



JOHANNES GUTENBERG
UNIVERSITÄT MAINZ

Studien zur elektrochemischen Synthese von C–N Funktionalitäten

Dissertation zur Erlangung des Grades
„Doktor der Naturwissenschaften“
im Promotionsfach Chemie

am Fachbereich Chemie, Pharmazie, Geographie und Geowissenschaften
der Johannes Gutenberg-Universität in Mainz

vorgelegt von

Lars Julian Wesenberg

geboren in Bad Schwalbach (Hessen)

Mainz, Juni 2020

Dekan:

████████████████████

Erster Gutachter:

██

Zweiter Gutachter:

██

Datum der mündlichen Prüfung:

Die vorliegende Arbeit wurde in der Zeit von September 2015 bis September 2019 am Department Chemie der Johannes Gutenberg-Universität Mainz unter Anleitung von [REDACTED] [REDACTED] angefertigt.

Hiermit versichere ich, dass die vorliegende Arbeit eigenständig und mit keinen anderen als den angegebenen Hilfsmitteln (Literatur, Apparaturen, Materialien) angefertigt wurde. Alle wörtlichen oder dem Inhalt nach ähnlichen Stellen aus fremden Arbeiten und Publikationen sowie adaptierte Abbildungen und Schemata wurden als solche eindeutig gekennzeichnet.

M. Sc. Chem. Lars Julian Wesenberg

*The most elementary and valuable statement in science,
the beginning of wisdom is 'I do not know'*
– **Lt. Commander Data**

Danksagung

An erster Stelle möchte ich mich bei [REDACTED] für die Aufnahme in seinen Arbeitskreis sowie die interessante und herausfordernde Aufgabenstellen bedanken. Durch zahlreiche Kooperationstreffen habe ich viel über die Schnittstelle Forschung und Industrie gelernt und erkannt wie wichtig die Kommunikation zwischen den einzelnen Gliedern einer Forschergemeinschaft sein kann. Man muss die Vokabeln lernen und prägnant die gesammelten Informationen aus dem letzten Forschungsquartal entsprechend net- und nagelfest vermitteln. Ich habe in diesem Abschnitt meiner Promotion viel über mich gelernt und erkannt welche Richtung ich mit meiner Promotion gehen möchte.

Die Forschung und die Erschließung neuer chemischer Verbindungen hat mich stets fasziniert und angetrieben. Ich möchte mich bei meinem Doktorvater noch für sein Vertrauen in meiner eigenverantwortlichen Erschließung neuer Themen und universitäts-internen Kooperationen bedanken. Durch diese Freiheiten war es möglich die rein organisch synthetisch orientierte Seite meiner Dissertation zu einer interdisziplinären anwendungsorientierten Promotion umzugestalten. In diesem Zuge möchte ich mich außerordentlich bei [REDACTED] und [REDACTED] für die biochemische Zusammenarbeit bedanken. Durch die herausfordernde und zeitintensive Laborarbeit von [REDACTED] konnten wir so potenzielle Inhibitoren der Zellviabilität auf der Prostatakrebs-Zelllinie LnCAP identifizieren.

Ein großer Dank gilt auch [REDACTED], [REDACTED], [REDACTED], [REDACTED], [REDACTED] und [REDACTED] die neben chemischen Fragestellungen stets Diskussionsbereitschaft zeigten und für eine entspannte und teilweise amüsante Atmosphäre im Quadranten sorgten. Darüber hinaus möchte ich mich auch noch bei [REDACTED] und [REDACTED] für ihre tatkräftige Unterstützung in der Synthese diverser Vorläuferverbindungen bedanken. Darüber hinaus gilt mein besonderer Dank [REDACTED] für ihre Mühen bei herausfordernden Trennproblemen stets Ruhe zu bewahren und mithilfe der präparativen HPLC und ihrer Expertise viele hochkomplexe Reaktionsgemische fein säuberlich isoliert wurden.

Inhaltsverzeichnis

1	EINLEITUNG	1
1.1	ELEKTROCHEMIE IN DER ORGANISCHEN SYNTHESE	2
1.2	RENAISSANCE DER ELEKTROCHEMIE	6
1.3	KONVENTIONELLER AUFBAU VON C–N FUNKTIONALITÄTEN	9
1.4	ELEKTROCHEMISCHER AUFBAU VON C–N FUNKTIONALITÄTEN.....	12
2	AUFGABENSTELLUNG	15
3	ERGEBNISSE & DISKUSSION	17
3.1	ELEKTROCHEMISCHE C–H AMINIERUNG VON PHENOXYESSIGSÄURE-METHYLESTERN ZUR DARSTELLUNG VON 1,4-BENZOXAZIN-3-ONEN	17
3.2	ZWEIFACHE ELEKTROCHEMISCHE C–H AMINIERUNG ZUR DARSTELLUNG VON MEDIZINISCH- RELEVANTEN VORLÄUFERMOLEKÜLEN.....	19
3.3	QUARTÄRE C(sp ²)–N FUNKTIONALITÄTEN ALS LADUNGSTRÄGER ZUR IDENTIFIZIERUNG VON METABOLITEN MITTELS EC-LC-MS METHODEN	21
4	ZUSAMMENFASSUNG	23
5	AUSBLICK	25
6	LITERATURVERZEICHNIS	29
7	ANHANG	37

1 Einleitung

Klimapolitische Interessen und die nachhaltige Ressourcennutzung werden in den nächsten Jahren auf globaler Ebene vordergründig sein. Eine wachsende Weltbevölkerung sowie steigende Lebensstandards verlangen von der Weltpolitik auf die einschneidende Veränderung unseres Ökosystems zu reagieren und eindämmende Maßnahmen einzuleiten. Die Energiewende wurde von der Bundesregierung beschlossen und setzt sich zentral aus einer nachhaltigen Energiegewinnung und der Reduktion des Energieverbrauchs im Allgemeinen zusammen.^[1] Mit einem nachhaltigen Ansatz werden quasi unerschöpfliche Energiequellen verwendet und umweltschonend elektromagnetische Strahlung (Licht) und mechanische Strömungen (z. B. Wind) in Elektrizität umgewandelt, welche in das Stromnetz eingespeist und von Privathaushalten und Industrie genutzt werden können. Die Problematik bei einer meteorologisch kontrollierten Energieeinspeisung liegt auf der Hand. Übersteigt die Produktion an Energie den Bedarf, muss diese gespeichert werden. Die nachhaltig gewonnene Energie wird somit in andere Substanzen beziehungsweise Energieträger transferiert, sei es in Form chemischer Bindungen „*Power-to-Chemistry*“, durch die Integration in die Wertschöpfungsketten der chemischen Industrie oder unter speziellen geographischen Anforderungen in Form von potentieller Energie in Pumpspeicherkraftwerken „*Power-to-Power*“ (Abbildung 1).^{[2]-[4]}

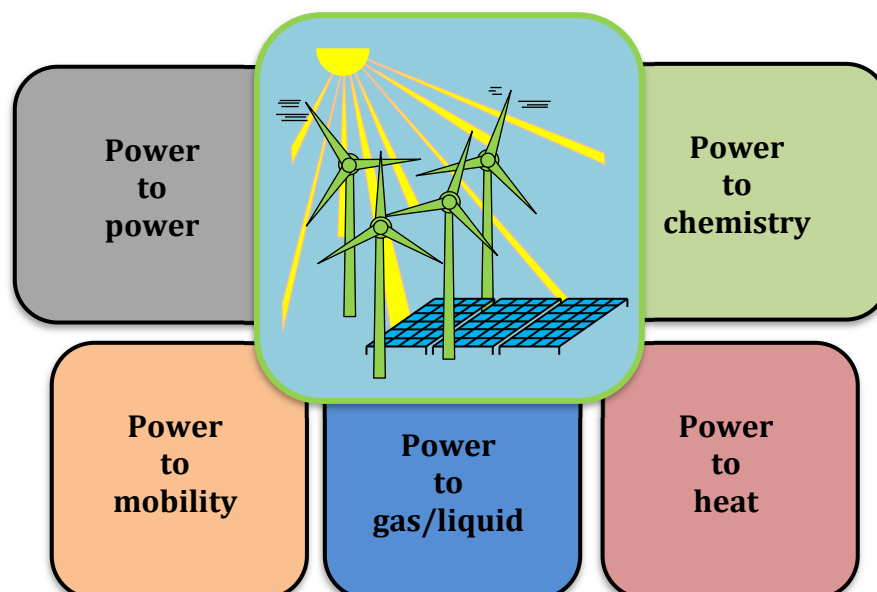
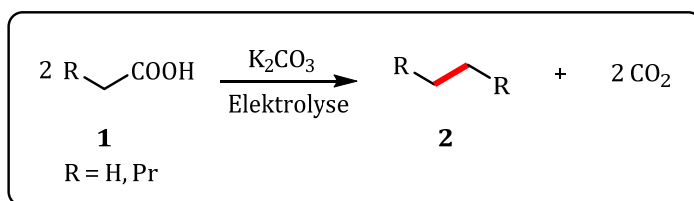


Abbildung 1: Energiespeichersysteme für Stromüberschüsse.

1.1 Elektrochemie in der organischen Synthese

ALESSANDRO VOLTA entdeckte im Jahr 1800 die Batterie, welche unter dem Namen „*Voltasche Säule*“ bekannt wurde. Diese Form der ersten Batterie bestand aus Kupfer- und Zinkplatten, welche systematisch übereinandergestapelt wurden. Die elektromotorische Kraft resultierte aus den Unterschieden der Redoxpotentiale der beiden unedlen Metalle.^[5] Er war somit der Begründer der Elektrochemie, wohingegen zu den ersten Vorreitern der Elektrosynthese MICHAEL FARADAY zählte. Dieser setzte eine wässrige Natriumacetat Lösung mithilfe einer Voltaschen Säule unter Strom, wobei er im Vergleich zur Kathode eine starke Gasentwicklung an der Anode beobachtete.^[6] Nähere Untersuchungen wurden anschließend von HERMANN KOLBE durchgeführt. Durch Elektrolyse von Valeriansäure bzw. Essigsäurelösung **1** konnten die entsprechenden gesättigten Kohlenwasserstoffe **2** teilweise identifiziert werden (Schema 1).^{[7],[8]}

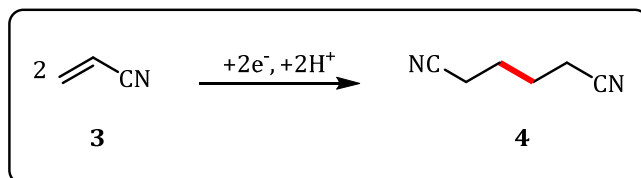


Schema 1: Anodische Dimerisierung durch Elektrolyse von verschiedenen aliphatischen Carbonsäuren nach Hermann Kolbe.

Die Arbeiten von FARADAY und KOLBE im 19. Jahrhundert ebneten somit den Weg für die Elektrochemie als vielversprechende Teildisziplin innerhalb der Chemie. Trotz des hohen Potentials wurde die elektroorganische Synthese erst Mitte des 20. Jahrhunderts wiederentdeckt.

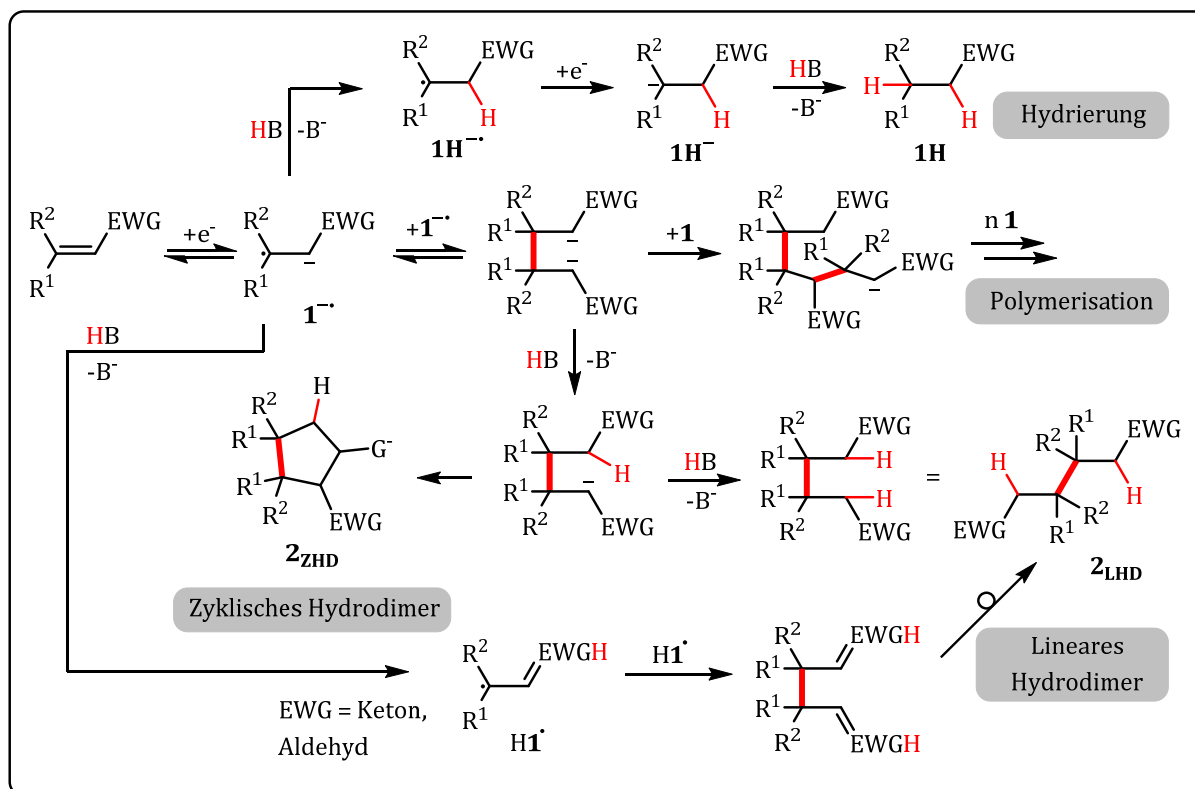
1960 entwickelte MANUEL BAIZER die elektrochemische Hydrodimerisierung (EHD) von Acrylnitril **3** zu Adipodinitril **4** in großtechnischem Maßstab. Adipodinitril ist ein wichtiges Vorläufermolekül für die Synthese von Polyamiden mit diversen Anwendungsgebieten wie z. B. technischem Plastik, Reifenkord und Textilien. Ende der 70er Jahre erreichte diese Produktion eine Größenordnung von über 100 000 Tonnen pro Jahr. Dieser Prozess legte somit den Grundbaustein für industrielle elektrochemische Verfahren.^{[9],[10]} Die konventionelle Synthese im industriellen Maßstab sieht vor, eine Hydrocyanierung an 1,3-Butadien bei hohen Temperaturen und Drücken von bis zu 130 °C und 50 bar durchzuführen.^[11] Die Nachteile dieser Strategie sind die extremen Reaktionsbedingungen und die Verwendung von toxischem Cyanwasserstoff, wodurch die Kontamination des Produktes kaum zu vermeiden ist. Der elektrochemische Ansatz

hingegen sieht vor in wässriger Lösung mit Cadmium, Quecksilber oder Blei und später mit weniger toxischen Kupfer-Blei-Legierungen als Kathodenmaterial zu arbeiten.^[12] Die Kontamination des Produktes wird durch den elektrochemischen Ansatz deutlich vermindert.^[13] Darüber hinaus kann die Reaktion bei milden Temperaturen und Drücken durchgeführt werden (Schema 2).



Schema 2: Reduktive Elektrodimerisierung von Acrylnitril zu Adipodinitril nach BAIZER.

Anhand der EHD soll gezeigt werden, welche Reaktionspfade elektrochemisch generierte Intermediate eingehen können. Dabei wird im Folgenden ausschließlich der mechanistische Verlauf innerhalb des Elektrolyten besprochen und auf Erklärungen des heterogenen Ladungstransfers (Elektrode – Elektrolyt) verzichtet. Die hier aufgeführte Reaktion behandelt einen reduktiven Prozess, somit werden Elektronen auf ein elektronendefizitäres Zentrum übertragen und ein elektronenreiches Zentrum geschaffen. Das durch diese *Umpolungsreaktion* resultierende intermediäre Radikal-Anion weist durch sein ungepaartes Elektron in einem „*single-occupied-molecular-orbital*“ (SOMO) eine besonders hohe Reaktivität auf. Bei der Synthesepaltung kommt es somit darauf, an diese Reaktivität zu nutzen respektive zu kontrollieren. Genaue Untersuchungen wurden bei der EHD von monoaktivierten ungesättigten Kohlenwasserstoffen durchgeführt. Diese Olefin-Derivate werden durch elektronenziehende Gruppen (EWG) aktiviert (Schema 3).^[14] Zwei wesentliche Nebenreaktionen können nach der Bildung des Radikal-Anions **1•** mit dem gewünschten Reaktionspfad der Hydrodimerisierung konkurrieren. Die *Umpolung* des elektronenarmen Olefins durch Aufnahme eines Elektrons führt zu einem hoch reaktiven Intermediat **1•** und damit Ausgangspunkt verschiedenster Reaktionssequenzen.^[15] Im protischen Medium kann das Radikal-Anion **1•** aufgrund der deutlich veränderten Reaktivität die Abstraktion eines Protons bewirken. Das Folgeprodukt dieser Reaktionssequenz bzw. der Hydrierung der Doppelbindung ist der gesättigte Aliphath **1H**. Hier ist die Acidität der Protonenquelle entscheidend für den Ausgang der Reaktion (Schema 3).



Schema 3: Mechanistische Untersuchungen zu verschiedenen Reaktionspfaden der EHD an einfach aktivierten Olefinen; G: Zyklisierung über z.B. Carbonyleinheit einer elektronenziehenden Gruppe.^[14]

In wasserfreien aprotischen Lösungsmitteln hingegen kann es im technischen Maßstab zu Polymerisation kommen. Neben der Abwesenheit von Protonen sind eine geringe Verdünnung, erhöhte Stabilität des Radikal-Anions **1^{••}** und die Reversibilität der Dimerisierung entscheidende Einflussgrößen. Die Natur des Substrates selbst und die damit verbundenen molekülbezogenen Eigenschaften werden unter Substratkontrolle zusammengefasst. Bei elektronenziehenden Gruppen wie Carbonsäuren, Nitrilen und Carbonylen kann der intramolekulare Angriff gegenüber einer weiteren Protonierung favorisiert sein und somit ein zyklisches Hydrodimer **2_{ZHD}** aufgebaut werden. Weiterhin ist die Enolisierung von Carbonylverbindungen nach Protonierung des Radikal-Anions **1^{••}** möglich. Das entstehende Radikal **H1[•]** ist reduktionsträge und rekombiniert leicht. Das Folgeprodukt ist nach Tautomerisierung das entsprechende lineare Hydrodimer **2_{LHD}**. Neben den genannten Größen können auch Additive entscheidenden Einfluss auf die Reaktion nehmen. Beispielsweise gewährleisten Leitsalze die Leitfähigkeit von organischen Lösungsmitteln und damit den Ladungstransport.^[16]

Im Jahr 2000 wurde von ANASTAS und WARNER der Begriff „Grüne Chemie“ vorgestellt und ausgearbeitet.^[17] Dieses Konzept umfasst 12 Prinzipien als Orientierungsgrundlage für die nachhaltige Entwicklung von neuen chemischen Produkten bzw. Prozessen. Durch die Verwendung von Elektronen als Reagenzien, können gefährliche, toxische und kostenintensive Chemikalien in Form von Oxidations- oder Reduktionsmitteln ersetzt werden. Folglich kann der Abfallstrom erheblich vermindert werden. Die organische Elektrosynthese zeichnet sich somit durch eine erheblich effizientere Atomökonomie und Energiebilanz aus. Außerdem kann die Elektrosynthese als inhärent sicher angesehen werden, da durch die Abschaltung der Stromquelle die Reaktivität dem System direkt entzogen wird. Die Elektroorganische Synthese erfüllt somit in gewissen Teilen die Prinzipien der „Grünen Chemie“ (Abbildung 2).^{[17]-[19]}

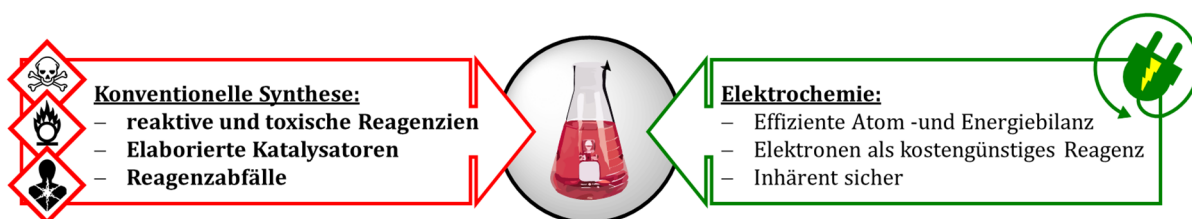


Abbildung 2: Schematischer Vergleich von konventioneller Synthese und Elektrochemie.

In den letzten Jahren hat sich die Elektroorganik innerhalb der organisch-chemischen Gemeinschaft als fähiges synthetisches Werkzeug präsentiert.^[17] Eine der großen Herausforderungen verbleibt in der Umsetzung bzw. Reproduzierbarkeit von elektrochemischen Methoden. Das zugrundeliegende Problem ist der systemtechnische Aspekt der nicht-standardisierten elektrochemischen Instrumente bezüglich Zelldesign, Stromquelle und Elektrodenmaterialien und -geometrien. Für eine Verbreitung der organischen Elektrosynthese bedarf es in einem kommerziellen Maßstab zugängliche Instrumente, standardisierte Verfahren und Anleitungen. Darüber hinaus muss der synthetische Nutzen bezüglich Skalierbarkeit und Zeiteffizienz gegenüber der konventionellen Methode konkurrenzfähig sein.^{[20],[21]}

1.2 Renaissance der Elektrochemie

Die elektroorganische Synthese erlebt derzeit eine *Renaissance*, da sie eine leistungsfähige und nachhaltige Alternative zu konventionellen Syntheserouten darstellt (Abbildung 3).^{[21]-[25]}

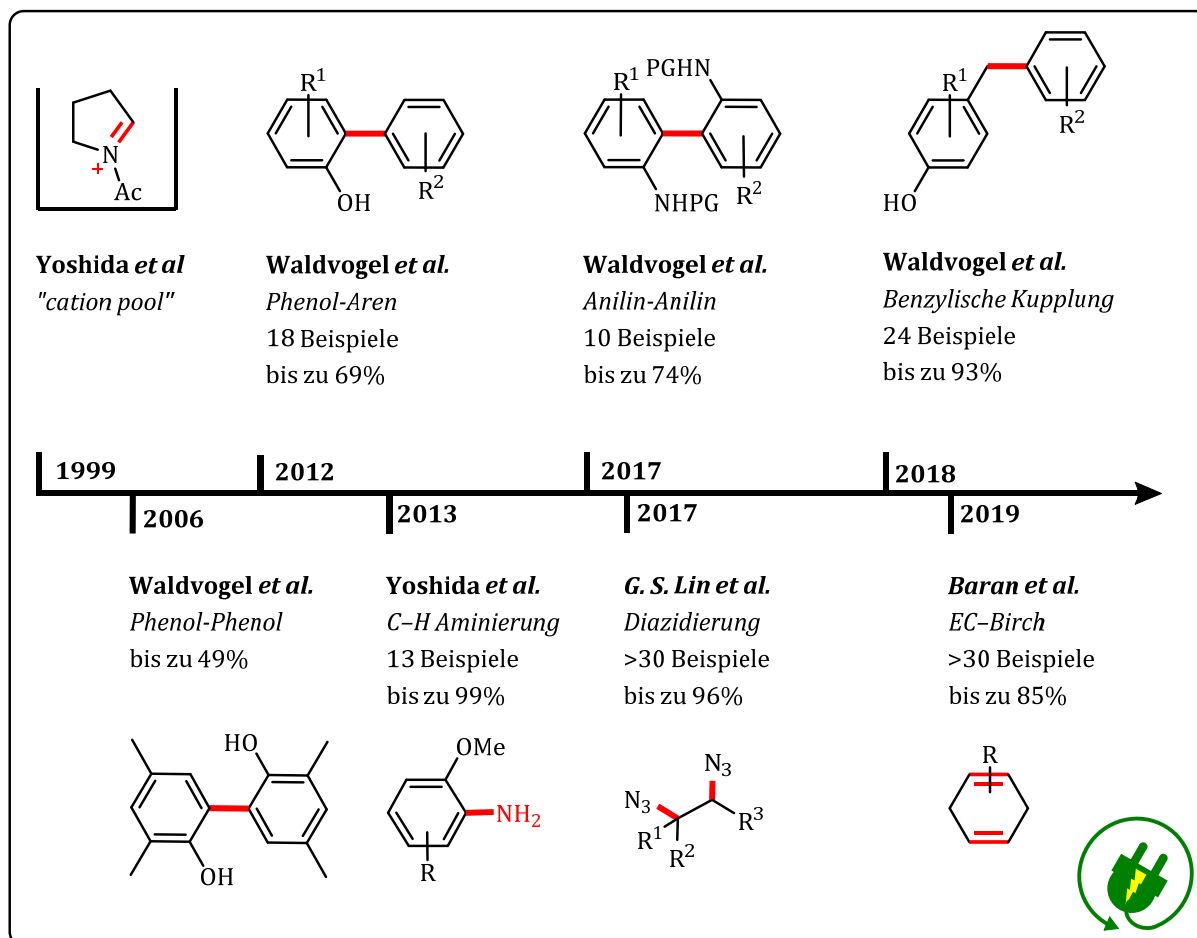
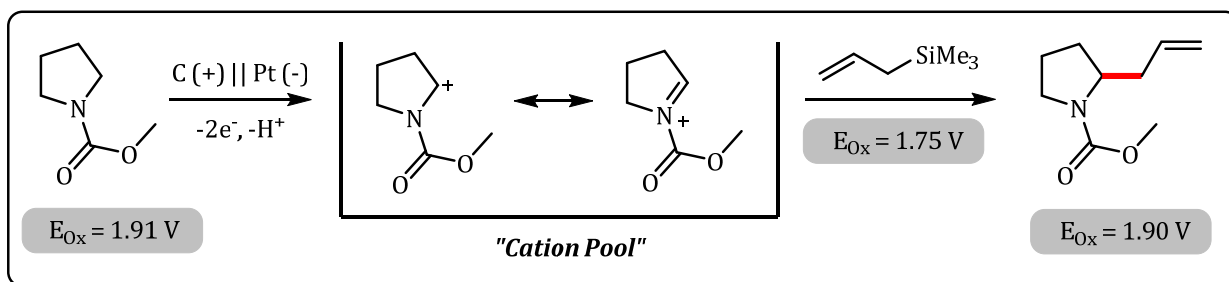


Abbildung 3: Ausgewählte elektrochemische Synthesen der letzten 20 Jahre.^{[26]-[33]}

YOSHIDA entwickelte im Jahr 1999 ein innovatives Konzept, Carbokationen in Lösung anzureichern und zu stabilisieren. Dieses Verfahren wurde ein fundamentaler Baustein der Elektrochemie und als „Cation Pool“ bekannt. Durch die *Umpolung* eines sp^3 -Kohlenstoff-Zentrums können, durch nachträgliches Hinzufügen eines oxidativ labilen und elektronenreichen Nucleophils, C-C Bindungen aufgebaut werden. Die Besonderheit liegt in der kryogenen Anreicherung eines oxidierten Substrates, welches ein höheres Oxidationspotential als das verwendete Nucleophil aufweist. Elektrolyse des Gemisches führte zur alleinigen Oxidation des Nucleophils und die gewünschte Produktbildung wurde nur in Spuren beobachtet (Schema 4).^{[26],[27]}



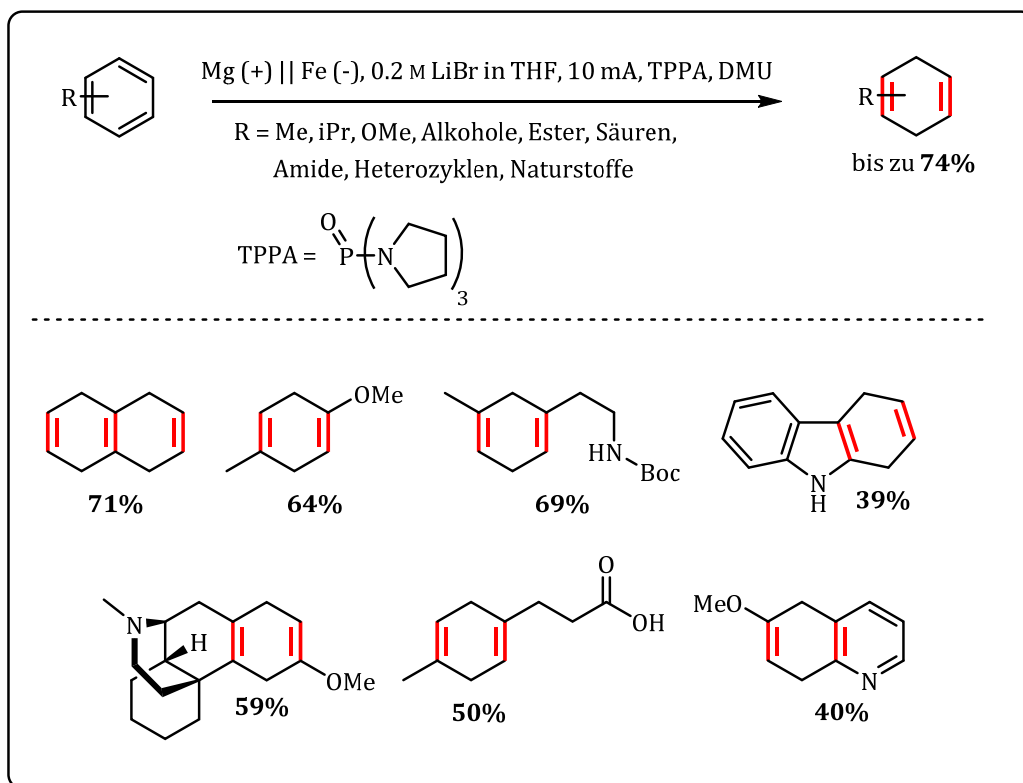
Schema 4: „Cation Pool“ Methode an geschützten Pyrrolidin-Derivaten, E_{ox} vs. Ag/AgCl in 0.1 M Bu_4NClO_4/CH_2Cl_2 .

Mithilfe des „Cation Pools“ konnte die Substratvielfalt der berühmten SHONO Oxidation erweitert werden.^{[21],[34]} Bei dieser Oxidation werden Alkylamide anodisch oxidiert und reaktive *N*-zentrierte Radikalkationen gebildet. Diese hochreaktiven Intermediate zerfallen zu *N*-Acyliminium Ionen, welche *in situ* durch geeignete Wahl von nukleophilen Lösungsmitteln wie Methanol als stabile *N,O*-Acetale eingefangen werden. Die gewünschte Folgereaktion mit einem Nucleophil ist nur durch gezielte Aktivierung des Acetals, durch z.B. Lewis-Säuren wie $TiCl_4$, möglich.^{[34]-[36]}

Seit 2006 haben WALDVOGEL und Mitarbeiter einen neuartigen elektrochemischen Synthesansatz zu aromatischen und benzyllischen Kupplungsreaktionen ausgearbeitet (Abbildung 3). Die Arbeitsgruppe etablierte zu Beginn die Synthese von 2,2'-Biphenolen über eine direkte anodische dehydrierende C-C-Kupplung.^[37] In den Folgejahren konnten zahlreiche Protokolle für Phenol-Phenol,^{[38]-[40]} Phenol-Aren^{[32],[41]} und *N*-geschützten Anilin-Anilin Kupplungsreaktionen entwickelt werden.^{[33],[42]}

2017 entwickelten S.LIN und Mitarbeiter ein leistungsfähiges Protokoll initial elektrochemisch Azid-Radikale zu generieren und mithilfe eines Radikaltransferreagens ($MnBr_2$) die Azidfunktion auf Olefine zu übertragen (Abbildung 3). Mit dieser Methodologie wurden diverse funktionelle Gruppen toleriert. Alkohole sowie Carbonyle, Ester, Alkine, Epoxide und Halogenalkane konnten zu den entsprechenden vicinalen Diaziden umgesetzt werden.^[30]

P. BARAN und Mitarbeiter etablierten im Jahr 2019 eine innovative und milde elektrochemische Alternative zur BIRCH-Reduktion. Als Opferanode fungiert Magnesium und als Kathode wird ein verzinkter Stahldraht verwendet. Das Elektrolytsystem besteht aus Lithiumbromid als Leitsalz in THF, Dimethylharnstoff (DMU) als Protonenquelle und Tris(pyrrolidin)phosphoramid (TPPA) als nicht-kanzerogenes Surrogat von Hexamethylphosphoramid. TPPA fungiert als Überladungsschutz an der Kathodenoberfläche, um eine Li^0 -Beschichtung zu verhindern (Schema 5).^[29]



Schema 5: Elektrochemische BIRCH-Reduktion nach P. BARAN mit hoher Toleranz gegenüber funktionellen Gruppen.

Neben der bekannten 1,4-Reduktion von aromatischen Systemen unter klassischen Birch-Bedingungen konnten auch elektroreduktive Transformationen wie Deoxygenierungen von Fluorenon, Epoxid-Ringöffnungen und intramolekulare MCMURRY Kupplungen bei Zimmertemperatur realisiert werden.

1.3 Konventioneller Aufbau von C-N Funktionalitäten

Die Kohlenstoff-Stickstoff-Bindung kann als elementares Strukturmotiv in mannigfaltigen Naturstoffen,^{[43]-[45]} Arzneistoffen,^{[46]-[49]} Farbstoffen,^{[50]-[52]} funktionellen Materialien sowie Polymeren^{[53]-[57]} wiedergefunden werden (Abbildung 4).

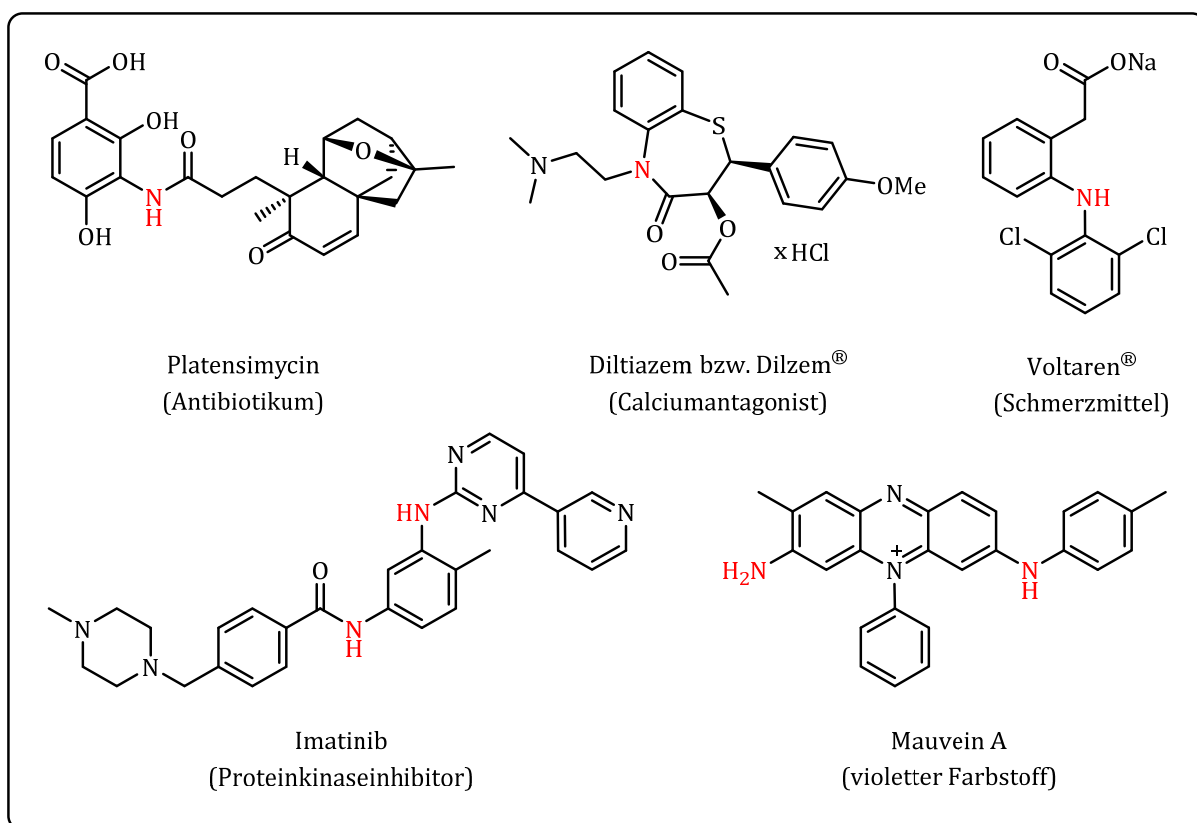
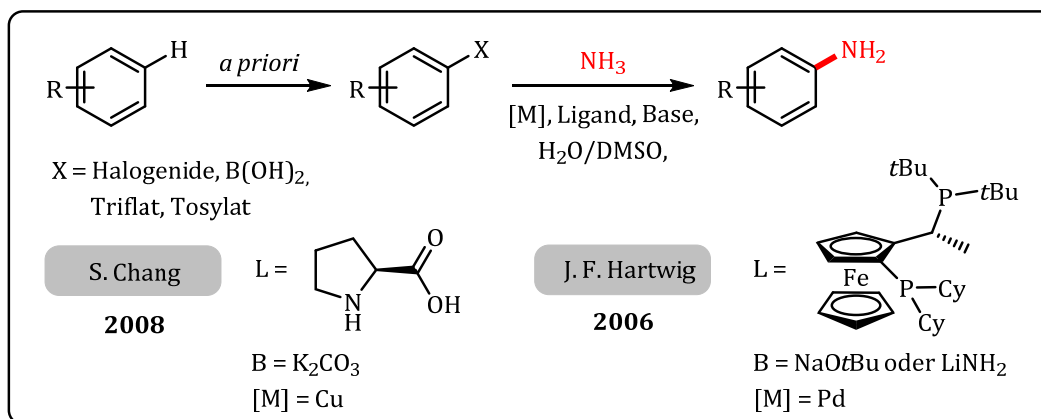


Abbildung 4: Diverse C-N Funktionalitäten in Pharmazeutika, Naturstoffen und Farbstoffen.

Die große Herausforderung bei der organisch-chemischen Synthese von C-N Funktionalitäten bleibt die Synthese von freien aromatischen primären Aminen.^{[58],[59]} Ein möglicher synthetischer Ansatz für den Aufbau von aromatischen primären Aminen ist die Nitrierung von aromatischen Systemen mit elektrophilen Nitronium-Ionen und anschließender Reduktion zur Aminfunktionalität. Der Einsatz toxischer Reagenzien, die teils aggressive Reaktionsführung sowie geringe Regioselektivitäten sind Nachteile dieser Methode. Häufig treten hierbei mehrfach nitrierte Produkte als unerwünschte Nebenkomponenten auf, welche aufwendig aus der Reaktionslösung entfernt werden müssen.^{[60],[61]} Eine deutlich verbesserte Regioselektivität kann durch potente Methoden wie die BUCHWALD-HARTWIG-Reaktion^{[62],[63]} oder CHAN-LAM-Reaktion^{[64],[65]} erreicht werden. Hierbei werden Übergangsmetalle als Katalysator und *a priori* funktionalisierte

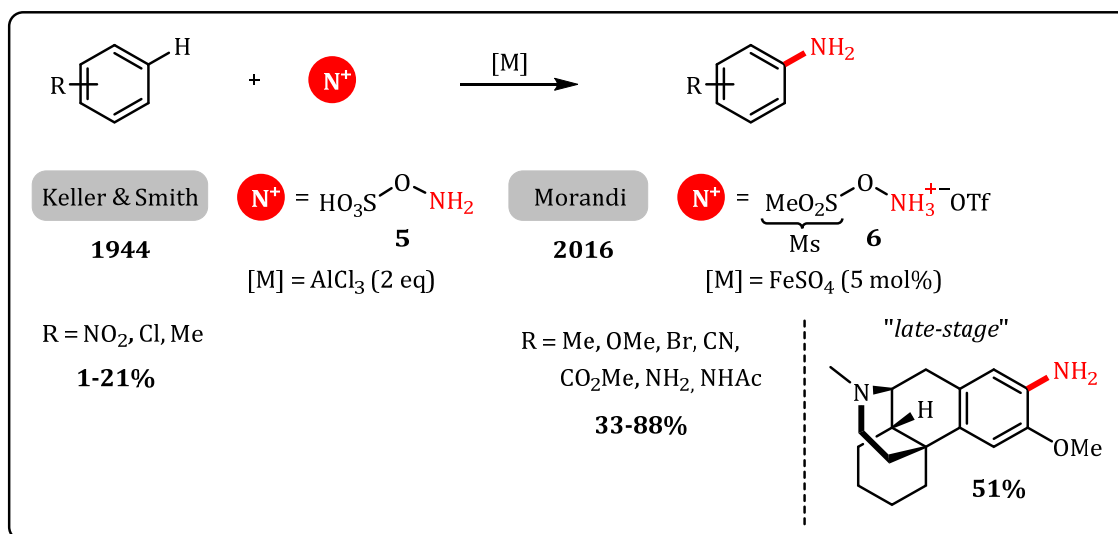
Substrate bei hohen Temperaturen und teilweise unter Einwirkung von starken Basen wie z.B. Kalium *tert.*-Butanolat (K*Ot*Bu) umgesetzt. Die BUCHWALD-HARTWIG-Reaktion findet industrielle Anwendung, wobei fast ausschließlich sekundäre und/oder *N*-geschützte C–N-Bindungen adressiert werden.^{[58],[66]} Eine unvorteilhafte Atomökonomie ist hierbei auf zusätzliche Syntheseschritte durch vorheriges Einführen der Abgangsfunctionalitäten zurückzuführen. Seit 1997 wurden stets die Synthesen von C–N Bindungen auf alternative Stickstoffquellen ausgedehnt und für die Synthese von freien aromatischen primären Aminen weiterentwickelt. Es wurden diverse Ammoniak-Äquivalente in Form von Silylamiden wie z.B. Zn[N(TMS)₂]₂,^[67] Phenylamiden^[68] oder Benzophenonimin Addukten^{[69],[70]} bei Palladium-katalysierten *N*-Arylierungen eingesetzt. Trotz dieser zahlreichen alternativen Stickstoffquellen ist ein weiterer Syntheseschritt für die Freisetzung des Amins unabdinglich und leistet damit einen negativen Beitrag zu der Atomökonomie und Energiebilanz. Moderne Methoden verwenden wässrige Ammoniak als Stickstoffquelle mit DMSO als Co-Solvens. Kupfer oder Palladium werden, in Gegenwart geeigneter und teilweise elaborierten Liganden, als Katalysatoren verwendet. Als Abgangsgruppen werden Boronsäuren, Halogenide, Triflate oder Tosylate genutzt (Schema 6).^{[71],[72]}



Schema 6: Moderne Synthesen von freien aromatischen primären Aminen über Palladium und Kupferkatalyse von CHANG und HARTWIG.

Im Jahr 1944 entwickelten KELLER und SMITH,^[73] basierend auf Arbeiten von SOMMER *et al.*,^[74] eine Alternative zur klassischen, nukleophilen Stickstoffquelle für die Synthese von freien aromatischen primären Aminen. Hydroxylamin-*O*-sulfonsäure (HSA) **5** wurde als neuartiges elektrophiles Reagenz eingesetzt. Mithilfe einer Lewis-Säure wie AlCl₃ konnten so aromatische Systeme in moderaten Ausbeuten von bis zu 21% aminiert werden. Das HSA-Reagenz **5** wurde von B. MORANDI im Jahr 2016 zum Ammoniummesylat-Salz **6** weiterentwickelt.^[75] Mit diesem innovativen C–H-

Aminierungsprotokoll mit Eisensulfat als Katalysator konnten sogar „late stage“ Funktionalisierung realisiert werden (Schema 7).^{[75]-[77]}



Schema 7: Direkte C–H Aminierung mittels elektrophiler Stickstoffquellen.

Trotz allen Bemühungen blieb die Verwendung präfunktionalisierte Reagenzien und Übergangsmetallkatalysatoren in den letzten Jahren unumgänglich, um direkt C–H Aminierungen realisieren zu können. In der organisch-synthetischen Gemeinschaft stellt die Entwicklung effizienter und nachhaltiger Methoden zum Aufbau von Aminfunktionalitäten weiterhin eine zentrale Herausforderung dar. Eine Vielzahl an Synthesen von C–N Bindungen wurden in den letzten Jahren durch homogene Katalyse realisiert, allerdings adressierten nur eine sehr geringe Anzahl freie aromatische primäre Amine *via* Ammoniak-Surrogate als Stickstoffquelle.^[59] Das grundlegende Problem bei der Verwendung von Ammoniak ist die Aktivierung der N–H Bindung. In den letzten Jahren gehören die direkte Hydroaminierung von Olefinen zur Gewinnung von primären aliphatischen Aminen und die direkte Kupplung von Ammoniak mit Arenen zur Darstellung von primären Anilinen zu den anspruchsvollsten Zielen in der Katalyse.^{[78]-[80]} Eines der Hauptprobleme ist die Tendenz des Stickstoffs, Lewis Säure-Base Komplexe in Form einer σ -Bindung über das freie Elektronenpaar mit einem Übergangsmetall einzugehen (WERNER-Komplex, Abbildung 5).^[81] Aufgrund der hohen Bindungsdissoziationsenergie ($\approx 107.4 \text{ kcal}\cdot\text{mol}^{-1}$)^[82] der N–H-Bindung ist die oxidative Addition thermodynamisch nicht begünstigt.

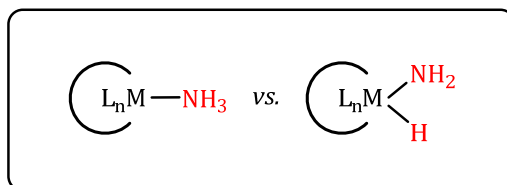
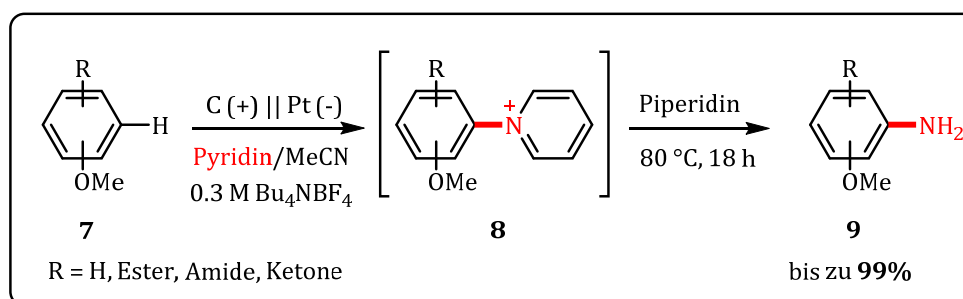


Abbildung 5: Vergleich einer σ -Bindungskoordination gegenüber einer oxidativen Addition an ein Metallzentrum.

1.4 Elektrochemischer Aufbau von C-N Funktionalitäten

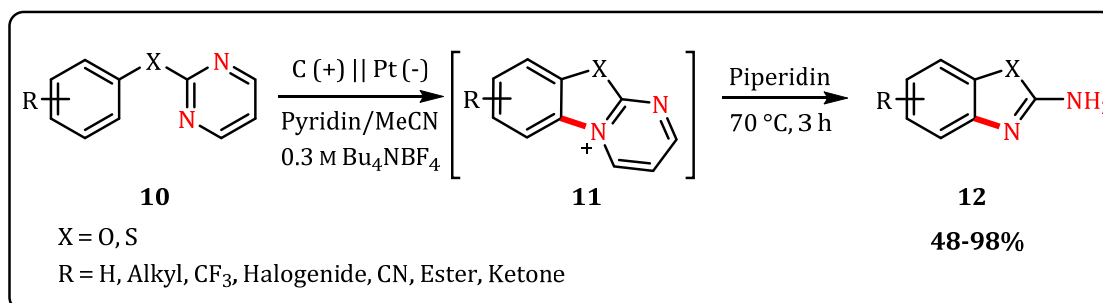
YOSHIDA und Mitarbeiter entwickelten im Jahr 2013 eine neuartige und potente Methode zum Aufbau von C-N-Funktionalitäten respektive freien aromatischen primären Aminen. Elektronenreiche Aromaten **7** werden anodisch zu Radikalkationen oxidiert und durch überschüssig eingesetztes Pyridin abgefangen. Pyridin fungiert somit zum einen als sogenannter „trapping agent“ und zum anderen als Stickstoffquelle. Durch einen weiteren Oxidationsschritt und Protonenabstraktion entsteht ein stabiles Pyridinium-Intermediat **8**. Dieses Zwischenprodukt **8** wird als ZINCKE-Salz bezeichnet. In einem Folgeschritt wird das freie primäre Amin **9**, durch einen nukleophilen Angriff eines sekundären zyklischen Amins in α -Position zum quartären Stickstoff, freigesetzt (Schema 8).^[28]



Schema 8: Elektrochemische C-H Aminierung von elektronenreichen Aromaten via ZINCKE-Salz nach YOSHIDA und Mitarbeitern.

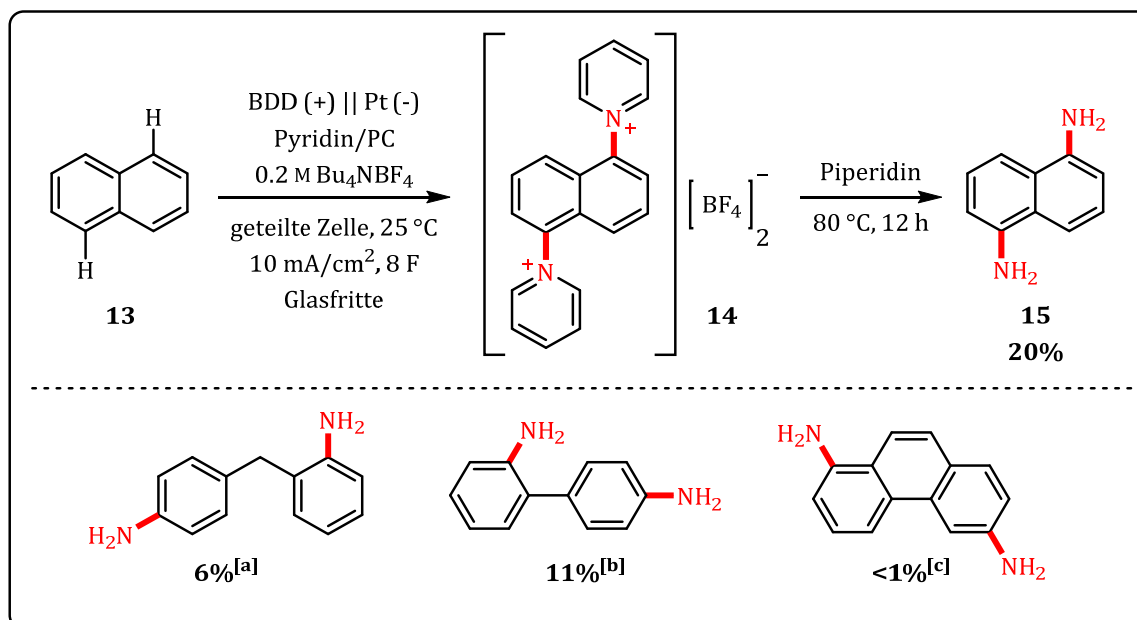
YOSHIDA postulierte, dass das intermediär gebildete Pyridinium-Kation **8**, aufgrund der positiven Ladung und des elektronenziehenden Effekts, vor Überoxidation geschützt ist und angereichert werden kann.^[28] Die positive Ladung des ZINCKE-Salzes **8** führt zur Coulomb-Abstoßung gegenüber der positiv polarisierten Anode, wodurch eine weitere Oxidation des Zwischenproduktes **8**, an der Anode sehr unwahrscheinlich ist. Der Pyridinium-Substituent fungiert zudem als EWG und verringert die Elektronendichte des aromatischen Systems. Diese Eigenschaften resultieren in einer signifikanten Erhöhung des Oxidationspotentials.

Darüber hinaus konnte YOSHIDA und Mitarbeiter neben dem intermolekularen ZINCKE-Salz **8** auch eine intramolekulare Variante **11** der C–H Aminierung etablieren. Mithilfe eines Pyrimidin substituierten Phenols bzw. Thiophenols **10** konnten auf diesem innovativen Weg 2-Aminobenzoxazole bzw. Aminobenzothiazole **12** erhalten werden (Schema 9).^[83]



Schema 9: Intramolekularer C–N Bindungsaufbau zur Darstellung von Benzoxazolen respektive Benzothiazolen.

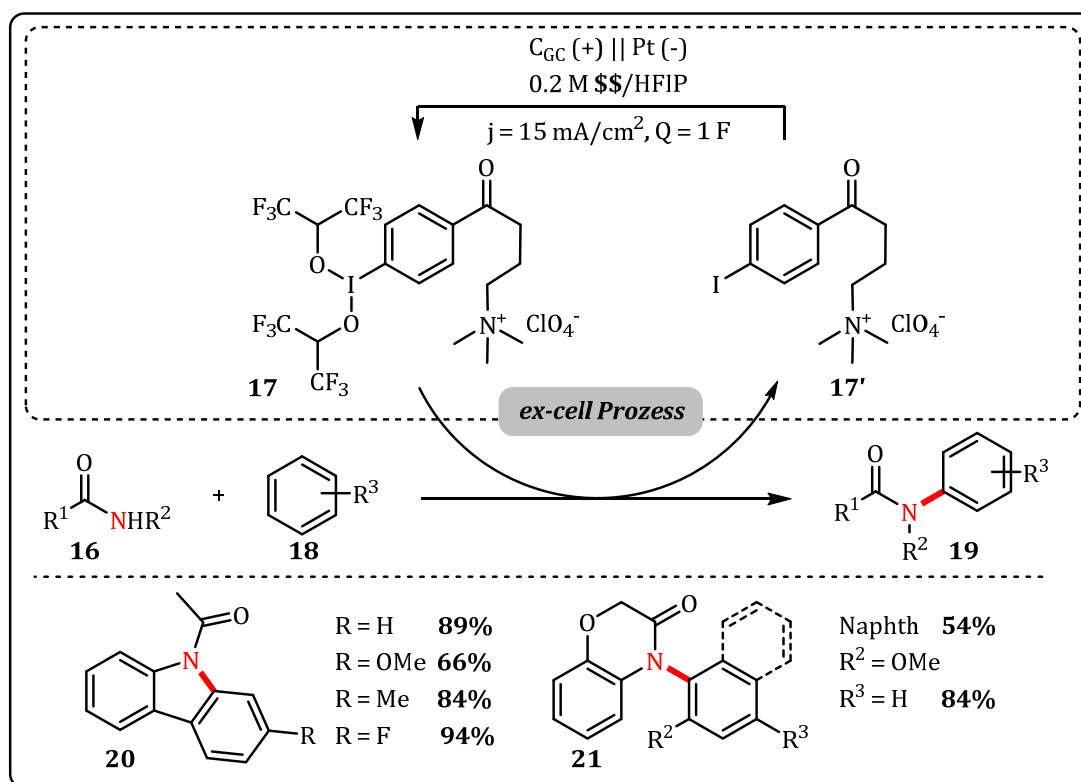
2017 entwickelten WALDVOGEL und Mitarbeiter die C–H Aminierung weiter und untersuchten die Möglichkeit, nicht aktivierte aromatische Systeme wie Naphthalin **13** und ähnliche Strukturen zu Dianilinen **15** zu überführen. Entgegen dem oben erwähnten Postulat von YOSHIDA konnten so von WALDVOGEL die gewünschten freien primären Dianiline **15** in Ausbeuten von bis zu 20% aufgebaut werden (Schema 10).^[84]



Schema 10: Elektrochemische Zweifach-Aminierung von Naphthalin und ausgewählten verwandten Strukturen; PC = Propylencarbonat, [a] = Acetonitril, Separator: Glasfritte, 20 mA/cm², 6 F, 60 °C; [b] = Acetonitril, Separator: Thomapor[®], 10 mA/cm², 6 F, 25 °C; [c] = Acetonitril, Separator: Celgard[®], 1 mA/cm², 3 F, 25 °C.

Diamine sind wichtige Vorläufermoleküle in der Produktion von Polyurethanen. Polyurethane werden über eine Polykondensation von Diisocyanaten mit Diolen

hergestellt. Um die gewünschten Ausgangsverbindung der Polymerisation herzustellen, wird das Diamin mittels zweifacher Phosgenierung zum Diisocyanat überführt.^{[85]–[87]} Die Firma Covestro AG verwendet dieses Verfahren bei der Herstellung von Vulkollan®.^[88] Eine nachhaltige, kosteneffiziente und weniger toxische Synthesestrategie zur Vorläufersynthese wurde in einer Kooperation mit der Waldvogel Gruppe angestrebt und durch den elektrochemischen Ansatz erfolgreich in teils moderaten Ausbeuten erzielt.^[84] Eine alternative Methode zum Aufbau von C–N-Funktionalitäten gelang im Jahr 2016 von R. FRANCKE und Mitarbeitern mit der indirekten elektrochemischen Arylierung von Carbonsäureamiden **16**. Der elektrochemische Ansatz sieht vor, ein Iodbenzol-Derivat (I^I) **17** anodisch in Gegenwart von 1,1,1,3,3,3-Hexafluorisopropanol (HFIP) zu oxidieren (I^{III}) **17'** und in einer „*ex-cell*“ Prozedur für die Oxidation des Substrates **16** zu nutzen. Die Leitfähigkeit der Reaktionslösung wird durch den Einbau einer quartären Ammonium-Struktur innerhalb des Iodaromaten **17** gewährleistet (Schema 8).^[89]

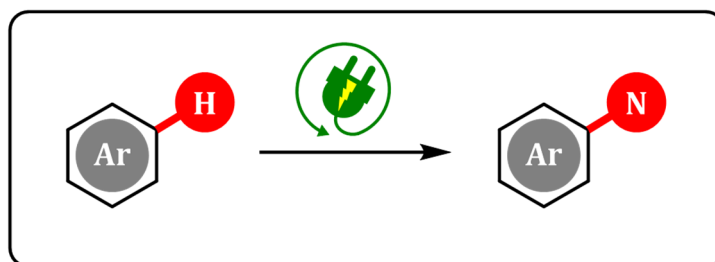


Schema 11: Intramolekulare und Intermolekulare C–N Arylierungen von Amidstrukturen nach R. FRANCKE; Anode: Glaskohlenstoff, Kathode: Platin.^[89]

Mit dieser Methode war es möglich, Methoxy-, Methyl- und Fluor-substituierte Carbazole **20** über einen intramolekularen C–N-Bindungsaufbau zu generieren. Darüber hinaus konnten auch intermolekular Benzoxazinonderivate mit Aren-Komponenten in teils sehr guten Ausbeuten von bis zu 86% gekuppelt werden.

2 Aufgabenstellung

Der nachhaltige und gleichzeitig effiziente Zugang zu Kohlenstoff-Stickstoff Bindungen gehört zu einer der großen Herausforderungen in der organischen Synthese. Eine geeignete Stickstoffquelle und die Wahl der Syntheseroute sind ausschlaggebend für den Erfolg der Reaktion. Ziel dieser Arbeit war es eine ressourcenschonende elektrochemische Syntheseroute für stickstoffhaltige und medizinisch-relevante Vorläufermoleküle zu etablieren.



Schema 12: Nachhaltiger Aufbau von Kohlenstoff-Stickstoff Bindungen mittels elektrochemischer Methoden.

3 Ergebnisse & Diskussion

3.1 Elektrochemische C–H Aminierung von Phenoxyessigsäuremethylestern zur Darstellung von 1,4-Benzoxazin-3-onen

Benzoxazinone kommen als Botenstoffe, natürliche Insektizide und Herbizide in der Natur in Nutzpflanzen wie Mais, Roggen und Weizen vor.^{[90]–[92]} Blepharin **22** mit 1,4-Benzoxazin-3-on als Grundgerüst wurde in Gräsern gefunden.^[93] Dieses Glykosid und auch andere glykosidisch verknüpfte Abkömmlinge zeigen eine hohe Aktivität in einer Reihe von Pflanzenabwehrmechanismen, die sich vor allem in Form der Pathogenabwehr ausdrücken (Abbildung 6).^[94] Benzoxazinone haben viel Aufmerksamkeit, bedingt durch ihre potentielle pharmakologische Wirkung, erfahren und sind grundlegende Bausteine in vielen medizinisch relevanten Verbindung. Das Benzoxazinone mit *N*-meta-Chlorbenzylrest **24** wirkt als Inhibitor der bakteriellen Histidinproteinkinase.^[95] Das synthetisch zugängliche Benzoxazinon-Derivat **23** wird als potentieller Wirkstoff für die Behandlung von Herzerkrankungen eingesetzt.^[96] Darüber hinaus finden die Guanidin Derivate **23** und **24** als Serotoninrezeptorantagonist Verwendung (Abbildung 6).^[97]

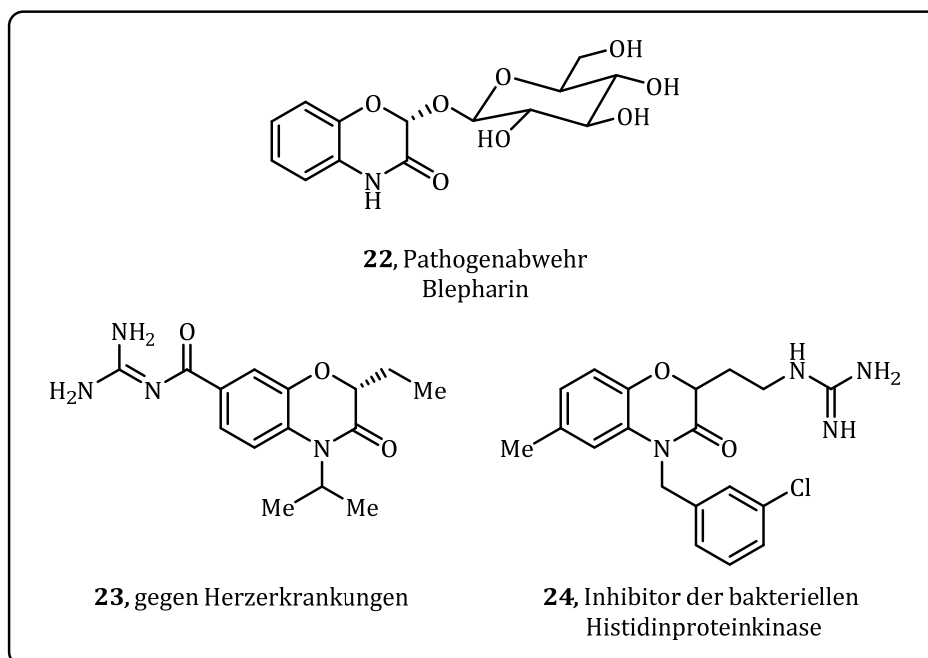
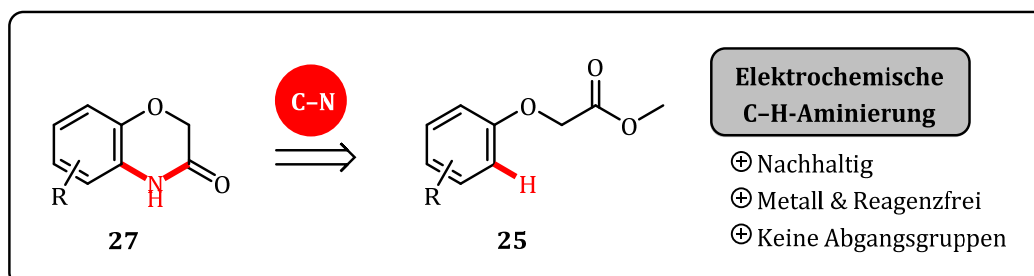


Abbildung 6: In Gräsern natürlich vorkommendes Blepharin **22** (oben), weitere synthetisch zugängliche Benzoxazinone für medizinisch-relevante Anwendungsgebiete (unten).

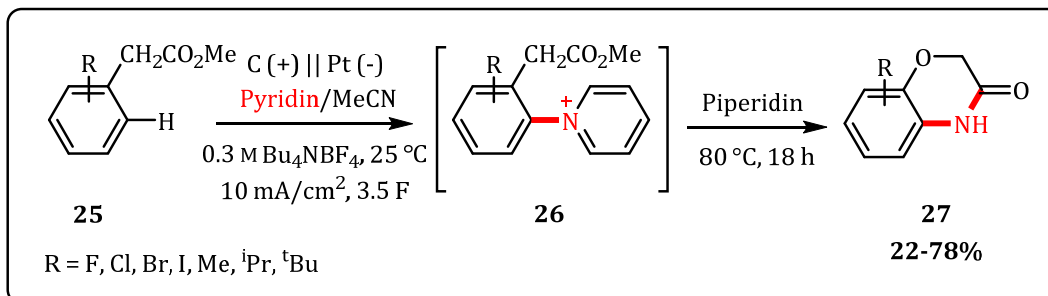
Basierend auf Vorarbeiten von YOSHIDA und WALDVOGEL wurde ein nachhaltiger synthetischer Zugang zu Benzoxazinone angestrebt. Diese Strategie sieht vor elektrochemisch die C–H Bindung in *ortho* Position zum Phenoxyessigsäuremethylestern

25 zum entsprechenden Pyridinium-Salz **26** umzusetzen. Anschließend wird das Amin freigesetzt und *in situ* zum 1,4-Benzoxazin-3-on **27** zyklisiert. Mithilfe elektrochemischer Methoden können so eine besonders hohe Atomökonomie und Energiebilanz erzielt werden (Schema 13).



Schema 13: Elektrochemische Synthesestrategie mittels C-H Aminierung nach YOSHIDA von Phenoxyessigsäuremethylestern zu 1,4-Benzoxazin-3-on.

Der obige Synthesepfad wurde nach vollständiger Optimierung der elektrochemischen Reaktionsbedingungen auf diverse Phenoxyessigsäuremethylester-Derivate **25** angewandt. Ein breites Substratspektrum mit Fluor-, Chlor-, Brom- und Iod- sowie Alkylsubstituenten konnten mit dieser Methodologie zu den gewünschten Heterozyklen **27** in Ausbeuten von bis zu 78% umgesetzt werden (Schema 14).^[98]



Schema 14: Elektrochemische C-H-Aminierung von Phenoxyessigsäuremethylestern.

Zu diesem Kapitel wurde ein Manuskript veröffentlicht:

Lars Julian Wesenberg, Sebastian Herold, Akihiro Shimizu, Jun-ichi Yoshida, und Siegfried R. Waldvogel, *Highly Selective Synthesis of 1,4-Benzoxazin-3-ones by Electrochemical C,H-Amination*, Eur. J. Chem. **2017, 23, 12096–12099.**

3.2 Zweifache elektrochemische C-H Aminierung zur Darstellung von medizinisch-relevanten Vorläufermolekülen

In diesem Projekt ging es um die Entwicklung einer potenten zweifachen C-H Aminierung von Phenoxyessigsäuremethylestern **28** und anschließende Modifikation zum Sulfonsäureamid **31**. Diese Verbindungsklasse wurde von YONG XU und Mitarbeitern als effizienter Inhibitor der Zellviabilität auf der Prostatakrebs-Zelllinie LnCAP eingesetzt, da es mit dem Bromodomänen-Protein 4 (BRD4) interagiert (Abbildung 7).^{[99],[100]}

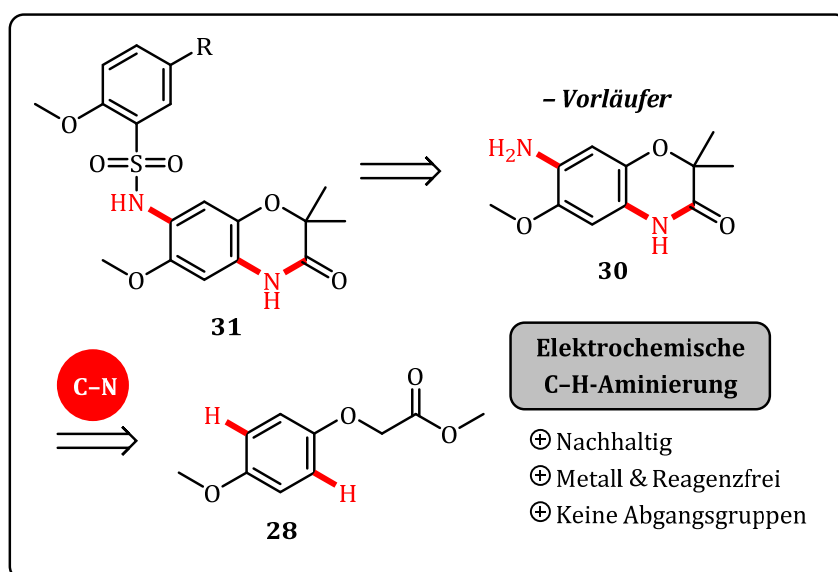
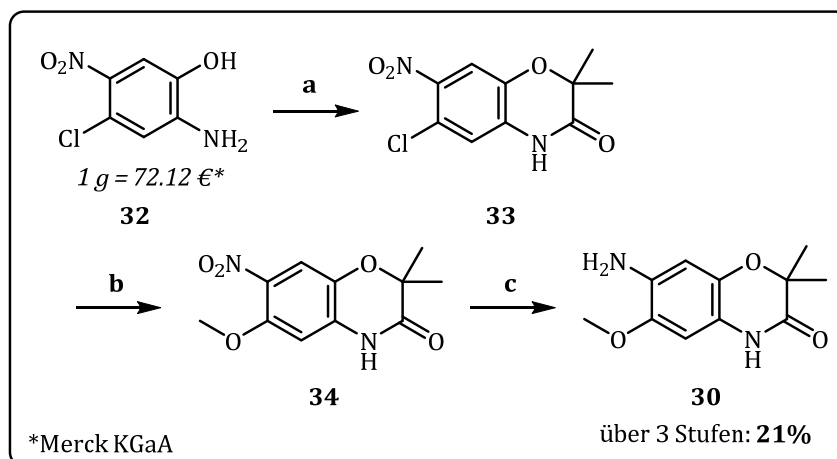


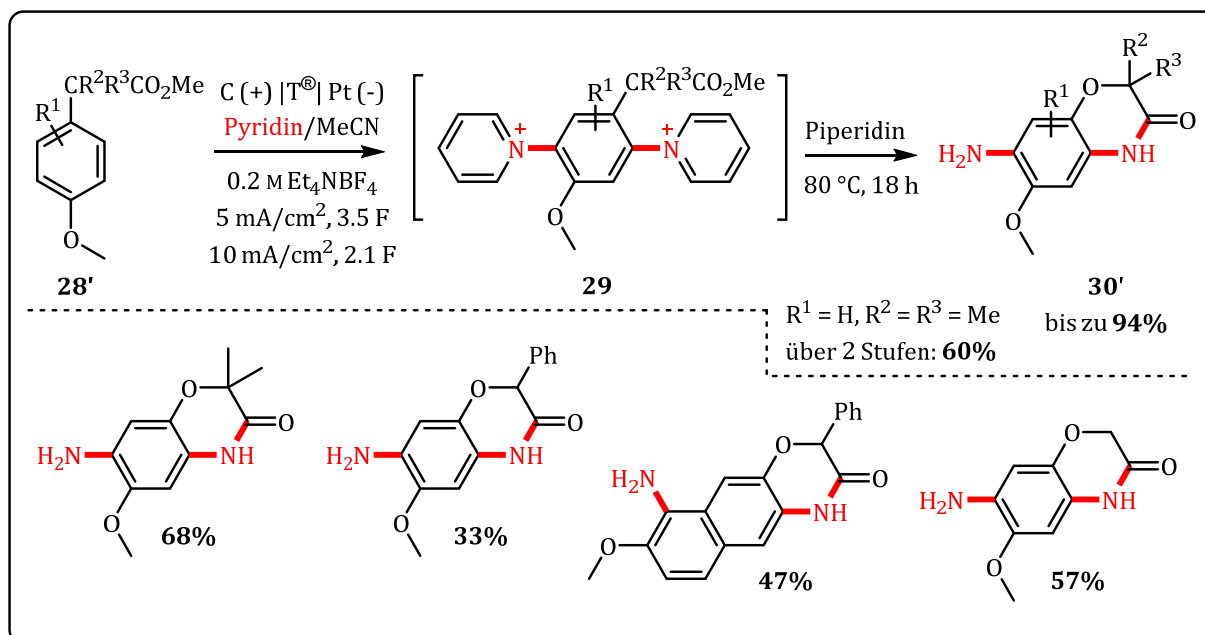
Abbildung 7: Medizinisch relevantes Benzoxazinon **30** als potentielles Krebs-Therapeutikum.

Bei der Herstellung von medizinisch und synthetisch relevanten Vorläufermolekülen ist die Verwendung von toxischen und umweltschädlichen Reagenzien mit geringer Atomökonomie und Energiebilanz nachteilig. Die Erforschung von effizienten und nachhaltigen Synthesen der zugrundeliegenden C-N-Bindungen ist von großem Interesse. Die hier angestrebte elektrochemische Reaktionssequenz verläuft, ausgehend vom 4-Methoxyphenol (500 g = 51,20 €, Merck KGaA), in nur 2 Stufen zur gewünschten Vorläufer-Verbindung **30** (Abbildung 7). Beide Reaktionen finden unter milden Reaktionsbedingungen statt und auf die Verwendung von Übergangsmetall-Katalysatoren kann verzichtet werden. Im Vergleich dazu werden bei der konventionellen Synthesestrategie, ausgehend von 2-Amino-5-chlor-4-nitrophenol **32** (1 g = 72.12 €, Merck KGaA) in 3 Stufen, Übergangsmetalle wie Palladium und Kupfer sowie teilweise komplexe Reaktionsbedingungen verwendet (Schema 15).^[100]



Schema 15: Konventionelle Synthese eines ausgewählten Vorläufermoleküls (a) (i) 2-Brom-2-methylpropansäure Bromid, Et₃N, DCM, 0 °C, 4 h; (ii) K₂CO₃, DMF, 80 °C, 4 h, 50%; (b) CH₃ONa, CuI, DMF, 100 °C, 18 h, 60%; (c) Pd/C, H₂, CH₃OH, RT, 5 h, 70%.

Die Gesamtausbeute der konventionellen Synthese der Vorläuferverbindungen für das oben aufgeführte Derivat **30** beträgt 21%. Die elektrochemische Alternativroute verläuft über eine Gesamtausbeute von 60%. Diese Synthesestrategie ist somit dem klassischen Ansatz in Atomökonomie und Energiebilanz überlegen (Schema 16).



Schema 16: Zweifache elektrochemische C-H Aminierung von Phenoxyessigsäuremethylestern.

Zu diesem Kapitel wurde ein Manuskript veröffentlicht:

Lars Julian Wesenberg, Erika Diehl, Till J. B. Zähringer, Carolin Dörr, Dieter Schollmeyer, Akihiro Shimizu, Jun-ichi Yoshida, Ute A. Hellmich und Siegfried R. Waldvogel, Metal-Free Twofold Electrochemical C-H Amination of Activated Arenes: Application to Medicinally Relevant Precursor Synthesis, Angew. Chemie 2020, manuscript submitted

3.3 Quartäre C(sp²)-N Funktionalitäten als Ladungsträger zur Identifizierung von Metaboliten mittels EC-LC-MS Methoden

Die meisten Wirkstoffe werden von der Leber in Stoffwechselprodukte umgewandelt. Um diese Produkte nach ihren pharmakologischen oder gar toxischen Effekten zu bewerten, ist es von großer Bedeutung, die Metabolite zu identifizieren und Erkenntnisse über ihre Wirkung zu gewinnen.^{[101]-[104]} In Phase-I des Wirkstoffwechsels führen enzymatische Transformationen in der Leber zu einer Oxidation, Hydrolyse oder Reduktion von Xenobiotika. Produkte dieser Umsetzungen weisen eine erhöhte Hydrophilie auf und können über die Niere ausgeschieden werden. Um die Hydrophilie zusätzlich zu steigern, werden reaktive Metabolite mit Glutathion, Sulfate, Aminosäuren oder Acetate konjugiert und unter der Phase-II des Wirkstoffwechsels zusammengefasst.^{[105],[106]} Der Phase-I-Wirkstoffwechsel wird hauptsächlich (zu 75%) von Cytochrom P450 Monooxygenasen (CYP450) durchgeführt.^{[106],[107]} Es wird angenommen, dass CYP450 elektrophile Oxoferryl-Porphyrin-Kation-Radikale verwenden, um *N*-Dealkylierung, *O*-Dealkylierung, aromatische Hydroxylierung, Oxidation von Alkoholen und Aldehyden und Baeyer-Villiger-Oxidation zu katalysieren (Abbildung 8).^{[107]-[109]}

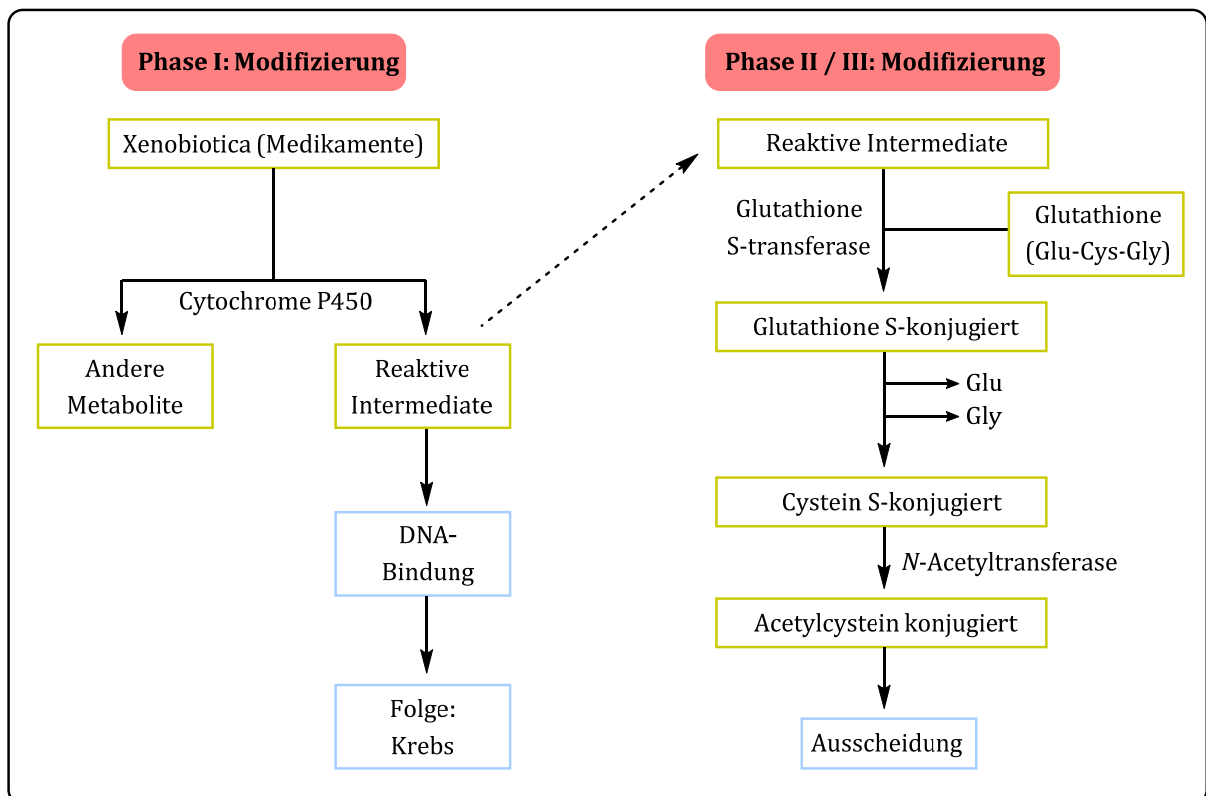


Abbildung 8: Ausgewähltes Beispiel über den Phase-I-Metabolismus und den Phase-II-Metabolismus; Rolle des Cytochrom-P450 (CYP450) und der Glutathion S-Transferase in Biotransformationen, welche in Teilen in der Leber und Niere stattfinden.^[110]

Elektrochemische Methoden haben das Potential, enzymatische Metabolisierungen von CYP450 des Phase-I-Stoffwechsels von Xenobiotika zu simulieren.^{[111]-[115]} Neben der Kosten-Nutzen-Bewertung ist es auch aus ethischen Gründen von großem Interesse, Alternativen zu *in-vivo* Experimenten zu finden.^{[116]-[119]} Darüber hinaus könnte die elektrochemische Synthese, durch die Verwendung von Elektronen als Reagenz, den Abfallstrom im Vergleich zu konventionellen Methoden deutlich verringern und somit eine nachhaltige und gleichzeitig effiziente Alternative darstellen.^{[120],[121]} Mithilfe von sogenannten „trapping agents“ können reaktive Intermediate abgefangen, angereichert und im Folgeschritt analysiert werden. Die daraus resultierenden Erkenntnisse helfen bei der Einstufung der Toxizität von Metaboliten und ferner im Bereich der Medikamentenentwicklung.^{[122]-[124]} Reaktive Zentren in Xenobiotika können so identifiziert und durch geeignete Derivatisierung hinsichtlich ihrer Verstoffwechslung modifiziert werden.^{[124],[125]}

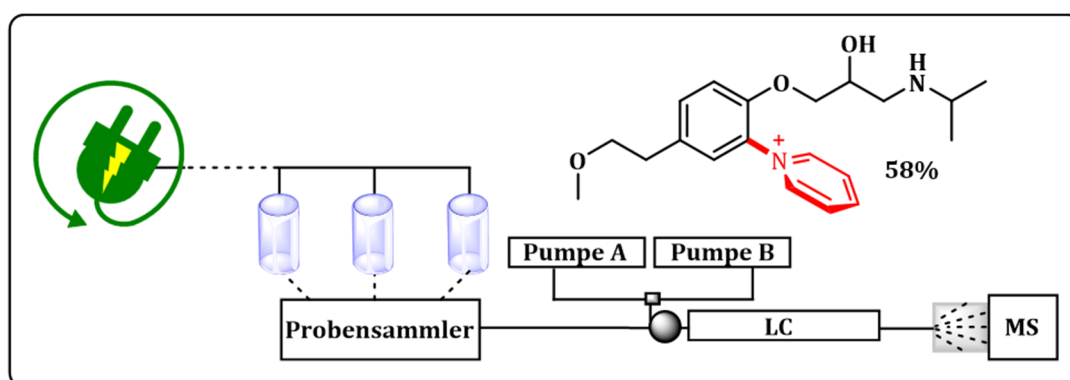


Abbildung 9: Elektrochemische Darstellung eines „charged-tag“ um reaktive Intermediate abzufangen, anzureichern und zu detektieren.

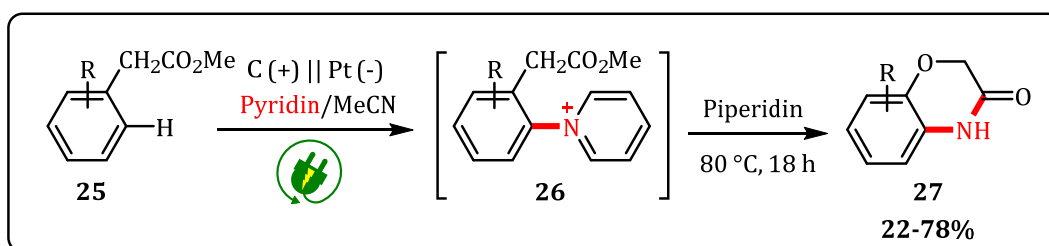
Metoprolol wurde für den Grundsatzbeweis „*proof-of-principle*“ gewählt. Dieses Medikament kann als Beta-Adrenozeptor-Antagonist fungieren und wird hauptsächlich bei der Behandlung von arteriellem Bluthochdruck,^[126] Herzinsuffizienz^[127] und Herzinfarkt^[128] eingesetzt. Darüber hinaus wurde in der Vergangenheit der Metoprolol-Metabolismus schon ausgiebig untersucht.^{[129]-[132]}

Zu diesem Kapitel wurde ein Manuskript veröffentlicht:

Alexandra Gutmann, Lars Julian Wesenberg, Nadine Peez, Siegfried R. Waldvogel, Thorsten Hoffmann, Charged tags for the Identification of Oxidative Drug Metabolites Based on Electrochemistry and Mass Spectrometry (EC-MS) ChemistryOpen 2020, 9, 568–572.

4 Zusammenfassung

Die Aufgabe dieser Arbeit war es nachhaltige elektrochemische Synthesen von medizinisch-relevanten C–N Funktionalitäten aufzubauen. Initial lag der Fokus auf der methodischen Ausarbeitung einer elektrochemischen Synthese von 1,4-Benzoxazin-3-onen. Der zugrundeliegende Heterozyklus hat in den letzten Jahren viel Aufmerksamkeit, bedingt durch eine potentielle pharmakologische Wirkung, erfahren und ist grundlegender Baustein in diversen medizinischen Anwendungsfeldern. Die elektrochemische Synthese von C–N-Funktionalitäten basiert auf der von YOSHIDA und Mitarbeitern ausgearbeiteten elektrochemischen C–H-Aminierungsmethode. Die intermediär generierten Pyridinium Salze werden in einem anschließenden nicht-elektrochemischen Syntheseschritt zum gewünschten freien aromatischen primären Amin umgesetzt. Bei der Synthese von Benzoxazinonen wurde ein aktivierter Phenoxyessigsäuremethylester **25** eingesetzt. Die Freisetzung des Amins bewirkte eine direkte Kondensationsreaktion mit dem benachbarten Ester zu einem zyklischen Amid **27** (Schema 17).

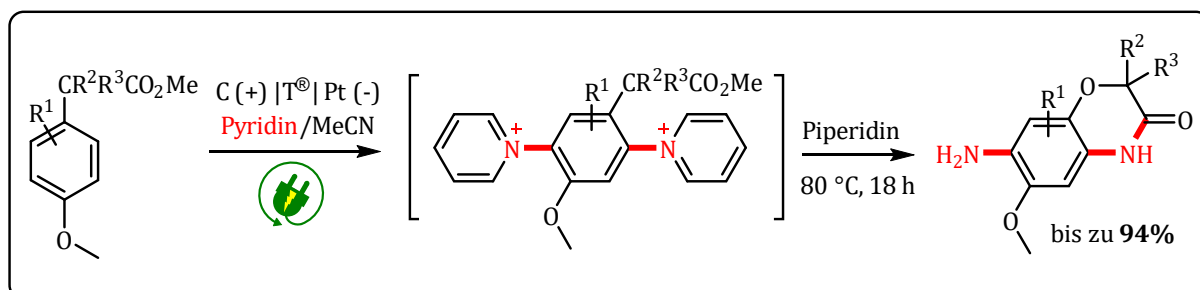


Schema 17: Elektrochemische C–H-Aminierung von Phenoxyessigsäuremethylestern.

So konnten erfolgreich elektronenreiche Aromaten in medizinisch-relevante Vorläuferverbindungen überführt werden. In dieser potenten Methodologie wurden diverse funktionelle Gruppen wie Fluor, Chlor, Brom und Iod Substituenten toleriert und Ausbeuten von bis zu 78% erzielt.

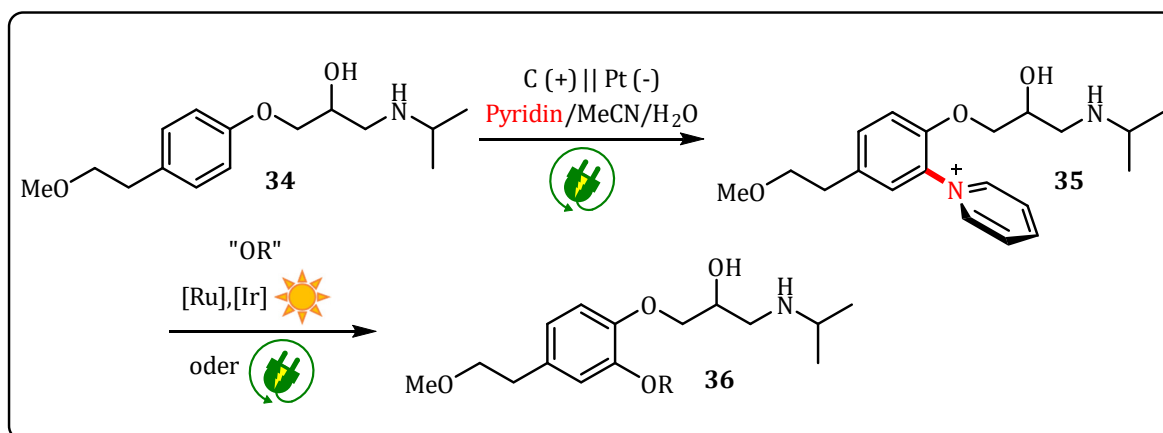
Basierend auf diesen Ergebnissen wurde in einem weiteren Projekt eine zweifache elektrochemische C–H-Aminierung von Methoxy-substituierten Phenoxyessigsäuremethylestern **28** angestrebt. Mithilfe von elektroanalytischen Methoden und mechanistischen Untersuchungen konnte gezeigt werden, dass dieser elektronenreiche Strukturtyp womöglich für den Aufbau von Bispyridinium-Intermediate **29** geeignet ist. Durch die zweifache elektrochemische C–H-Aminierung konnten so erfolgreich ein zyklisches Amid und ein freies aromatisches primäres Amin **30** in einer Eintopf-Synthese

eingebaut werden. Durch anschließende Umsetzung zum Sulfonsäureamid **31** wurde diese Verbindungsklasse als potentieller Inhibitor der Zellviabilität auf der Prostatakrebs-Zelllinie LnCAP untersucht (Schema 18, Manuskriptverweis unter Kapitel 3.2).



Schema 18: Zweifache elektrochemische C-H Aminierung von aktivierten Phenoxyessigsäuremethylestern.

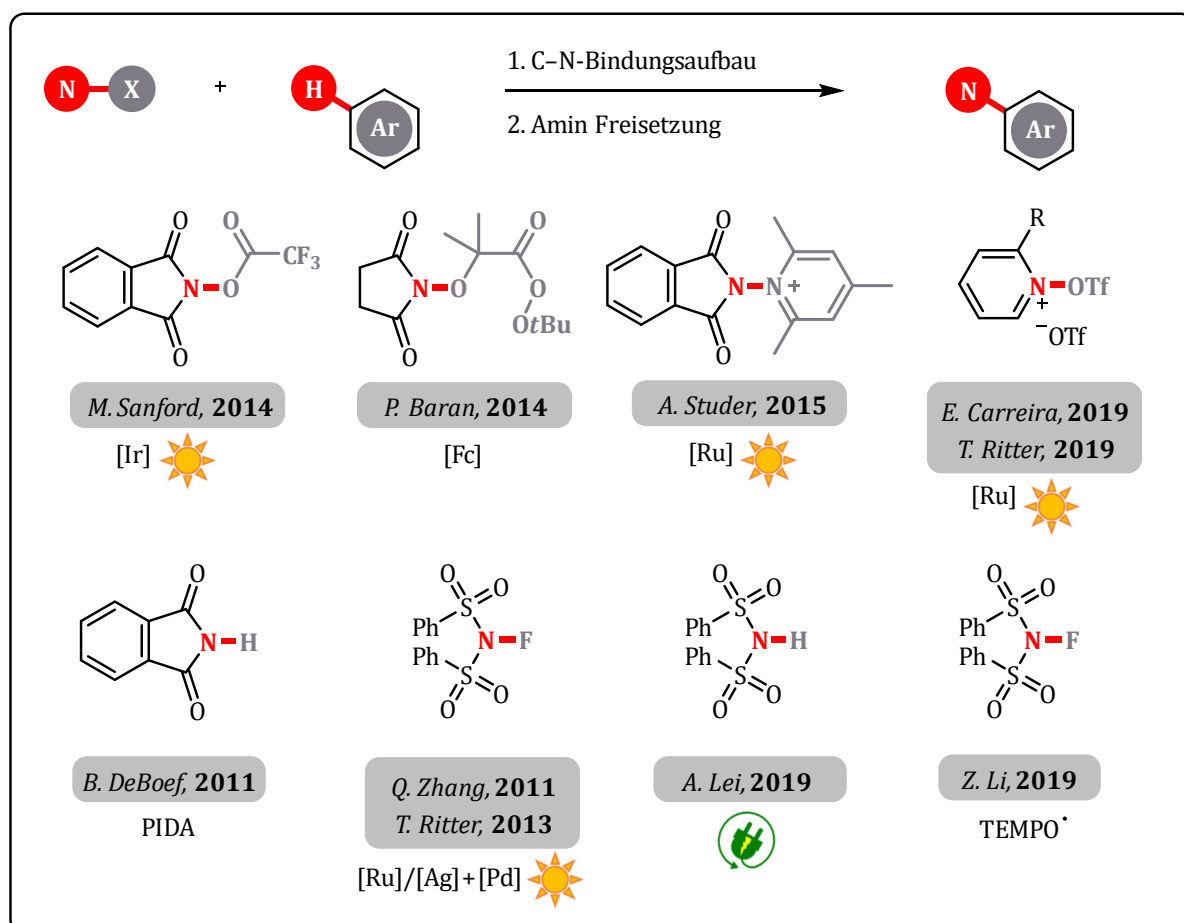
Elektrochemisch generierte Pyridinium-Salze **34** wurden in einem weiteren Projekt als quartäre C(sp²)-N-Funktionalitäten in Form von „charged-tags“ für die Analyse von Metoprolol-Metaboliten **36** verwendet. Mithilfe von EC-LC-MS gekoppelten Methoden war es möglich elektrochemisch oxidierte Metoprolol-Intermediate mittels Pyridin abzufangen, anzureichern und zu detektieren. Diese Studie ermöglichte die Synthese von C(sp²)-N-Funktionalitäten an Metoprolol und zeigte eine bevorzugte Ausbildung der Pyridinium-Gruppe an der *ortho*-Position des Phenoxyethers von Metoprolol **35**. Nebenreaktionen wie Dealkylierungen und Oxidation der Amin- und/oder der Alkoholfunktionalität konnten unterdrückt werden. Darüber hinaus ermöglicht die Pyridinium-Substitution, das als redox-aktives Gruppentransfer-Reagenz fungieren kann, potentiell die Einführung von Sauerstoff-Nukleophilen (Schema 19).



Schema 19: Elektrochemische Synthese von C(sp²)-N-Funktionalitäten an Metoprolol; Pyridinium-Salz als redox-aktive Gruppentransfer-Reagenz in einem weiteren Syntheseschritt zur Einführung von Sauerstoff-Nukleophilen

5 Ausblick

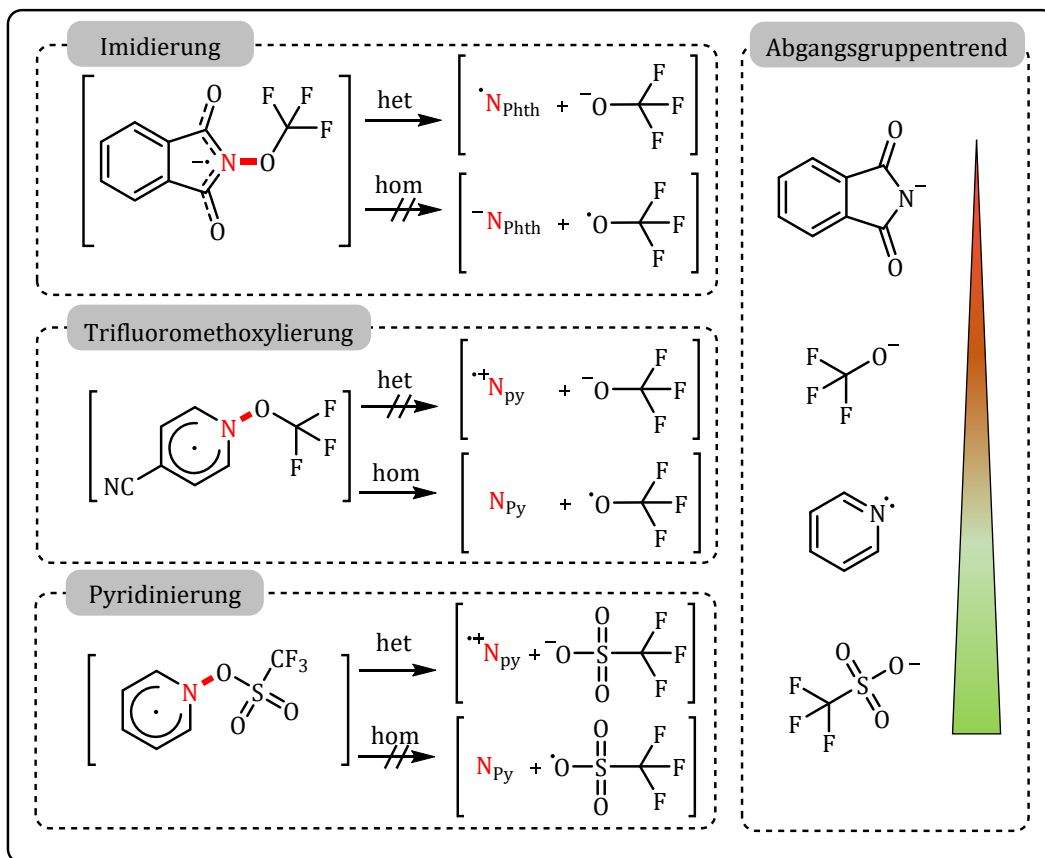
Übergangsmetall-katalysierte und teils photochemische Reaktionen haben bewiesen, dass die Verwendung von Stickstoffquellen wie Phthalimid, Succinimid, Sulfonimide oder Pyridinium-Salze mit Abgangsgruppen mit Abgangsgruppen potente Ammoniak Surrogate darstellen (Schema 20).



Schema 20: Inspiration für alternative Syntheserouten für den Aufbau von C-N-Funktionalitäten; Fc = Ferrocen, PIDA = Diacetyoxydibenzol, TEMPO = 2,2,6,6-Tetramethylpiperidinyloxy.^{[133]-[142]}

Der angeregte Photoredox-Katalysator fungiert als Reduktionsmittel und überträgt ein Elektron („single-electron-transfer“ = SET) auf die Stickstoffverbindung, wodurch intermediär ein elektronisch übersättigter Zustand geschaffen wird. Die Reaktivität der Stickstoffquelle wird durch die Verwendung von Abgangsgruppen gezielt adressiert. Nach dem SET muss die Bindung zwischen Stickstoff und Nukleofug gespalten werden. TOGNI und CARREIRA haben untersucht, ob es zu einer heterolytischen oder homolytischen Spaltung der Bindungselektronen kommt. Die Abgangsgruppen-Tendenz und die

Stabilisierung der Ladung sind entscheidende Einflussgrößen bei diesem Spaltungsprozess (Schema 21).^{[143]-[145]}



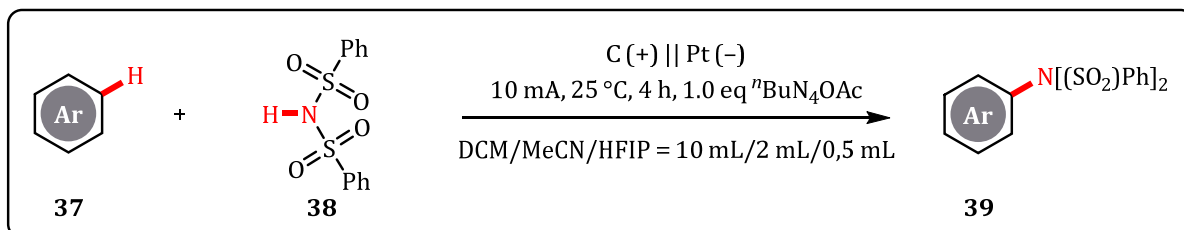
Schema 21: Einfluss der Abgangsgruppe auf die heterolytische (het)/homolytische (hom) Spaltung der N-O-Bindung nach einem SET in einer photokatalytischen Reaktion.^{[143]-[145]}

Anstelle von Photoredox-Katalysatoren, die als SET-Reagenzien fungieren, könnten elektrochemische Methoden eine vielversprechende Alternative für die reduktive C-H-Imidierung bzw. Pyridinierung darstellen.

Vorarbeiten auf dem Gebiet der oxidativen C-H-Imidierung von Naphthalin mit einer elektrochemisch generierten hypervalenten I^{III}-Spezies wurden von S. MÖHLE angefertigt. Angelehnt an die Synthese von R. FRANCKE (Kapitel 1.4) konnte so mit Iodbenzol in einem „*ex-cell*“ Prozess 1,4-Benzoxazin-3-on mit Naphthalin gekuppelt werden. Allerdings konnte diese Methodologie nicht auf die oxidative Kupplung mit Phthalimid übertragen werden. Unsubstituierte Iodbenzole neigen nach der Oxidation zur Dimerisierung, wodurch diese nicht mehr als Oxidationsmittel für den Aufbau der C-N-Funktionalität zur Verfügung stehen.^[146]

2019 beobachtete A. LEI bei der Verwendung von Phenylsulfonsäureimid **38** in einem Elektrolytssystem bestehend aus *n*Bu₄NOAc als Leitsalz in einem DCM/ACN/HFIP-

Gemisch die Ausbildung eines $N_{\text{Imid}}\text{-H-Acetat}$ Komplexes, wodurch die Oxidation zum Imidyl-Radikal begünstigt wird. Die anschließende radikalische Addition an ein aromatisches Kohlenstoffzentrum **37** lieferte die neue C-N-Funktionalität **39**. Die Verwendung einer schwachen und nicht-nukleophilen Base als Gegenion im Leitsalz scheint essentiell für diese elektrochemische C-H-Imidierung zu sein (Schema 22).^[134]



Schema 22: Elektrochemische C-H-Imidierung von aromatischen Systemen **37 nach A. LEI.**

Zukünftige Synthesestrategien könnten diese Überlegungen auf Phthalimid übertragen und Leitsalz-Anionen verwenden, die ähnliche Eigenschaften wie Acetat aufweisen. Als vielversprechende Kandidaten könnten sich Carbonate oder Salze der schwefel- oder phosphorhaltigen Oxosäuren (z. B. Phosphate, Phosphonate, Sulfate, Sulfonate, etc.) herausstellen. Diese Verbindungen verteilen ihre negative Ladung ähnlich wie Acetat in der Sauerstoff-Peripherie des Anionmoleküls und damit könnten diese Salze als schwache und nicht-nukleophile Basen fungieren. Darüber hinaus könnten Additive wie nicht-nukleophile Stickstoffbasen (z.B. Hünig-Base) die Oxidation der Imidverbindung begünstigen.

6 Literaturverzeichnis

- [1] Bundesministerium für Wirtschaft und Energie (BMWi), *Schlaglichter der Wirtschaftspolitik* **2019**; Monatsbericht: Oktober.
- [2] F. Ausfelder, C. Beilmann, M. Bertau, S. Bräuninger, A. Heinzl, R. Hoer, W. Koch, F. Mahlendorf, A. Metzethin, M. Peuckert et al., *Chem. Ing. Tech.* **2015**, *87*, 17–89.
- [3] A. Sternberg, A. Bardow, *Energy Environ. Sci.* **2015**, *8*, 389–400.
- [4] H.-M. Henning, A. Palzer, *Renewable and Sustainable Energy Rev.* **2014**, *30*, 1003–1018.
- [5] A. Volta, *Phil. Trans. R. Soc. Lon* **1800**, *90*, 403–431.
- [6] M. Faraday, *Phil. Trans. R. Soc. Lon* **1834**, *124*, 77–122.
- [7] H. Kolbe, *Ann. Chem. Pharm.* **1849**, *69*, 257–294.
- [8] H. Kolbe, *Q. J. Chem. Soc.* **1850**, *2*, 157–184.
- [9] Y. Kado in *Encyclopedia of Applied Electrochemistry* (Eds.: G. Kreysa, K.-i. Ota, R. F. Savinell), Springer New York, New York, NY, **2014**, 153–154.
- [10] T. Fuchigami, M. Atobe, S. Inagi, *Fundamentals and applications of organic electrochemistry. Synthesis, materials, devices*, John Wiley & Sons Inc, Chichester, West Sussex, **2015**.
- [11] D. E. Blanco, A. Z. Dookhith, M. A. Modestino, *React. Chem. Eng.* **2019**, *4*, 8–16.
- [12] M. M. Baizer, *J. Electrochem. Soc.* **1964**, *111*, 215.
- [13] J. Schwarz, B. Beloff, E. Beaver, *Chem. Eng. Prog.* **2002**, *98*, 58–63.
- [14] H. Lund, O. Hammerich (Eds.) *Organic electrochemistry*, Marcel Dekker, New York, NY, **2001**.
- [15] F. Tang, C. Chen, K. Moeller, *Synthesis* **2007**, 3411–3420.
- [16] L. Meites, P. Zuman, H. W. Nurnberg, *Pure Appl. Chem.* **1985**, *57*, 1491–1505.
- [17] P. T. Anastas, J. C. Warner, *Green chemistry. Theory and practice*, 1. Aufl., Oxford Univ. Press, Oxford, **2000**.
- [18] J. A. Linthorst, *Found. Chem.* **2010**, *12*, 55–68.
- [19] B. A. Frontana-Uribe, R. D. Little, J. G. Ibanez, A. Palma, R. Vasquez-Medrano, *Green Chem.* **2010**, *12*, 2099.
- [20] C. Kingston, M. D. Palkowitz, Y. Takahira, J. C. Vantourout, B. K. Peters, Y. Kawamata, P. S. Baran, *Acc. Chem. Res.* **2019**.
- [21] M. Yan, Y. Kawamata, P. S. Baran, *Chem. Rev.* **2017**, *117*, 13230–13319.

- [22] S. R. Waldvogel, B. Janza, *Angew. Chem.* **2014**, *126*, 7248–7249; *Angew. Chem. Int. Ed.* **2014**, *53*, 7122–7123.
- [23] J. L. Röckl, D. Pollok, R. Franke, S. R. Waldvogel, *Acc. Chem. Res.* **2020**, *53*, 45–61.
- [24] S. Möhle, M. Zirbes, E. Rodrigo, T. Gieshoff, A. Wiebe, S. R. Waldvogel, *Angew. Chem. Int. Ed.* **2018**, *57*, 6018–6041; *Angew. Chem.* **2018**, *130*, 6124–6149.
- [25] A. Wiebe, T. Gieshoff, S. Möhle, E. Rodrigo, M. Zirbes, S. R. Waldvogel, *Angew. Chem. Int. Ed.* **2018**, *57*, 5594–5619; *Angew. Chem.* **2018**, *130*, 5694–5721.
- [26] J.-i. Yoshida, S. Suga, S. Suzuki, N. Kinomura, A. Yamamoto, K. Fujiwara, *J. Am. Chem. Soc.* **1999**, *121*, 9546–9549.
- [27] J.-i. Yoshida, S. Suga, *Chem. Eur. J.* **2002**, *8*, 2650.
- [28] T. Morofuji, A. Shimizu, J.-i. Yoshida, *J. Am. Chem. Soc.* **2013**, *135*, 5000–5003.
- [29] B. K. Peters, K. X. Rodriguez, S. H. Reisberg, S. B. Beil, D. P. Hickey, Y. Kawamata, M. Collins, J. Starr, L. Chen, S. Udyavara et al., *Science* **2019**, *363*, 838–845.
- [30] N. Fu, G. S. Sauer, A. Saha, A. Loo, S. Lin, *Science* **2017**, *357*, 575–579.
- [31] Y. Imada, J. L. Röckl, A. Wiebe, T. Gieshoff, D. Schollmeyer, K. Chiba, R. Franke, S. R. Waldvogel, *Angew. Chem. Int. Ed.* **2018**, *57*, 12136–12140; *Angew. Chem.* **2018**, *130*, 12312–12317.
- [32] A. Kirste, B. Elsler, G. Schnakenburg, S. R. Waldvogel, *J. Am. Chem. Soc.* **2012**, *134*, 3571–3576.
- [33] L. Schulz, M. Enders, B. Elsler, D. Schollmeyer, K. M. Dyballa, R. Franke, S. R. Waldvogel, *Angew. Chem.* **2017**, *129*, 4955–4959; *Angew. Chem. Int. Ed.* **2017**, *56*, 4877–4881.
- [34] J.-i. Yoshida, K. Kataoka, R. Horcajada, A. Nagaki, *Chem. Rev.* **2008**, *108*, 2265–2299.
- [35] O. Onomura, *Heterocycles* **2012**, *85*, 2111.
- [36] A. M. Jones, C. E. Banks, *Beilstein J. Org. Chem.* **2014**, *10*, 3056–3072.
- [37] I. M. Malkowsky, U. Griesbach, H. Pütter, S. R. Waldvogel, *Eur. J. Org. Chem.* **2006**, *2006*, 4569–4572.
- [38] A. Kirste, M. Nieger, I. M. Malkowsky, F. Stecker, A. Fischer, S. R. Waldvogel, *Chem. Eur. J.* **2009**, *15*, 2273–2277.
- [39] B. Elsler, D. Schollmeyer, K. M. Dyballa, R. Franke, S. R. Waldvogel, *Angew. Chem. Int. Ed.* **2014**, *53*, 5210–5213; *Angew. Chem.* **2014**, *126*, 5079.
- [40] A. Wiebe, D. Schollmeyer, K. M. Dyballa, R. Franke, S. R. Waldvogel, *Angew. Chem. Int. Ed.* **2016**, *55*, 11801–11805.

-
- [41] A. Kirste, G. Schnakenburg, F. Stecker, A. Fischer, S. R. Waldvogel, *Angew. Chem. Int. Ed.* **2010**, *49*, 971–975; *Angew. Chem.* **2010**, *122*, 983–987.
- [42] L. Schulz, R. Franke, S. R. Waldvogel, *ChemElectroChem.* **2018**, *5*, 2069–2072.
- [43] K. C. Nicolaou, A. Li, D. J. Edmonds, *Angew. Chem. Int. Ed.* **2006**, *45*, 7086–7090; *Angew. Chem.* **2006**, *118*, 7244–7248.
- [44] A. L. Bowie, C. C. Hughes, D. Trauner, *Org. Lett.* **2005**, *7*, 5207–5209.
- [45] T. Fukuyama, L. Xu, S. Goto, *J. Am. Chem. Soc.* **1992**, *114*, 383–385.
- [46] A. Wissner, D. M. Berger, D. H. Boschelli, M. B. Floyd, L. M. Greenberger, B. C. Gruber, B. D. Johnson, N. Mamuya, R. Nilakantan, M. F. Reich et al., *J. Med. Chem.* **2000**, *43*, 3244–3256.
- [47] A. W. Czarnik, *Acc. Chem. Res.* **1996**, *29*, 112–113.
- [48] J. A. Bikker, N. Brooijmans, A. Wissner, T. S. Mansour, *J. Med. Chem.* **2009**, *52*, 1493–1509.
- [49] R. Hili, A. K. Yudin, *Nat. Chem. Biol.* **2006**, *2*, 284–287.
- [50] W. H. Perkin, *Q. J. Chem. Soc.* **1862**, *14*, 230–255.
- [51] M. M. Sousa, M. J. Melo, A. J. Parola, P. J. T. Morris, H. S. Rzepa, J. S. S. de Melo, *Chem. Eur. J.* **2008**, *14*, 8507–8513.
- [52] O. Meth-Cohn, M. Smith, *J. Chem. Soc., Perkin Trans. 1* **1994**, *5*.
- [53] A. Yella, H.-W. Lee, H. N. Tsao, C. Yi, A. K. Chandiran, M. K. Nazeeruddin, E. W.-G. Diao, C.-Y. Yeh, S. M. Zakeeruddin, M. Grätzel, *Science* **2011**, *334*, 629–634.
- [54] H. Letheby, *J. Chem. Soc.* **1862**, *15*, 161–163.
- [55] A. G. Green, A. E. Woodhead, *J. Chem. Soc., Trans.* **1910**, *97*, 2388–2403.
- [56] A. D. Schlüter, J. P. Rabe, *Angew. Chem.* **2000**, *112*, 860–880; *Angew. Chem. Int. Ed.* **2000**, *39*, 864–883.
- [57] H.-J. Arpe, K. Weissemel, *Industrielle organische Chemie. Bedeutende Vor- und Zwischenprodukte*, 6. Aufl., Wiley-VCH, Weinheim, **2007**.
- [58] P. Ruiz-Castillo, S. L. Buchwald, *Chem. Rev.* **2016**, *116*, 12564–12649.
- [59] L. Legnani, B. Bhawal, B. Morandi, *Synthesis* **2017**, *49*, 776–789.
- [60] G. A. Olah, R. Malhotra, S. C. Narang, *Nitration. Methods and Mechanisms*, Wiley, New York, **1989**.
- [61] R. S. Downing, P. J. Kunkeler, H. van Bekkum, *Catal. Today* **1997**, *37*, 121–136.
- [62] J. F. Hartwig, *Acc. Chem. Res.* **1998**, *31*, 852–860.

- [63] J. P. Wolfe, S. Wagaw, J.-F. Marcoux, S. L. Buchwald, *Acc. Chem. Res.* **1998**, *31*, 805–818.
- [64] P. Y.S. Lam, G. Vincent, C. G. Clark, S. Deudon, P. K. Jadhav, *Tetrahedron Lett.* **2001**, *42*, 3415–3418.
- [65] D. M.T. Chan, K. L. Monaco, R.-P. Wang, M. P. Winters, *Tetrahedron Lett.* **1998**, *39*, 2933–2936.
- [66] R. Dorel, C. P. Grugel, A. M. Haydl, *Angew. Chem. Int. Ed.* **2019**, *58*, 17118–17129; *Angew. Chem.* **2019**, *131*, 17276–17287.
- [67] D.-Y. Lee, J. F. Hartwig, *Org. Lett.* **2005**, *7*, 1169–1172.
- [68] T. Ikawa, T. E. Barder, M. R. Biscoe, S. L. Buchwald, *J. Am. Chem. Soc.* **2007**, *129*, 13001–13007.
- [69] J. P. Wolfe, J. Åhman, J. P. Sadighi, R. A. Singer, S. L. Buchwald, *Tetrahedron Lett.* **1997**, *38*, 6367–6370.
- [70] G. A. Grasa, M. S. Viciu, J. Huang, S. P. Nolan, *Am. J. Org. Chem.* **2001**, *66*, 7729–7737.
- [71] Q. Shen, J. F. Hartwig, *J. Am. Chem. Soc.* **2006**, *128*, 10028–10029.
- [72] J. Kim, S. Chang, *Chem. Commun.* **2008**, 3052–3054.
- [73] R. N. Keller, P. A. S. Smith, *J. Am. Chem. Soc.* **1944**, *66*, 1122–1124.
- [74] F. Sommer, O. F. Schulz, M. Nassau, *Z. Anorg. Allg. Chem.* **1925**, *147*, 142–155.
- [75] L. Legnani, G. Prina Cerai, B. Morandi, *ACS Catal.* **2016**, *6*, 8162–8165.
- [76] P. Kovacic, R. P. Bennett, *J. Am. Chem. Soc.* **1961**, *83*, 221–224.
- [77] L. Legnani, G. Prina-Cerai, T. Delcaillau, S. Willems, B. Morandi, *Science* **2018**, *362*, 434–439.
- [78] J. Haggin, *Chem. Eng. News* **1993**, *71*, 23–27.
- [79] J. I. van der Vlugt, *Chem. Soc. Rev.* **2010**, *39*, 2302–2322.
- [80] T. E. Müller, m. Beller, *Chem. Rev.* **1998**, *98*, 675–704.
- [81] A. Werner, *Z. Anorg. Chem.* **1893**, *3*, 267–330.
- [82] D. F. McMillen, D. M. Golden, *Annu. Rev. Phys. Chem.* **1982**, *33*, 493–532.
- [83] T. Morofuji, A. Shimizu, J.-i. Yoshida, *Chem. - Eur. J.* **2015**, *21*, 3211–3214.
- [84] S. Möhle, S. Herold, F. Richter, H. Nefzger, S. R. Waldvogel, *ChemElectroChem.* **2017**, *4*, 2196–2210.
- [85] H.-W. Engels, H.-G. Pirkl, R. Albers, R. W. Albach, J. Krause, A. Hoffmann, H. Casselmann, J. Dormish, *Angew. Chem.* **2013**, *125*, 9596–9616; *Angew. Chem. Int. Ed.* **2013**, *52*, 9422–9441.

-
- [86] O. Bayer, *Angew. Chem.* **1947**, *59*, 257–272.
- [87] J. Laue, C. Steffens, J. Krause, S. Wershofen, W. Kilian, M. Seekamp, M. Ruhland, US20150246873 A1, **2015**.
- [88] S. Reiter, H. Nefzger, J. Krause, WO 2013/000912, **2012**.
- [89] T. Broese, R. Francke, *Org. Lett.* **2016**, *18*, 5896–5899.
- [90] M. R. Freitas, Matias, Stella V B G, R. L. G. Macedo, M. P. Freitas, N. Venturin, *J. Agric. Food Chem.* **2013**, *61*, 8499–8503.
- [91] F. A. Macías, D. Marín, A. Oliveros-Bastidas, J. M. G. Molinillo, *Nat. Prod. Rep.* **2009**, *26*, 478.
- [92] F. A. Macias, D. Marin, A. Oliveros-Bastidas, D. Castellano, A. M. Simonet, J. M. G. Molinillo, *J. Agric. Food Chem.* **2006**, *54*, 1040–1048.
- [93] H. M. Niemeyer, *Phytochemistry* **1988**, *27*, 3349–3358.
- [94] X.-F. Wu, m. Beller, *Heterocycles from double-functionalized arenes. Transition metal catalyzed coupling reactions*, Royal Society of Chemistry, Cambridge, **2015**.
- [95] R. Frechette, M. Beach, WO97/28167, **1996**.
- [96] M. Hori, W. Ikuo, H. Ohtaka, H. Kengo, M. Joji, M. Tominori, Y. Takeshi, T. Hisayoshi, US5597820, **1997**.
- [97] T. Kawakita, T. Kuroita, M. Yasumoto, M. Sano, K. Inaba, T. Fukuda, T. Tahara, *Chem. Pharm. Bull.* **1992**, *40*, 624–630.
- [98] L. J. Wesenberg, S. Herold, A. Shimizu, J.-i. Yoshida, S. R. Waldvogel, *Chem. - Eur. J.* **2017**, *23*, 12096–12099.
- [99] X. Xue, Y. Zhang, C. Wang, M. Zhang, Q. Xiang, J. Wang, A. Wang, C. Li, C. Zhang, L. Zou et al., *Eur. J. Med. Chem.* **2018**, *152*, 542–559.
- [100] Q. Xiang, Y. Zhang, J. Li, X. Xue, C. Wang, M. Song, C. Zhang, R. Wang, C. Li, C. Wu et al., *ACS Med. Chem. Lett.* **2018**, *9*, 262–267.
- [101] A. F. Stepan, D. P. Walker, J. Bauman, D. A. Price, T. A. Baillie, A. S. Kalgutkar, M. D. Aleo, *Chem. Res. Toxicol.* **2011**, *24*, 1345–1410.
- [102] S. D. Krämer, B. Testa, *Chem. Biodiversity* **2009**, *6*, 1477–660.
- [103] B. Testa, S. D. Krämer, *Chem. Biodiversity* **2006**, *3*, 1053–1101.
- [104] J. Genovino, D. Sames, L. G. Hamann, B. B. Touré, *Angew. Chem. Int. Ed.* **2016**, *55*, 14218–14238; *Angew. Chem.* **2016**, *128*, 14430–14451.
- [105] S. Sozzani, D. Bosisio, A. Mantovani, P. Ghezzi, *Eur. J. Immunol.* **2005**, *35*, 3095–3098.

- [106]K. Schroer, M. Kittelmann, S. Lütz, *Biotechnol. Bioeng.* **2010**, *106*, 699–706.
- [107]R. Bernhardt, *J. Biotechnol.* **2006**, *124*, 128–145.
- [108]A. Chefson, K. Auclair, *Mol. BioSyst.* **2006**, *2*, 462–469.
- [109]F. P. Guengerich, *AAPS J.* **2006**, *8*, E101-11.
- [110]T. Simic, A. Savic-Radojevic, M. Pljesa-Ercegovac, M. Matic, J. Mimic-Oka, *Nat. Rev. Urol.* **2009**, *6*, 281–289.
- [111]K. G. Madsen, J. Olsen, C. Skonberg, S. H. Hansen, U. Jurva, *Chem. Res. Toxicol.* **2007**, *20*, 821–831.
- [112]R. Stalder, G. P. Roth, *ACS Med. Chem. Lett.* **2013**, *4*, 1119–1123.
- [113]K. Pelivan, L. Frensemeier, U. Karst, G. Koellensperger, B. Bielec, S. Hager, P. Heffeter, B. K. Keppler, C. R. Kowol, *Analyst* **2017**, *142*, 3165–3176.
- [114]T. Wigger, A. Seidel, U. Karst, *Chemosphere* **2017**, *176*, 202–211.
- [115]U. Jurva, H. V. Wikstrom, L. Weidolf, A. P. Bruins, *Rapid Commun. Mass Spectrom.* **2003**, *17*, 800–810.
- [116]H. Zhang, D. Zhang, W. Li, M. Yao, C. D'Arienzo, Y.-X. Li, W. R. Ewing, Z. Gu, Y. Zhu, N. Murugesan et al., *Drug Metab. Dispos.* **2007**, *35*, 795–805.
- [117]*Safety Testing of Drug Metabolites. Guidance for Industry*; U.S. Department of Health and Human Services, zu finden unter:
<https://www.fda.gov/media/72279/download>, **2016**.
- [118]*Guidance for Industry. S6 Preclinical Safety Evaluation of Biotechnology-Derived Pharmaceuticals*; U.S. Department of Health and Human Services, zu finden unter:
<https://www.fda.gov/media/72028/download>, **1997**.
- [119]D. Wendler, *The Ethics of Clinical Research*; Metaphysics Research Lab, Stanford University, zu finden unter:
<https://plato.stanford.edu/archives/win2017/entries/clinical-research/>, **2017**.
- [120]J. Atzrodt, V. Derdau, W. Holla, M. Sandvoss, *Arkivoc* **2011**, *2012*, 257.
- [121]A. Zöllner, D. Buchheit, M. R. Meyer, H. H. Maurer, F. T. Peters, M. Bureik, *Bioanalysis* **2010**, *2*, 1277–1290.
- [122]B. B. Brodie, W. D. Reid, A. K. Cho, G. Sipes, G. Krishna, J. R. Gillette, *Proceedings of the National Academy of Sciences of the United States of America* **1971**, *68*, 160–164.
- [123]E. C. Miller, J. A. Miller, *J. Natl. Cancer Inst.* **1955**, *15*, 1571–1590.
- [124]C. Ionescu, M. R. Caira, *Drug Metabolism*, Springer-Verlag, Berlin/Heidelberg, **2005**.

-
- [125]D. Zhang, M. Zhu, W. G. Humphreys, *Drug metabolism in drug design and development. Basic concepts and practice*, Wiley-Interscience, Hoboken, N.J, **2008**.
- [126]L. Hansson, L. H. Lindholm, T. Ekbom, B. Dahlöf, J. Lanke, B. Scherstén, P.-O. Wester, T. Hedner, U. de Faire, *The Lancet* **1999**, *354*, 1751–1756.
- [127]*The Lancet* **1999**, *353*, 2001–2007.
- [128]*The Lancet* **2005**, *366*, 1622–1632.
- [129]T. Johansson, L. Weidolf, U. Jurva, *Rapid Commun. Mass Spectrom.* **2007**, *21*, 2323–2331.
- [130]J. C. McGourty, J. H. Silas, M. S. Lennard, G. T. Tucker, H. F. Woods, *Br. J. Clin. Pharmacol.* **1985**, *20*, 555–566.
- [131]N. Bodor, P. Buchwald, *AAPS J.* **2005**, *7*, E820-33.
- [132]S. S. Murthy, H.U. Shetty, W. L. Nelson, p. R. Jackson, M. S. Lennard, *Biochem. Pharmacol.* **1990**, *40*, 1637–1644.
- [133]Q. Miao, Z. Shao, C. Shi, L. Ma, F. Wang, R. Fu, H. Gao, Z. Li, *Chem. Commun.* **2019**, *55*, 7331–7334.
- [134]X. Hu, G. Zhang, L. Nie, T. Kong, A. Lei, *Nat. Commun.* **2019**, *10*, 5467.
- [135]G. B. Boursalian, M.-Y. Ngai, K. N. Hojczyk, T. Ritter, *J. Am. Chem. Soc.* **2013**, *135*, 13278–13281.
- [136]K. Sun, Y. Li, T. Xiong, J. Zhang, Q. Zhang, *J. Am. Chem. Soc.* **2011**, *133*, 1694–1697.
- [137]A. A. Kantak, S. Potavathri, R. A. Barham, K. M. Romano, B. DeBoef, *J. Am. Chem. Soc.* **2011**, *133*, 19960–19965.
- [138]W. S. Ham, J. Hillenbrand, J. Jacq, C. Genicot, T. Ritter, *Angew. Chem.* **2019**, *131*, 542–546; *Angew. Chem. Int. Ed.* **2019**, *58*, 532–536.
- [139]S. L. Rössler, B. J. Jelier, P. F. Tripet, A. Shemet, G. Jeschke, A. Togni, E. M. Carreira, *Angew. Chem.* **2019**, *131*, 536–541; *Angew. Chem. Int. Ed.* **2019**, *58*, 526–531.
- [140]T. W. Greulich, C. G. Daniliuc, A. Studer, *Org. Lett.* **2015**, *17*, 254–257.
- [141]K. Foo, E. Sella, I. Thomé, M. D. Eastgate, P. S. Baran, *J. Am. Chem. Soc.* **2014**, *136*, 5279–5282.
- [142]L. J. Allen, P. J. Cabrera, M. Lee, M. S. Sanford, *J. Am. Chem. Soc.* **2014**, *136*, 5607–5610.
- [143]B. J. Jelier, P. F. Tripet, E. Pietrasiak, I. Franzoni, G. Jeschke, A. Togni, *Angew. Chem. Int. Ed.* **2018**, *57*, 13784–13789; *Angew. Chem.* **2018**, *130*, 13980–13985.

[144]A. Togni, S. L. Rössler, B. J. Jelier, E. Magnier, G. Dagousset, E. M. Carreira, *Angew. Chem. Int. Ed.* **2019**; *Angew. Chem.* **2019**.

[145]T. Fuchigami, T. Fujita, *Am. J. Org. Chem.* **1994**, *59*, 7190–7192.

7 Anhang

Inhaltsverzeichnis – Anhang

Seitenzahl im Anhang

Lars Julian Wesenberg, Sebastian Herold, Akihiro Shimizu, Jun-ichi Yoshida, und Siegfried R. Waldvogel <i>Eur. J. Chem.</i> 2017 , <i>23</i> , 12096–12099.	001 – 004
Supporting Information	005 – 047
Lars Julian Wesenberg, Erika Diehl, Till J. B. Zähringer, Dieter Schollmeyer, Akihiro Shimizu, Jun-ichi Yoshida, Ute A. Hellmich und Siegfried R. Waldvogel <i>Angew. Chem.</i> 2020 , manuscript submitted.	048 – 055
Supporting Information	056 – 118
Alexandra Gutmann, Lars Julian Wesenberg, Nadine Peez, Siegfried R. Waldvogel, Thorsten Hoffmann <i>ChemistryOpen</i> 2020 , manuscript accepted.	119 – 123
Supporting Information	124 – 140

C–H Amination | Very Important Paper |

VIP New Approach to 1,4-Benzoxazin-3-ones by Electrochemical C–H Amination

Lars Julian Wesenberg,^[a] Sebastian Herold,^[a, b] Akihiro Shimizu,^[c] Jun-ichi Yoshida,^[c] and Siegfried R. Waldvogel*^[a, b]

Dedicated to Hans J. Schäfer on the occasion of his 80th birthday

Abstract: 1,4-Benzoxazin-3-ones are important structural motifs in natural products and bioactive compounds. Usually, the synthesis of benzoxazinones requires transition-metal catalysts and pre-functionalized substrates such as aryl halides. However, the anodic C–H amination of phenoxy acetates offers a very efficient and sustainable access to these heterocycles. The presented electrochemical protocol can be applied to a broad scope of alkylated substrates. Even *tert*-butyl moieties or halogen substituents are compatible with this versatile method.

The 1,4-benzoxazin-3-one scaffold has been recognized as an important heterocyclic motif in natural products as well as in pharmaceutically active compounds.^[1] Naturally occurring benzoxazin-3-ones, like 2,4-dihydroxy-1,4-benzoxazin-3-one (DIBOA, **1**) and 2,4-dihydroxy-7-methoxy-1,4-benzoxazin-3-one (DIMBOA, **2**) were found in gramineous plants like maize, wheat, rye, and rice (Figure 1).^[2,3] Biosynthesis of DIMBOA (**2**) is accomplished by the hydroxylation of indole derivatives using P450 monooxygenase. Intermediates of this reaction pathway can also be found in tryptophan biosynthesis.^[4] Alternatively, benzoxazinones **3** and **4** are interesting compounds for pharmaceutical applications. The former is an inhibitor of bacterial histidine protein kinase,^[5] whereas the latter is a potential

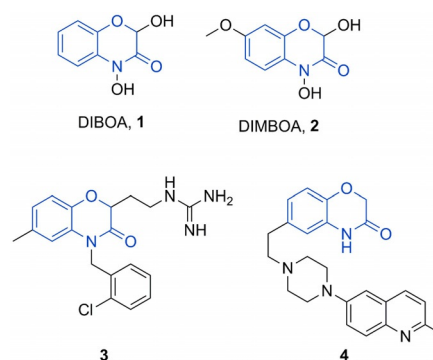


Figure 1. Naturally occurring 1,4-benzoxazin-3-ones DIBOA (**1**) and DIMBOA (**2**) and pharmaceutically relevant compounds **3** and **4** with the benzoxazinone scaffold.

agent for the treatment of anxiety and depression symptoms (Figure 1).^[6,7]

Common synthetic strategies to construct benzoxazin-3-ones employ *ortho*-substituted nitrophenols or halophenols as starting materials.^[2,8] Recently, El Kaïm et al. reported a three-component reaction to access the benzoxazinone scaffold through a Passerini–Smiles rearrangement, followed by hydrogenation and in situ cyclization.^[9] Moreover, Liu and co-workers developed a copper(I)-catalyzed one-pot synthesis of benzoxazinones.^[6] In this approach, *ortho*-halophenols react with α -chloroacetamides in the presence of a metal promoter. However, a disadvantage of such approaches is the need for transition-metal catalysts as well as pre-functionalized substrates, for example, aryl halogenides or nitroaromatic compounds. In particular, nitroaromatic starting materials are sometimes difficult to obtain selectively because nitration usually leads to regioisomeric mixtures.^[10] Purification of such mixtures often is a tedious process. Recently, Yoshida and co-workers reported in a series of accounts a powerful and selective electrochemical C–N bond-formation reactions,^[11–13] including a novel method for the synthesis of benzoxazoles **7** (Scheme 1).^[14]

The phenolic substrates for the electrochemical synthesis of oxazoles **7** were initially modified with a pyrimidine moiety. This promotes an intramolecular electrochemical C–N coupling reaction. The anodic amination proceeds via positively charged Zincke intermediates **6** and **9**, which prevent further anodic degradation, thus increasing the selectivity. The corresponding amino moieties can be liberated in a later step at non-electrolytic conditions.

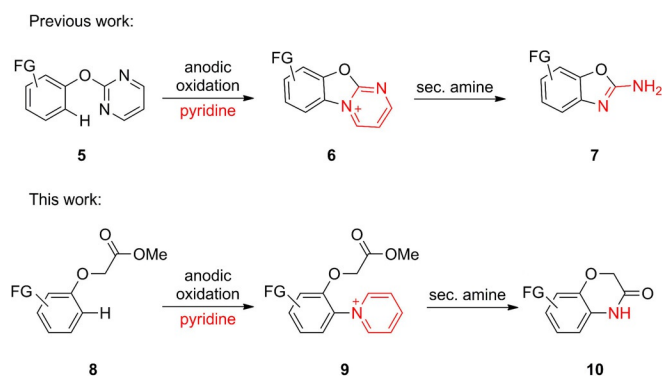
[a] L. J. Wesenberg, Dr. S. Herold, Prof. Dr. S. R. Waldvogel
Institut für Organische Chemie
Johannes Gutenberg Universität Mainz
Duesbergweg 10–14, 55128 Mainz (Germany)
E-mail: waldvogel@uni-mainz.de
Homepage: <http://www.chemie.uni-mainz.de/OC/AK-Waldvogel/>

[b] Dr. S. Herold, Prof. Dr. S. R. Waldvogel
Graduate School Material Science in Mainz
Johannes Gutenberg Universität Mainz
Staudingerweg 9, 55128 Mainz (Germany)

[c] Dr. A. Shimizu, Prof. Dr. J.-i. Yoshida
Department of Synthetic Chemistry and Biological Chemistry
Graduate School of Engineering, Kyoto University
Nishikyo-ku, Kyoto 615-8510 (Japan)

Supporting information and the ORCID number(s) for the author(s) of this article can be found under <https://doi.org/10.1002/chem.201701979>.

Part of a Special Issue to celebrate the 150th anniversary of the German Chemical Society (GDCh). To view the complete issue, visit <https://doi.org/chem.v23.50>.

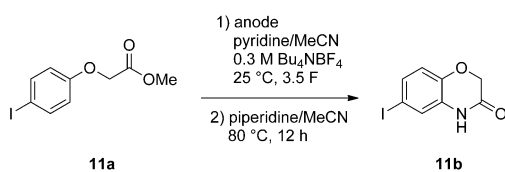


Scheme 1. Electrochemical synthesis of oxazoles **7**^[14] and oxazinones **10**.

In this work, we present a novel and innovative synthetic approach to the benzoxazinone scaffold by means of electrochemistry. Electrosynthetic conversions usually are considered sustainable as they take place at ambient conditions and avoid the use of stoichiometric amounts of oxidizing or reducing agents. As direct C–H functionalization can be achieved, pre-functionalized starting materials are not necessary. Thus, electro-synthetic processes can offer a higher atom economy compared to traditional methodologies.^[15] As extraordinary reaction pathways can be realized by electrochemical oxidation or reduction, electro-synthesis has recently experienced a renaissance.^[16,17]

Phenoxyacetate derivatives **8** served as starting materials for the envisioned electrochemical conversion to benzoxazinones. Anodic oxidation of such phenoxyacetates **8** in the presence of pyridine should lead to the positively charged pyridinium intermediates **9** (Zincke-type salts).^[11,18] Upon treatment with piperidine, the released primary aniline immediately attacks the ester moiety to form the desired benzoxazinones **10**. However, the anodic functionalization by pyridine needs to take place at the position *ortho* to the carboxymethoxy substituent. Only in this case, the desired fused heterocycle with the 1,4-oxazin-3-one substitution pattern will be formed. Therefore, an accessible and activated *ortho* position is required for the direct electrochemical C–H amination.

At first, a screening for suitable electrode materials was carried out because previous studies revealed a significant impact of the anode material on the anodic amination.^[19] For this investigation, methyl 4-iodophenoxyacetate (**11a**) was chosen as test substrate (Scheme 2). Phenoxyacetate **11a** fulfilled all requirements, such as good access to the position *ortho* to the phenoxy moiety and additionally, a leaving group for subse-



Scheme 2. Electrochemical amination of methyl 4-iodophenoxyacetate (**11a**) as test substrate for electrochemical synthesis of benzoxazinone (**11b**).

quent functionalization reactions. The optimization experiments were conducted in divided Teflon cells with a porous glass-frit as separator (see the Supporting Information). This screening methodology is simple and allows the variation of different important electrolysis parameters, for example, current density and applied charge, in a time-efficient manner.^[20] As anode materials, different carbon felts, carbon fleeces, boron-doped diamond as well as isotactic graphite were employed. The outcome of these screening reactions was quantified by ¹H NMR analysis with 1,1,2,2-tetrachloroethane as internal standard (ISTD).

Porous electrode materials like carbon fleece and carbon felt can be beneficial in electro-synthetic transformations because they exhibit a high surface area. However, anodically generated highly reactive intermediates need to diffuse into the bulk solution for desired follow-up reactions. This diffusion can be inhibited by absorption of the intermediates by the porous material. For carbon felt and carbon fleece as anode materials, a current of 8 mA was applied. These conditions were adopted from previous studies by Yoshida and co-workers.^[11] With an applied charge of 3.5 F, a maximum yield of 37% (NMR, ISTD) of **11b** was obtained. Next, boron-doped diamond, which has recently attracted a lot of attention in electro-synthesis, was evaluated.^[17,21] Initially, a current density of 10 mA cm⁻² and an applied charge of 3.5 F were investigated. At these conditions, the desired benzoxazinone **11b** was formed in 45% yield (NMR, ISTD). So far, the best results were obtained by using an isotactic graphite anode at similar reaction conditions as used before. Therefore, this anode material was investigated in detail. First, the current density was altered in the range of 0.5–13 mA cm⁻² at an applied charge of 3.5 F. We anticipated that a low current density might be beneficial for the selectivity as the amount of reactive intermediates generated is lower than at a high current density (Figure 2).

However, low current densities of up to 1 mA cm⁻² resulted in moderate yields of up to 45% (¹H NMR, ISTD). The best performance was observed at an elevated current density of 10 mA cm⁻² with 61% yield of **11b** (¹H NMR, ISTD). Thus, for further experiments, a current density of 10 mA cm⁻² was used. Furthermore, the applied charge was varied in a range of 2.0–5.0 F in steps of 0.5 F (see the Supporting Information). Best results were obtained at an applied charge of 3.5 F (61% of

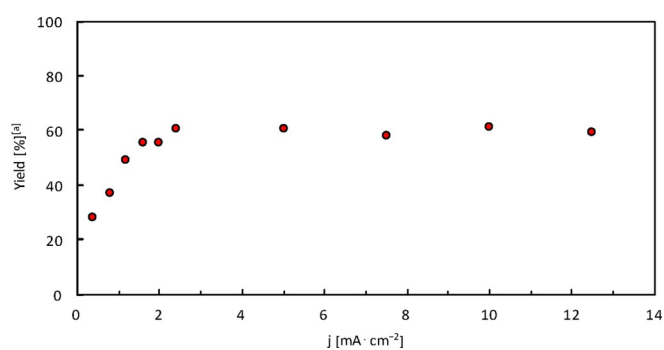
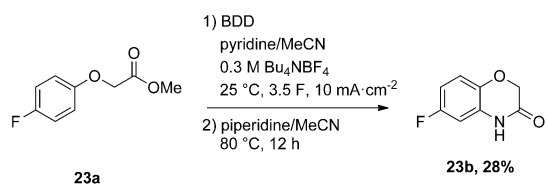


Figure 2. Electrochemical amination of methyl 4-iodophenoxy acetic acid (**11a**); screening of current density at isotactic graphite. [a] ¹H NMR yield, internal standard: 1,1,2,2-tetrachloroethane.

11 b). At lower applied charge, the yield decreased drastically to approx. 30% of **11 b** (¹H NMR, ISTD). In this case, incomplete conversion was observed. Application of more charge, for example, 5 F led to roughly 40% of benzoxazinone **11 b**. The identified, optimized electrolysis conditions consist of an isostatic graphite anode, a current density of 10 mA cm⁻², and an applied charge of 3.5 F. These optimized reaction conditions were then subjected to a collection of phenoxy acetates (Table 1).

As illustrated by Table 1, the electrochemical protocol is applicable to a broad scope of phenoxy acetates. Halide derivatives, for example, chloro, bromo, and iodo phenoxy acetates (**11 a–16 a**), were compatible with this methodology. The corresponding benzoxazinones (**11 b–16 b**) were obtained in moderate to good yields of up to 78% (Table 1, Entries 1–6). *Para*-substituted alkyl derivatives **17 a**, **18 a**, and **19 a** were transformed to the corresponding heterocycles **17 b**, **18 b**, and **19 b** in yields of up to 62% (Table 1, Entries 7–9). Despite the cationic nature of intermediates, this method is even suitable for *tert*-butyl groups, in which case the corresponding benzoxazinone **19 b** was obtained in a good yield of 62% (Table 1, Entry 9). Substrates like **19 a** might undergo dealkylation processes upon anodic treatment thus causing by-products. However, this seemed not to be the case. Starting materials **20 a** and **21 a** exhibit two alkyl substituents in both *meta* positions, leading to a lower yield than the congener with a single substituent (Table 1, Entries 10 and 11). Surprisingly, even the more sterically demanding alkyl substrate **21 a** with two *tert*-butyl groups was more easily accessible than phenoxy acetate **20 a**. However, to circumvent more hindered adjacent locations, we tested different substitution patterns. Unfortunately, an *ortho* and *para* alkyl substituent did not result in better yields (Table 1, Entry 12). Furthermore, we investigated the less-activated fluoro derivative **23 a** as a substrate. However, in this case the use of an isostatic graphite anode did not lead to the desired benzoxazinone **23 b**. Next, we used boron-doped diamond as the anode because this material proved to be a powerful tool for the electroconversion of electron-deficient starting materials.^[19] Indeed, by employing boron-doped diamond as the anode, **23 b** was obtained in a moderate yield of 28% (Scheme 3).

In conclusion, the use of phenoxy acetates as substrates for the electrochemical amination reaction results in the formation of 1,4-benzoxazinones, which are valuable scaffolds in natural products as well as pharmaceutically active compounds. The sequence includes the electrochemical amination via Zincke intermediates followed by liberation of the aniline function,



Scheme 3. Electrochemical transformation of electron-deficient phenoxyacetate **23 a** using boron-doped diamond electrodes.

Table 1. Scope of the anodic benzoxazinone formation.			
Entry	Substrate	Product	Yield [%] ^[a]
1			51
2			38
3			39
4			54
5			66
6			78
7			42
8			58
9			62
10			12
11			22
12			23

which finally undergoes the ring closure by a condensation reaction. The protocol presented allows a simple access to the benzoxazinone skeleton at ambient conditions highlighting the performance of electrochemical approaches to such complex heterocycles.

Acknowledgements

The support by The Advanced Lab for Electrochemistry and Electrosynthesis—ELYSION (Carl Zeiss Stiftung) is highly appreciated.

Conflict of interest

The authors declare no conflict of interest.

Keywords: amination · benzoxazinone · electrochemistry · nitrogen heterocycles · sustainable chemistry

- [1] K. Brahma, B. Das, C. Chowdhury, *Tetrahedron* **2014**, *70*, 5863–5871.
- [2] D. Chen, G. Shen, W. Bao, *Org. Biomol. Chem.* **2009**, *7*, 4067–4073.
- [3] a) J. Atkinson, P. Morand, J. T. Arnason, H. M. Niemeyer, H. R. Bravo, *J. Org. Chem.* **1991**, *56*, 1788–1800; b) H. M. Niemeyer, *Phytochemistry* **1988**, *27*, 3349–3358; c) F. A. Macias, D. Marin, A. Oliveros-Bastidas, J. M. G. Molinillo, *Nat. Prod. Rep.* **2009**, *26*, 478.
- [4] a) M. Frey, *Science* **1997**, *277*, 696–699; b) S. R. Desai, P. Kumar, W. S. Chilton, *Chem. Commun.* **1996**, 1321.
- [5] R. Frechette, M. Beach, WO97/28167, **1996**.
- [6] E. Feng, H. Huang, Y. Zhou, D. Ye, H. Jiang, H. Liu, *J. Org. Chem.* **2009**, *74*, 2846–2849.
- [7] B. Bertani, M. Borriello, A. Bozzoli, S. M. Bromidge, E. Granci, C. P. Leslie, H. Serafinowska, L. Stasi, A. Vong, V. Zucchelli, WO 2004/046124 A1, **2004**.
- [8] a) T. Hasui, N. Matsunaga, T. Ora, N. Ohyabu, N. Nishigaki, Y. Imura, Y. Igata, H. Matsui, T. Motoyaji, T. Tanaka, N. Habuka, S. Sogabe, M. Ono, C. S. Siedem, T. P. Tang, C. Gauthier, L. A. De Meese, S. A. Boyd, S. Fukumoto, *J. Med. Chem.* **2011**, *54*, 8616–8631; b) A. R. Gangloff, J. Brown, R. de Jong, D. R. Dougan, C. E. Grimshaw, M. Hixon, A. Jennings, R. Kamran, A. Kiryanov, S. O'Connell, E. Taylor, P. Vu, *Bioorg. Med. Chem. Lett.* **2013**, *23*, 4501–4505; c) C. Rajitha, P. K. Dubey, V. Sunku, V. R. Veeramaneni, M. Pal, *J. Heterocycl. Chem.* **2013**, *50*, 630–637; d) C. Ramesh, B. R. Raju, V. Kavala, C.-W. Kuo, C.-F. Yao, *Tetrahedron* **2011**, *67*, 1187–1192; e) Y. Lv, M. Li, T. Liu, L. Tong, T. Peng, L. Wei, J. Ding, H. Xie, W. Duan, *ACS Med. Chem. Lett.* **2014**, *5*, 592–597; f) T. P. C. Rooney, P. Filippakopoulos, O. Fedorov, S. Picaud, W. A. Cortopassi, D. A. Hay, S. Martin, A. Tumber, C. M. Rogers, M. Philpott, M. Wang, A. L. Thompson, T. D. Heightman, D. C. Pryde, A. Cook, R. S. Paton, S. Müller, S. Knapp, P. E. Brennan, S. J. Conway, *Angew. Chem. Int. Ed.* **2014**, *53*, 6126–6130; *Angew. Chem.* **2014**, *126*, 6240–6244.
- [9] a) E. Martinand-Lurin, L. El Kaïm, L. Grimaud, *Tetrahedron Lett.* **2014**, *55*, 5144–5146; b) E. Martinand-Lurin, A. Dos Santos, L. El Kaim, L. Grimaud, P. Retailleau, *Chem. Commun.* **2014**, *50*, 2214–2217.
- [10] a) R. S. Downing, P. J. Kunkeler, H. van Bekkum, *Catal. Today* **1997**, *37*, 121–136; b) G. A. Olah, R. Malhotra, S. C. Narang, *Nitration. Methods and Mechanisms*, Wiley, Hoboken, **1989**.
- [11] T. Morofuji, A. Shimizu, J.-i. Yoshida, *J. Am. Chem. Soc.* **2013**, *135*, 5000–5003.
- [12] a) T. Morofuji, A. Shimizu, J.-i. Yoshida, *J. Am. Chem. Soc.* **2015**, *137*, 9816–9819; b) R. Hayashi, A. Shimizu, Y. Song, Y. Ashikari, T. Nokami, J.-i. Yoshida, *Chem. Eur. J.* **2017**, *23*, 61–64.
- [13] S. R. Waldvogel, S. Möhle, *Angew. Chem. Int. Ed.* **2015**, *54*, 6398–6399; *Angew. Chem.* **2015**, *127*, 6496–6497.
- [14] T. Morofuji, A. Shimizu, J.-i. Yoshida, *Chem. Eur. J.* **2015**, *21*, 3211–3214.
- [15] a) H. J. Schäfer, *C. R. Chim.* **2011**, *14*, 745–765; b) B. A. Frontana-Urbe, R. D. Little, J. G. Ibanez, A. Palma, R. Vasquez-Medrano, *Green Chem.* **2010**, *12*, 2099; c) E. Steckhan, T. Arns, W. R. Heineman, G. Hilt, D. Hoormann, J. Jörissen, L. Kröner, B. Lewall, H. Pütter, *Chemosphere* **2001**, *43*, 63–73.
- [16] a) J.-i. Yoshida, K. Kataoka, R. Horcajada, A. Nagaki, *Chem. Rev.* **2008**, *108*, 2265–2299; b) E. J. Horn, B. R. Rosen, Y. Chen, J. Tang, K. Chen, M. D. Eastgate, P. S. Baran, *Nature* **2016**, *533*, 77–81; c) E. J. Horn, B. R. Rosen, P. S. Baran, *ACS Cent. Sci.* **2016**, *2*, 302–308; d) B. R. Rosen, E. W. Werner, A. G. O'Brien, P. S. Baran, *J. Am. Chem. Soc.* **2014**, *136*, 5571–5574; e) S. R. Waldvogel, B. Janza, *Angew. Chem. Int. Ed.* **2014**, *53*, 7122–7123; *Angew. Chem.* **2014**, *126*, 7248–7249; f) T. Gieshoff, D. Schollmeyer, S. R. Waldvogel, *Angew. Chem. Int. Ed.* **2016**, *55*, 9437–9440; *Angew. Chem.* **2016**, *128*, 9587–9590; g) S. Lips, A. Wiebe, B. Elsler, D. Schollmeyer, K. M. Dyballa, R. Franke, S. R. Waldvogel, *Angew. Chem. Int. Ed.* **2016**, *55*, 10872–10876; *Angew. Chem.* **2016**, *128*, 11031–11035; h) R. Francke, R. D. Little, *J. Am. Chem. Soc.* **2014**, *136*, 427–435; i) T. Broese, R. Francke, *Org. Lett.* **2016**, *18*, 5896–5899; j) R. Francke, *Beilstein J. Org. Chem.* **2014**, *10*, 2858–2873.
- [17] B. Elsler, D. Schollmeyer, K. M. Dyballa, R. Franke, S. R. Waldvogel, *Angew. Chem. Int. Ed.* **2014**, *53*, 5210–5213; *Angew. Chem.* **2014**, *126*, 5311–5314.
- [18] a) B. Reitstöen, V. D. Parker, K.-P. Lillerud, E. Högfeldt, P. Spielbüchler, J. B. Pedersen, P. Krosggaard-Larsen, *Acta Chem. Scand.* **1992**, *46*, 464–468; b) H. Lund, C. Tegnér, B. Takman, *Acta Chem. Scand.* **1957**, *11*, 1323–1330.
- [19] S. Herold, S. Möhle, M. Zirbes, F. Richter, H. Nefzger, S. R. Waldvogel, *Eur. J. Org. Chem.* **2016**, 1274–1278.
- [20] C. Gütz, B. Klöckner, S. R. Waldvogel, *Org. Process Res. Dev.* **2016**, *20*, 26–32.
- [21] a) T. A. Ivandini, Y. Einaga, *Chem. Commun.* **2017**, *53*, 1338–1347; b) S. R. Waldvogel, S. Mentizi, A. Kirste, *Top. Curr. Chem.* **2012**, *320*, 1–31; c) S. R. Waldvogel, A. Kirste, S. Mentizi in *Synthetic Diamond Films* (Eds.: E. Brillas, C. A. Martínez-Huitle), Wiley, Hoboken, **2011**, pp. 483–510; d) S. R. Waldvogel, B. Elsler, *Electrochim. Acta* **2012**, *82*, 434–443.

Manuscript received: May 3, 2017

Accepted manuscript online: June 12, 2017

Version of record online: July 10, 2017

CHEMISTRY

A **European** Journal

Supporting Information

New Approach to 1,4-Benzoxazin-3-ones by Electrochemical C–H Amination

Lars Julian Wesenberg,^[a] Sebastian Herold,^[a, b] Akihiro Shimizu,^[c] Jun-ichi Yoshida,^[c] and Siegfried R. Waldvogel^{*[a, b]}

chem_201701979_sm_miscellaneous_information.pdf

Supporting Information

General aspects

All reagents were used in analytical grades. Cyclohexane and ethyl acetate were of technical grade and were purified *via* distillation prior to use. Acetonitrile was of HPLC grade (Fisher Scientific). Pyridine was purchased from Acros Organics and tetrabutylammonium tetrafluoroborate from Sigma-Aldrich. BDD electrodes (DIACHEM®, 10 µm boron-doped diamond layer on 3 mm silicon support wafer) were purchased from CONDIAS GmbH, Itzhoë, Germany.

Column chromatography

Column chromatography was performed on silica gel 60 M (0.040-0.063 mm, Macherey-Nagel GmbH & Co, Düren, Germany) with a maximum pressure of 2.0 bar. A preparative chromatography system (Büchi-Labortechnik GmbH, Essen, Germany) was used with a Büchi Control Unit C-620, an UV detector Büchi UV photometer C-635, Büchi fraction collector C-660 and two Pump Modules C-605 for adjusting the solvent mixtures. Mixtures of cyclohexane and ethyl acetate were used as eluents. Silica gel 60 sheets on aluminium (F254, Merck, Darmstadt, Germany) were employed for thin layer chromatography.

Gas chromatography

GC was performed on a Shimadzu GC-2010 (Shimadzu, Japan) using a Zebron ZB-5MSi column (Phenomenex, USA, dim.: 30 m · 0.25 mm · 0.25 µm, carrier gas: hydrogen).

GC-MS measurements were carried out on a Shimadzu GC-2010 (Shimadzu, Japan) using a HP 1 column (Agilent Technologies, USA; length: 30 m, inner diameter: 0.25 mm, film: 0.25 µm, carrier gas: hydrogen). The method was coupled with mass spectrometry on a Shimadzu GCMS-QP2010.

Method "hart": 50 °C starting temperature for 1 min, heating rate 20 °C/min, final temperature: 190 °C for 5 min.

Spectroscopy and spectrometry

¹H NMR and ¹³C NMR spectra were recorded at 25 °C on a Bruker Avance II 400 or Avance III HD 300 instrument (*Bruker*, Analytische Messtechnik, Karlsruhe, Germany). Chemical shifts (δ) are reported in parts per million (ppm). Traces of non-deuterated solvents were used as internal standard for calibration. Mass spectra and high resolution mass spectra

were obtained by using a QToF Ultima 3 (Waters, Milford, Massachusetts) apparatus employing the ESI+ mode.

General protocol 1 for the synthesis of methyl phenoxyacetates

In a round-bottom flask (250 mL) the phenol derivative (18 mmol, 1.0 eq) was dissolved in 120 mL *N,N*-dimethylformamide (DMF) and potassium carbonate (45 mmol, 2.5 eq) was added. Followed by a slow addition of methyl α -bromoacetate (20 mmol, 1.1 eq) to the suspension. The reaction mixture was stirred at room temperature for 18 hours.

Thin layer chromatography (TLC) indicated almost disappearance of the phenolic component (ethyl acetate/cyclohexane = 1/1). Water (200 mL) was added to the reaction mixture. The aqueous layer was extracted three times with ethyl acetate (200 mL). The combined organic fractions were washed two times with water (50 mL) and two times with saturated sodium chloride solution (50 mL). The organic layer was dried (MgSO_4) and filtered. Concentration of the solution provided the crude product.

Solid products were purified by recrystallization from ethanol/water = 9/1. Liquid products were distilled at reduced pressure. Alternatively, the crude products were purified by column chromatography using ethyl acetate/cyclohexane as eluent-mixtures.

General protocol 2 for the synthesis of 1,4-benzoxazin-3-ones

The electrochemical conversion was conducted in divided cells made of Teflon.^[1,2] A porous glass frit (P4) was used as separator. As cathode a platinum plate was employed and as anodic material different electrodes, based on sp^2 and sp^3 carbon, were investigated (dimension: 1 cm \times 7 cm \times 0.3 cm).^[2] The anolyte consisted of 0.5 mmol substrate, 1 mL (12 mmol) pyridine and 5 mL 0.3 M Bu_4NBF_4 in acetonitrile. To the cathodic compartment 6 mL 0.3 M Bu_4NBF_4 in acetonitrile and 0.4 mL trifluoromethane sulfonic acid were added. The electrolyses were conducted at constant current conditions at 20 °C.

Anolyte and catholyte were transferred into a pressure tube and 1 mL of piperidine or pyrrolidine was added. This solution was heated to 80 °C for 12 hours. The solvent was removed under reduced pressure and the crude product was purified *via* column chromatography (ethyl acetate/cyclohexane).

Applied charge

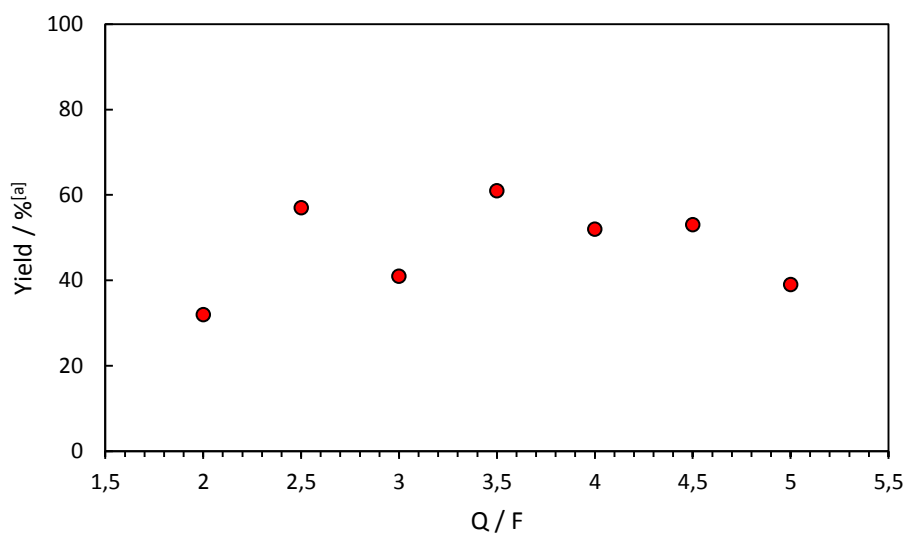


Figure 1. Electrochemical amination of methyl 4-iodophenoxy acetic acid, screening of applied charge at isostatic graphite. [a] ^1H NMR yield, internal standard: 1,1,2,2-tetrachloroethane.

Experimental setup

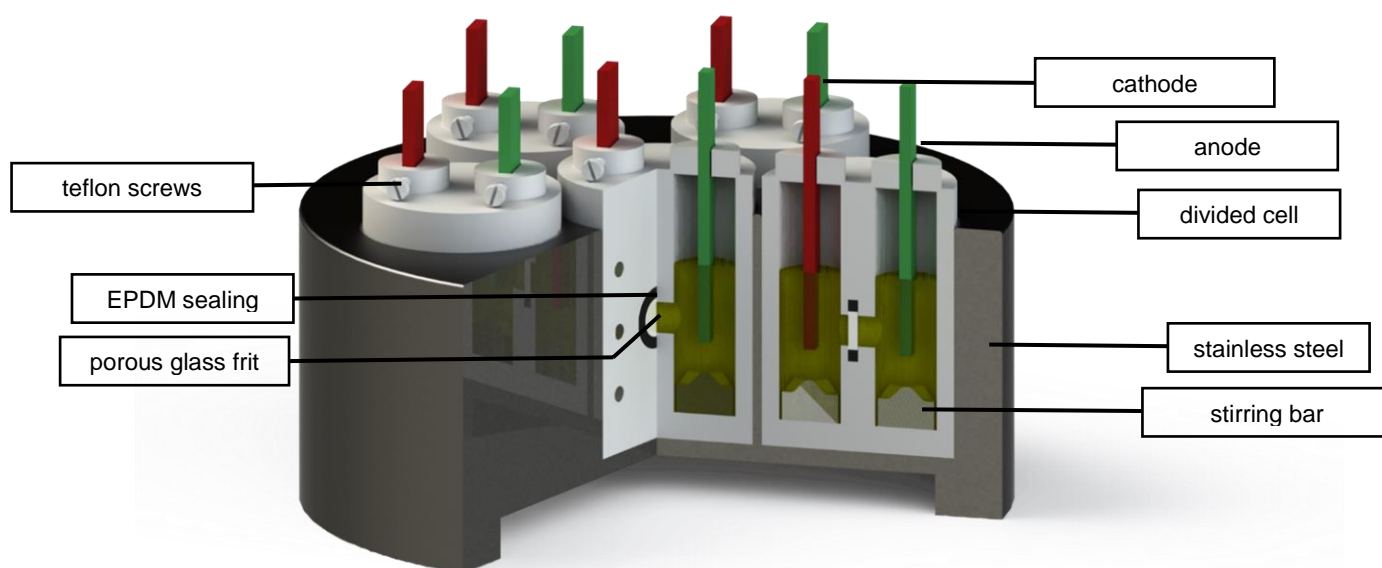
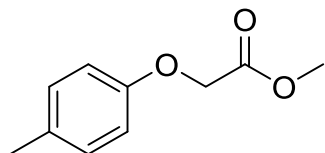


Figure 2: Screening system with 6 divided electrolysis cells fitting on a common magnetic stirrer; electrode gap: 2 cm; active surface of each planar electrode: 3 cm²; dimensions of carbon fleece: 5.0 x 1.0 cm; dimensions of carbon felt: 5.0 x 1.0 x 0.5 cm.

This setup allows convenient screening of several electrolysis parameters in an efficient way and short time.^[2]

Analytical data

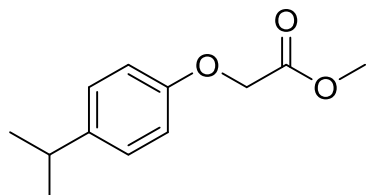
Methyl (4-methylphenoxy)acetate (17a)



Preparation according to general protocol 1 afforded **17a** (1.7 g, 9.4 mmol, 85%) as colorless liquid. $R_f = 0.50$, (ethyl acetate/cyclohexane = 1/2). $^1\text{H NMR}$ (400 MHz, CDCl_3): δ [ppm] = 2.29 (s, 3H), 3.80 (s, 3H), 4.61 (s, 2H), 6.77–6.86 (m, 2H), 7.05–7.14 (m, 2H). $^{13}\text{C NMR}$ (101 MHz, CDCl_3): δ [ppm] = 20.6, 52.3, 65.7, 114.6, 130.1, 131.2, 155.8, 169.7. HRMS (m/z) for $[\text{M}+\text{Na}] \text{C}_{10}\text{H}_{12}\text{NaO}_3$: calc: 203.0684, found: 203.0681.

The spectroscopic data match those reported in literature.^[3]

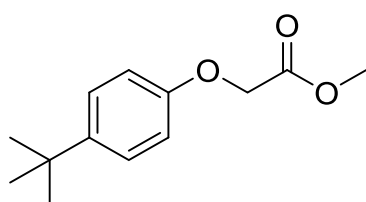
Methyl (4-(1-methylethyl)phenoxy)acetate (18a)



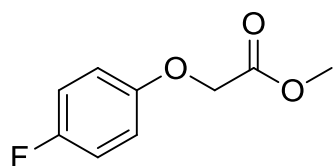
Preparation according to general protocol 1 afforded **18a** (2.1 g, 10 mmol, 90%) as colorless liquid. $R_f = 0.54$, (ethyl acetate/cyclohexane = 1/2). $^1\text{H NMR}$ (400 MHz, CDCl_3): δ [ppm] = 1.22 (d, $J = 6.9$ Hz, 6H), 2.87 (hept, $J = 6.9$ Hz, 1H), 3.81 (s, 3H), 4.62 (s, 2H), 6.80–6.89 (m, 2H), 7.10–7.20 (m, 2H). $^{13}\text{C NMR}$ (101 MHz, CDCl_3): δ [ppm] = 24.3, 33.4, 52.3, 65.6, 114.6, 127.5, 142.3, 156.0, 169.7. HRMS (m/z) for $[\text{M}+\text{Na}] \text{C}_{12}\text{H}_{16}\text{NaO}_3$: calc: 231.0998, found: 231.0986.

The spectroscopic data match those reported in literature.^[4]

Methyl (4-(1,1-dimethylethyl)phenoxy)acetate (19a)

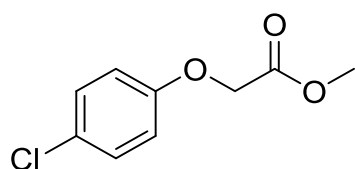


Preparation according to general protocol 1 afforded **19a** (1.73 g, 7.8 mmol, 70%) as colorless liquid. $R_f = 0.54$, (ethyl acetate/cyclohexane = 1/2). $^1\text{H NMR}$ (400 MHz, CDCl_3): δ [ppm] = 1.30 (s, 9H), 3.81 (s, 3H), 4.62 (s, 2H), 6.75–6.94 (m, 2H), 7.25–7.40 (m, 2H). $^{13}\text{C NMR}$ (101 MHz, CDCl_3): δ [ppm] = 31.6, 34.3, 52.4, 65.6, 114.2, 126.5, 144.6, 155.6, 169.8. HRMS (m/z) for $[\text{M}+\text{Na}-\text{H}] \text{C}_{13}\text{H}_{17}\text{NaO}_3$: calc: 245.1154, found: 245.1149. Elemental analysis for $\text{C}_{13}\text{H}_{18}\text{O}_3$: calc: C: 70.24%, H: 8.16%, found: C: 70.21%, H: 8.25%.

Methyl (4-fluorophenoxy)acetate (23a)

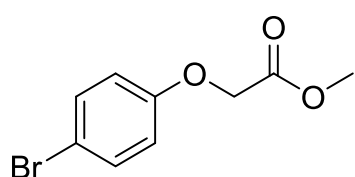
Preparation according to general protocol 1 afforded **23a** (1,70 g, 9.2 mmol, 83%) as slightly brown solid. $R_f = 0.45$ (ethyl acetate/cyclohexane = 1/2). $^1\text{H NMR}$ (300 MHz, CDCl_3) δ [ppm] = 3.80 (s, 3H), 4.60 (s, 2H), 6.80–6.92 (m, 2H), 6.91–7.06 (m, 2H). $^{13}\text{C NMR}$ (101 MHz, CDCl_3): δ [ppm] = 52.4, 66.1, 116.0, 116.2 (d, $J = 15.8$ Hz), 154.0 (d, $J = 2.3$ Hz), 158.0 (d, $J = 239.7$ Hz), 169.4. $^{19}\text{F NMR}$ (376 MHz, CDCl_3) δ [ppm] = 122.65 (tt, 8.3 Hz, 4.4 Hz, 1F). HRMS (m/z) for $[\text{M}+\text{H}] \text{C}_9\text{H}_{10}\text{FO}_3$: calc: 185.0614, found: 185.0609.

The spectroscopic data match those reported in literature.^[5]

Methyl (4-chlorophenoxy)acetate (13a)

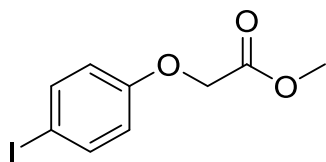
Preparation according to general protocol 1 afforded **13a** (0.6 g, 3.0 mmol, 27%) as colorless solid. $R_f = 0.50$, (ethyl acetate/cyclohexane = 1/2). $^1\text{H NMR}$ (400 MHz, CDCl_3): δ [ppm] = 3.82 (s, 3H), 4.63 (s, 2H), 6.80–6.93 (m, 2H), 7.20–7.32 (m, 2H). $^{13}\text{C NMR}$ (101 MHz, CDCl_3): δ [ppm] = 52.5, 65.6, 116.1, 126.9, 129.6, 156.5, 169.2. mp: 37.7–38.7 °C, crystallized from cyclohexane/ethyl acetate, 35–37 °C (lit.).^[6] HRMS (m/z) for $[\text{M}+\text{Na}-\text{H}] \text{C}_9\text{H}_9^{35}\text{ClNaO}_3$: calc: 223.0138, found: 223.0141.

The spectroscopic data match those reported in literature.^[6]

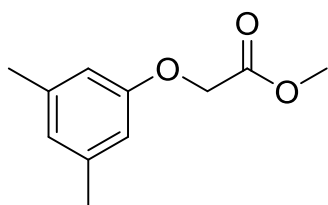
Methyl (4-bromophenoxy)acetate (12a)

Preparation according to general protocol 1 afforded **12a** (1.21 g, 5.0 mmol, 44%) as colorless solid. $R_f = 0.50$, (ethyl acetate/cyclohexane = 1/2). $^1\text{H NMR}$ (400 MHz, CDCl_3): δ [ppm] = 3.80 (s, 3H), 4.61 (s, 2H), 6.74–6.84 (m, 2H), 7.33–7.43 (m, 2H). $^{13}\text{C NMR}$ (101 MHz, CDCl_3): δ [ppm] = 52.5, 65.6, 116.1, 126.9, 129.6, 156.5, 169.2. mp: 45.9–47.1 °C, crystallized from cyclohexane/ethyl acetate, 46–47 °C (lit.).^[6] HRMS (m/z) for $[\text{M}+\text{Na}] \text{C}_9\text{H}_9^{79}\text{BrNaO}_3$: calc: 266.9633, found: 266.9639.

The spectroscopic data match those reported in literature.^[6]

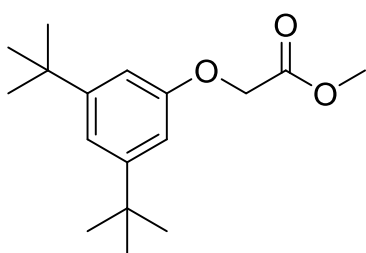
Methyl (4-iodophenoxy)acetate (11a)

Preparation according to general protocol 1 afforded **11a** (6.24 g, 24.1 mmol, 79%) as colorless solid. $R_f = 0.48$, (ethyl acetate/cyclohexane = 1/2). $^1\text{H NMR}$ (400 MHz, CDCl_3): δ [ppm] = 3.8 (s, 3H), 4.6 (s, 2H), 6.7–6.8 (m, 2H), 7.3–7.4 (m, 2H). $^{13}\text{C NMR}$ (101 MHz, CDCl_3): δ [ppm] = 31.1, 52.5, 65.5, 114.2, 116.6, 132.6, 157.0, 169.1. mp: 73.4–74.6 °C, crystallized from ethanol. HRMS (m/z) for $[\text{M}+\text{Na}] \text{C}_9\text{H}_9\text{INO}_3$: calc: 314.9495, found: 314.9497. Elemental analysis for $\text{C}_{12}\text{H}_9\text{INO}_2$: calc: C: 37.01%, H: 3.11%, found: C: 36.97%, H: 3.13%.

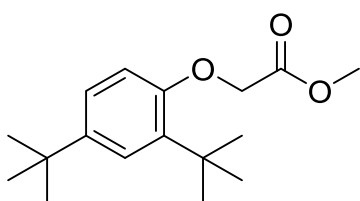
Methyl (3,5-dimethylphenoxy)acetate (20a)

Preparation according to general protocol 1 afforded **20a** (1.45 g, 7.5 mmol, 83%) as colorless oil. $^1\text{H NMR}$ (400 MHz, CDCl_3): δ [ppm] = 2.29 (s, 6H), 3.81 (s, 3H), 4.61 (s, 2H), 6.50–6.59 (m, 2H), 6.60–6.71 (m, 2H). $^{13}\text{C NMR}$ (101 MHz, CDCl_3): δ [ppm] = 21.6, 52.4, 65.3, 112.4, 123.7, 139.5, 157.9, 168.7. HRMS (m/z) for $[\text{M}+\text{Na}] \text{C}_{11}\text{H}_{14}\text{NaO}_3$: calc: 217.0841, found: 217.0846.

The spectroscopic data match those reported in literature.^[7]

Methyl (3,5-bis(1,1-dimethylethyl)phenoxy)acetate (21a)

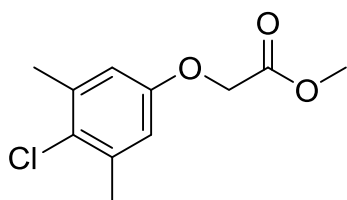
Preparation according to general protocol 1 afforded **21a** (1.45 g, 7.5 mmol, 83%) as colorless solid. $^1\text{H NMR}$ (400 MHz, CDCl_3): δ [ppm] = 1.31 (s, 18H), 3.82 (s, 3H), 4.64 (s, 2H), 6.77 (d, $J = 1.6$ Hz, 2H), 7.07 (t, $J = 1.6$ Hz, 1H). $^{13}\text{C NMR}$ (101 MHz, CDCl_3): δ [ppm] = 21.4, 52.2, 65.2, 112.3, 123.6, 139.4, 157.8, 169.6. mp: 70.7–71.7 °C, crystallized from ethanol. HRMS (m/z) for $[\text{M}+\text{Na}] \text{C}_{17}\text{H}_{26}\text{NaO}_3$: calc: 301.1780, found: 301.1784. Elemental analysis for $\text{C}_{17}\text{H}_{26}\text{O}_3$: calc: C: 73.35%, H: 9.41%, found: C: 73.07%, H: 9.58%.

Methyl (2,4-bis(1,1-dimethylethyl)phenoxy)acetate (22a)

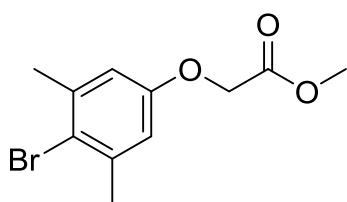
Preparation according to general protocol 1 afforded **22a** (3.39 g, 12.2 mmol, 61%) as colorless liquid. $^1\text{H NMR}$ (400 MHz, CDCl_3): δ [ppm] = 1.31 (s, 9H), 1.44 (s, 9H), 3.82 (s, 3H), 4.64 (s, 2H), 6.65 (d, $J = 8.5$ Hz, 1H), 7.16 (dd, $J = 8.5, 2.5$ Hz, 1H), 7.36 (d, $J = 2.5$ Hz, 1H). $^{13}\text{C NMR}$ (101 MHz, CDCl_3) δ

[ppm] = 30.0, 31.7, 34.4, 35.2, 52.2, 65.4, 111.3, 123.5, 124.4, 137.8, 143.7, 154.4, 169.8. HRMS (m/z) for [M+Na] C₁₇H₂₆NaO₃: calc: 301.1780, found: 301.1774. Elemental analysis for C₁₇H₂₆O₃: calc: C: 73.35%, H: 9.41%, found: C: %, H: %.

Methyl (4-chloro-3,5-dimethylphenoxy)acetate (16a)



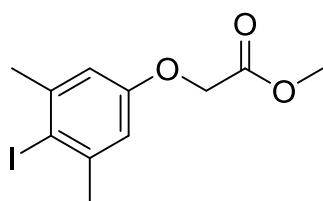
Preparation according to general protocol 1 afforded **16a** (2.66 g, 11.6 mmol, 77%) as colorless solid. ¹H NMR (400 MHz, CDCl₃) δ = 2.34 (s, 6H), 3.80 (s, 3H), 4.59 (s, 2H), 6.64 (s, 2H). ¹³C NMR (101 MHz, CDCl₃) δ = 21.1, 52.4, 65.5, 114.7, 127.5, 137.5, 155.7, 169.5. mp: 47.4–48.8 °C, crystallized from ethyl acetate/cyclohexane. HRMS (m/z) for [M+Na] C₁₁H₁₃³⁵ClNaO₃: calc: 251.0451, found: 251.0447. Elemental analysis for C₁₁H₁₃ClO₃: calc: C: 57.78%, H: 5.73, found: C: 57.93%, H: 5.92%.



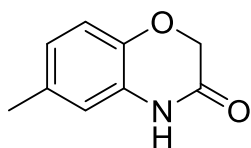
Methyl (4-bromo-3,5-dimethylphenoxy)acetate (15a)

Preparation according to general protocol 1 afforded **15a** (2.5 g, 9.8 mmol, 98%) as colorless solid. ¹H NMR (400 MHz, CDCl₃) δ = 2.37 (s, 6H), 3.80 (s, 3H), 4.59 (s, 2H), 6.65 (s, 2H). ¹³C NMR (101 MHz, CDCl₃) δ = 24.2, 52.4, 65.4, 114.6, 119.6, 139.5, 156.3, 169.4. mp: 65.2–66.5 °C, crystallized from ethyl acetate/cyclohexane. HRMS (m/z) for [M+Na] C₁₁H₁₃⁷⁹BrNaO₃: calc: 294.9946, found: 294.9940. Elemental analysis for C₁₁H₁₃ClO₃: calc: C: 48.37%, H: 4.80, found: C: 48.74%, H: 5.01%.

Methyl (4-iodo-3,5-dimethylphenoxy)acetate (14a)

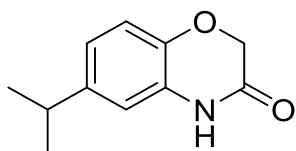


Preparation according to general protocol 1 afforded **14a** (1.45 g, 7.5 mmol, 84%) as colorless solid. ¹H NMR (400 MHz, CDCl₃) δ = 2.43 (s, 6H), 3.80 (s, 3H), 4.60 (s, 2H), 6.66 (s, 2H). ¹³C NMR (101 MHz, CDCl₃) δ = 29.9, 52.5, 65.3, 98.7, 113.6, 143.3, 157.5, 169.4. mp: 60.2–62.3 °C, crystallized from ethyl acetate/cyclohexane. HRMS (m/z) for [M+Na] C₁₁H₁₃I NaO₃: calc: 342.9807, found: 342.9814. Elemental analysis for C₁₁H₁₃IO₃: calc: C: 41.27%, H: 4.09, found: C: %, H: %.

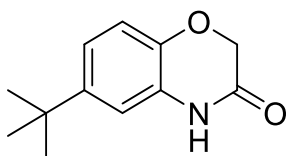
2H-2,3-Dihydro-6-methylbenzo[*b*]-1,4-oxazin-3-one (17b)

Preparation according to general protocol 2 afforded **17b** (34 mg, 0.21 mmol, 42%) as colorless solid. $R_f = 0.25$, (ethyl acetate/cyclohexane = 1/2). $^1\text{H NMR}$ (300 MHz, DMSO- d_6): δ [ppm] = 2.28 (s, 3H), 4.60 (s, 2H), 6.67 (d, $J = 1.2$ Hz, 1H), 6.77 (dd, $J = 8.3, 1.2$ Hz, 1H), 6.86 (d, $J = 8.3$ Hz, 1H), 9.34 (s, 1H). $^{13}\text{C NMR}$ (101 MHz, DMSO- d_6): δ [ppm] = 20.4, 66.8, 115.9, 116.1, 123.3, 127.0, 131.4, 141.1, 165.1. mp: 205.6–207.0 °C, crystallized from ethyl acetate/cyclohexane, 205–207 °C (lit.).^[8] HRMS (m/z) for [M+H] $\text{C}_9\text{H}_{10}\text{NO}_2$: calc: 164.0712, found: 164.0724.

The spectroscopic data match those reported in literature.^[8]

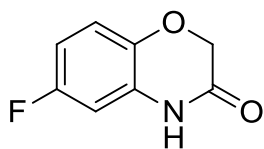
2H-2,3-Dihydro-6-(1-methylethyl)benzo[*b*]-1,4-oxazin-3-one (18b)

Preparation according to general protocol 2 afforded **18b** (62 mg, 0.29 mmol, 58%) as slightly yellow solid. $R_f = 0.25$, (ethyl acetate/cyclohexane = 1/2). $^1\text{H NMR}$ (400 MHz, DMSO- d_6): δ [ppm] = 1.15 (d, $J = 6.9$ Hz, 6H), 2.79 (hept, $J = 6.9$ Hz, 1H), 4.51 (s, 2H), 6.75 (d, $J = 2.0$ Hz, 1H), 6.78 (dd, $J = 8.2, 2.0$ Hz, 1H), 6.85 (d, $J = 8.2$ Hz, 1H), 10.60 (s, 1H). $^{13}\text{C NMR}$ (101 MHz, DMSO- d_6): δ [ppm] = 24.0, 32.8, 66.8, 113.6, 115.9, 120.7, 127.0, 141.4, 142.6, 165.1. mp: 132.1–133.7 °C, crystallized from ethyl acetate/cyclohexane. HRMS (mf/z) for [M+H] $\text{C}_{11}\text{H}_{14}\text{NO}_2$: calc: 192.1025, found: 192.1022. Elemental analysis for $\text{C}_{11}\text{H}_{14}\text{NO}_2$: calc: C: 69.09%, H: 6.85%, N: 7.32%, found: C: 69.60%, H: 6.83%, N: 6.96%.

2H-2,3-Dihydro-6-(1,1-dimethylethyl)benzo[*b*]-1,4-oxazin-3-one (19b)

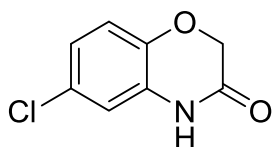
Preparation according to general protocol 2 afforded **19b** (63 mg, 0.31 mmol, 62%) as colorless solid. $R_f = 0.25$, (ethyl acetate/cyclohexane = 1/2). $^1\text{H NMR}$ (300 MHz, CDCl_3): δ [ppm] = 1.29 (s, 9H), 4.60 (s, 2H), 6.82 (d, $J = 2.2$ Hz, 1H), 6.90 (d, $J = 8.5$ Hz, 1H), 7.00 (dd, $J = 8.5, 2.2$ Hz, 1H), 8.80 (s, 1H). $^{13}\text{C NMR}$ (101 MHz, CDCl_3): δ [ppm] = 31.2, 34.0, 66.8, 112.8, 115.6, 119.7, 126.7, 141.1, 145.0, 165.0. mp: 149.3–150.2 °C, crystallized from ethyl acetate/cyclohexane, 150–151 °C (lit.).^[8] HRMS (m/z) for [M+H] $\text{C}_{12}\text{H}_{16}\text{NO}_2$: calc: 206.1181, found: 206.1173.

The spectroscopic data match those reported in literature.^[8]

2H-6-Fluoro-2,3-dihydro-benzo[*b*]-1,4-oxazin-3-one (23b)

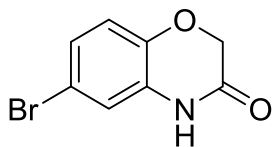
Preparation according to general protocol 2 afforded **23b** (24 mg, 0.14 mmol, 28%) as colorless solid. $R_f = 0.20$, (ethyl acetate/cyclohexane) = 1/2). $^1\text{H NMR}$ (400 MHz, CD_3CN) $\delta = 4.5$ (s, 2H), 6.5–6.8 (m, 2H), 6.8–7.0 (m, 1H), 8.7 (s, 1H). $^{13}\text{C NMR}$ (101 MHz, CDCl_3): δ [ppm] = 67.4, 103.5 (d, $J = 27.7$ Hz), 110.4 (d, $J = 23.2$ Hz), 117.7 (d, $J = 9.2$ Hz), 139.9 (d, $J = 2.5$ Hz), 158.2 (d, $J = 241.0$ Hz), 166.3. $^{19}\text{F NMR}$ (376 MHz, CD_3CN): δ [ppm] = -123.33 (td, $J = 8.9, 5.0$ Hz, 1F). mp: 202.6–204.1 °C, crystallized from acetonitrile/dichloromethane, 203–205 °C (lit.).^[10] HRMS (m/z) for [M+H] $\text{C}_8\text{H}_7\text{FNO}_2$: calc: 168.0461, found: 168.0474.

The spectroscopic data match those reported in literature.^[10]

2H-6-Chloro-2,3-dihydro-benzo[*b*]-1,4-oxazin-3-one (13b)

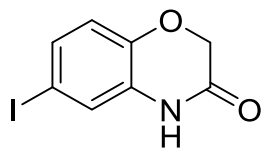
Preparation according to general protocol 2 afforded **13b** (38 mg, 0.20 mmol, 39%) as colorless solid. $R_f = 0.27$, (ethyl acetate/cyclohexane) = 1/2). $^1\text{H NMR}$ (400 MHz, DMSO-d_6): δ [ppm] = 4.59 (s, 2H), 6.89 (dd, $J = 2.1, 0.6$ Hz, 1H), 6.94 (dd, $J = 8.5, 2.1$ Hz, 1H), 6.97 (dd, $J = 8.5, 0.6$ Hz, 1H), 10.81 (s, 1H). $^{13}\text{C NMR}$ (101 MHz, DMSO-d_6): δ [ppm] = 66.7, 115.2, 117.6, 122.4, 125.7, 128.7, 142.2, 164.7. mp: 215.9–216.6 °C, crystallized from ethyl acetate/cyclohexane, 214 °C (lit.).^[9] HRMS (m/z) for [M+H] $\text{C}_8\text{H}_7^{35}\text{ClNO}_2$: calc: 184.0165, found: 184.0161.

The spectroscopic data match those reported in literature.^[10]

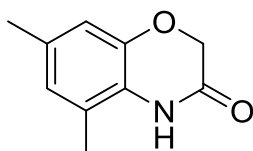
2H-6-Bromo-2,3-dihydro-benzo[*b*]-1,4-oxazin-3-one (12b)

Preparation according to general protocol 2 afforded **12b** (37 mg, 0.16 mmol, 31%) as slightly brown solid. $R_f = 0.27$, (ethyl acetate/cyclohexane) = 1/2). $^1\text{H NMR}$ (400 MHz, DMSO-d_6): δ [ppm] = 4.59 (s, 2H), 6.91 (d, $J = 8.5$ Hz, 1H), 7.02 (d, $J = 2.3$ Hz, 1H), 7.07 (dd, $J = 8.5, 2.4$ Hz, 1H), 10.79 (s, 1H). $^{13}\text{C NMR}$ (101 MHz, DMSO-d_6): δ [ppm] = 52.5, 65.6, 114.3, 116.6, 132.6, 157.0, 169.1. mp: 221.7–223.9 °C, crystallized ethyl acetate/cyclohexane, 221–223 °C (lit.).^[11] HRMS (m/z) for [M+H] $\text{C}_8\text{H}_7^{79}\text{BrNO}_2$: calc: 227.9660, found: 227.9652.

The spectroscopic data match those reported in literature.^[11]

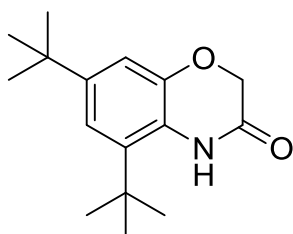
2H-2,3-Dihydro-6-iodobenzo[b]-1,4-oxazin-3-one (11b)

Preparation according to general protocol 2 afforded **11b** (70 mg, 0.26 mmol, 51%) as slightly yellow solid. $R_f = 0.30$, (ethyl acetate/cyclohexane = 1/2). $^1\text{H NMR}$ (400 MHz, DMSO-d_6): δ [ppm] = 4.58 (s, 2H), 6.77 (d, $J = 8.4$, 1H), 7.17 (d, $J = 2.1$, 1H), 7.22 (dd, $J = 8.4$, 2.1, 1H), 10.75 (s, 1H). $^{13}\text{C NMR}$ (101 MHz, DMSO-d_6): δ [ppm] = 66.6, 84.6, 118.5, 123.7, 129.2, 131.3, 143.2, 164.6. mp: 261–264 °C (decomposition), crystallized from ethyl acetate/cyclohexane. HRMS (m/z) for $[\text{M}+\text{H}] \text{C}_8\text{H}_7\text{INO}_2$: calc: 275.9521, found: 275.9518. Elemental analysis for $\text{C}_8\text{H}_6\text{INO}_2$: calc: C: 34.94%, H: 2.20%, N: 5.09%, found: C: 36.57%, H: 2.56%, N: 4.73%.

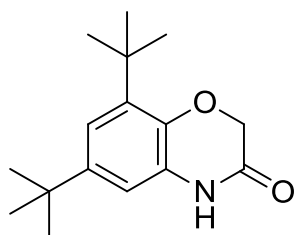
2H-2,3-Dihydro-5,7-dimethylbenzo[b]-1,4-oxazin-3-one (20b)

Preparation according to general protocol 2 afforded **20b** (11 mg, 0.06 mmol, 12%) as slightly brown solid. $R_f = 0.20$, (ethyl acetate/cyclohexane = 1/5). $^1\text{H NMR}$ (300 MHz, CDCl_3) $\delta = 2.23$ (s, 3H), 2.25 (s, 3H), 4.55 (s, 2H), 6.65 (s, 1H), 6.66 (s, 1H), 8.17 (s, 1H). $^{13}\text{C NMR}$ (101 MHz, DMSO-d_6) $\delta = 16.8$, 20.3, 66.8, 114.4, 123.3, 124.7, 131.9, 143.9, 165.4. mp: 205.1–206.0 °C, crystallized from ethyl acetate/cyclohexane, 205–209 °C (lit.).^[12] HRMS (m/z) for $[\text{M}+\text{H}] \text{C}_{10}\text{H}_{12}\text{NO}_2$: calc: 178.0868, found: 178.0862.

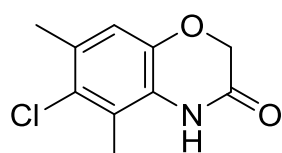
The spectroscopic data match those reported in literature.^[12]

2H-2,3-Dihydro-5,7-bis(dimethylethyl)benzo[b]-1,4-oxazin-3-one (21b)

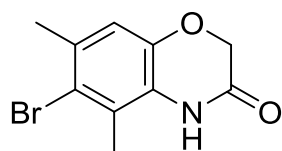
Preparation according to general protocol 2 afforded **21b** (29 mg, 0.11 mmol, 22%) as slightly brown solid. $R_f = 0.20$, (ethyl acetate/cyclohexane = 1/5). $^1\text{H NMR}$ (300 MHz, CDCl_3): $\delta = 1.29$ (s, 9H), 1.43 (s, 9H), 4.55 (s, 2H), 6.93 (d, $J = 1.7$ Hz, 1H), 7.05 (d, $J = 2.1$ Hz, 1H), 7.71 (s, 1H). $^{13}\text{C NMR}$ (75 MHz, CDCl_3) $\delta = 30.7$, 31.5, 34.6, 34.8, 67.2, 117.6, 122.2, 135.4, 144.6, 146.9, 165.3. mp: 205.1–206.0 °C, crystallized from ethyl acetate/cyclohexane, HRMS (m/z) for $[\text{M}+\text{H}] \text{C}_{16}\text{H}_{24}\text{NO}_2$: calc: 262.1807, found: 262.1805. Elemental analysis for $\text{C}_{16}\text{H}_{23}\text{NO}_2$: calc: C: 73.53%, H: 8.87%, N: 5.36%, found: C: 73.61%, H: 9.14%, N: 4.98%.

2H-2,3-Dihydro-6,8-bis(dimethylethyl)benzo[b]-1,4-oxazin-3-one (22b)

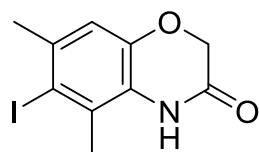
Preparation according to general protocol 2 afforded **22b** (31 mg, 0.12 mmol, 23%) as slightly brown solid. $R_f = 0.20$, (ethyl acetate/cyclohexane = 1/5). $^1\text{H NMR}$ (400 MHz, CDCl_3) $\delta = 1.29$ (s, 9H), 1.38 (s, 9H), 4.54 (s, 2H), 6.67 (d, $J = 2.2$ Hz, 1H), 7.01 (d, $J = 2.2$ Hz, 1H), 8.10 (s, 1H). $^{13}\text{C NMR}$ (101 MHz, CDCl_3) $\delta = 29.8, 31.6, 34.7, 35.0, 67.0, 111.5, 118.9, 126.6, 138.6, 140.5, 145.5, 166.6$. Elemental analysis for $\text{C}_{16}\text{H}_{23}\text{NO}_2$: calc: C: 73.53%, H: 8.87%, N: 5.36%, found: C: 73.52%, H: 8.94%, N: 5.05%.

2H-6-Chloro-2,3-dihydro-5,7-dimethylbenzo[b]-1,4-oxazin-3-one (16b)

Preparation according to general protocol 2 afforded **16b** (83 mg, 0.39 mmol, 78%) as colorless solid. $R_f = 0.21$, (ethyl acetate/cyclohexane = 1/5). $^1\text{H NMR}$ (400 MHz, DMSO-d_6) $\delta = 2.24$ (s, 3H), 2.26 (s, 3H), 4.49 (s, 2H), 6.86 (s, 1H), 10.34 (s, 1H). $^{13}\text{C NMR}$ (101 MHz, DMSO-d_6) $\delta = 14.4, 20.0, 66.7, 116.0, 122.7, 125.1, 127.1, 129.9, 142.4, 165.5$. mp: 256.6–257.1 °C (decomposition), crystallized from methanol. HRMS (m/z) for $[\text{M}+\text{H}] \text{C}_{10}\text{H}_{10}^{35}\text{ClNO}_2$: calc: 212.0478 found: 212.0484. Elemental analysis for $\text{C}_{10}\text{H}_{10}\text{ClNO}_2$: calc: C: 56.75%, H: 4.76%, N: 6.62%, found: C: 56.84%, H: 4.57%, N: 6.64%.

2H-6-Bromo-2,3-dihydro-5,7-dimethylbenzo[b]-1,4-oxazin-3-one (15b)

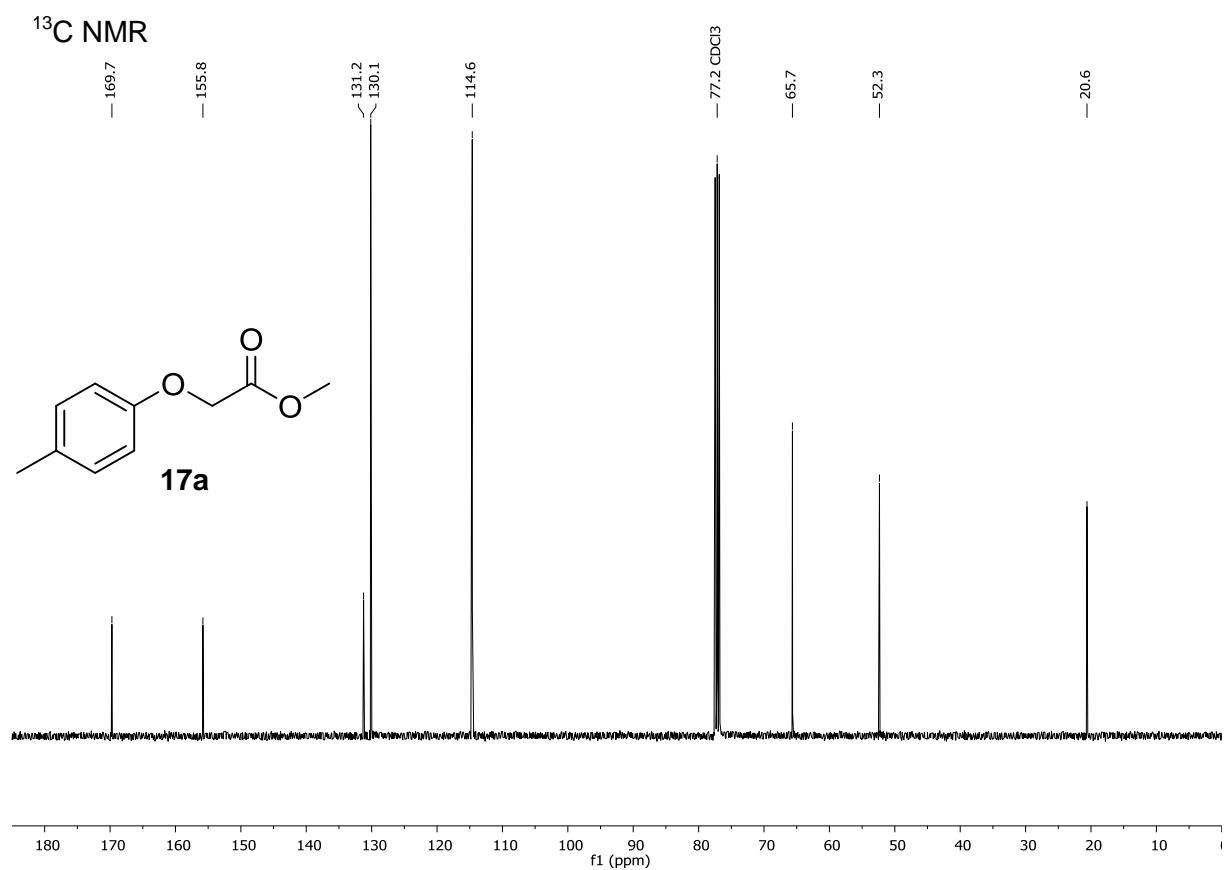
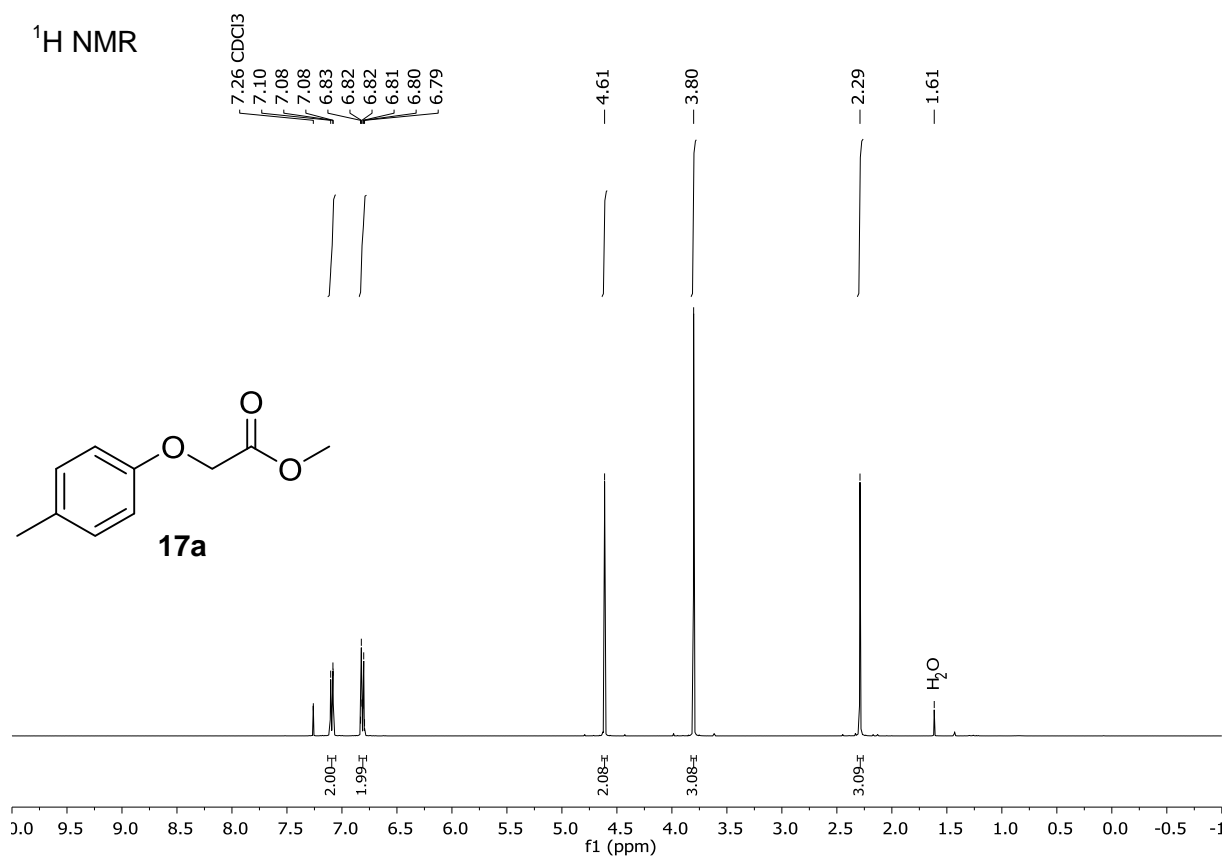
Preparation according to general protocol 2 afforded **15b** (79 mg, 0.33 mmol, 66%) as colorless solid. $R_f = 0.22$, (ethyl acetate/cyclohexane = 1/5). $^1\text{H NMR}$ (400 MHz, DMSO-d_6) $\delta = 2.27$ (s, 3H), 2.32 (s, 3H), 4.50 (s, 2H), 6.89 (s, 1H), 10.34 (s, 1H). $^{13}\text{C NMR}$ (101 MHz, DMSO-d_6) $\delta = 17.6, 23.2, 66.7, 116.0, 119.9, 124.4, 124.9, 131.9, 143.1, 165.5$. mp: 269.4–270.3 °C (decomposition), crystallized from methanol. HRMS (m/z) for $[\text{M}+\text{H}] \text{C}_{10}\text{H}_{11}^{79}\text{BrNO}_2$: calc: 255.9973 found: 255.9977. Elemental analysis for $\text{C}_{10}\text{H}_{10}\text{BrNO}_2$: calc: C: 46.90%, H: 3.94%, N: 5.47%, found: C: 46.81%, H: 4.22%, N: 5.27%.

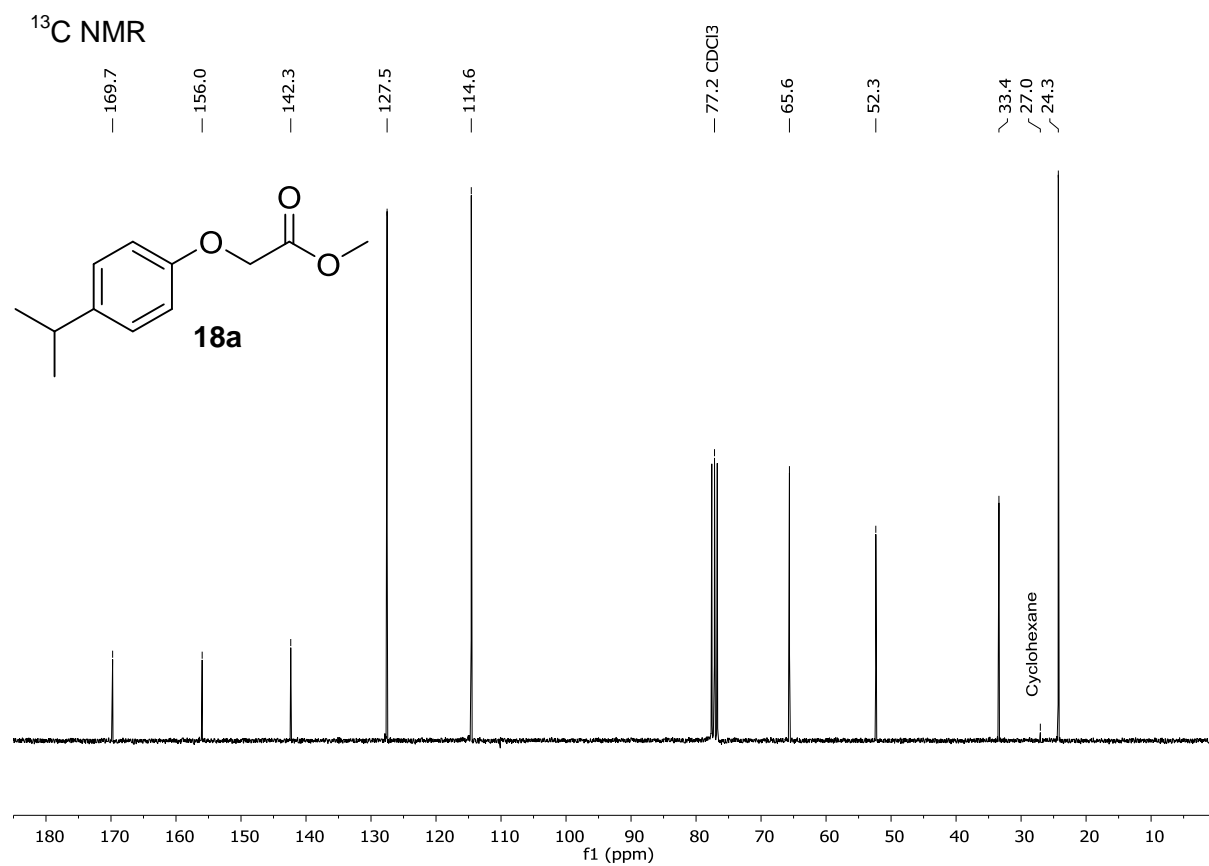
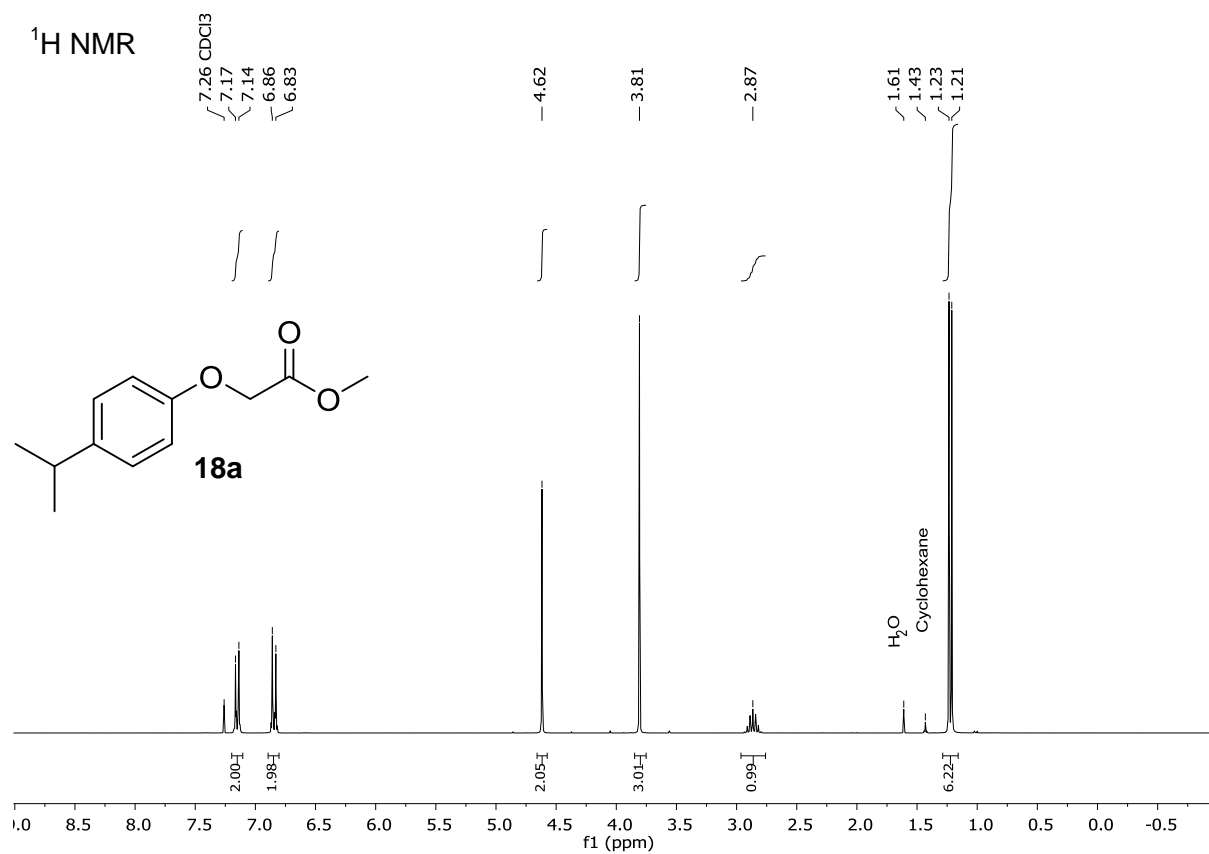
2H-2,3-Dihydro-6-iodo-5,7-dimethylbenzo[b]-1,4-oxazin-3-one (14b)

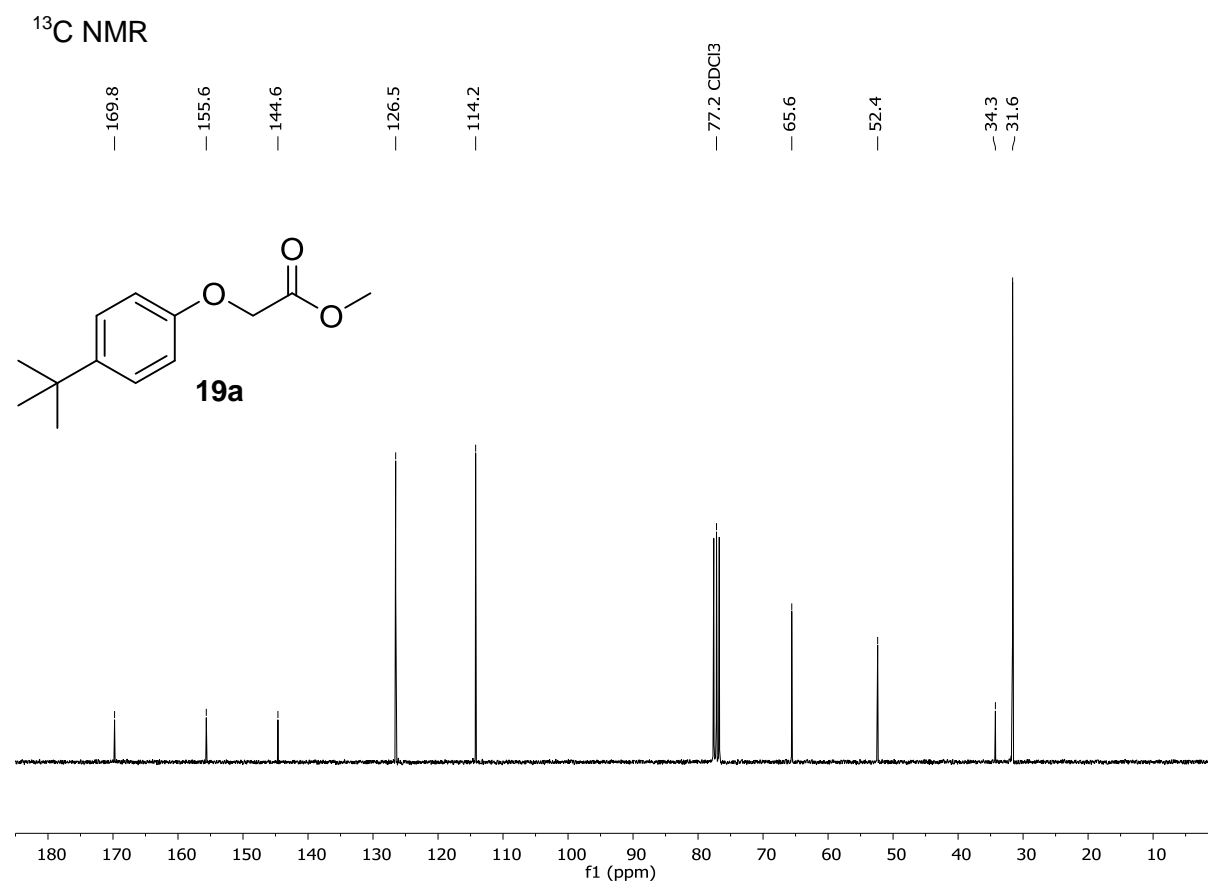
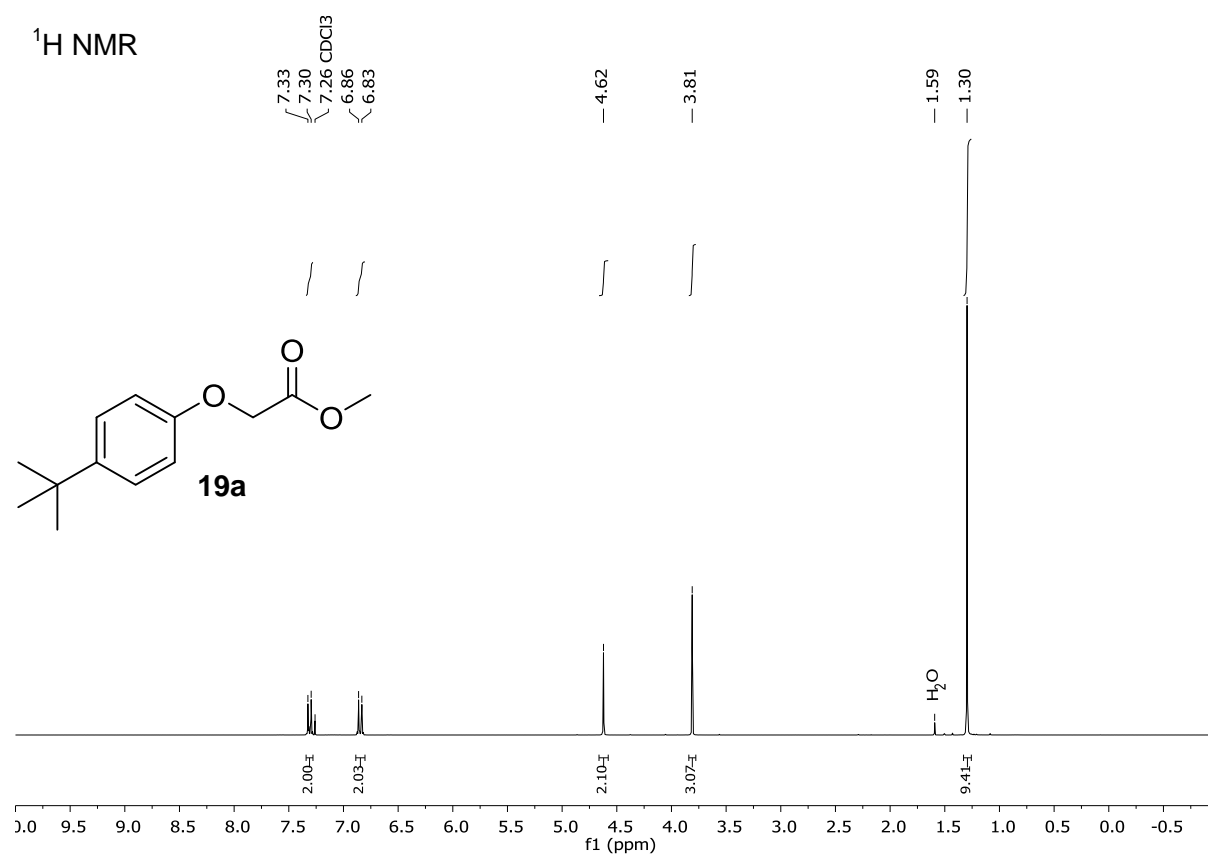
Preparation according to general protocol 2 afforded **14b** (82 mg, 0.27 mmol, 54%) as colorless solid. The product was purified by crystallization due to slow addition of water to a solution of DMF. $^1\text{H NMR}$ (400 MHz, DMSO-d_6) $\delta = 2.27$ (s, 3H), 2.32 (s, 3H), 4.50 (s, 2H), 6.89 (s, 1H), 10.34 (s, 1H). $^{13}\text{C NMR}$ (101 MHz, DMSO-d_6) $\delta = 23.6, 29.0, 66.7, 100.6, 115.3, 123.8, 127.7, 135.8, 144.0, 165.6$. mp: 270.0–270.6 °C (decomposition), crystallized

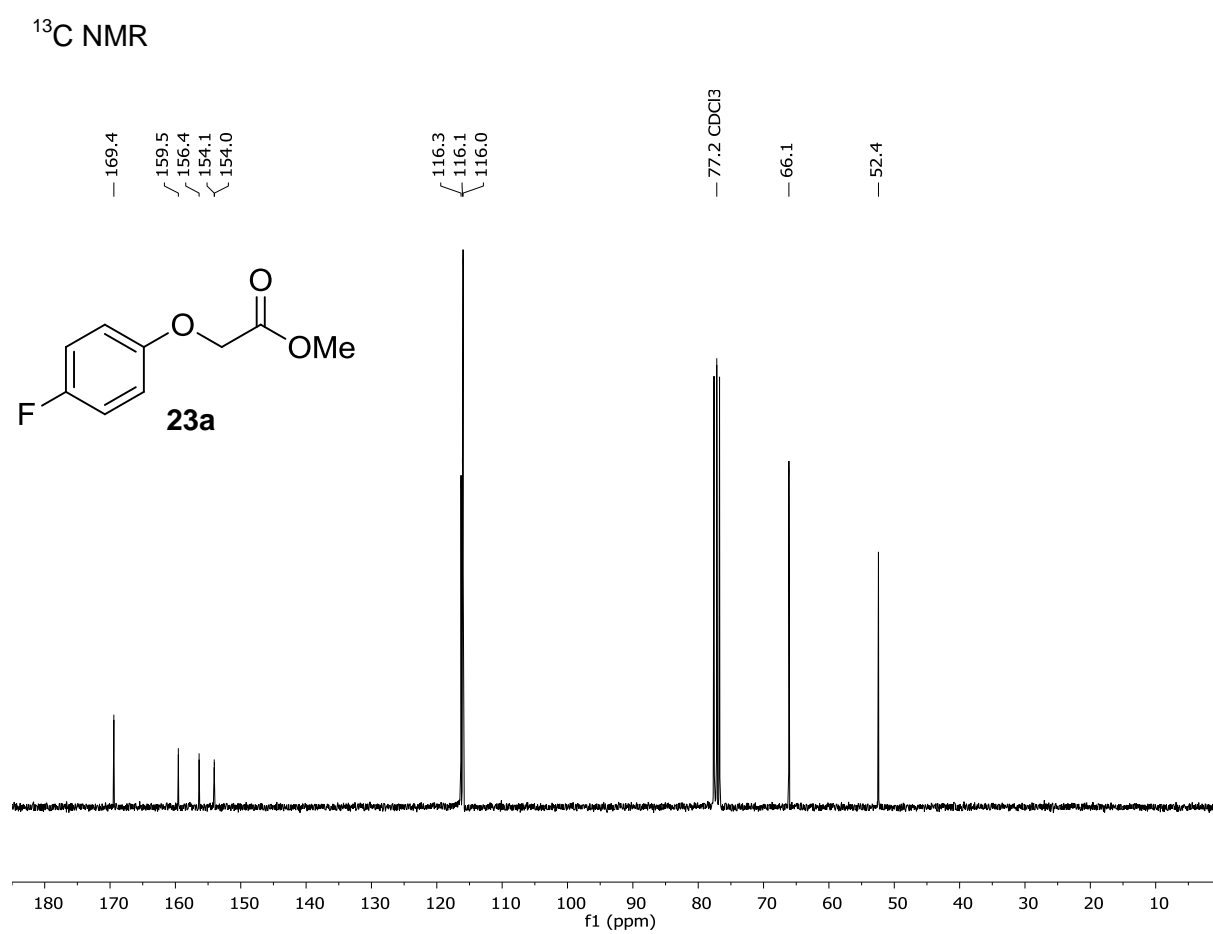
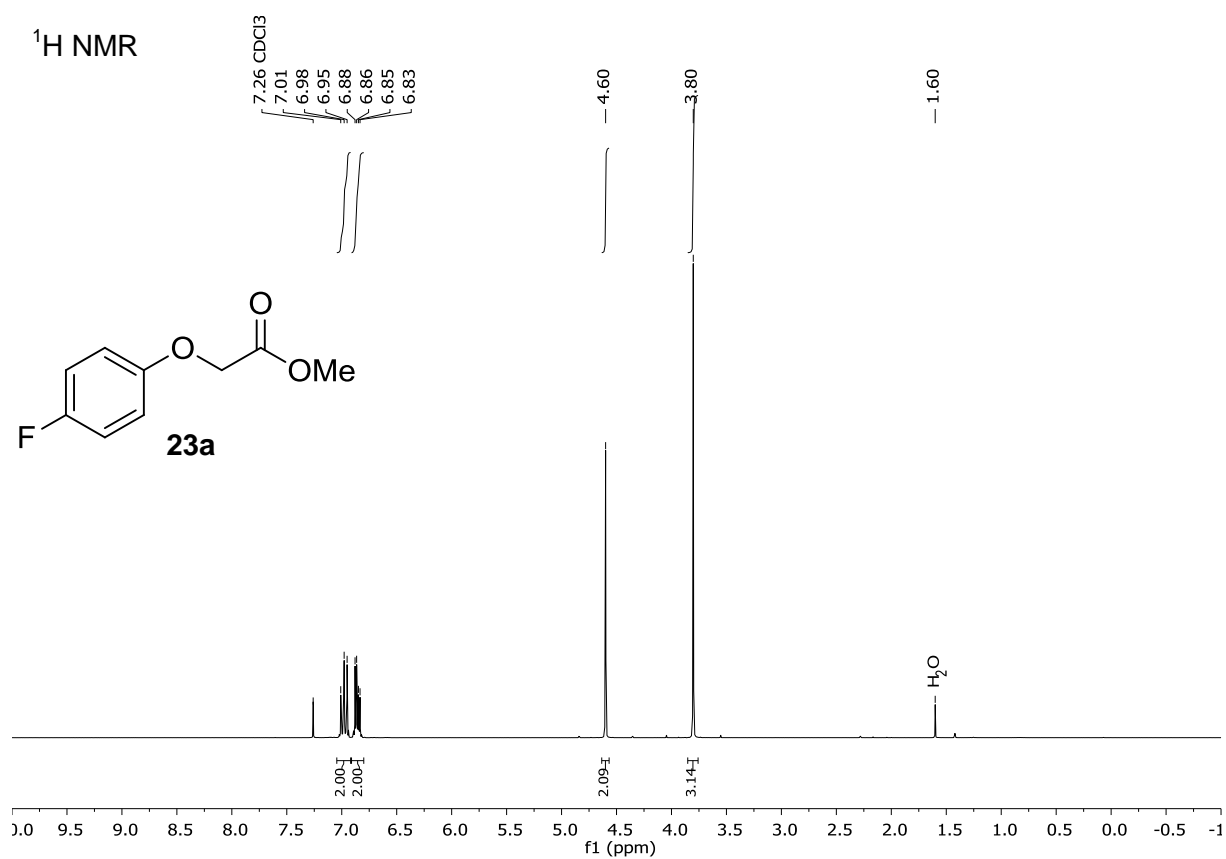
from methanol. HRMS (m/z) for [M+H] $C_{10}H_{11}INO_2$ calc: 303.9835 found: 303.9825.
Elemental analysis for $C_{10}H_{10}INO_2$: calc: C: 39.63%, H: 3.33%, N: 4.62%, found: C: 39.36%,
H: 3.70%, N: 4.58%.

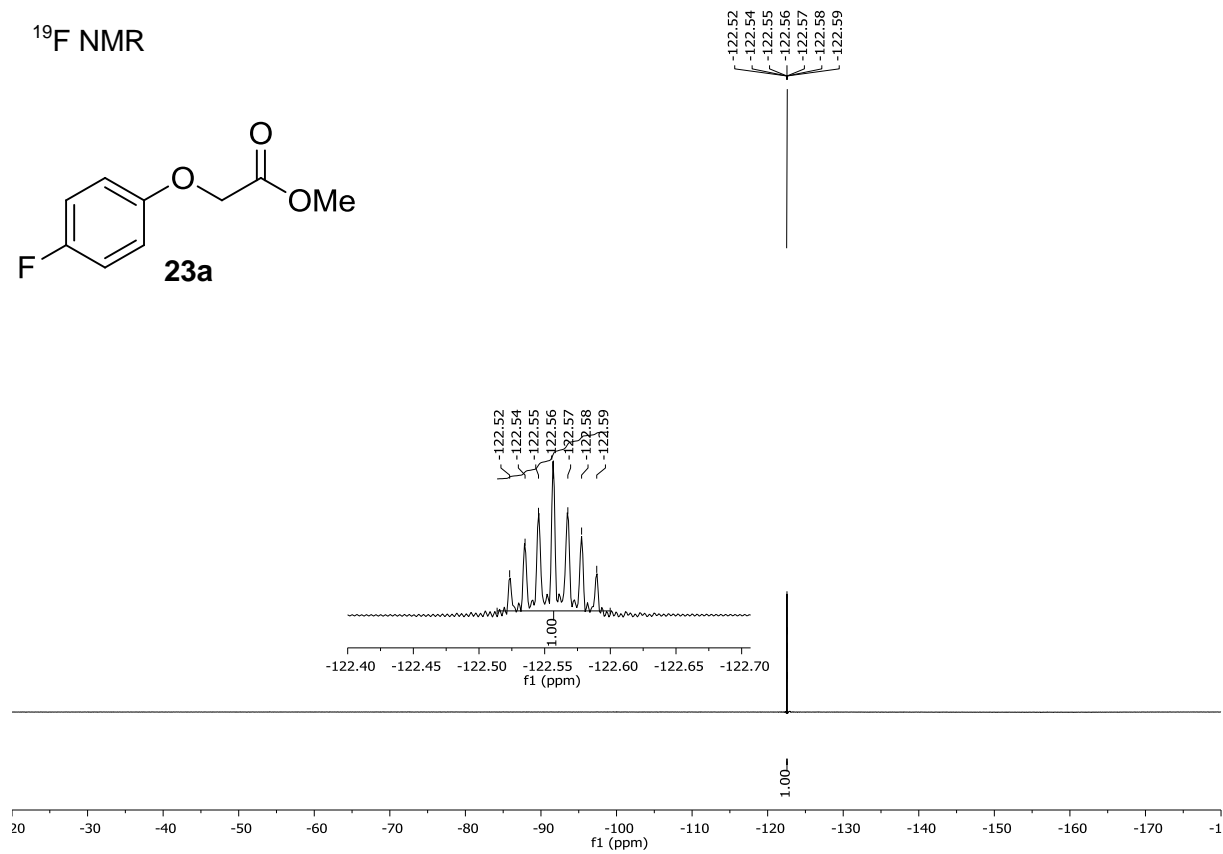
NMR spectra

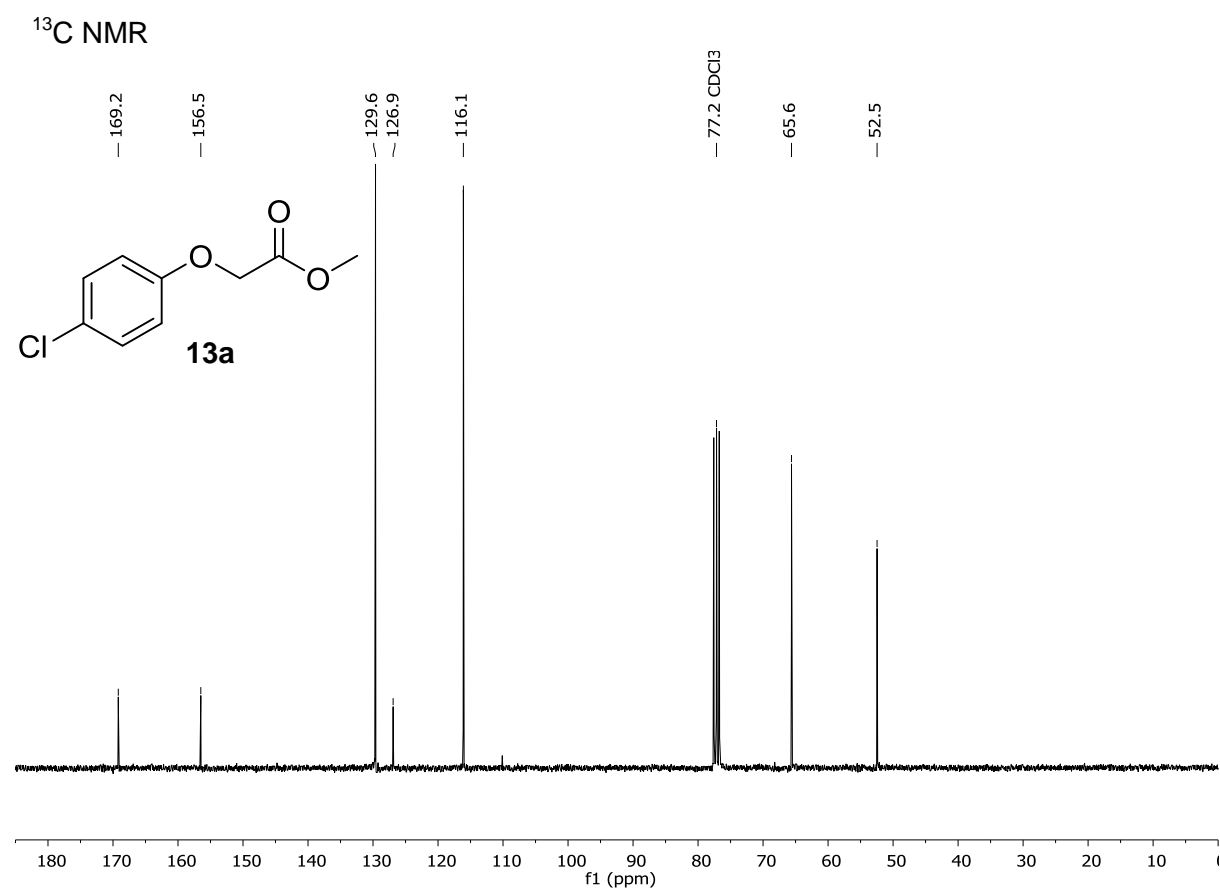
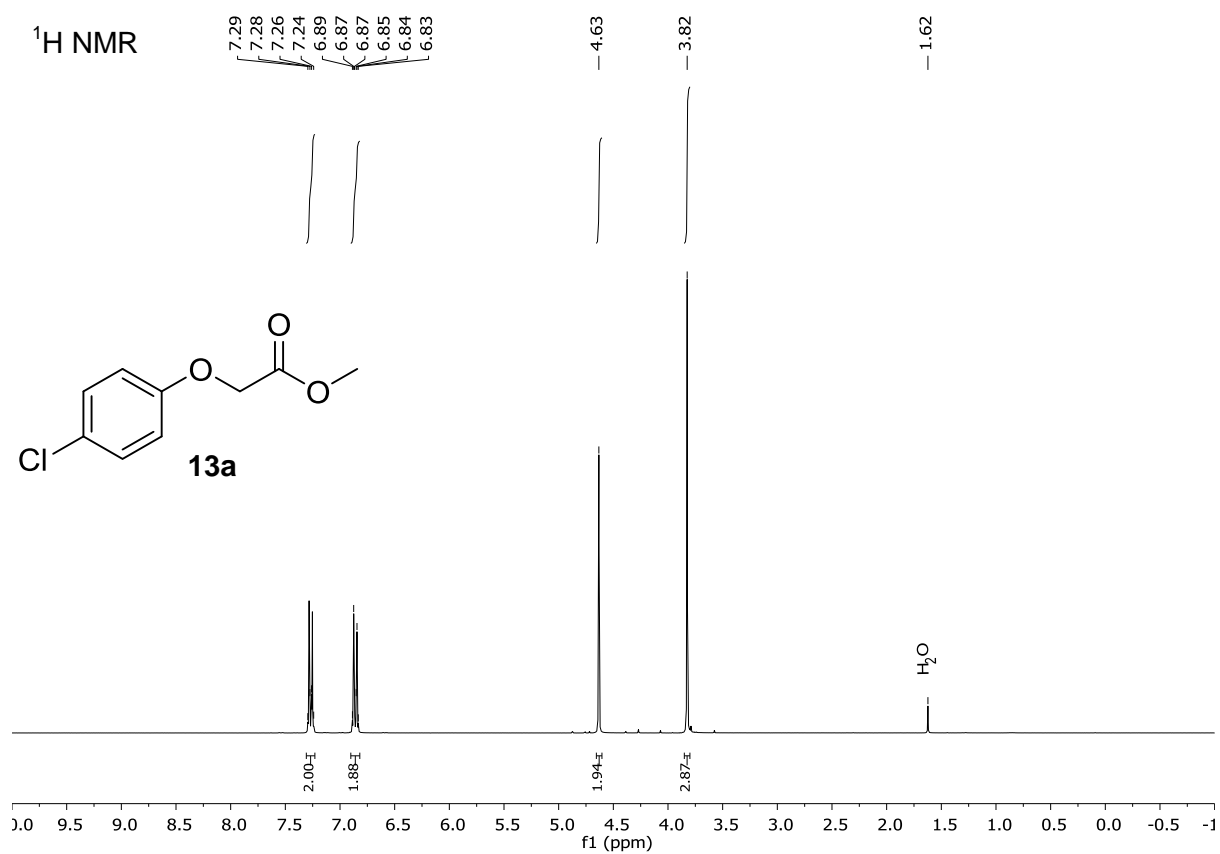


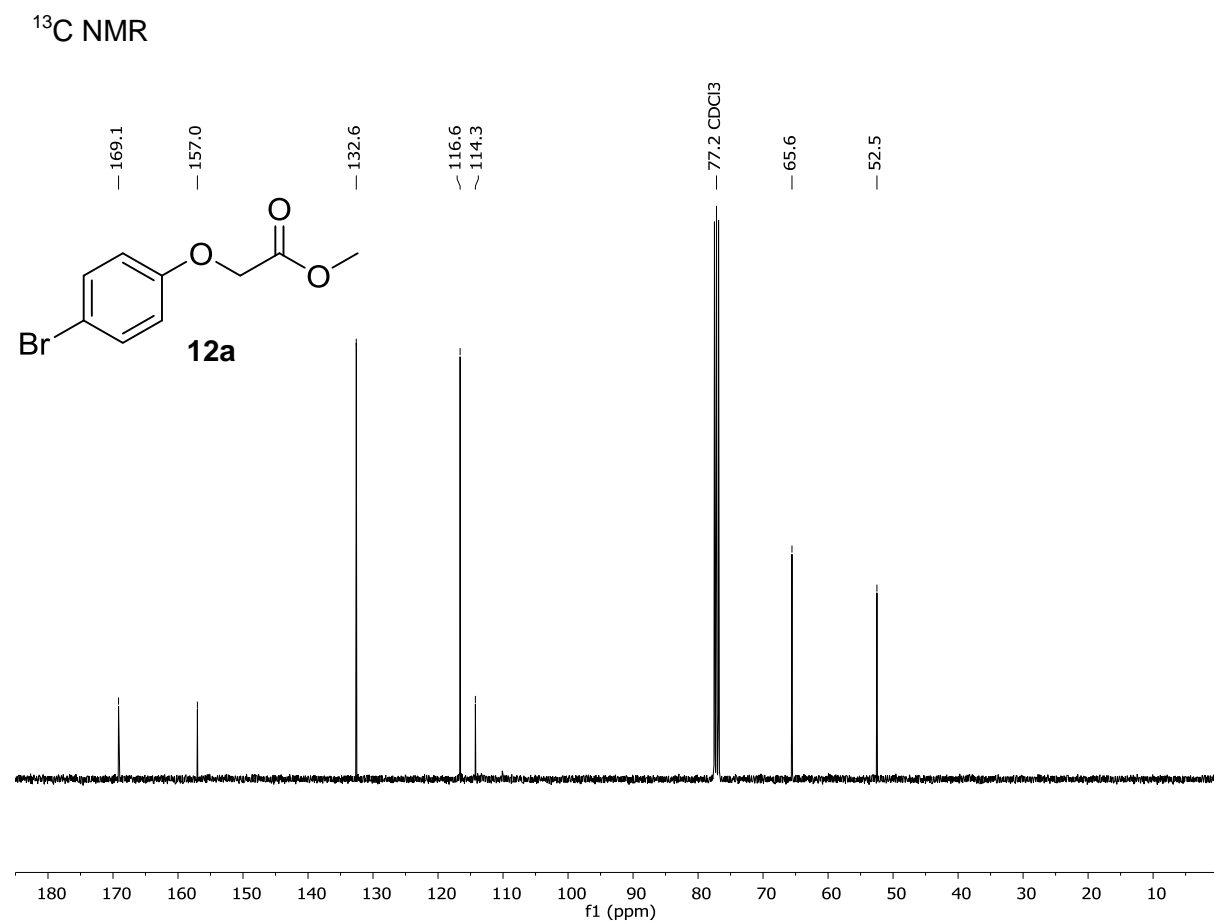
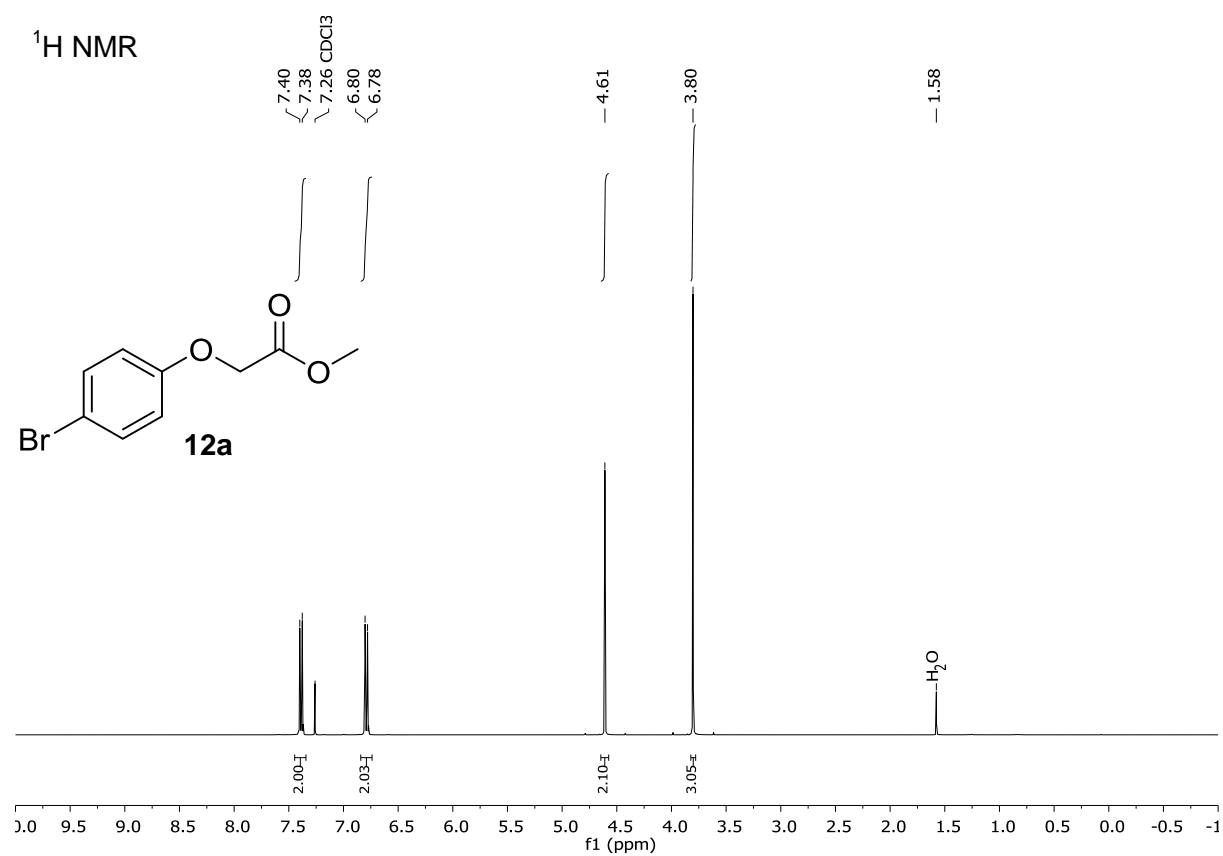


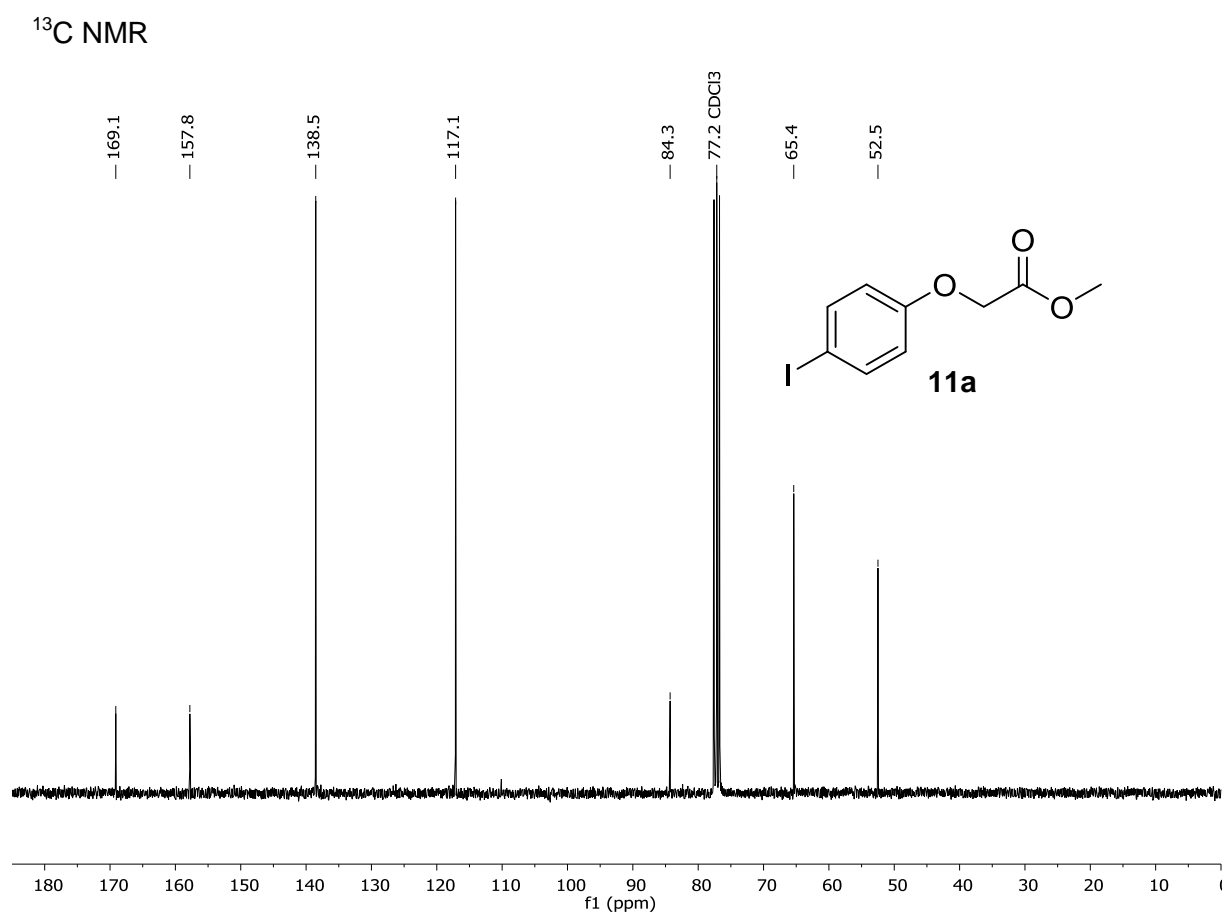
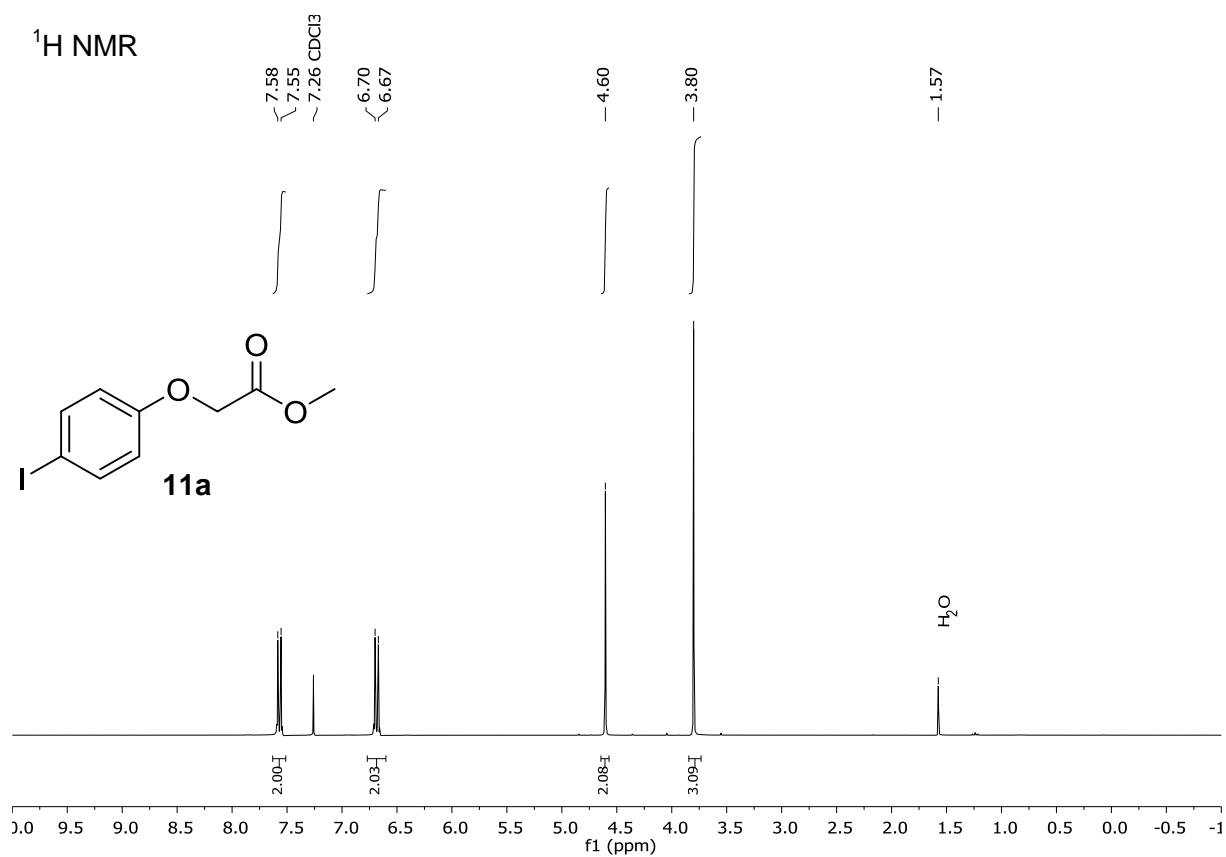


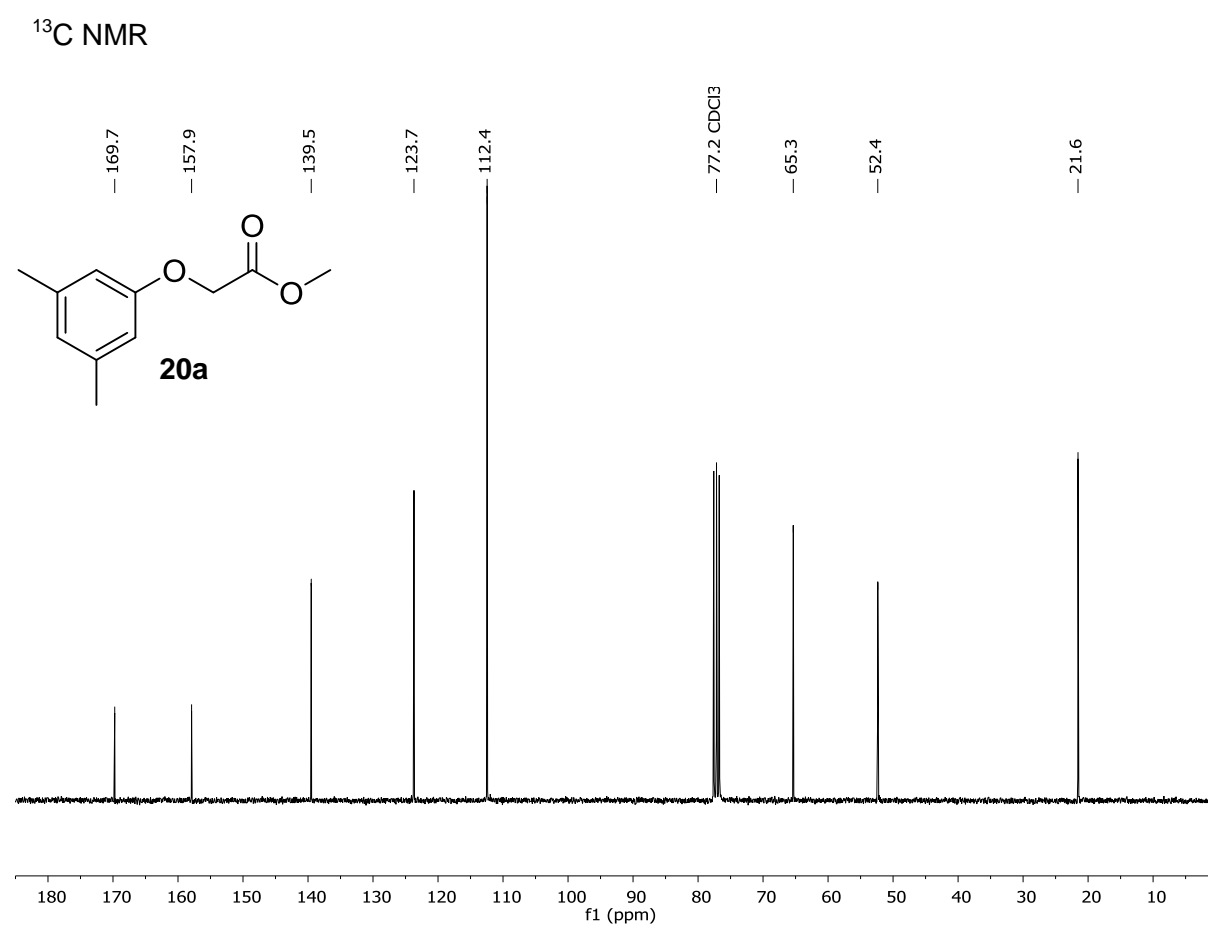
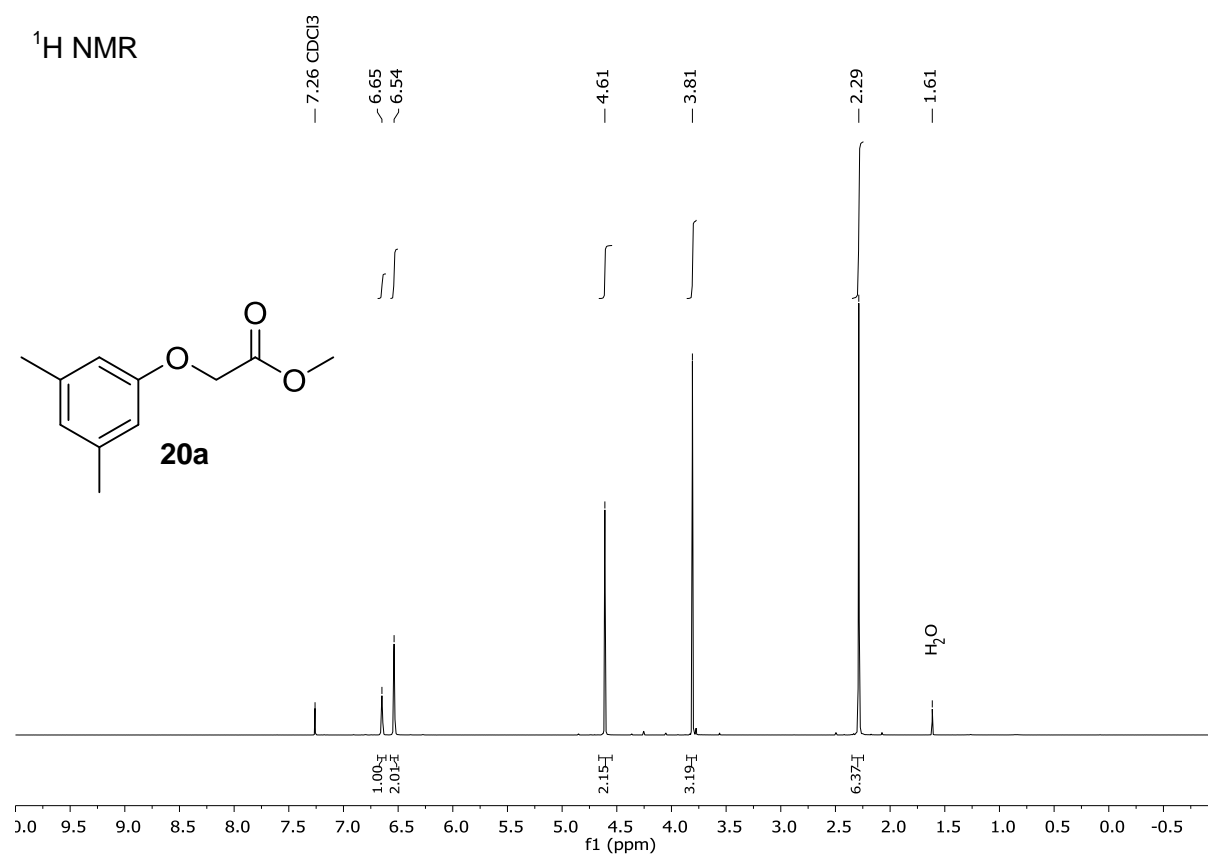


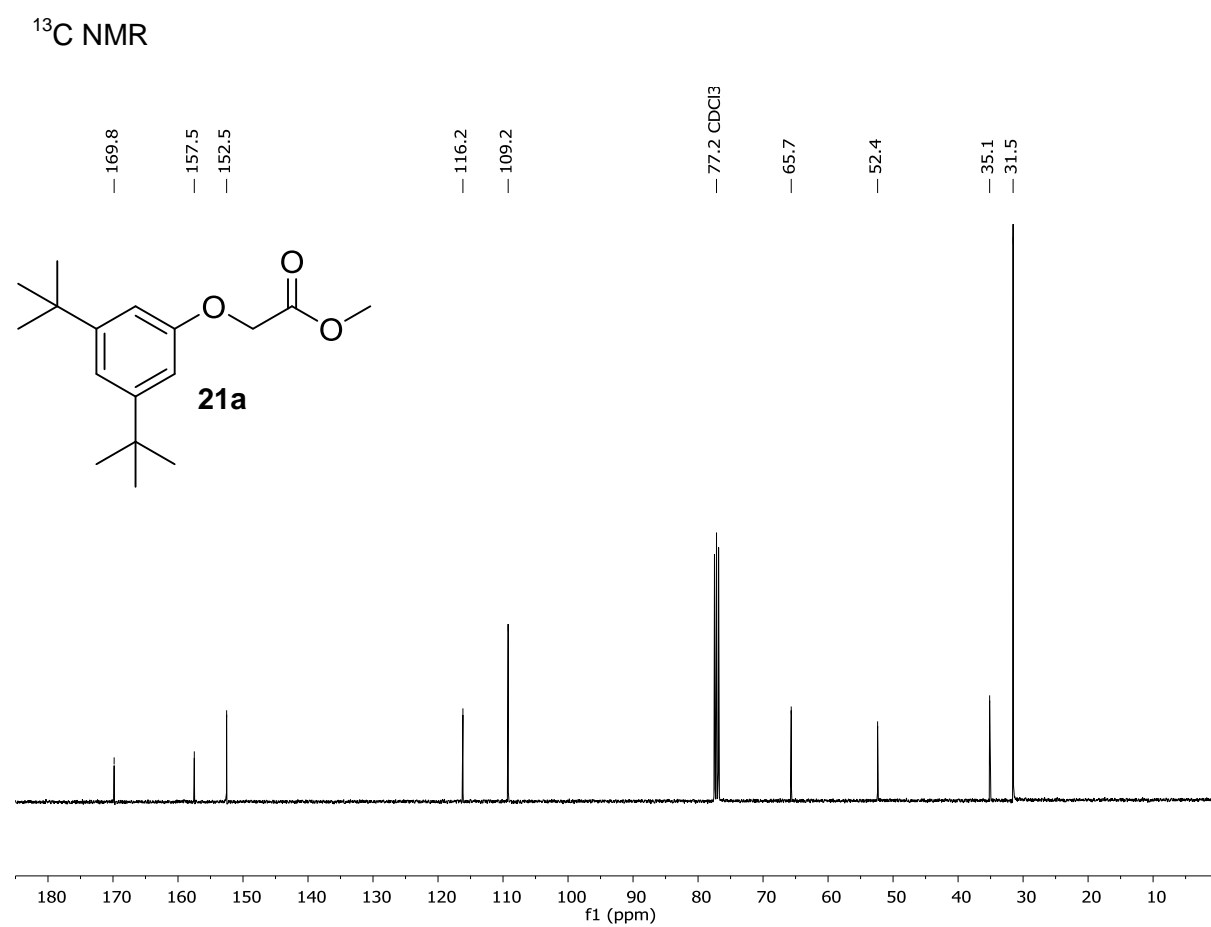
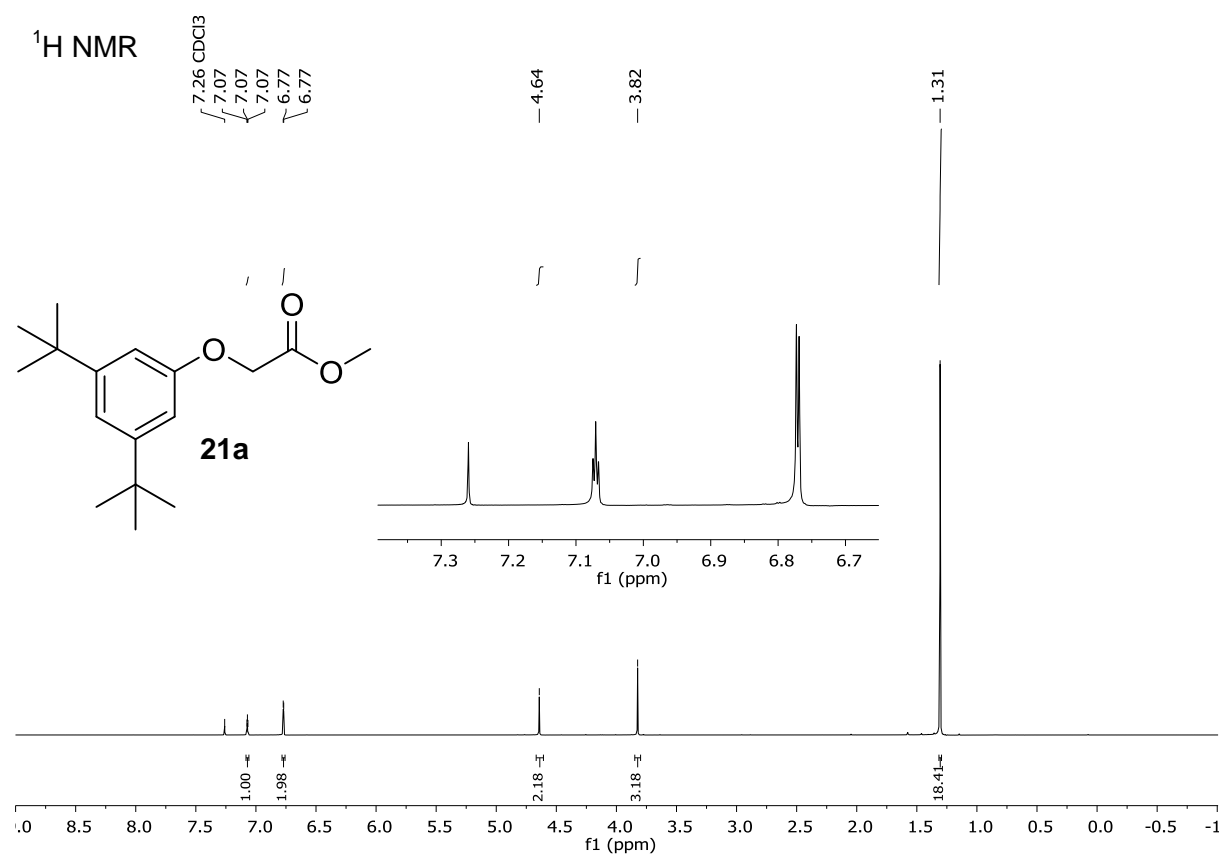


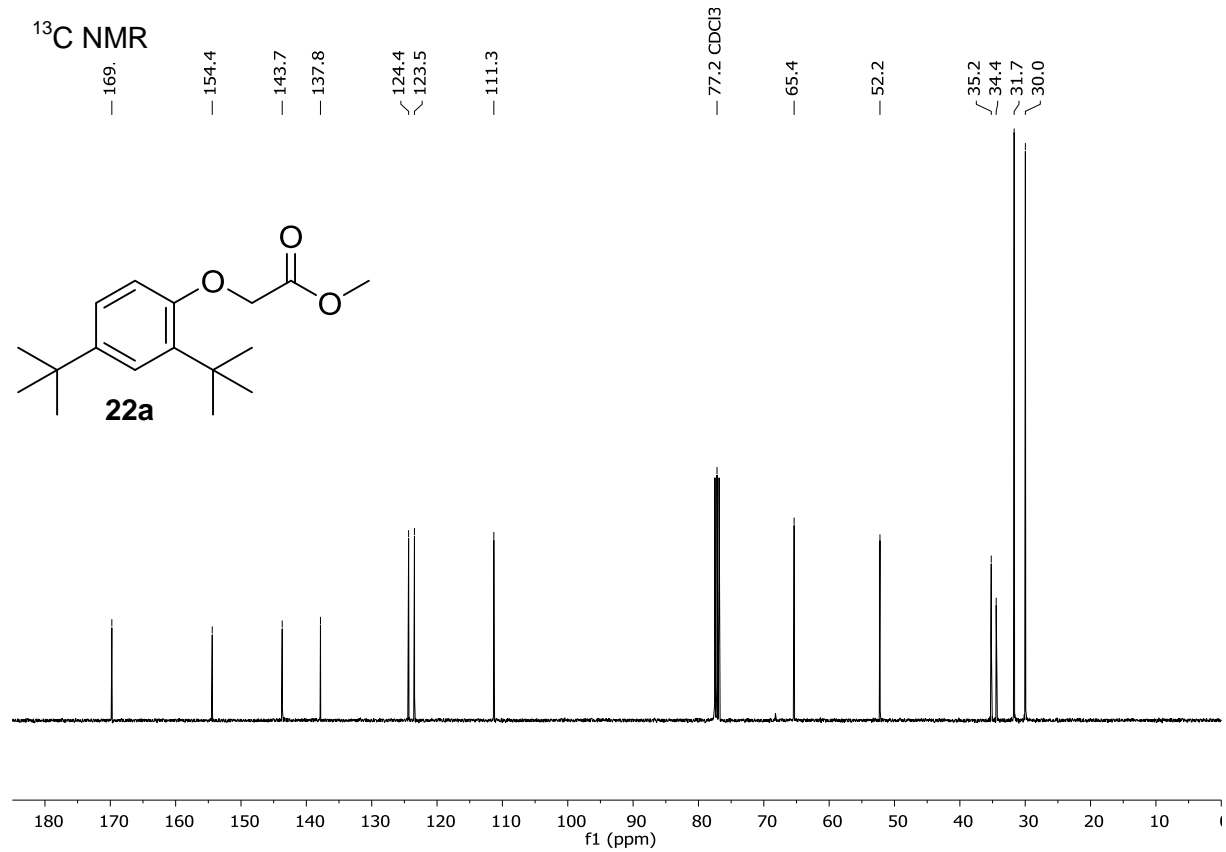
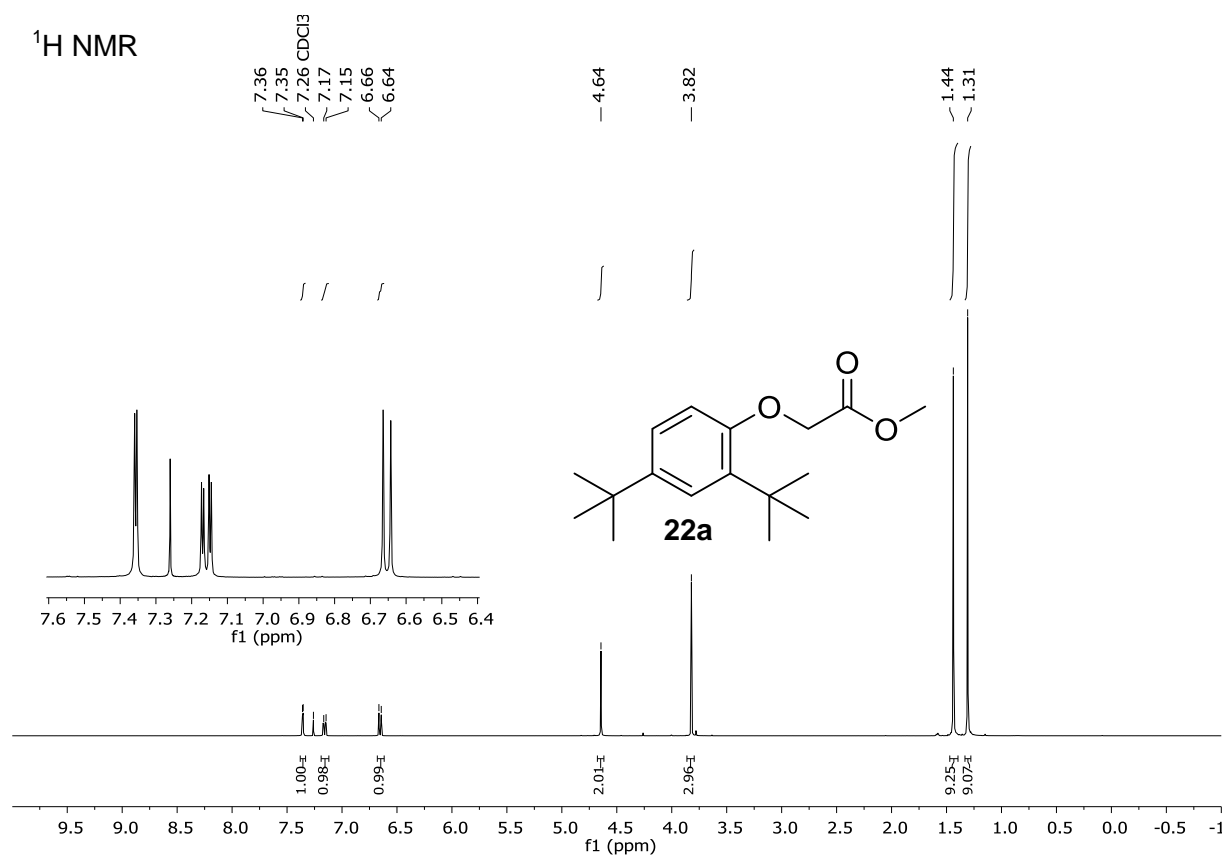


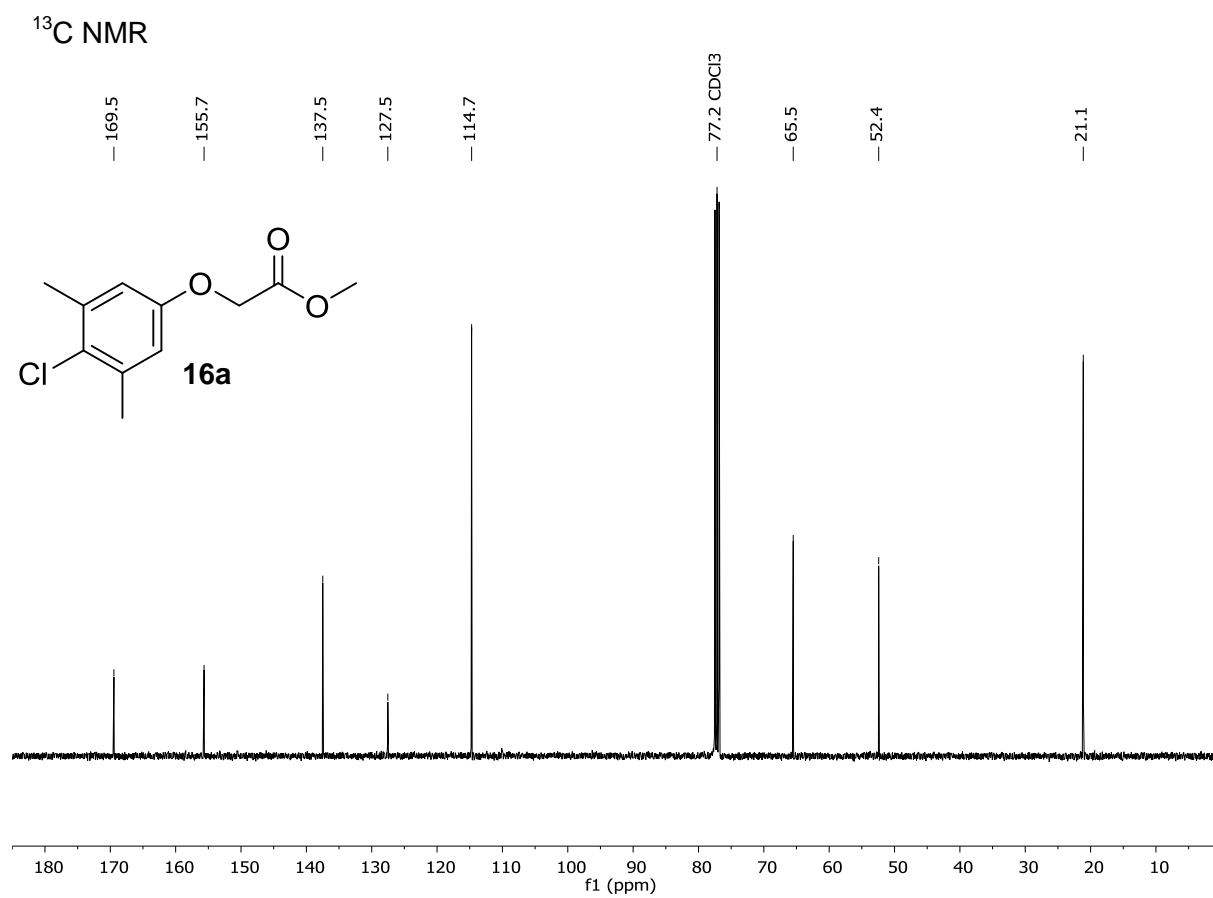
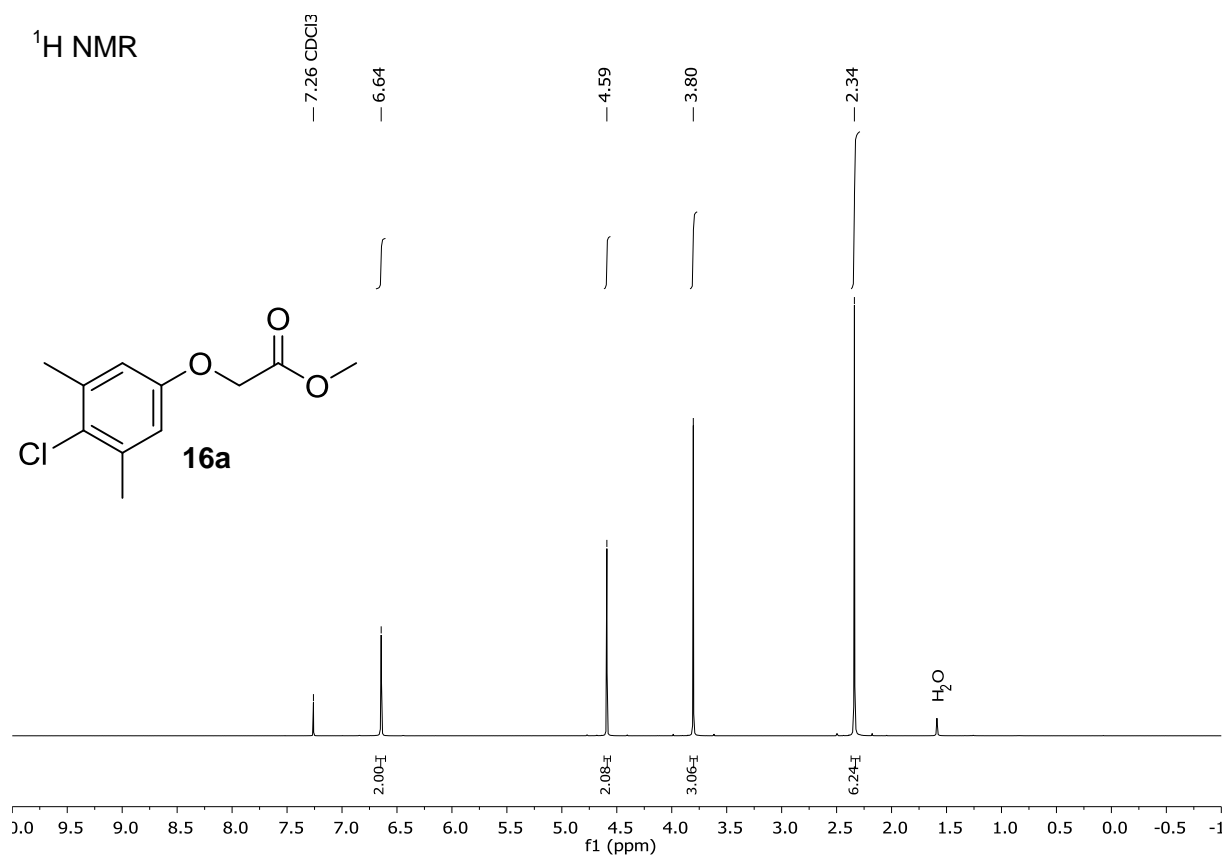


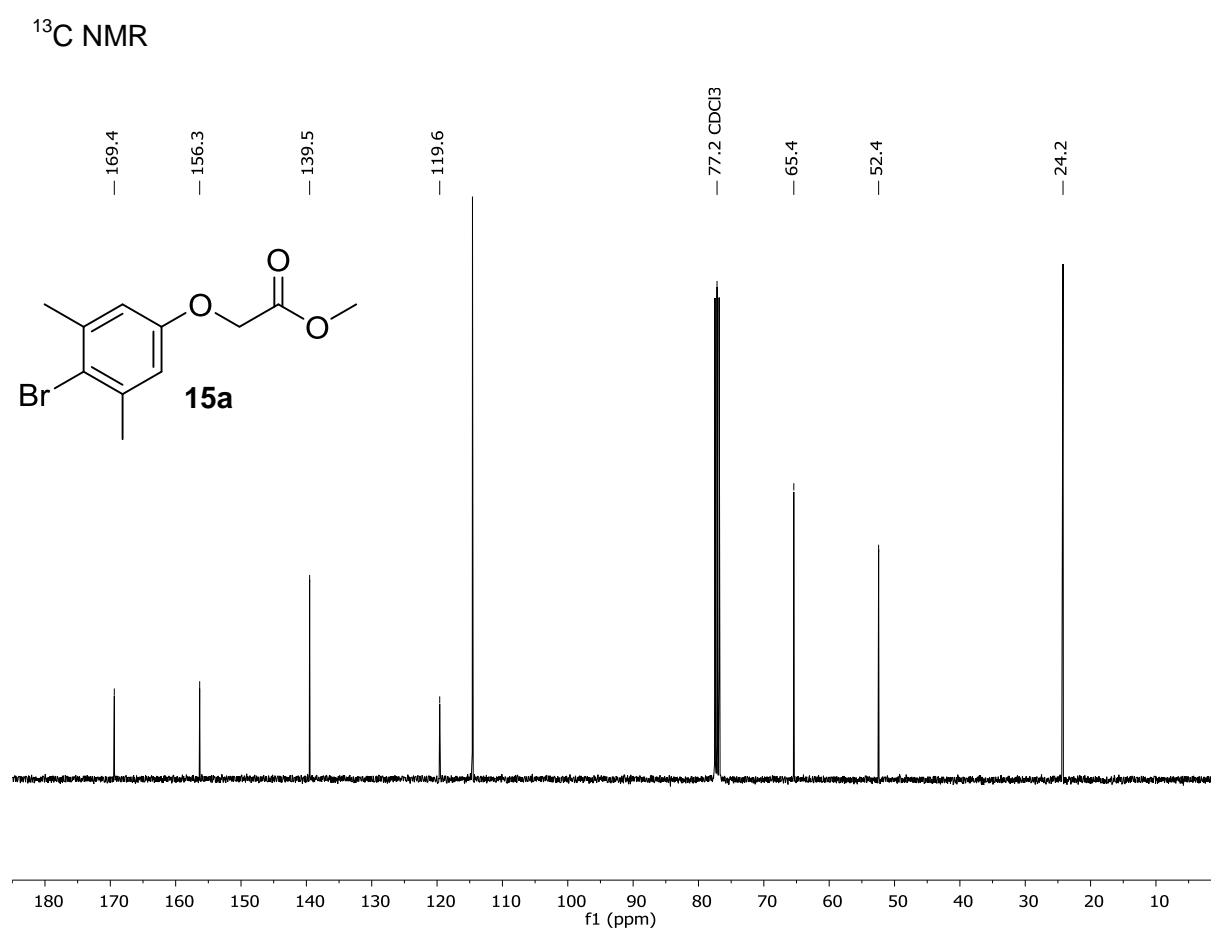
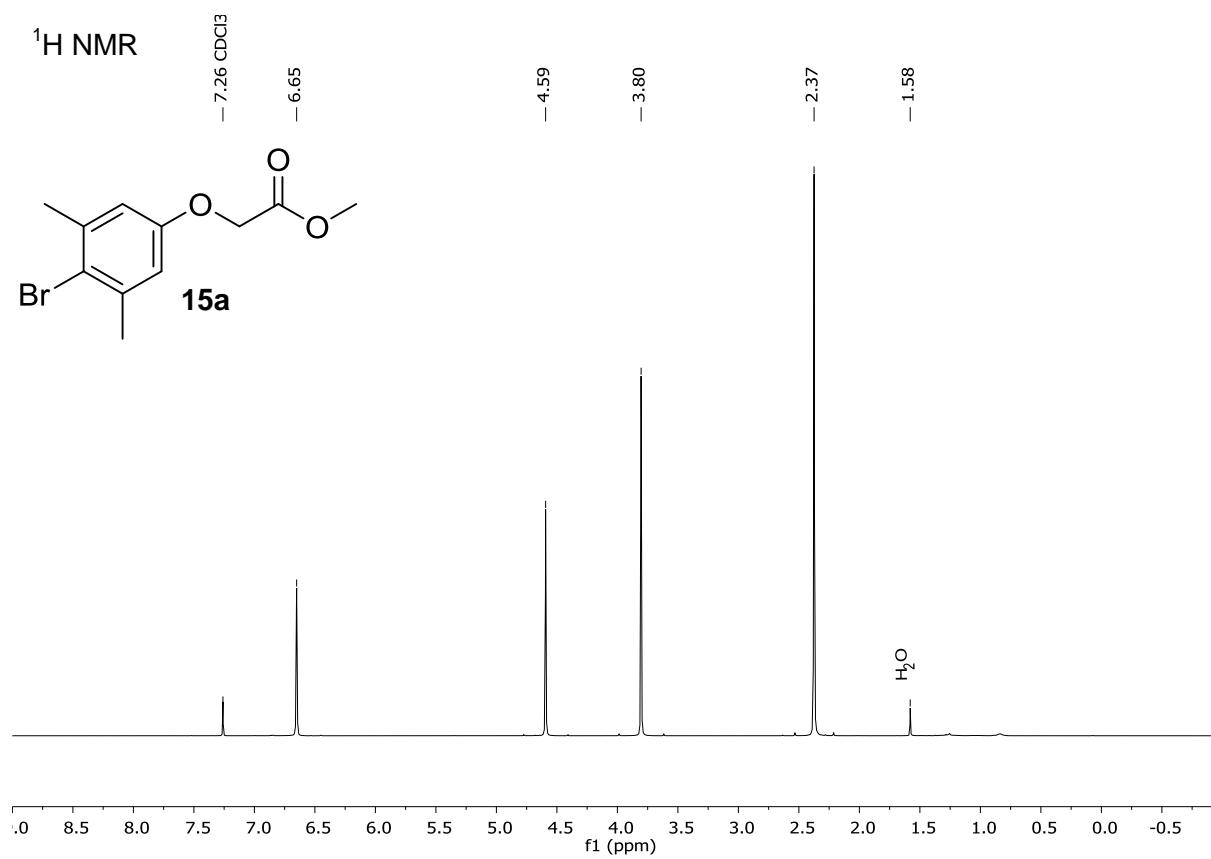


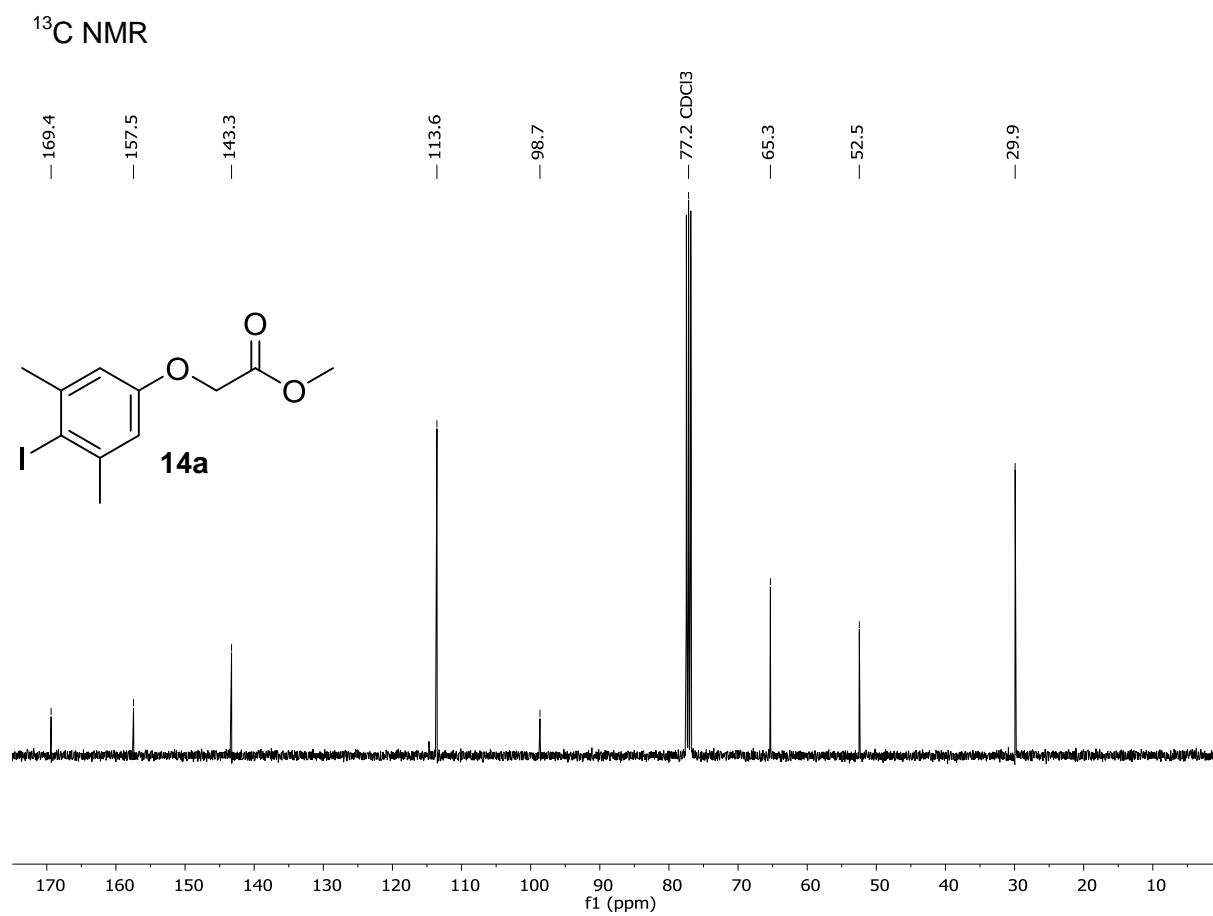
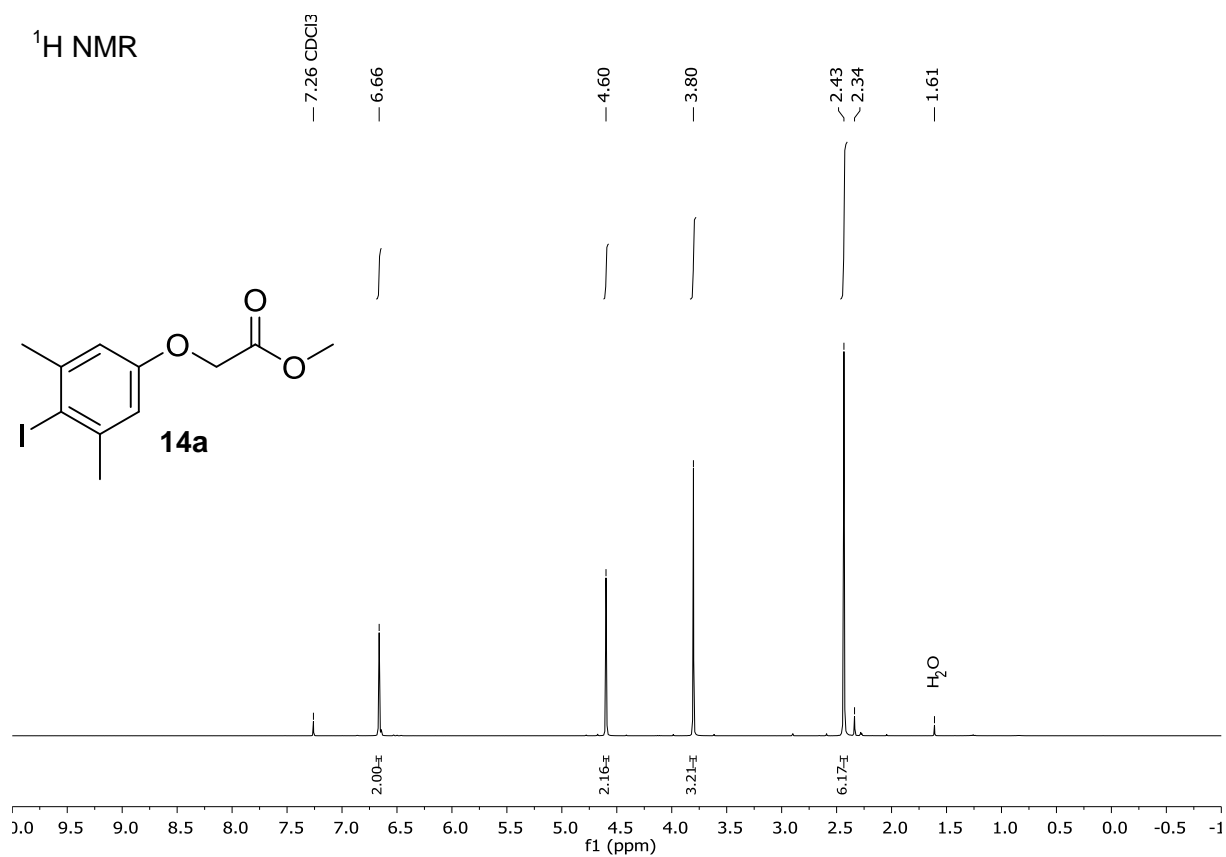


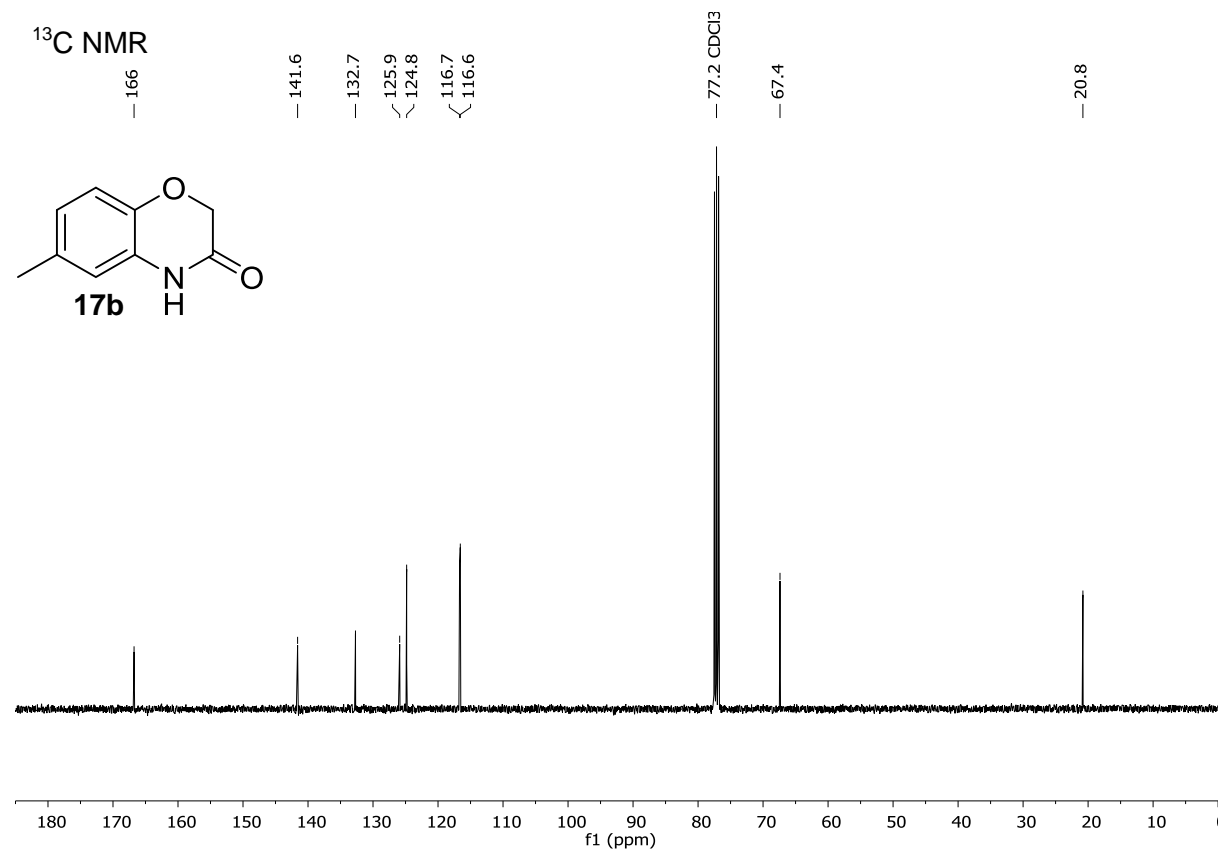
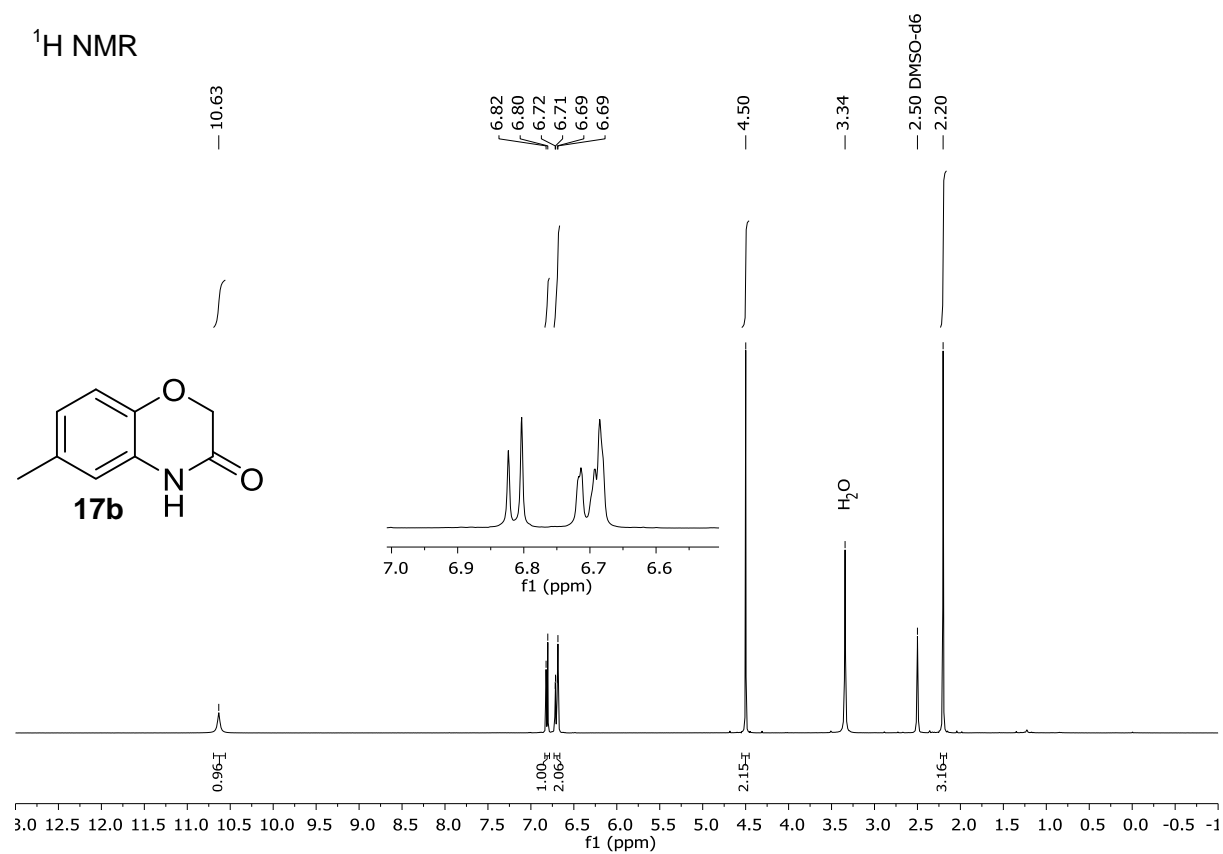


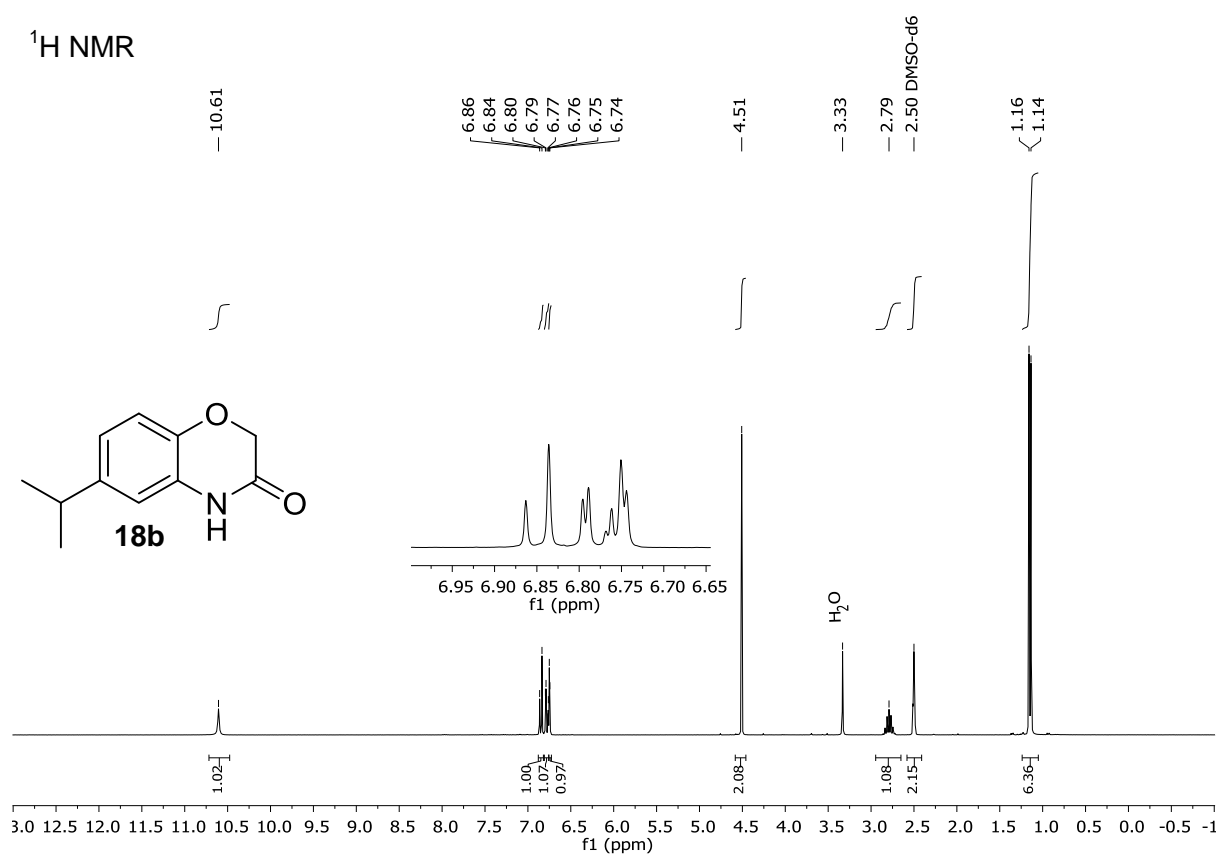
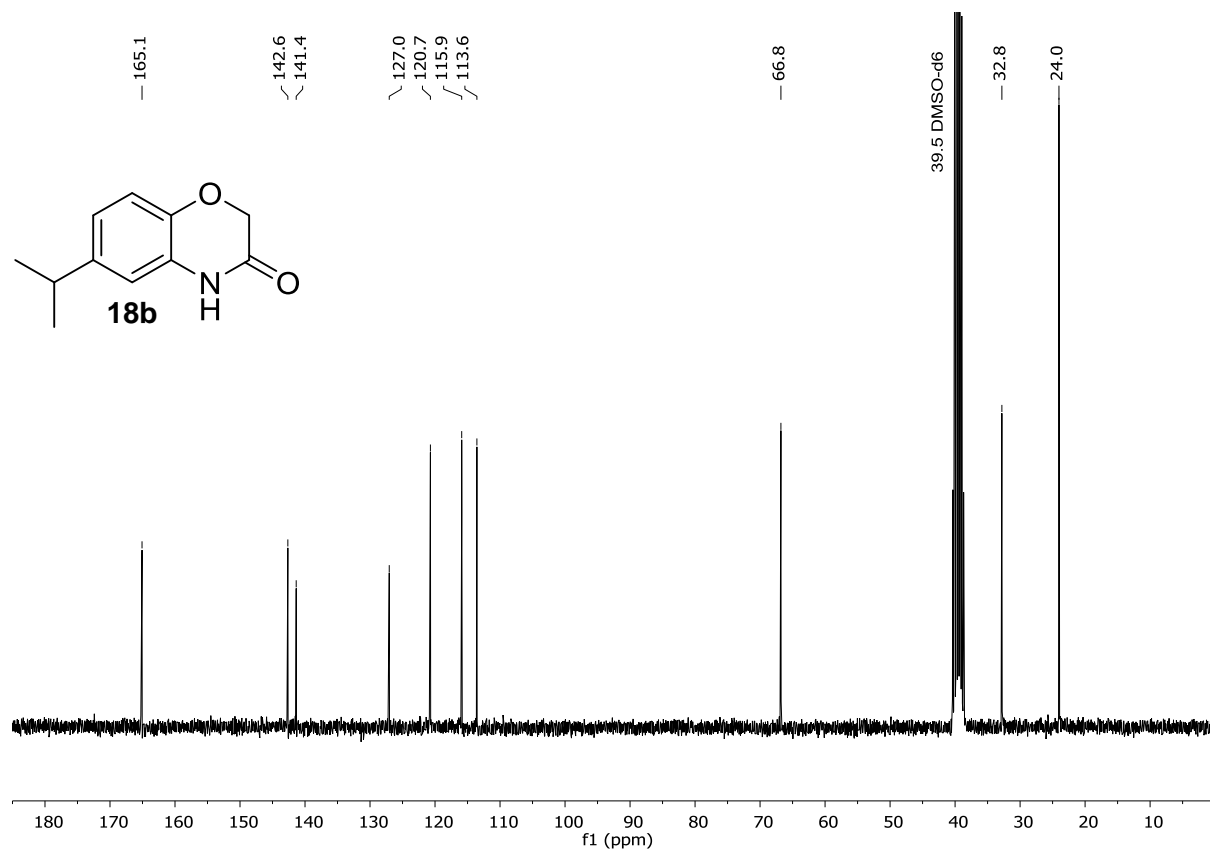


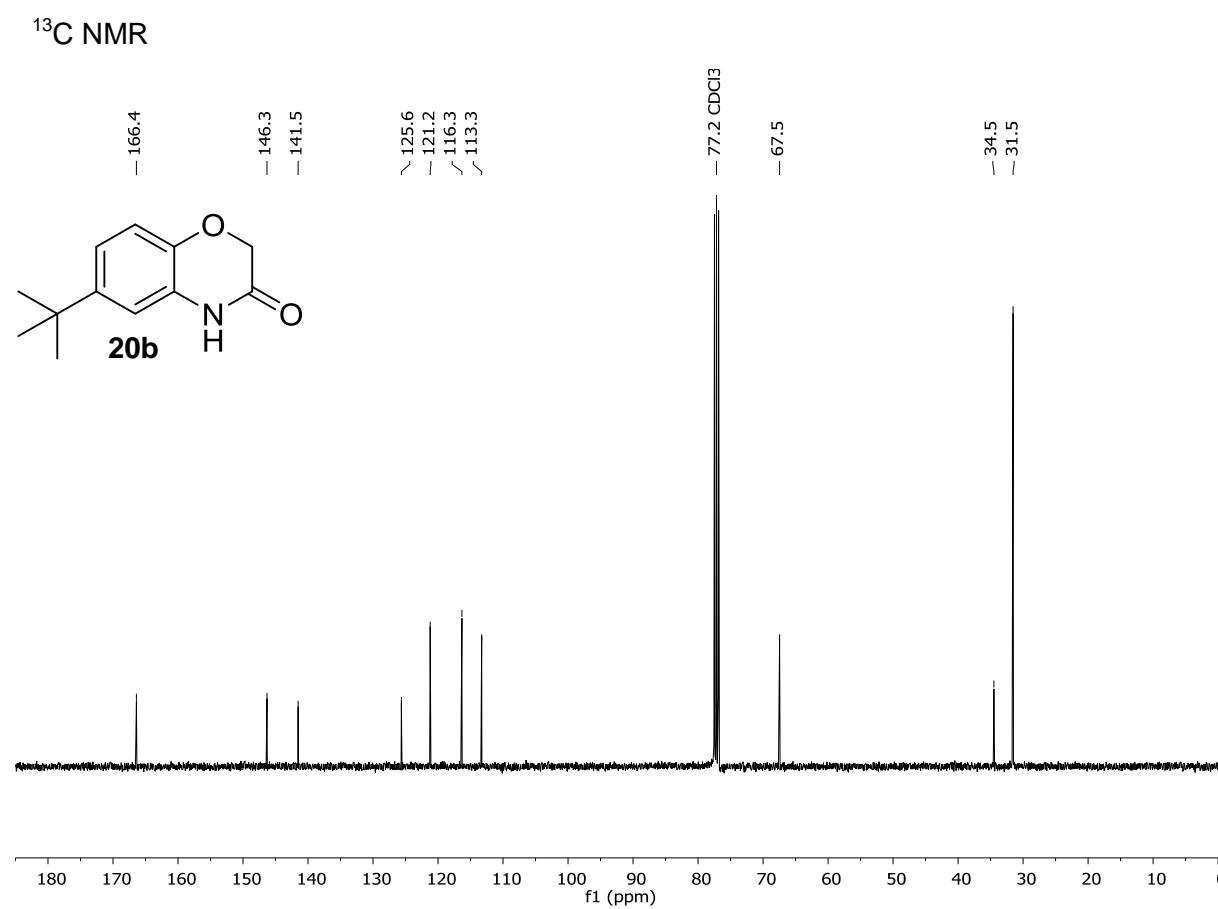
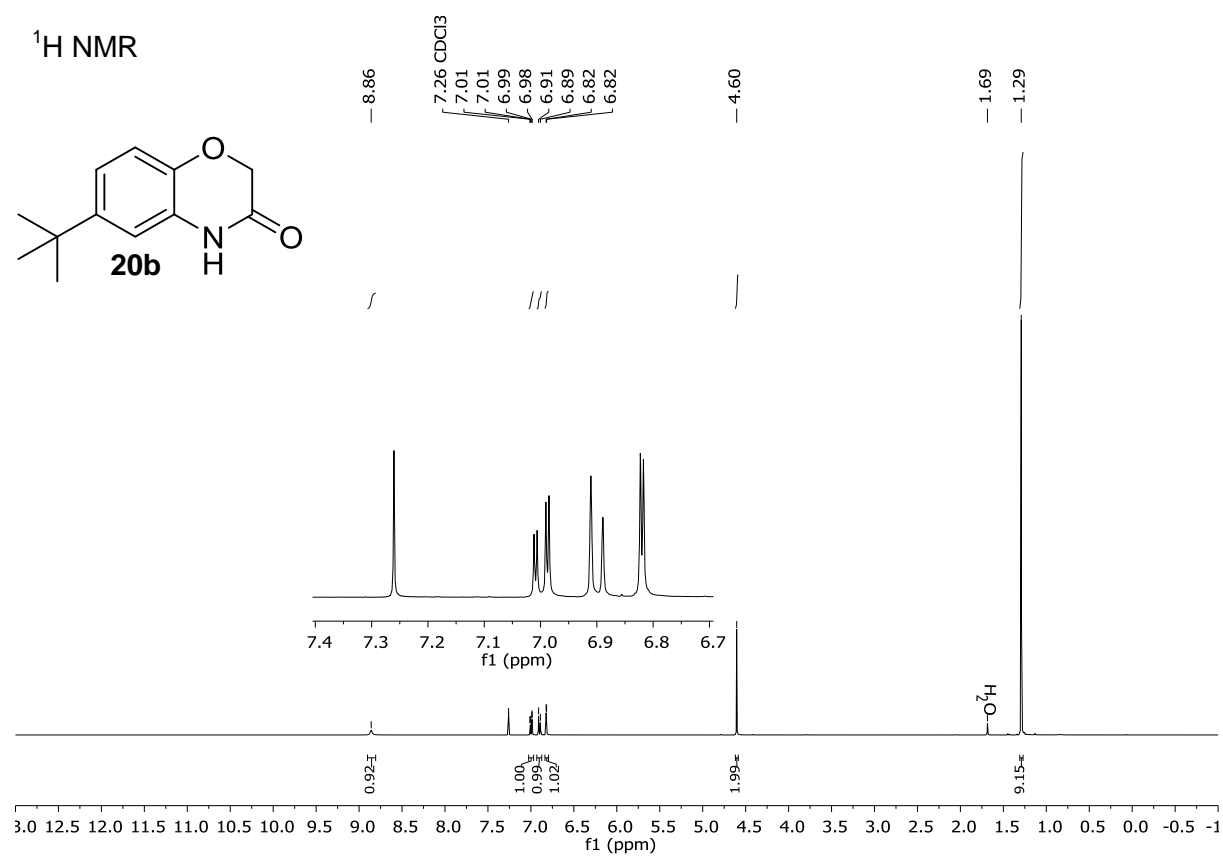


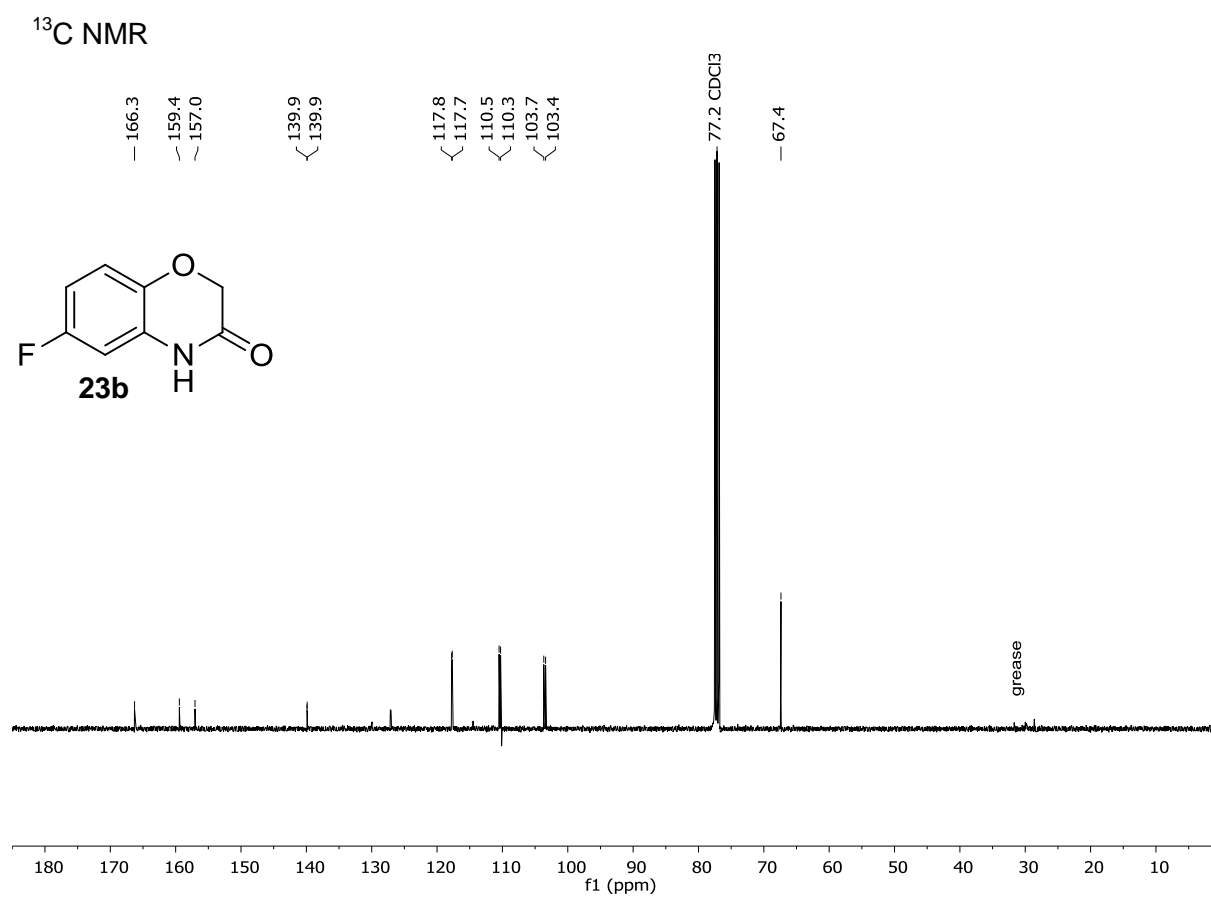
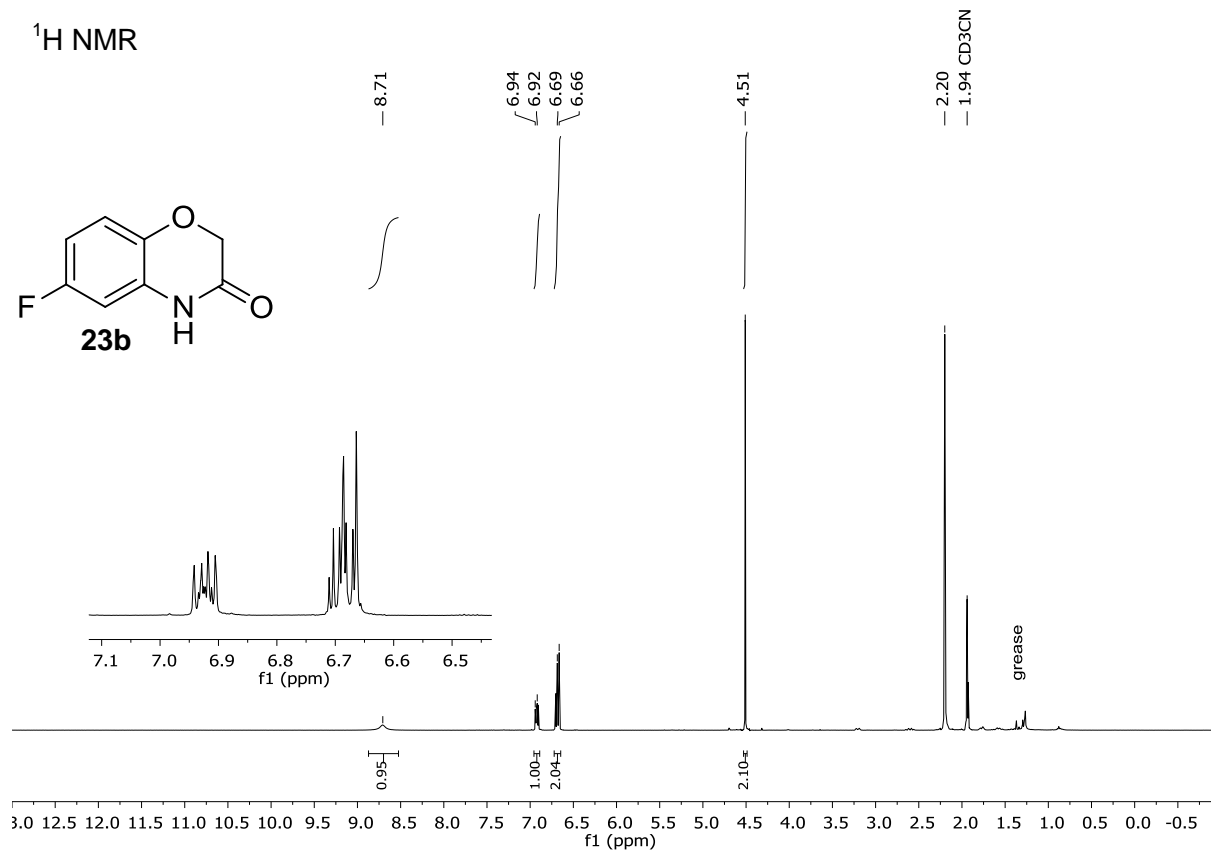






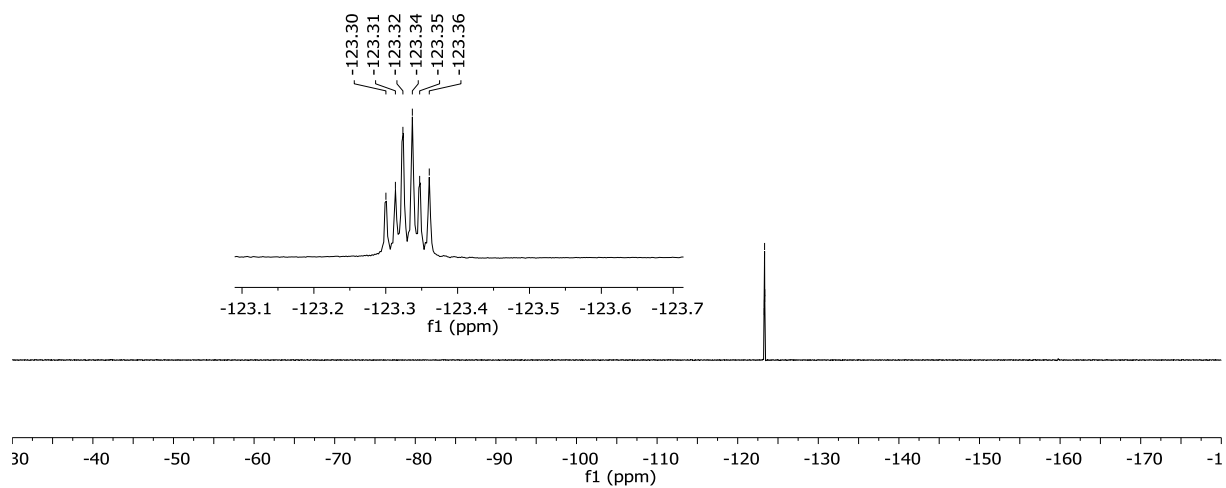
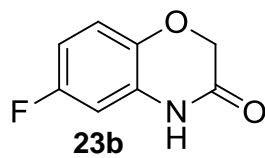
^1H NMR ^{13}C NMR

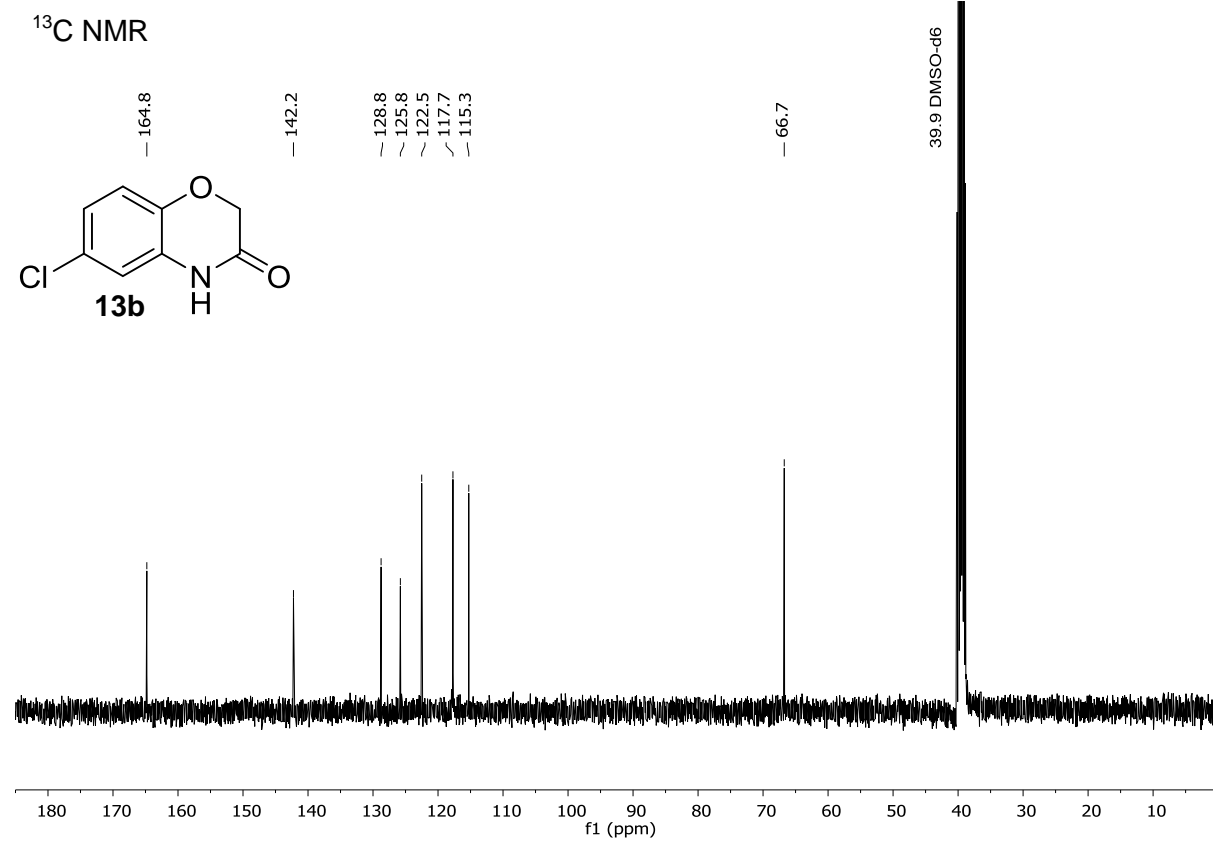
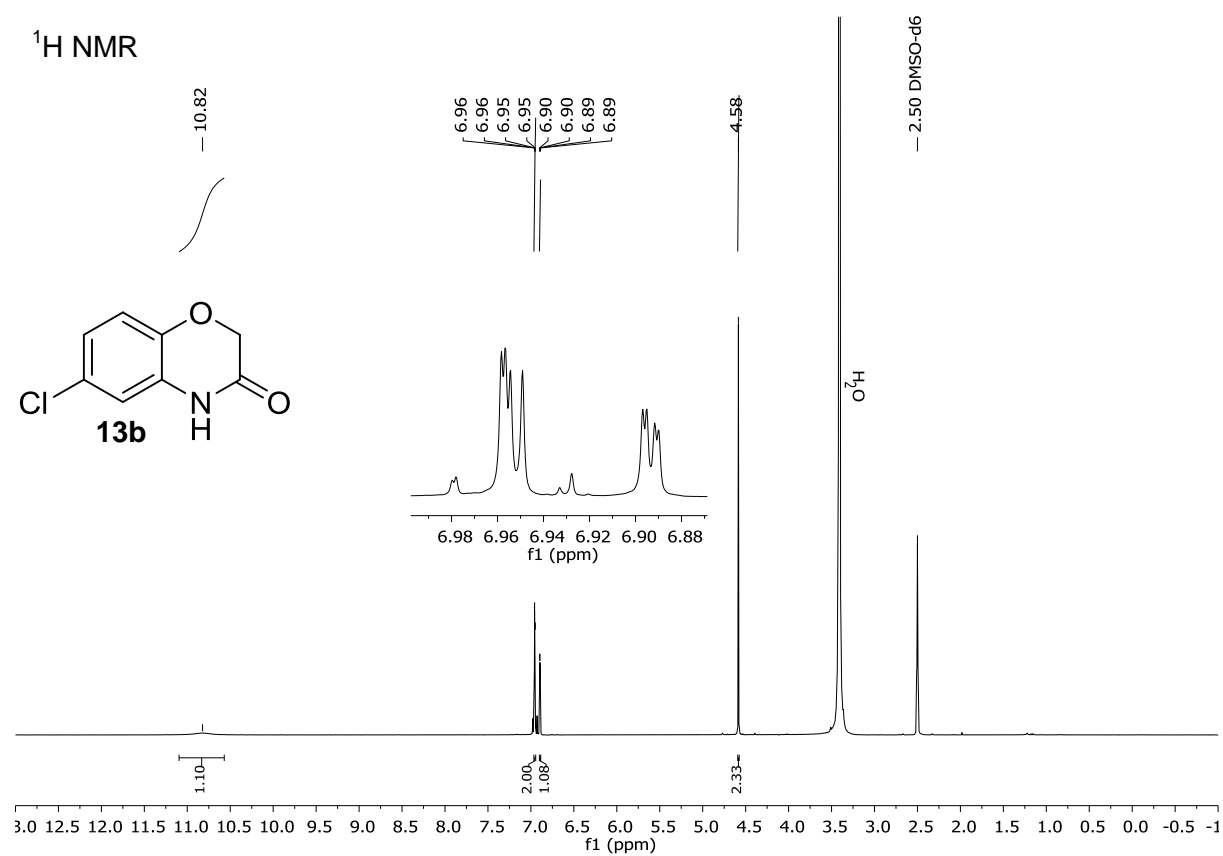


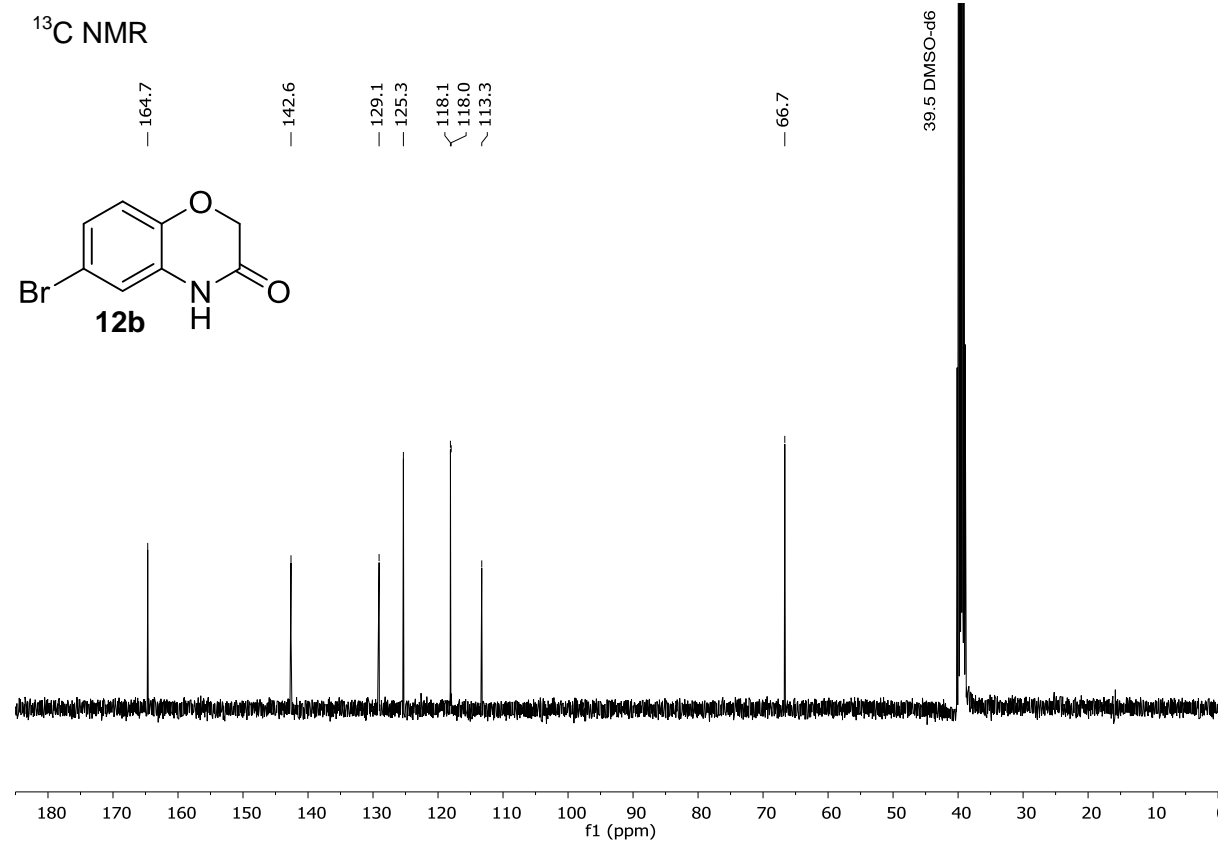
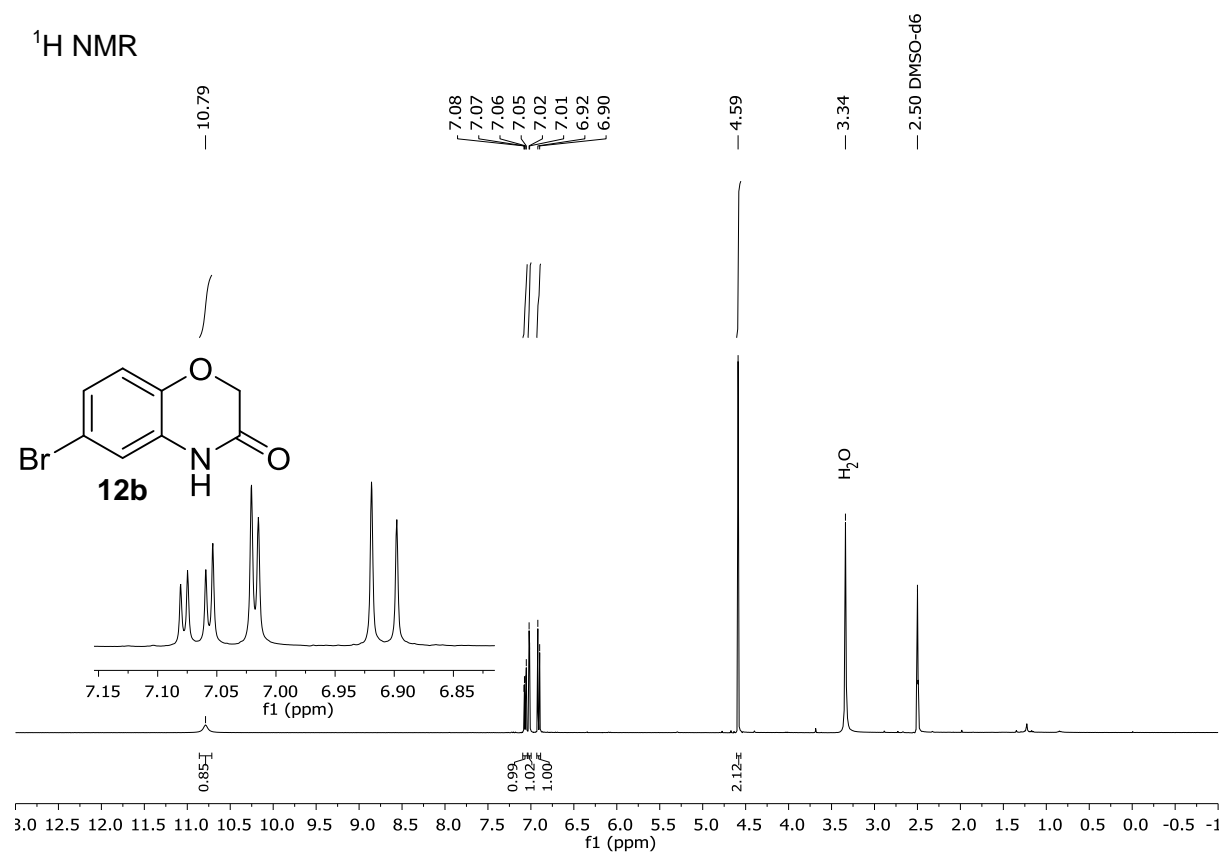


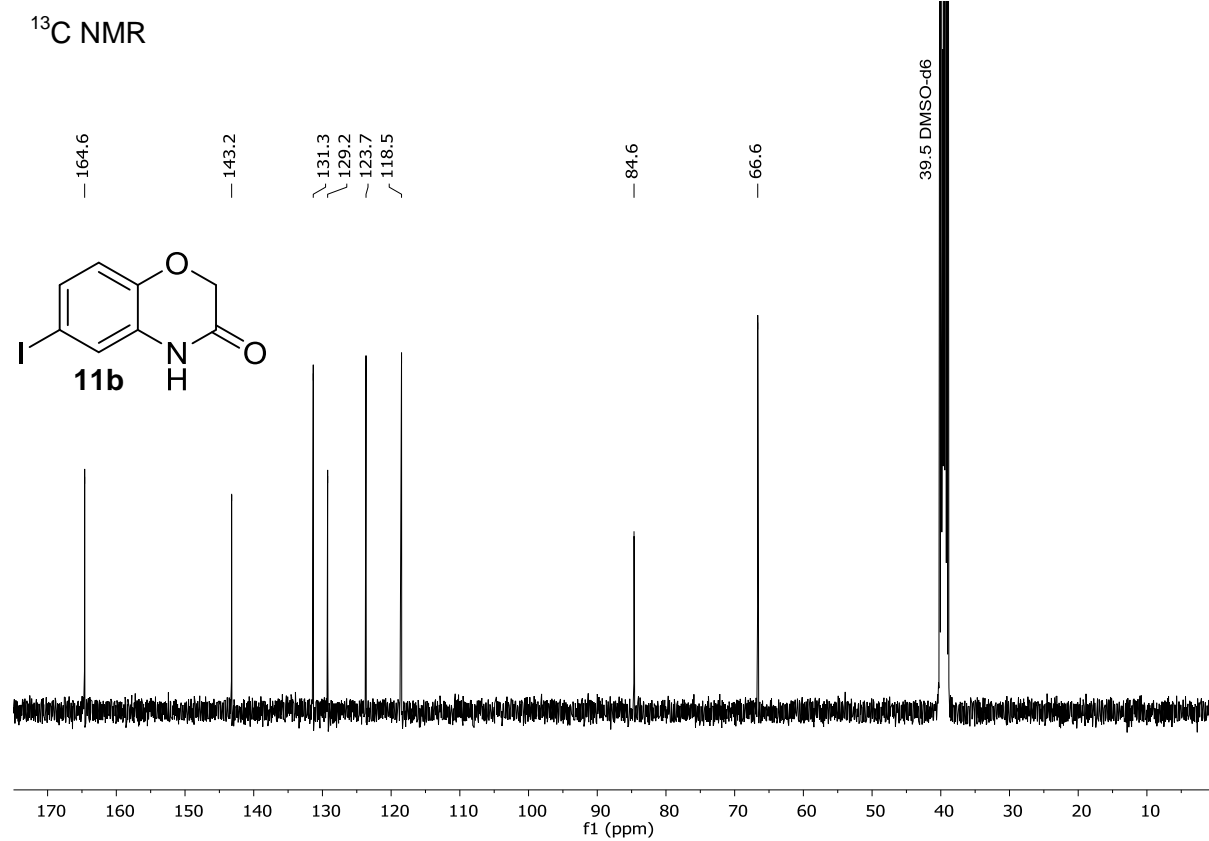
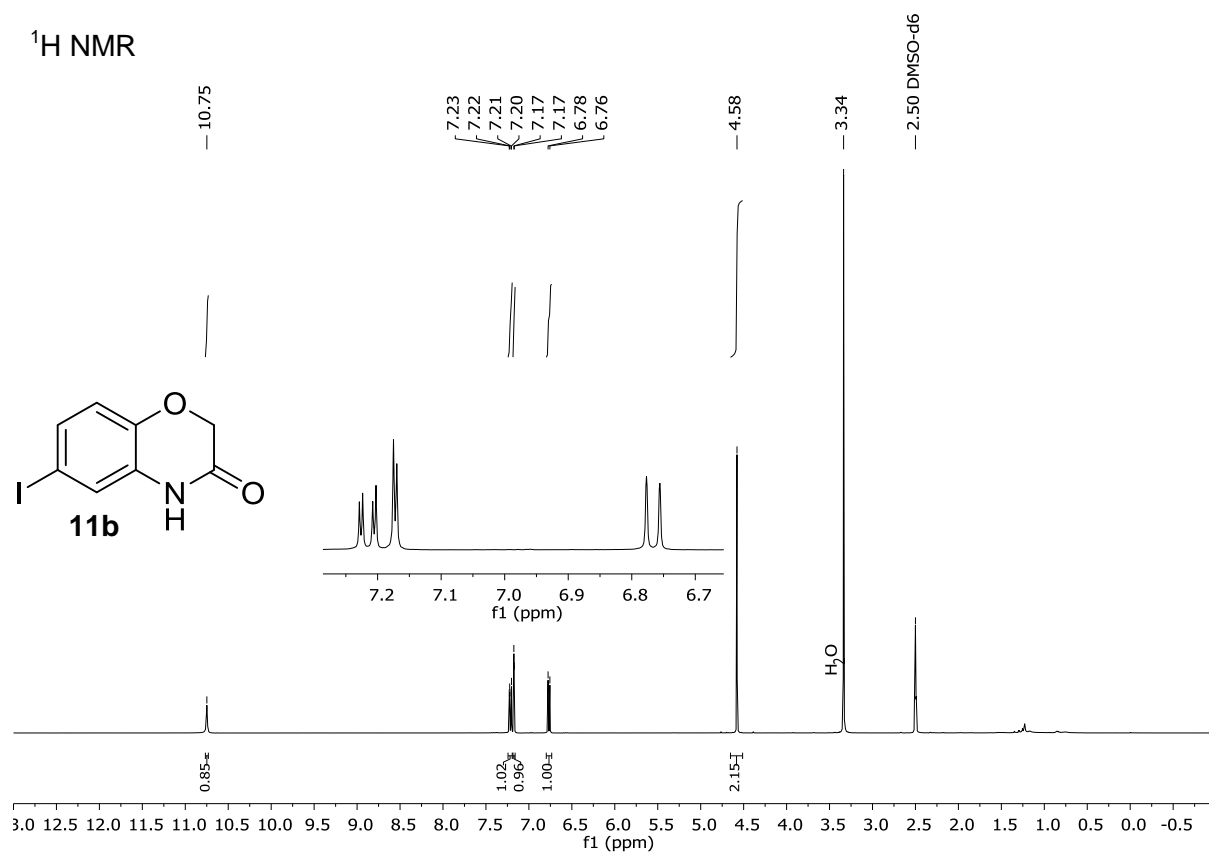
^{19}F NMR

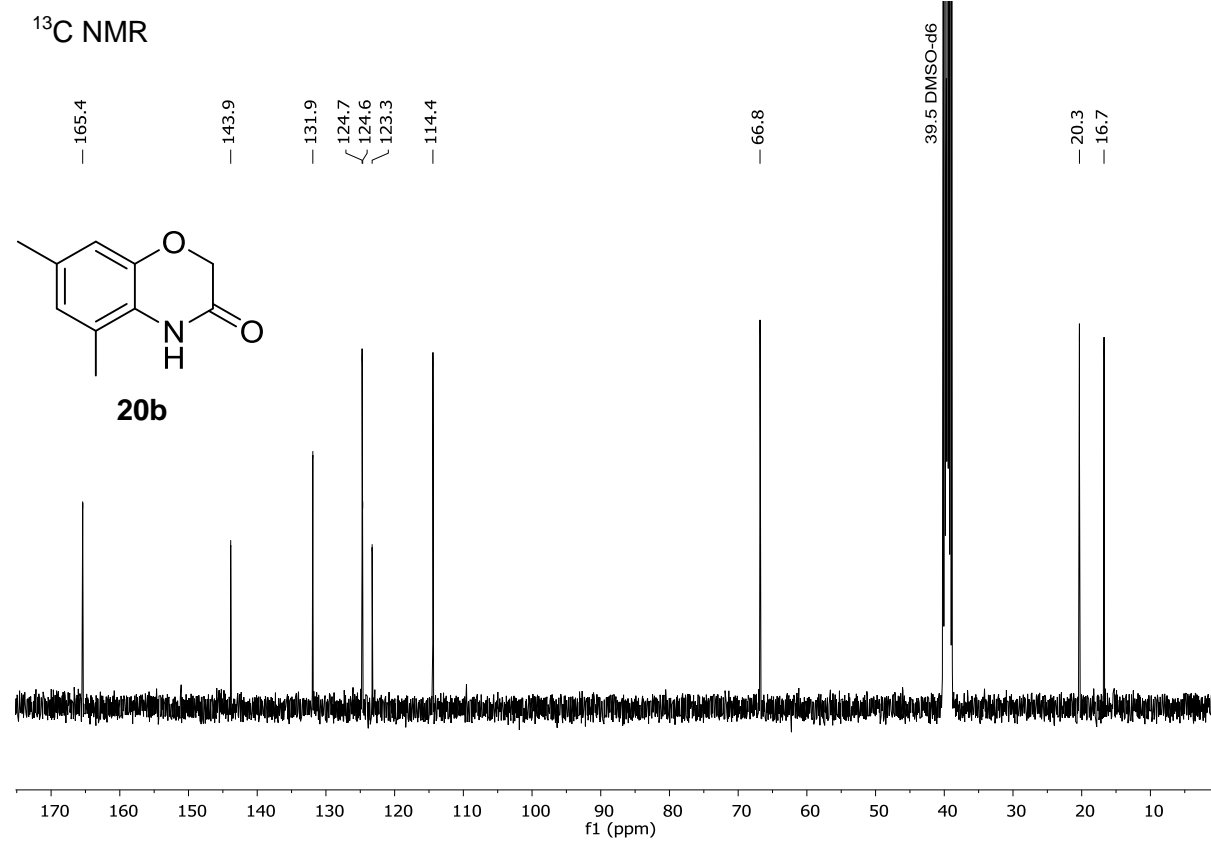
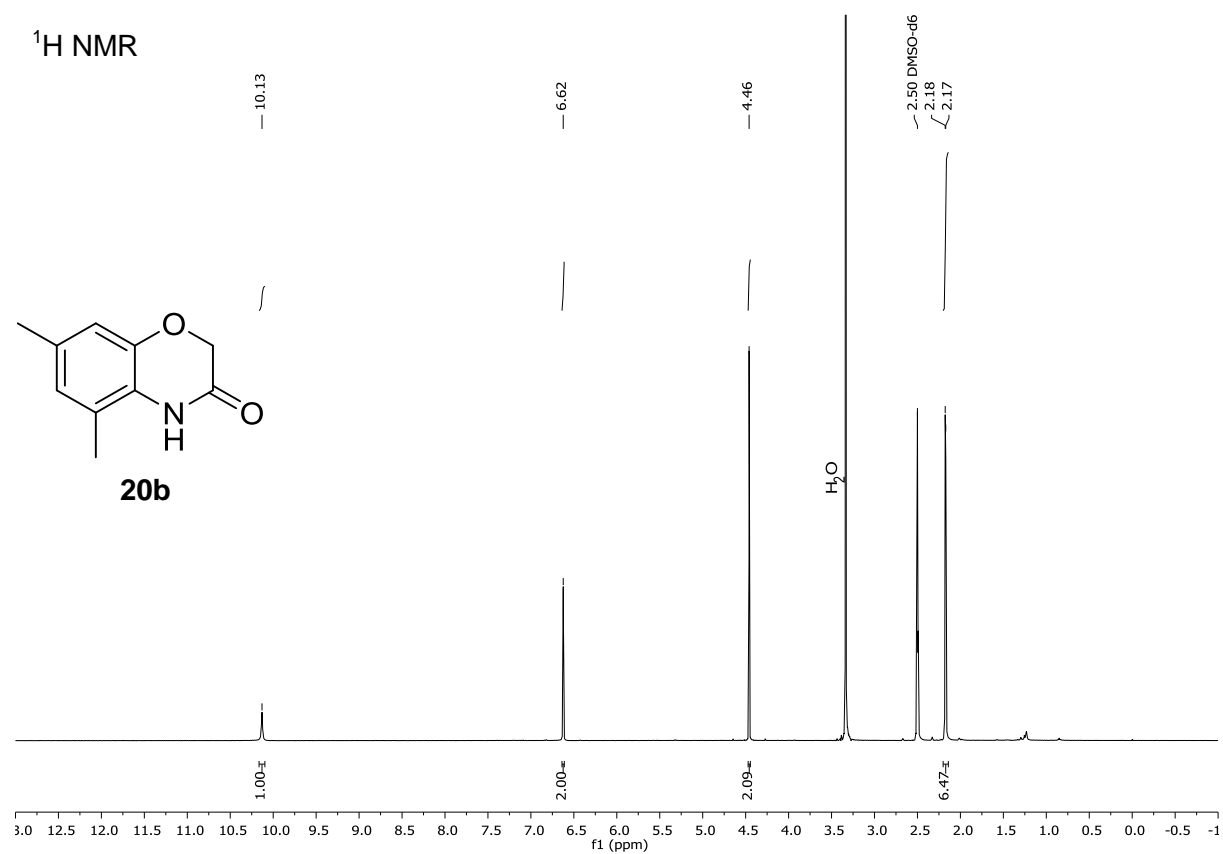
-123.30
-123.31
-123.32
-123.34
-123.35
-123.36

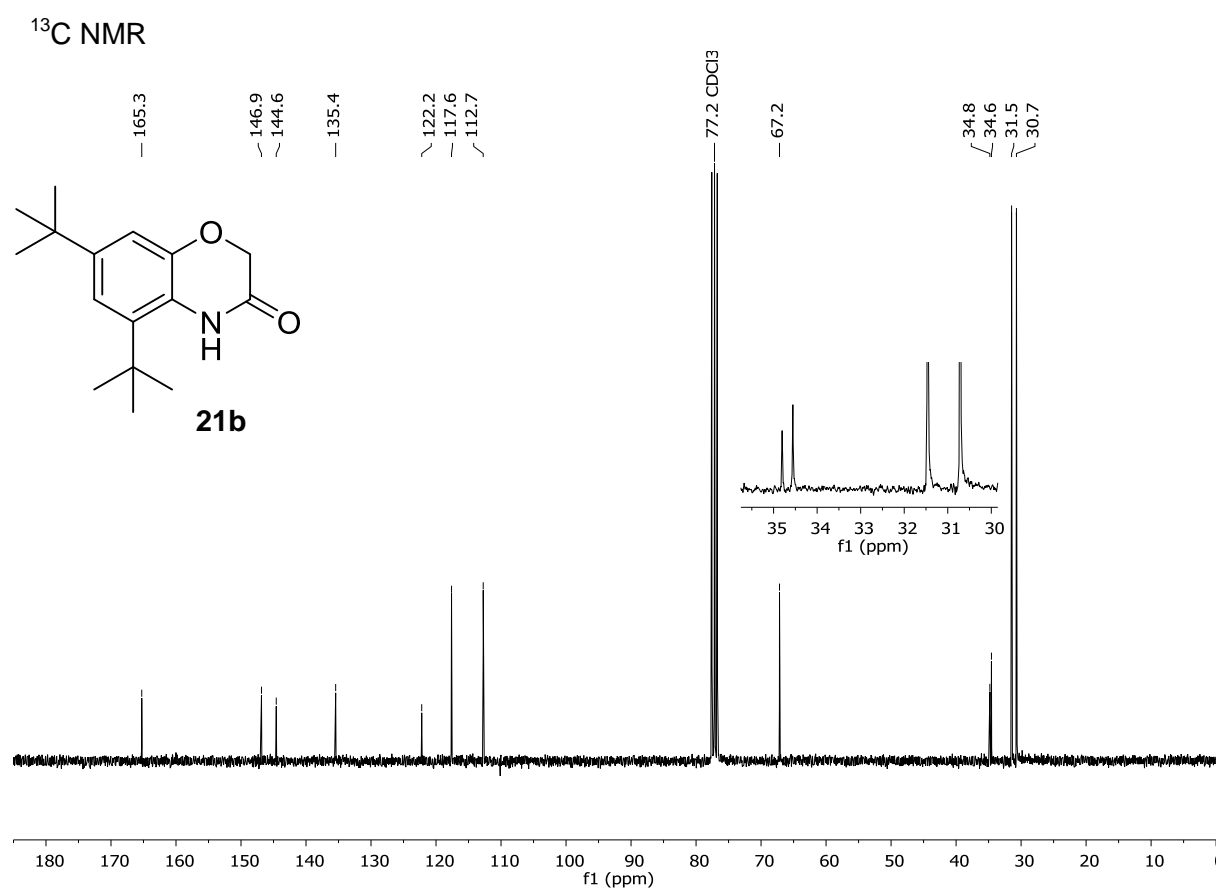
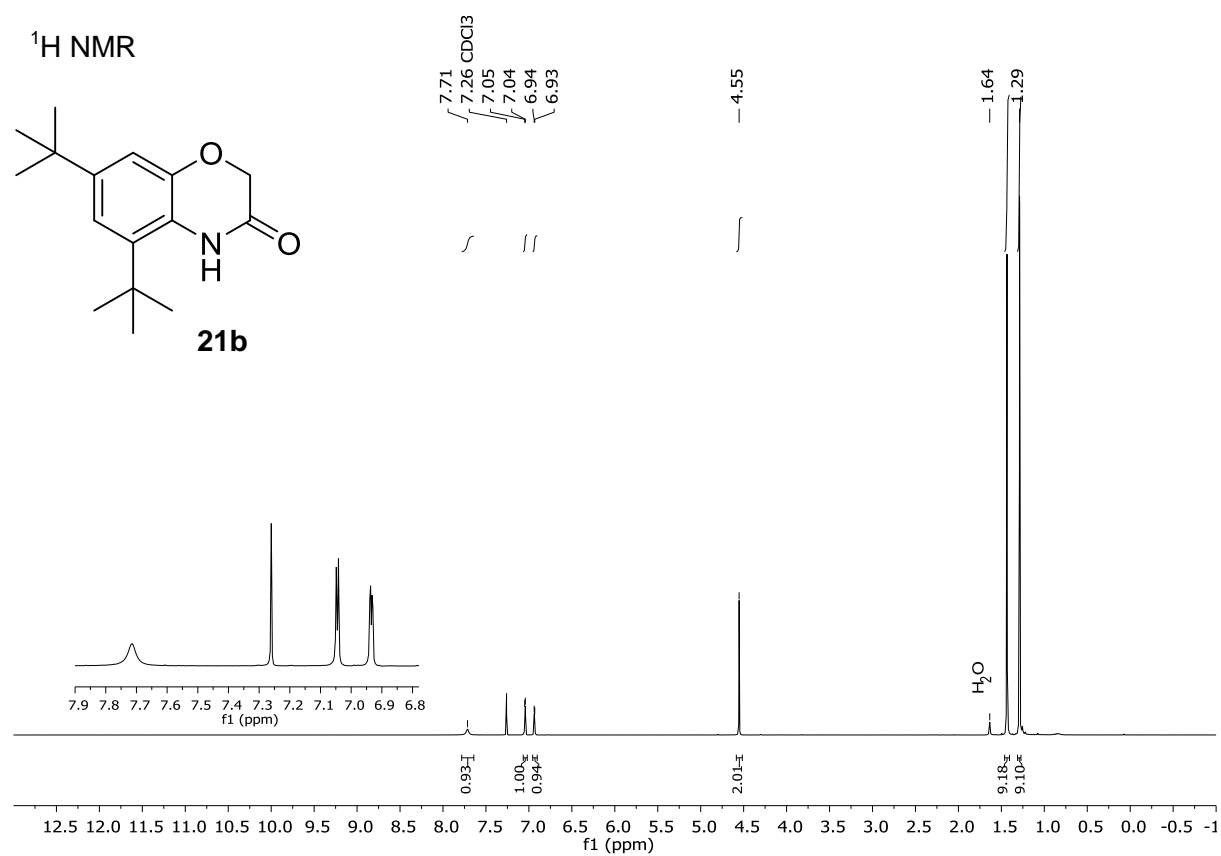


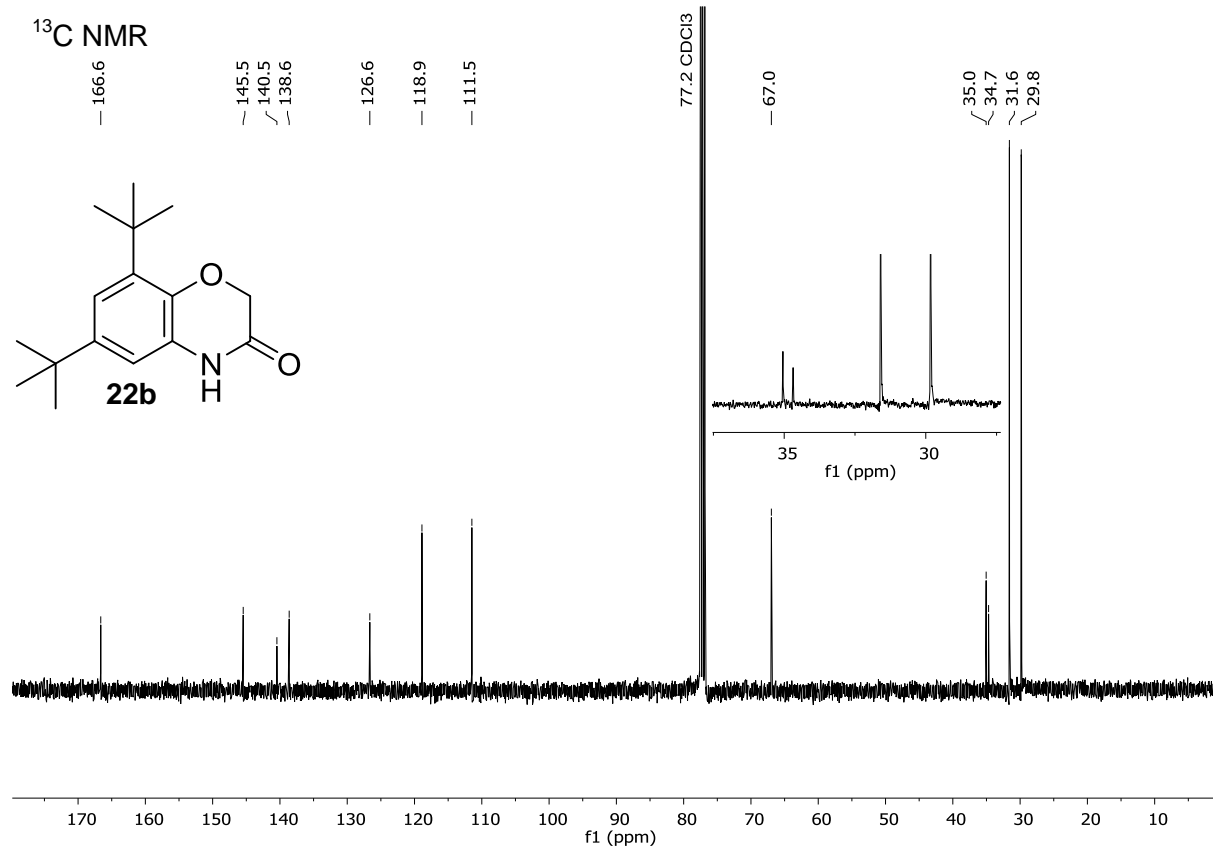


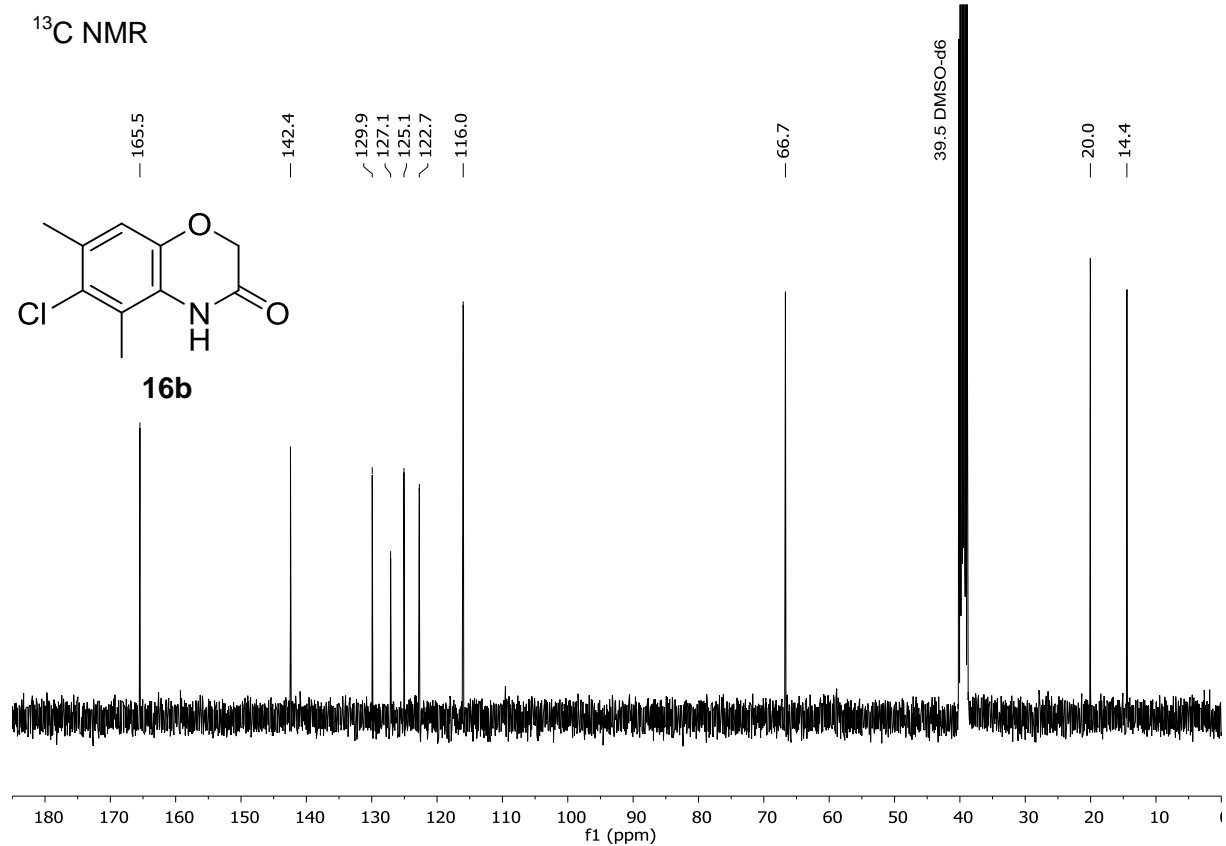
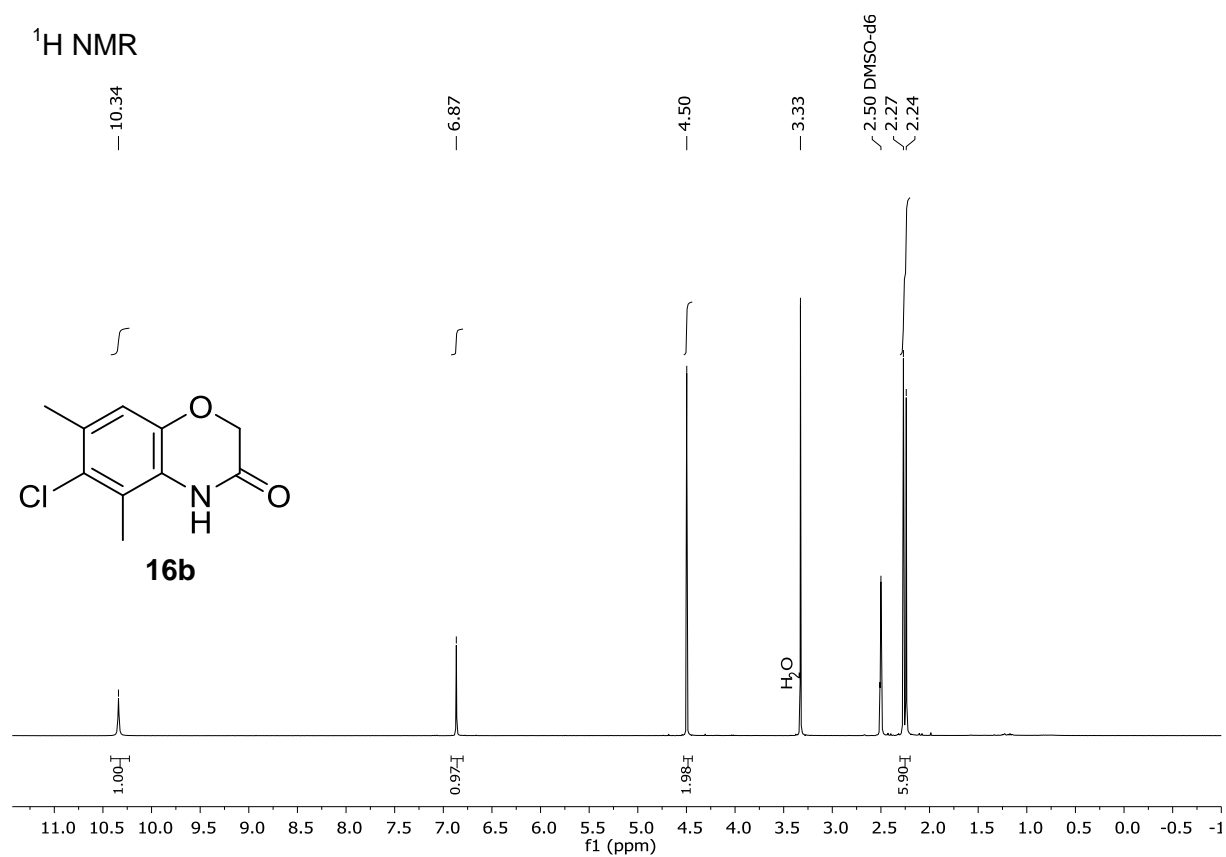


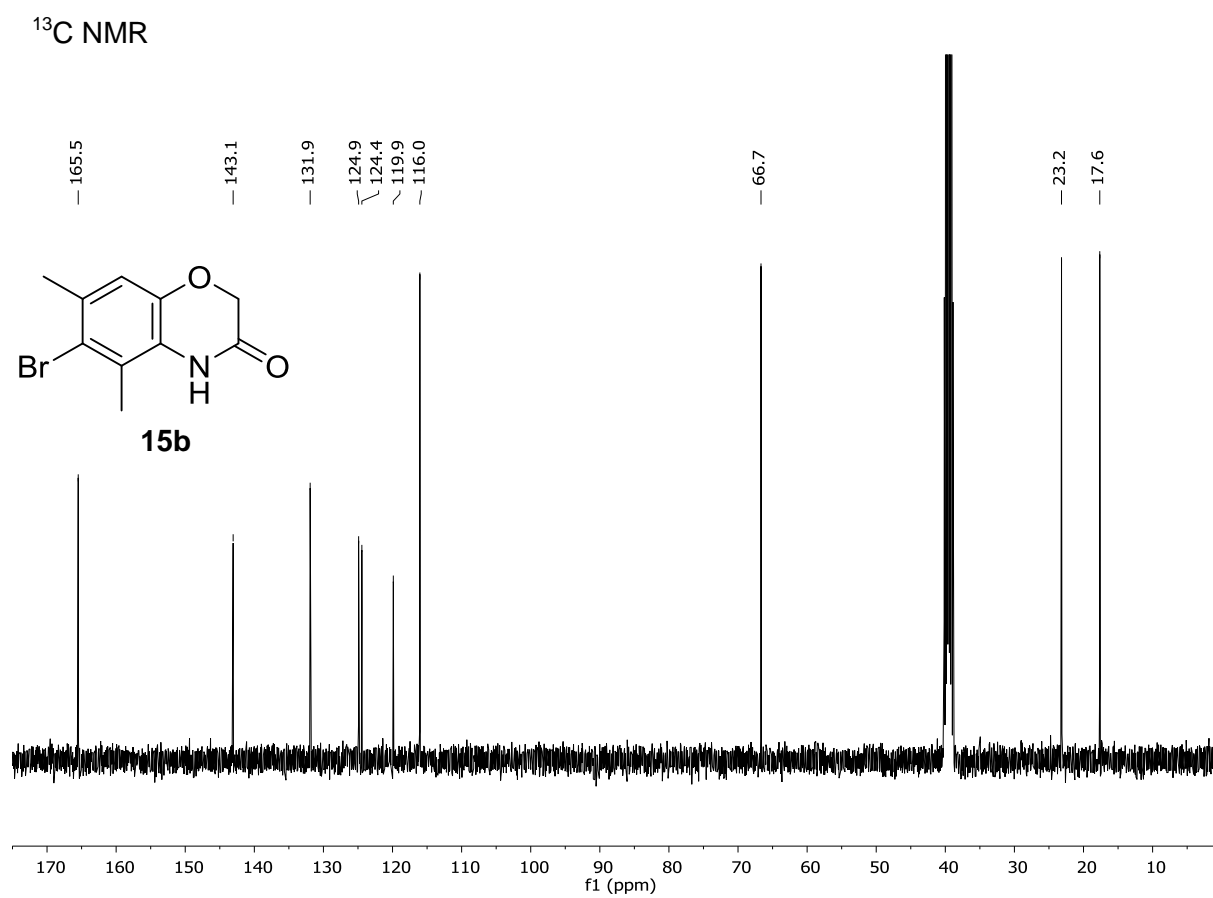
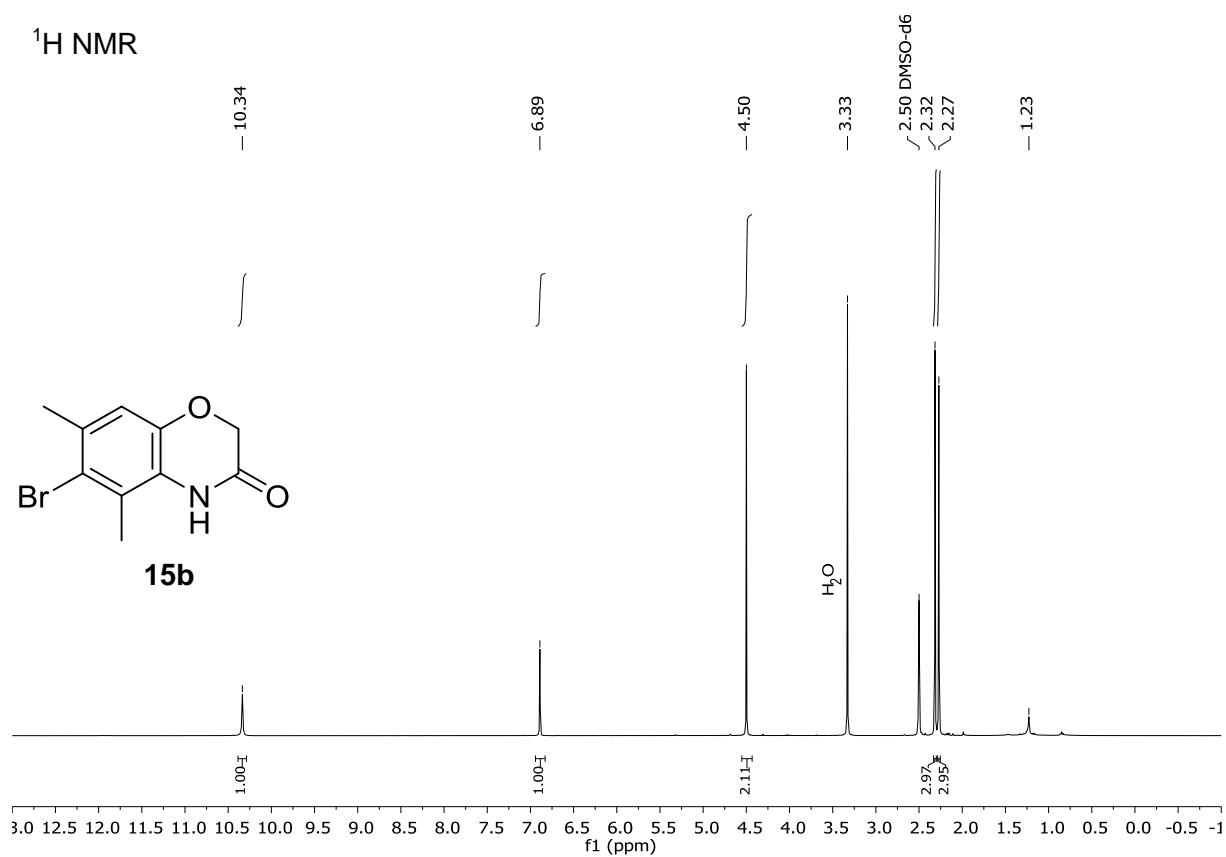


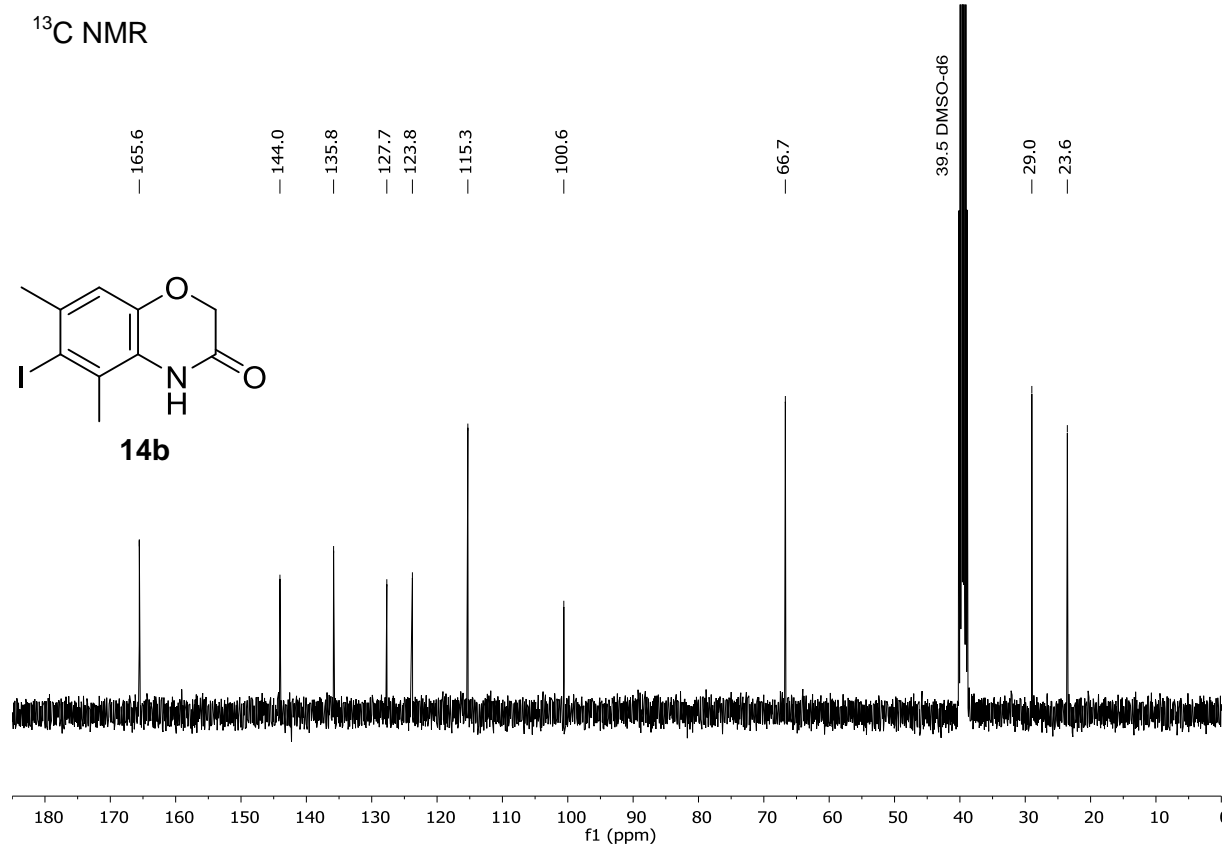
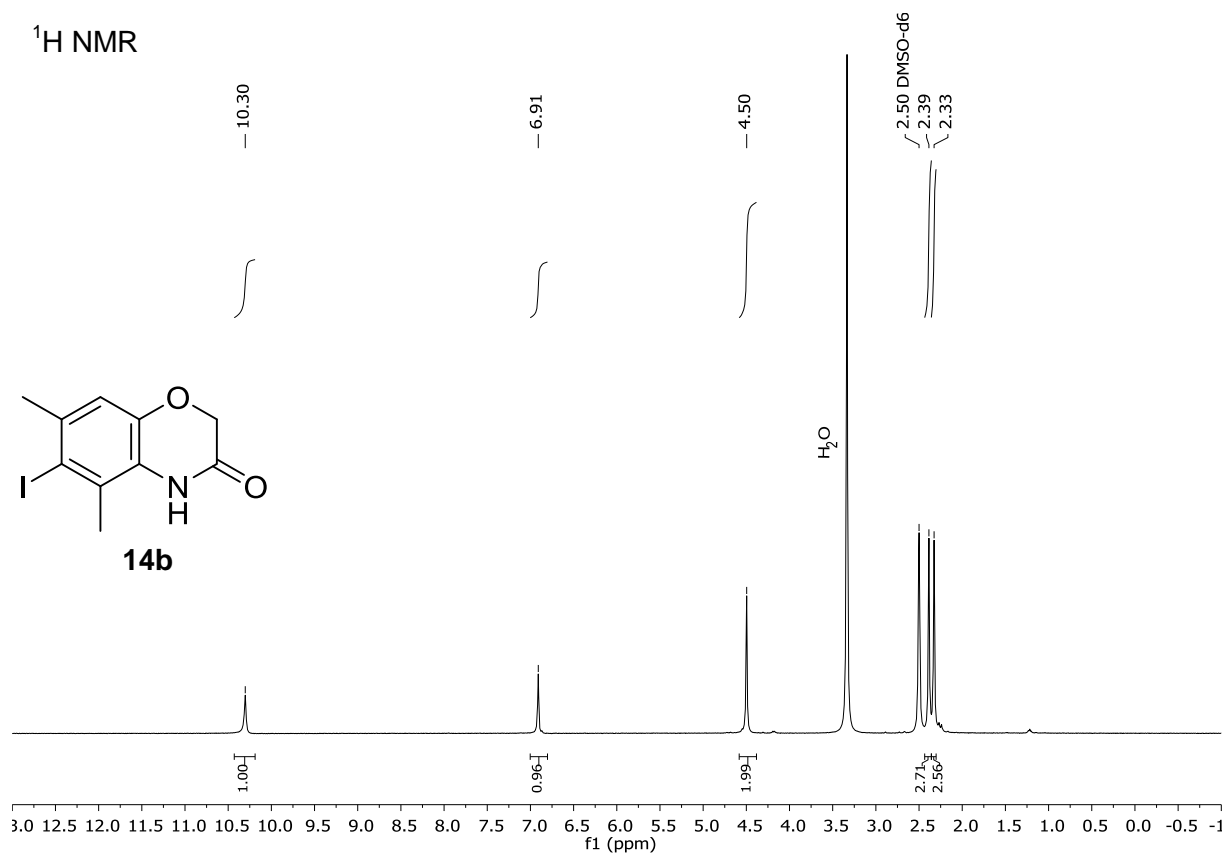












References

- [1] C. Gütz, M. Bänziger, C. Bucher, T. R. Galvão, S. R. Waldvogel, *Org. Process Res. Dev.* **2015**, *19*, 1428.
- [2] C. Gütz, B. Klöckner, S. R. Waldvogel, *Org. Process Res. Dev.* **2016**, *20*, 26.
- [3] M. d. C. Cruz, M. Salazar, Y. Garciafigueroa, D. Hernández, F. Díaz, G. Chamorro, J. Tamariz, *Drug Dev. Res.* **2003**, *60*, 186.
- [4] R. Sarges, R. F. Hank, J. F. Blake, J. Bordner, D. L. Bussolotti, D. M. Hargrove, J. L. Treadway, E. M. Gibbs, *J. Med. Chem.* **1996**, *39*, 4783.
- [5] H. Mori, R. Wada, J. Li, T. Ishimoto, M. Mizuguchi, T. Obita, H. Gouda, S. Hirono, N. Toyooka, *Bioorg. Med. Chem. Lett.* **2014**, *24*, 3732.
- [6] H. M. Abdel Hamid, E. Sayed Ramadan, M. Hagar, E. S. H. El Ashry, *Synth. Commun.* **2004**, *34*, 377.
- [7] J. Belleney, J. Vebrel, E. Cerutti, *J. Heterocycl. Chem.* **1984**, *21*, 1431.
- [8] D. Chen, G. Shen, W. Bao, *Org. Biomol. Chem.* **2009**, *7*, 4067.
- [9] D. R. Shridhar, M. Jogibhukta, V. S. H. Krishnan, *Org. Prep. Proced. Int.* **2009**, *14*, 195.
- [10] C. Ramesh, B. R. Raju, V. Kavala, C.-W. Kuo, C.-F. Yao, *Tetrahedron* **2011**, *67*, 1187.
- [11] M. von Wantoch Rekowski, A. Pyriochou, N. Papapetropoulos, A. Stossel, A. Papapetropoulos, A. Giannis, *Bioorg. Med. Chem.* **2010**, *18*, 1288.
- [12] D. J. Drain, M. J. Daly, B. Davy, M. Horlington, J. G. B. Howes, J. M. Scruton, R. A. Selway, *J. Pharm. Pharmacol.* **1970**, *22*, 684.

RESEARCH ARTICLE

Metal-free Twofold Electrochemical C-H Amination of Activated Arenes: Application to Medicinally Relevant Precursor Synthesis

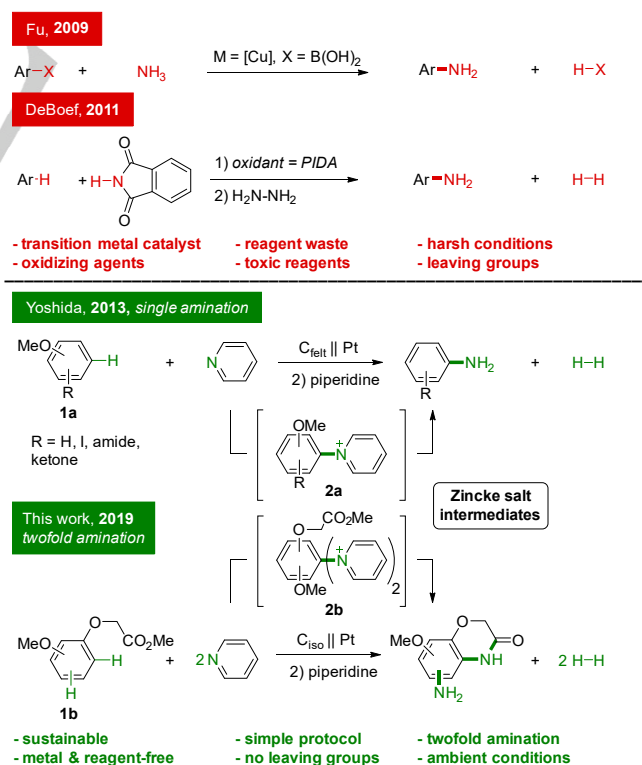
Lars J. Wesenberg,^[a] Erika Diehl,^[b,c] Till J. B. Zähringer,^[a] Carolin Dörr,^[b] Dieter Schollmeyer,^[a] Akihiro Shimizu,^[d] Jun-ichi Yoshida[†],^[e] Ute A. Hellmich^[b,c], and Siegfried R. Waldvogel^{*[a]}

Abstract: The efficient production of many medicinally or synthetically important starting materials suffers from wasteful or toxic precursors for the synthesis. In particular, the aromatic non-protected primary amine function represents a versatile synthetic precursor, but its synthesis typically requires toxic oxidizing agents and transition metal catalysts. The twofold electrochemical amination of activated benzene derivatives via Zincke intermediates provides an alternative sustainable strategy for the formation of new C–N bonds of high synthetic value. As a proof of concept, we use our approach to generate a benzoxazinone scaffold that gained attention as a starting structure against castrate-resistance prostate cancer. Further improvement of the structure led to significantly increased cancer cell line toxicity. Thus, exploiting environmentally benign electrooxidation, we present a new versatile and powerful method based on direct C–H activation that is applicable for e.g. the production of medicinally relevant compounds.

Introduction

The carbon–nitrogen functionality represents an important basic element in synthetic organic chemistry. This structural motif has been utilized for the synthesis of manifold natural products,^[1] pharmaceuticals,^[2] dyes,^[3] as well as polymers and functional materials.^[4] Thus, efficient and selective synthetic approaches for new ways to form C–N bonds and especially to aromatic primary amine functions are highly desired. However, common synthesis strategies suffer from excessive use of toxic chemicals including reagents for nitration, pre-functionalization

such as aryl halides, or transition metal catalysts. In addition, nitration reactions are highly exothermic processes that frequently lead to regioisomeric mixtures^[5] and the subsequent separation of such mixtures is often tedious. The major challenge regarding new synthetic approaches for primary amines remains unsolved. State of the art methods for higher regioselectivity to produce new C–N bonds are the application of palladium or copper-catalyzed protocols, such as Buchwald-Hartwig and Chan-Lam-coupling.^[6] Nevertheless, these methods focus almost exclusively on protected and/or secondary amine functionalities. Modern approaches employ ammonia as the nitrogen source for the synthesis of aromatic primary amines (Scheme 1).^[7] However, all these methods suffer from high catalyst loading, excessive use of toxic and expensive chemicals, pre-functionalized substrates and harsh reaction conditions such as strong bases and elevated temperatures. For instance, DeBoef and co-workers established a synthesis of primary amines via stoichiometric amounts of hypervalent iodine reagents (Scheme 1). Unfortunately, this strategy generates significant waste and is highly unfavorable with regard to the ecological and sustainable footprint of organic synthesis.^[8]



Scheme 1. Common synthesis strategies for the synthesis of aromatic unprotected primary amine functions in comparison with the single and twofold electrochemical C–H-amination procedures.

[a] L. J. Wesenberg, T. J. B. Zähringer, Dr. D. Schollmeyer, Prof. Dr. S. R. Waldvogel <https://orcid.org/0000-0002-7949-9638>

Department of Chemistry
 Johannes Gutenberg University Mainz
 Duesbergweg 10-14, 55128 Mainz, Germany

E-mail: waldvogel@uni-mainz.de

[b] E. Diehl, C. Dörr, Prof. Dr. U. A. Hellmich <https://orcid.org/0000-0001-7162-285X>

Department of Chemistry
 Johannes Gutenberg University Mainz
 Johann-Joachim Becherweg 30, 55128 Mainz, Germany
 E-Mail: u.hellmich@uni-mainz.de

[c] E. Diehl, Prof. Dr. U. A. Hellmich

Centre for Biomolecular Magnetic Resonance (BMRZ)
 Goethe-University Frankfurt
 Max-von-Laue Str. 9, D-60438 Frankfurt/M, Germany

[d] Dr. A. Shimizu <https://orcid.org/0000-0001-9392-2087>

Department Materials Engineering Science
 Graduate School of Engineering Science, Osaka University
 Toyonaka, Osaka 560-8531, Japan
 E-mail: shimizu@chem.es.osaka-u.ac.jp

[e] Prof. Dr. J.-i. Yoshida[†], deceased 09/19.

Supporting information is given at the end of the document.

RESEARCH ARTICLE

Compared to conventional synthetic approaches electrochemistry offers a sustainable and green alternative. Furthermore, electrochemical transformations have an efficient atom economy and avoid oxidizing or reducing agents and reagent waste.^[9]

Yoshida and co-workers established a remarkable electrochemical C–N bond formation with electron-rich arenes **1a** (Scheme 1).^[10,11] Based on these reports Waldvogel and co-workers could demonstrate the electrochemical synthesis of benzoxazinones, which gained interest as basic heterocycle motifs in potential anti-cancer drugs.^[12–14]

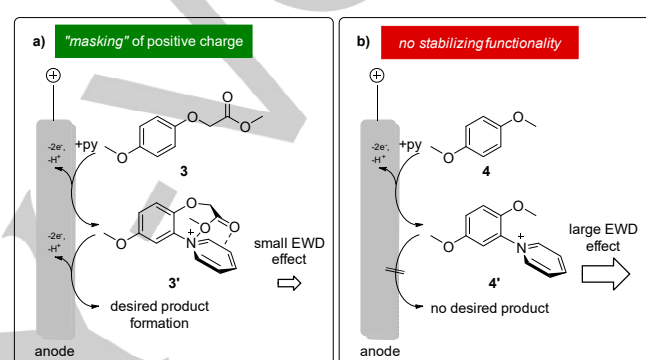
Recently, electrosynthetic conversions have gained more interest in the academic community as the use of inexpensive, environmental benign reactants - such as simple electrons and recyclable electrodes - is superior to expensive and toxic reactants like elaborate transition metal complexes.^[15] Waldvogel and co-workers were able to establish versatile electrochemical approaches for direct C–C coupling reactions,^[16,17] C–N functionalizations,^[12,17–19] and intramolecular C–N, N–N, and S–S bond formations.^[20]

Due to the importance of aromatic primary amines as fundamental scaffolds in natural products and pharmaceutically relevant substances such as benzoxazinones, we thus aimed to further extend our electrochemical approaches toward the direct twofold amination of methyl phenoxyacetate structure **3** (Scheme 2). Besides providing access to a valuable heterocycle, the ester functionality plays a crucial role in stabilizing intermediates. Anodic oxidation of electron-rich aromatic compounds **1a** in the presence of pyridine usually leads to relatively stable and positively charged pyridinium intermediates (Zincke-type salts **2a**, Scheme 1). Upon treatment with piperidine these cationic species liberate the aromatic primary amine function in a second step. Yoshida et al. postulated that due to the electron withdrawing effect (EWG) of the pyridinium intermediate and the electrostatic repulsion from the anode, further oxidation and pyridination processes were suppressed.^[11] However, Waldvogel et al. recently reported a twofold amination process of polycyclic aromatic compounds, albeit with low yields since electron donating substituents were found to play a crucial role in stabilizing the pyridinium intermediates. Furthermore, the regioselectivity of the electrochemical amination procedure is associated with electron releasing functional groups, thus the aminated products consisted of regioisomers.^[19]

Results and Discussion

Based on Yoshida's hypothesis regarding the reaction intermediate dependent suppression of oxidation processes, we aimed to evaluate whether overoxidation of the Zincke-type salt is truly suppressed and the first pyridinium intermediate accumulates. We thus designed substrates capable of efficiently masking the electron-withdrawing effect of the first pyridinium moiety. In contrast to the prior hypothesis, these compounds were capable of further oxidation and consequently provide an

expeditious route to valuable product synthesis. Efficient electrochemical C–H amination requires electron-rich arenes with electron donating and radical cation stabilizing substituents such as methoxy groups.^[11] Initially, we compared activated compounds such as 1,4-dimethoxybenzene (**4**) and Methyl 2-(4-methoxyphenoxy)-acetate (**3**) with regards to their ability to undergo a second pyridination process (Scheme 2). We hypothesized that the ester functionality of the phenoxy acetate derivative **3** might be able to stabilize the pyridinium moiety via σ - σ or π - π interactions. Stabilization of the electron-deficient substituent can be beneficial for further oxidation. These interactions act as shielding effects to disguise the positive charge, thus the electron withdrawing effect diminishes and further oxidation of **3'** at the anode can occur (Scheme 2).



Scheme 2: a) Proposed masking effect of the pyridinium moiety via a stabilizing ester function by σ - σ or π - π interactions, b) the absence of a side chain on substrate **4** results in the lack of desired product formation.

Initially, we conducted various cyclic voltammetry experiments to evaluate the phenoxy acetate **3** and to observe whether the ester moiety provides the expected beneficial impact (Figure 2). The electron-rich arene 1,4-dimethoxybenzene (**4**) was used for comparison (Figure 1).

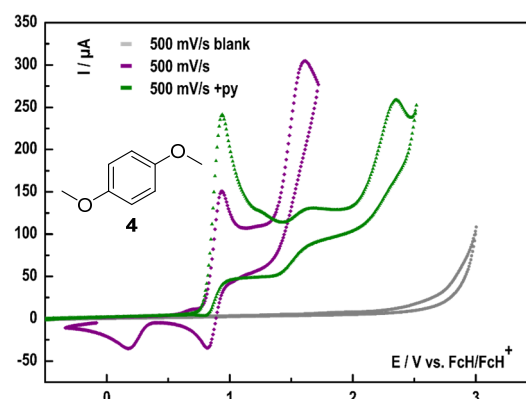


Figure 1: Cyclic voltammograms of 0.1 M Et₄NBF₄/CH₃CN with 1,4-dimethoxybenzene (**4**) (purple line) and with pyridine (py) as additive (4 eq) (green line); working electrode: boron-doped diamond (BDD); counter electrode: glassy carbon; reference electrode: Ag/AgNO₃; scan rate 500 mV/s, (for more information: see SI).

RESEARCH ARTICLE

In the cyclic voltammogram of 1,4-dimethoxybenzene (**4**) (Figure 1, purple line), one quasi-reversible oxidation step and another oxidation peak were observed ($E_{\text{Ox1a}} = 0.94$ V, $E_{\text{Ox2a}} = 1.61$ V vs. FcH/FcH^+ , respectively). With the addition of pyridine (Figure 1, green line) the second oxidation peak is shifted to elevated values ($E_{\text{Ox1b}} = 0.94$ V, $E_{\text{Ox2b}} = 2.43$ V vs. FcH/FcH^+ , respectively). These data are in line with the mechanism postulated by Yoshida, where initially a radical cation is formed and then trapped in-situ by pyridine. This molecule is stabilized by deprotonation and further oxidation to establish the first pyridinium intermediate (for more details on the mechanism see Supporting Information). The trapping mechanism is related to the absence of a reduction wave ($E_{\text{Red1a}} = 0.90$ V vs. FcH/FcH^+ , Figure 1, green line). Subsequently, radical cations are generated and consumed by a follow-up reaction with pyridine. The presence of pyridine (Figure 1, green line) shifts the second pyridination peak close to the electrochemical window of the electrolyte ($E_{\text{Ox2b}} = 2.43$ V vs. FcH/FcH^+). This suggests that the electron withdrawing effect of the positively charged scaffold destabilizes the benzene system. Our data thus strongly support Yoshida's original proposal that the pyridinium intermediate and its electron withdrawing nature will prevent further oxidation processes.

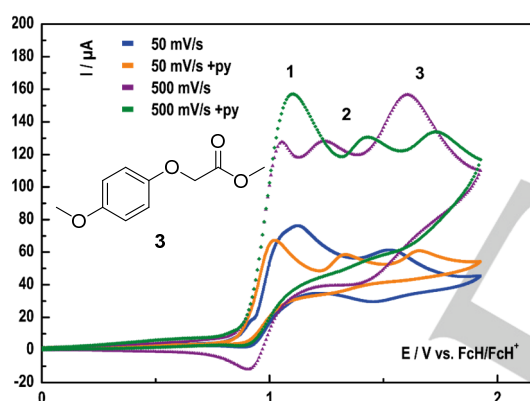
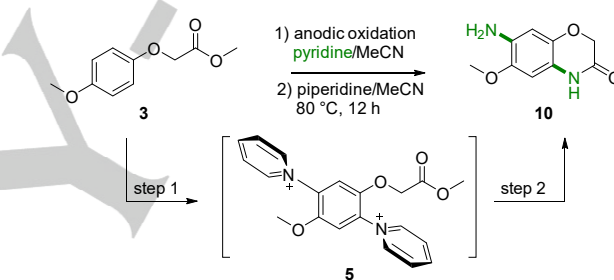


Figure 2: Cyclic voltammograms of 0.1 M $\text{Et}_4\text{NBF}_4/\text{CH}_3\text{CN}$ with methyl 2-(4-methoxyphenoxy)acetate (**3**); scan rate: 50 mV/s (blue line); scan rate: 500 mV/s (purple line); and with additive pyridine (py) (4eq); scan rate: 50 mV/s (orange line); scan rate: 500 mV/s (green line); working electrode: BDD; counter electrode: glassy carbon; reference electrode: Ag/AgNO_3 .

In the cyclic voltammogram of methyl 2-(4-methoxyphenoxy)acetate (**3**) (Figure 2, purple line), three distinct oxidation peaks are observed ($E_{\text{Ox1}} = 1.05$ V, $E_{\text{Ox2}} = 1.24$ V, and $E_{\text{Ox3}} = 1.61$ V vs. FcH/FcH^+ , respectively). The first oxidation peak is quasi-reversible at high scan rates (Figure 2, purple line, peak 1). By reducing the scan rate from 500 mV/s to 50 mV/s, the first two oxidation peaks unite to one broad peak ($E_{\text{Ox1+2}} = 1.12$ V, Figure 2, blue line). This suggests that the resolution of this experiment on a fast time scale corresponds approximately to two narrow single electron transfers (SETs). At a slow time scale chemical reactions become observable and might interfere with emerging radical cations. Consequently, the two peaks merge and appear almost indistinguishable. With the addition of pyridine, the time scale of the electron transfer process become inconsequential for the reaction progress (Figure 2, orange and green lines). Hence,

three oxidation peaks are observed at slow and fast scan rates. The formation of any radical cation species will be trapped in-situ by pyridine. The presence of pyridine also influences and shifts the equilibrium of the electron transfer towards the oxidized substrate, thus the peak current is increased substantially ($E_{\text{Ox1}} = 1.05$ V vs. FcH/FcH^+ , Figure 2, green line). Interestingly, no significant elevated oxidation peaks appear in contrast to what is observed with the 1,4-dimethoxybenzene derivative **4**. This indicates a shielding and stabilizing effect provided by the dangling ester function (for more details see Supporting Information).

The promising results obtained by cyclic voltammetry experiments in combination with our earlier successful electrochemical synthesis of benzoxazinones^[12] prompted us to test further amination procedures, in particular with regards to the synthesis of aromatic non-protected primary amines with benzoxazinone scaffolds.^[12] The cyclic voltammetry data revealed beneficial properties with respect to a twofold electrochemical C–H amination (Scheme 3).



Scheme 3: Electrochemical twofold amination of **3** as the test substrate and the proposed Zincke-type intermediate **5**.

The optimization reactions were carried out in divided Teflon cells with a porous glass-frit or an anion exchange membrane like Thomapor® as separators (SI, Figure 1 and Figure 2).^[21] This screening technique is time and cost efficient and allows the simultaneous variation of several electrochemical parameters, e.g. current density and applied charge (for the experimental setup see Supporting Information). The results of the screening experiments were determined via ^1H NMR analysis with 1,1,2,2-tetrachloroethane as an internal standard (ISTD). Tetraethylammonium tetrafluoroborate (NEt_4BF_4) was used as the supporting electrolyte. The increased salt character of tetraethyl ammonium compared to the corresponding butyl salts facilitated the workup procedure by column chromatography.

Previous work has shown that isostatic graphite anodes can be used in electrochemical oxidation reaction for electron-rich phenoxyacetates to generate efficiently new C–N functionalities.^[12] To determine the optimal diamination conditions of phenoxy acetate **3**, we systematically investigated the influence of the current density, the amount of charge and different membranes with isostatic graphite as anode material (Table 1). In principle, the current density is directly correlated to the concentration of radical cations close to the electrode surface, thus higher current densities could favor further oxidation of

RESEARCH ARTICLE

relative inert Zincke-type salt **3'**. Recently, when using naphthalene as the starting material we observed that low current densities $1\text{--}6\text{ mA/cm}^2$ benefit the single amination process, whereas higher current densities lead to competing pathways.^[19] Based on these results, it was envisioned that a two-step electrolysis might be feasible.

Optimal reaction conditions were achieved when Thomapor[®], an anion exchange membrane, was applied as a separator. Due to its superior properties such as permeaselectivity and low electrical resistivity to glass frits, the envisioned two-step electrolysis led to optimal results (for more details on the condition screening see Table 1 and Table 2, SI). Previous studies on C–H amination have shown that the actual demand of charge is significantly higher compared to theory.^[12] Therefore, the electrochemical conditions for the two-step electrolysis were set to 3.4 F with 5 mA/cm^2 and 2.1 F with 10 mA/cm^2 . This approach resulted in high yields of 69% with compound **10** (entry 16, Table 1).

Table 1. Screening of different electrolysis conditions for the twofold amination process. 0.5 mmol substrate, 0.2 M supporting electrolyte, 12 mmol pyridine, 5 mmol trifluoromethanesulfonic acid (TfOH), isostatic graphite anode, platinum cathode, divided cell.

#	Separator	Supporting electrolyte	Current density / mA/cm^2	Applied charge / F	Yield / % ^[a]
1	glass frit	NBu_4BF_4	10	4.2	0 ^[b]
2	glass frit	NEt_4BF_4	10	4.2	30
3	glass frit	NEt_4BF_4	10	5.0	29
4	glass frit	NEt_4BF_4	10	6.0	25
5	glass frit	NEt_4BF_4	10	7.0	0
6	Thomapor [®]	NEt_4BF_4	1	4.2	34
7	Thomapor [®]	NEt_4BF_4	3	4.2	40
8	Thomapor [®]	NEt_4BF_4	7	4.2	50
9	Thomapor [®]	NEt_4BF_4	10	4.2	49
10	Thomapor [®]	NEt_4BF_4	13	4.2	49
11	Thomapor [®]	NEt_4BF_4	16	4.2	46
12	Thomapor [®]	NEt_4BF_4	10	4.5	56
13	Thomapor [®]	NEt_4BF_4	10	5.0	57
14	Thomapor [®]	NEt_4BF_4	10	5.5	59
15	Thomapor [®]	NEt_4PF_6	10	5.5	50
16	Thomapor [®]	NEt_4BF_4	i) 5, ii) 10	i) 3.4, ii) 2.1	69 ^[c]

[a] determined via $^1\text{H NMR}$ with 1,1,2,2-tetrachloroethane as ISTD [b] work-up procedure did not fully lead to isolation of desired product [c] achieved via two-step electrolysis.

The optimized electrolysis conditions consist of a divided cell setup with isostatic graphite as the anode and platinum as the cathodic material, Thomapor[®] as the separator and a two-step-electrolysis of 3.4 F with 5 mA/cm^2 and 2.1 F with 10 mA/cm^2 at $25\text{ }^\circ\text{C}$. These optimized reaction conditions were then used on a collection of activated arene systems (Figure 3).

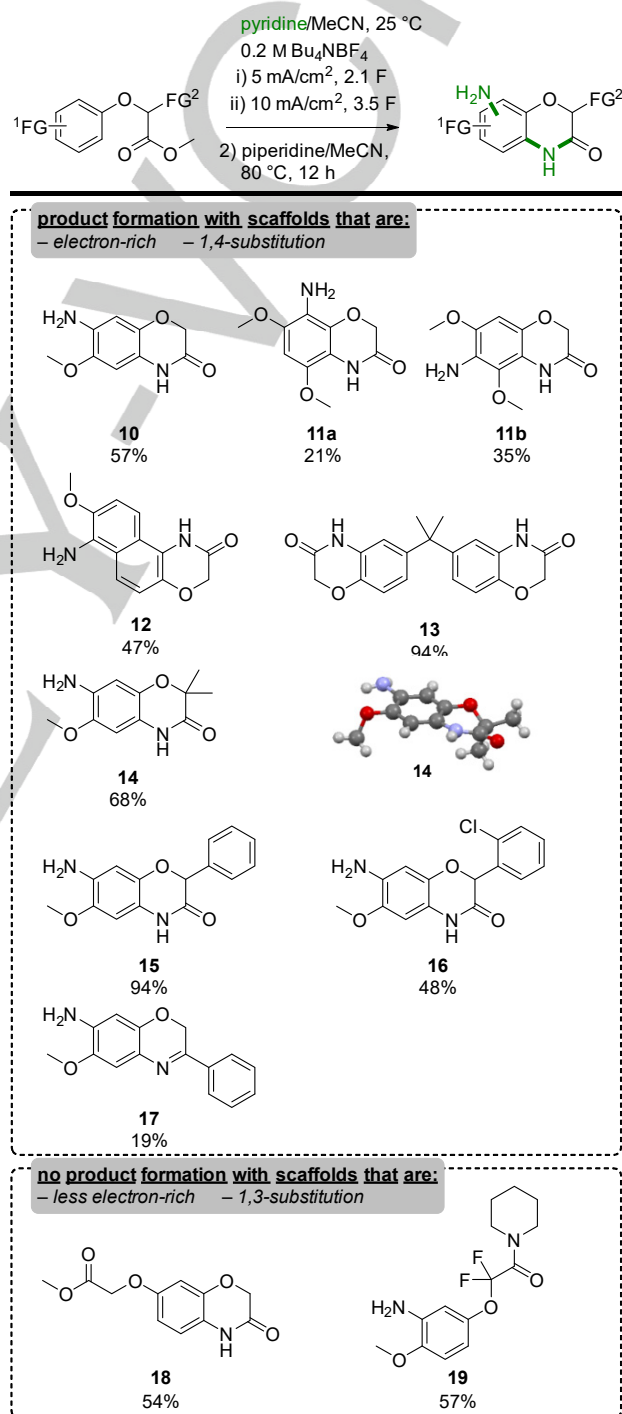


Figure 3. Scope of diaminated products with various substitution patterns obtained via optimized reaction conditions. Divided cell; separator: Thomapor[®].

RESEARCH ARTICLE

Importantly, our improved electrochemical protocol for a twofold amination process is applicable to a broad scope of different 1,4-activated phenoxy systems as seen in Figure 3. Other substitution patterns including 1,3-activated phenoxy systems were also investigated. However, even with an increased amount of charge only a single aminated product **18** of 54% yield was generated (Figure 3). By attaching two fluoride functions, the desired conversion was not observed and instead only a single amination product **19** of 57% yield was obtained. This is presumably due to the electron withdrawing nature of fluorine, stereoelectronic effects, and the consequently destabilized benzene system.

1,4-activated phenoxy systems like compound **10** could be isolated with a yield of 57%. For specific scaffolds such as highly activated benzene systems, we still obtained a relatively high yield of 56%, but regioisomers were formed (see **11a** and **11b**). Based on our results, we then focused on the effect of larger aromatic systems including naphthyl derivatives. For instance, the 2,6-substituted naphthyl derivative was successfully transformed into the desired product **12** with yields of up to 47%.

Next, we investigated the influence of the electron withdrawing effect of the positive charged pyridinium moiety in comparison to the electrostatic repulsion by applying the electrochemical twofold amination protocol to a separated pi-system. Surprisingly, this resulted in almost quantitative yield of 94% for **13**. This suggests that the electrostatic repulsion has a less adverse effect on the second pyridination process than the electron-withdrawing effect of the Zincke-type intermediate. The best reactivity and selectivity were observed with 1,4-substituted aromatic compounds, due to the low steric demands of two attached pyridinium intermediates and their respective electrostatic properties. Thus, other substituent patterns close to the ring system were investigated to assess whether they may show reduced influence on the electron-density of the aromatic compound. By attaching two methyl groups to the side chain, the resulting product **14** was formed in satisfactory yields of up to 68%. Next, a phenyl-substituted scaffold was transformed into the diaminated product **15** with 33% yield. Surprisingly, even a halo function such as a chloro-substituent was compatible with this methodology, obtaining **16** with a yield of 48%. Furthermore, our protocol was even capable of transforming phenyl ketones intramolecular into cyclic aminated imine structures with a yield of 19% with **17**. These lower yields may be explained by the inevitably occurring enamine formation with piperidine during the transformation. Nevertheless, the electro-conversion of these phenyl ketones provides a novel synthetic access route towards precursors of asymmetrical imine reduction.^[22]

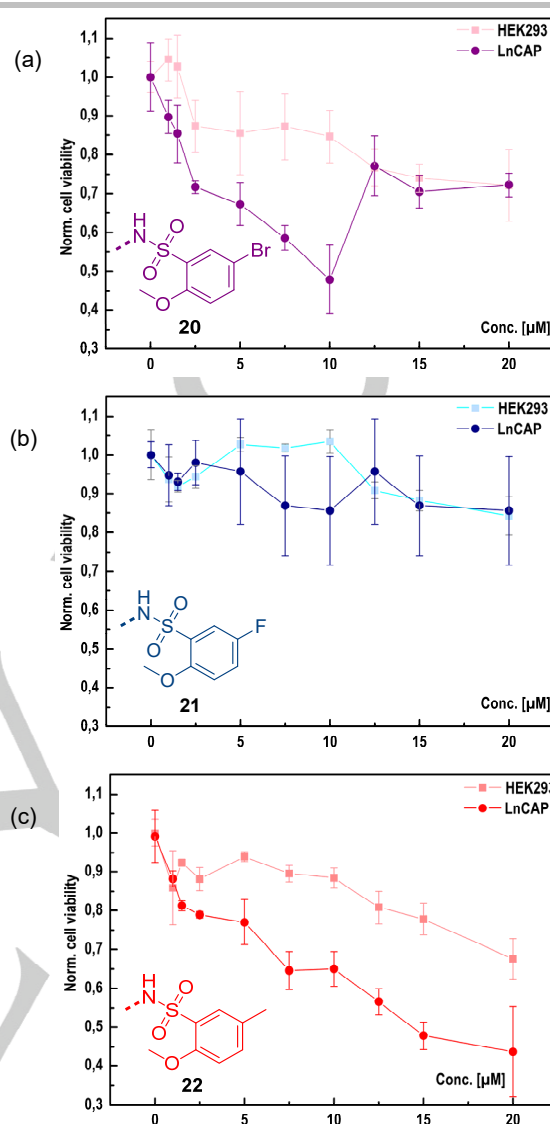


Figure 4: Effects of compound **20** (a), **21** (b), **22** (c) on cell viability of the prostate cancer cell line LnCAP and HEK293 as the control cell line. Cells were treated with increasing concentrations of compounds, with a final DMSO concentration of 0.5 % (v/v). Cell viability was measured by MTT assays. Results represent three independent experiments with four technical replicates each. Boxed molecule shows the electrochemically generated benzoxazinone backbone precursor for the synthesis of compounds **20**, **21** and **22**.

Recently, benzoxazinones similar to compound **20** gained attention as general structures for novel drugs against so-called castrate-resistance prostate cancer (CRPC).^[13,14] Currently, patients that display CRPC ultimately always succumb to this disease. Androgen deprivation therapy (ADT) drugs are being heavily investigated for their potential to counteract the proliferative effects of the androgen receptor in prostate cancer cells. However, cancer patients develop the above-mentioned

RESEARCH ARTICLE

resistance due to various biochemical survival adaptations of the cancer.^[23,24] Therefore, there is an urgent need for the development of alternative ADT therapeutics.

Xu *et al.* recently demonstrated that benzoxazinone **20** can be used as an efficient inhibitor ($IC_{50} = 4.41 \mu\text{M}$) of cell viability of the prostate cancer cell line LnCAP by interacting with bromodomain containing protein 4 (BRD4).^[14] BRD4 belongs to the so-called Bromodomain and Extra-Terminal Domain (BET) protein family and interacts with the N-terminus of the androgen receptor. Inhibiting this protein interaction with BRD4 inhibitors ultimately leads to an anti-proliferative effect, which is especially pronounced in prostate cancer cells.^[23]

To evaluate the effect of our electrochemically generated benzoxazinone **20** and select derivatives against prostate-cancer cell lines, we carried out cell-viability assays with LnCAP and non-cancerous HEK293 cells as a control. In contrast to what was observed previously,^[14] we did not observe a complete cell growth inhibition at increasing concentrations of compound **20** (Figure 4a). Rather, the dose-response curve is bell-shaped. Bell-shaped dose-response curves could indicate the formation of colloidal drug aggregates and consequently a decreased ability of the compound to penetrate cellular membranes and to ultimately interact with their cellular target such as the nuclear protein BRD4.^[25] Intriguingly, our crystal structure of benzoxazinone **20** indeed shows a distinct 3D linkage via H-bond formation of the bromine (for more information see SI, Figure 8). To examine the role of the halide moiety for compound oligomerization and cell toxicity, we thus substituted bromine with fluorine, resulting in benzoxazinone **21**. Fluorine as substituent possesses a higher electronegativity but simultaneous less polarizability than bromine, which could thus avoid H-bond formation. Indeed, the crystal structure of the fluoro compound **21** (for more information see SI, Figure 7) revealed the loss of the 3D linkage previously observed for **20**. At the same time, however, cell toxicity of **21** was lost (Figure 4b).

The crystal structure of BRD4 in complex with benzoxazinone **20**^[14] indicates that the 5-bromo-2-methoxybenzene moiety of benzoxazinone **20** interacts with the WPF shelf of BRD4, a hydrophobic cavity within BRD4 (see SI, Figure 9). The substitution of bromine with fluorine could thus lead to an impaired BRD4 binding behavior and consequently a decreased inhibitory effect on LnCAP cell growth. On the other hand, this encouragingly indicates that the overall toxicity of this compound for human cells is low and that off-target effects are minimal thus fulfilling important requirements for a putative drug. To evaluate whether the inhibitory effect of compound **20** relies on the polarizability of bromine or its space requirement, we substituted the bromine with a methyl group to yield compound **22**. With increasing compound **22** concentrations, LnCAP viability decreases (Figure 4c). Compared to sulfonamide **20**, derivative **22** shows a clear dependence of cell viability for LnCAP cells on compound concentration, indicating no compound aggregation at higher concentrations. This is in agreement with our crystal structure of **22** (for more information see SI, Figure 10) which does not show H-bond acceptor abilities such as bromine and

therefore no 3D linking and aggregation. With the methyl derivative **22** obtained using our optimized electrochemical protocol, we provide a compound that displays a significant boost in solubility and, in contrast to related molecules, a dose-dependent toxicity against a prostate cancer cell line. Our findings thus combine the design of an anti-prostate cancer drug precursor with improved properties with a significantly enhanced electrochemical protocol for the selective amination of important molecular scaffolds for many downstream applications.

Conclusion

In conclusion, the application of the phenoxy-acetate moiety revealed a new and interesting reactivity towards twofold amination products. We introduced a versatile and powerful method to electrochemically generate doubly positive charged Zincke intermediates. These pyridinium intermediates liberate one aromatic non-protected primary amine function and one amine which induces the formation of an intramolecular heterocycle. We conducted detailed cyclic voltammetry studies of activated arene systems to elucidate their reactivity and behavior towards a twofold amination protocol. With our new electrochemical C–H amination procedure, twofold aminated products with more than 90% yields were accessible. This process does not require leaving groups and transition metal catalysts and thus represents a new and powerful approach for C–N bond formation. Furthermore, we also could show a new way to synthesize pharmaceutical key compounds with sustainable electrochemistry, which will be highly valuable for future pharmaceutical productions against the background of environment protection and shortage of raw materials.

Experimental Section

For experimental details, setup and analytical data see Supporting Information.

Acknowledgements

Financial support by Deutsche Forschungsgemeinschaft (DFG: Wa1276/17-1) is highly appreciated. ED acknowledges a TransMED PhD Fellowship and the Sibylle Kalkhof-Rose-Stiftung. This work was supported by the Center for Biomolecular Magnetic Resonance (BMRZ), Frankfurt University funded by the state of Hesse.

Keywords: benzoxazinone • drug scaffold • electrochemistry • sustainable chemistry • twofold amination

- [1] K. C. Nicolaou, A. Li, D. J. Edmonds, *Angew. Chem.* **2006**, *118*, 7244–7248; *Angew. Chem. Int. Ed.* **2006**, *45*, 7086–7090.
 [2] a) R. Hill, A. K. Yudin, *Nat. Chem. Biol.* **2006**, *2*, 284–287; b) A. W. Czarnik, *Acc. Chem. Res.* **1996**, *29*, 112–113; c) J. A. Bikker, N. Brooijmans, A. Wissner, T. S. Mansour, *J. Med. Chem.* **2009**, *52*, 1493–1509; d) A. Wissner, D. M. Berger, D. H. Boschelli, M. B. Floyd, L. M.

RESEARCH ARTICLE

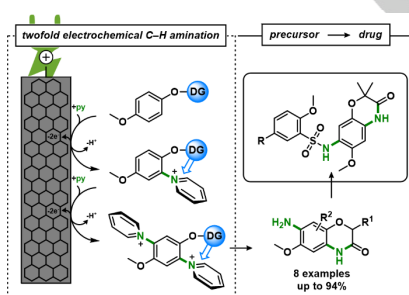
- Greenberger, B. C. Gruber, B. D. Johnson, N. Mamuya, R. Nilakantan, M. F. Reich et al., *J. Med. Chem.* **2000**, *43*, 3244–3256.
- [3] a) O. Meth-Cohn, M. Smith, *J. Chem. Soc., Perkin Trans. 1* **1994**, *5*; b) M. M. Sousa, M. J. Melo, A. J. Parola, P. J. T. Morris, H. S. Rzepa, J. S. S. de Melo, *Chem. Eur. J.* **2008**, *14*, 8507–8513; c) W. H. Perkin, *Q. J. Chem. Soc.* **1862**, *14*, 230–255.
- [4] a) A. D. Schlüter, J. P. Rabe, *Angew. Chem.* **2000**, *112*, 860–880; *Angew. Chem. Int. Ed.* **2000**, *39*, 864–883; b) A. G. Green, A. E. Woodhead, *J. Chem. Soc., Trans.* **1910**, *97*, 2388–2403; c) H. Letheby, *J. Chem. Soc.* **1862**, *15*, 161–163; d) Q.-L. Yang, X.-Y. Wang, J.-Y. Lu, L.-P. Zhang, P. Fang, T.-S. Mei, *J. Am. Chem. Soc.* **2018**, *140*, 11487–11494; e) A. Yella, H.-W. Lee, H. N. Tsao, C. Yi, A. K. Chandiran, M. K. Nazeeruddin, E. W.-G. Diau, C.-Y. Yeh, S. M. Zakeeruddin, M. Grätzel, *Science* **2011**, *334*, 629–634.
- [5] a) R. S. Downing, P. J. Kunkeler, H. van Bekkum, *Catal. Today* **1997**, *37*, 121–136; b) G. A. Olah, R. Malhotra, S. C. Narang, *Nitration. Methods and Mechanisms*, Wiley, New York, **1989**.
- [6] a) J. F. Hartwig, *Acc. Chem. Res.* **1998**, *31*, 852–860; b) J. P. Wolfe, S. Wagaw, J.-F. Marcoux, S. L. Buchwald, *Acc. Chem. Res.* **1998**, *31*, 805–818; c) D. M. T. Chan, K. L. Monaco, R.-P. Wang, M. P. Winters, *Tetrahedron Lett.* **1998**, *39*, 2933–2936; d) P. Y. S. Lam, G. Vincent, C. G. Clark, S. Deudon, P. K. Jadhav, *Tetrahedron Lett.* **2001**, *42*, 3415–3418.
- [7] a) N. Xia, M. Taillefer, *Angew. Chem.* **2009**, *121*, 343–345; *Angew. Chem. Int. Ed.* **2009**, *48*, 337–339; b) H. Rao, H. Fu, Y. Jiang, Y. Zhao, *Angew. Chem. Int. Ed.* **2009**, *48*, 1114–1116.
- [8] a) A. A. Kantak, S. Potavathri, R. A. Barham, K. M. Romano, B. DeBoef, *J. Am. Chem. Soc.* **2011**, *133*, 19960–19965; b) H. J. Kim, J. Kim, S. H. Cho, S. Chang, *J. Am. Chem. Soc.* **2011**, *133*, 16382–16385.
- [9] a) E. Steckhan, T. Arns, W. R. Heineman, G. Hilt, D. Hoormann, J. Jörissen, L. Kröner, B. Lewall, H. Pütter, *Chemosphere* **2001**, *43*, 63–73; b) B. A. Frontana-Urbe, R. D. Little, J. G. Ibanez, A. Palma, R. Vasquez-Medrano, *Green Chem.* **2010**, *12*, 2099; c) H. J. Schäfer, *C. R. Chim.* **2011**, *14*, 745–765.
- [10] a) T. Morofuji, A. Shimizu, J.-i. Yoshida, *J. Am. Chem. Soc.* **2015**, *137*, 9816–9819; b) T. Morofuji, A. Shimizu, J.-i. Yoshida, *Chem. - Eur. J.* **2015**, *21*, 3211–3214; c) T. Morofuji, A. Shimizu, J.-i. Yoshida, *J. Am. Chem. Soc.* **2014**, *136*, 4496–4499; d) R. Hayashi, A. Shimizu, Y. Song, Y. Ashikari, T. Nokami, J.-i. Yoshida, *Chem. - Eur. J.* **2017**, *23*, 61–64.
- [11] T. Morofuji, A. Shimizu, J.-i. Yoshida, *J. Am. Chem. Soc.* **2013**, *135*, 5000–5003.
- [12] L. J. Wesenberg, S. Herold, A. Shimizu, J.-i. Yoshida, S. R. Waldvogel, *Chem. - Eur. J.* **2017**, *23*, 12096–12099.
- [13] X. Xue, Y. Zhang, C. Wang, M. Zhang, Q. Xiang, J. Wang, A. Wang, C. Li, C. Zhang, L. Zou et al., *Eur. J. Med. Chem.* **2018**, *152*, 542–559.
- [14] Q. Xiang, Y. Zhang, J. Li, X. Xue, C. Wang, M. Song, C. Zhang, R. Wang, C. Li, C. Wu et al., *ACS Med. Chem. Lett.* **2018**, *9*, 262–267.
- [15] a) M. Yan, Y. Kawamata, P. S. Baran, *Chem. Rev.* **2017**, *117*, 13230–13319; b) E. J. Horn, B. R. Rosen, P. S. Baran, *ACS Cent. Sci.* **2016**, *2*, 302–308; c) M. D. Kärkäs, *Chem. Soc. Rev.* **2018**, *47*, 5786–5865; d) A. Wiebe, T. Gieshoff, S. Möhle, E. Rodrigo, M. Zirbes, S. R. Waldvogel, *Angew. Chem.* **2018**, *130*, 5694–5721; *Angew. Chem. Int. Ed.* **2018**, *57*, 5594–5619; e) S. Möhle, M. Zirbes, E. Rodrigo, T. Gieshoff, A. Wiebe, S. R. Waldvogel, *Angew. Chem.* **2018**, *130*, 6124–6149; *Angew. Chem. Int. Ed.* **2018**, *57*, 6018–6041; f) S. R. Waldvogel, S. Lips, M. Selt, B. Riehl, C. J. Kampf, *Chem. Rev.* **2018**, *118*, 6706–6765.
- [16] a) A. Wiebe, S. Lips, D. Schollmeyer, R. Franke, S. R. Waldvogel, *Angew. Chem.* **2017**, *129*, 14920–14925; *Angew. Chem. Int. Ed.* **2017**, *56*, 14727–14731; b) S. Lips, A. Wiebe, B. Elsler, D. Schollmeyer, K. M. Dyballa, R. Franke, S. R. Waldvogel, *Angew. Chem. Int. Ed.* **2016**, *55*, 10872–10876; *Angew. Chem.* **2016**, *128*, 11031–11035; c) S. Lips, B. A. Frontana-Urbe, M. Dörr, D. Schollmeyer, R. Franke, S. R. Waldvogel, *Chem. Eur. J.* **2018**, *24*, 6057–6061; d) S. Lips, D. Schollmeyer, R. Franke, S. R. Waldvogel, *Angew. Chem.* **2018**, *130*, 13509–13513; *Angew. Chem. Int. Ed.* **2018**, *57*, 13325–13329; e) A. Lipp, D. Ferenc, C. Gütz, M. Geffe, N. Vierengel, D. Schollmeyer, H. J. Schäfer, S. R. Waldvogel, T. Opatz, *Angew. Chem.* **2018**, *130*, 11221–11225; *Angew. Chem. Int. Ed.* **2018**, *57*, 11055–11059; f) J. L. Röckl, D. Schollmeyer, R. Franke, S. R. Waldvogel, *Angew. Chem.* **2020**, *132*, 323–327; *Angew. Chem. Int. Ed.* **2020**, *59*, 315–319.
- [17] S. Herold, S. Möhle, M. Zirbes, F. Richter, H. Nefzger, S. R. Waldvogel, *Eur. J. Org. Chem.* **2016**, *2016*, 1274–1278.
- [18] S. R. Waldvogel, S. Möhle, *Angew. Chem.* **2015**, *127*, 6496–6497; *Angew. Chem. Int. Ed.* **2015**, *54*, 6496–6497.
- [19] S. Möhle, S. Herold, F. Richter, H. Nefzger, S. R. Waldvogel, *ChemElectroChem.* **2017**, *4*, 2196–2210.
- [20] a) T. Gieshoff, D. Schollmeyer, S. R. Waldvogel, *Angew. Chem.* **2016**, *128*, 9587–9590; *Angew. Chem. Int. Ed.* **2016**, *55*, 9437–9440; b) A. Kehl, V. M. Breising, D. Schollmeyer, S. R. Waldvogel, *Chem. Eur. J.* **2018**, *24*, 17230–17233; c) V. M. Breising, T. Gieshoff, A. Kehl, V. Kilian, D. Schollmeyer, S. R. Waldvogel, *Org. Lett.* **2018**, *20*, 6785–6788.
- [21] C. Gütz, B. Klöckner, S. R. Waldvogel, *Org. Process Res. Dev.* **2016**, *20*, 26–32.
- [22] a) S. Fleischer, S. Zhou, S. Werkmeister, K. Junge, m. Beller, *Chem. Eur. J.* **2013**, *19*, 4997–5003; b) J.-H. Xie, S.-F. Zhu, Q.-L. Zhou, *Chem. Rev.* **2011**, *111*, 1713–1760.
- [23] I. A. Asangani, V. L. Dometti, X. Wang, R. Malik, M. Cieslik, R. Yang, J. Escara-Wilke, K. Wilder-Romans, S. Dhanireddy, C. Engelke et al., *Nature* **2014**, *510*, 278–282.
- [24] C. D. Chen, D. S. Welsbie, C. Tran, S. H. Baek, R. Chen, R. Vessella, M. G. Rosenfeld, C. L. Sawyers, *Nature medicine* **2004**, *10*, 33–39.
- [25] a) S. C. Owen, A. K. Doak, A. N. Ganesh, L. Nedyalkova, C. K. McLaughlin, B. K. Shoichet, M. S. Shoichet, *ACS Chem. Biol.* **2014**, *9*, 777–784; b) S. C. Owen, A. K. Doak, P. Wassam, M. S. Shoichet, B. K. Shoichet, *ACS Chem. Biol.* **2012**, *7*, 1429–1435.

RESEARCH ARTICLE

Entry for the Table of Contents (Please choose one layout)

Layout 1:

Efficient and sustainable access to medicinally and synthetically important C–N bonds is in high demand. However, aromatic primary amine functions via direct C–H amination still remain the major challenge in synthetic organic chemistry. Herein, we report a new environmentally benign twofold electrochemical C–H amination procedure to provide versatile primary amines and valuable heterocycles for biomedical applications.



Lars J. Wesenberg, Erika Diehl, Till J. B. Zähringer, Dieter Schollmeyer, Akihiro Shimizu, Jun-ichi Yoshida†, Ute A. Hellmich, and Siegfried R. Waldvogel

Page No. – Page No.

Metal-free Twofold Electrochemical C–H Amination of Activated Arenes: Application to Medicinally Relevant Precursor Synthesis

Inhaltsverzeichnis

Supporting Information	S5
General aspects	S5
Column chromatography	S5
Gas chromatography	S5
Spectroscopy and spectrometry	S6
X-ray analysis	S6
High Performance Liquid Chromatography (HPLC)	S6
Cyclic Voltammetry (CV)	S6
A: General protocol for the synthesis of methyl phenoxyacetates.....	S7
B: General protocol for the synthesis of Weinreb amides	S7
C: General protocol for the synthesis of arylketones (Grignard method)	S8
D: General protocol for the synthesis of arylketones (α -halo-acetone)	S8
E: General protocol for the synthesis of 1,4-benzoxazin-3-ones.....	S9
F: General protocol or the synthesis of benzenesulfonyl chloride	S9
G: General protocol for the synthesis of sulfonamides.....	S9
Cell culture and Cell Viability Assay:	S10
Experimental setup.....	S11
Thomapor [®] membrane	S12
Cyclic Voltammetry.....	S13
Analysis of 1,4-dimethoxybenzene (4)	S13
Analysis of methyl 2-(4-methoxyphenoxy)acetate (3)	S15
Screening of Electrolytic Conditions	S17
Porous Glass Frit.....	S17
Supporting Electrolyte Tetraethylammonium Hexafluorophosphate	S17
Analytical data	S18
Methyl 2-(4-methoxyphenoxy)acetate (3).....	S18
Methyl 2-(3,5-dimethoxyphenoxy)acetate (18).....	S18
Methy 2-(6-methoxynaphthoxy)acetate (19).....	S18

2,2-Bis(4'-methoxycarbonyl-methyl-phenoxy)propane (23).....	S19
<i>N</i> -Methoxy-2-(4-methoxyphenoxy)- <i>N</i> -methylacetamide (24)	S20
2-(4-Methoxyphenoxy)acetophenone (25)	S20
Methyl 2-(4-methoxyphenoxy)-2-methylpropionate (26).....	S20
Methyl 2-(4-methoxyphenoxy)-2-phenylacetate (27).....	S20
Methyl 2-(2-chlorophenyl)-2-(4-methoxyphenoxy)acetate (28)	S21
Ethyl 2,2-difluoro-2-(4-methoxyphenoxy)acetate (29)	S21
2 <i>H</i> -7-Amino-2,3-dihydro-6-methoxybenzo[<i>b</i>]-1,4-oxazin-3-one (10).....	S22
2 <i>H</i> -8-Amino-2,3-dihydro-7-methoxynaphtho[<i>b</i>]-1,4-oxazin-3-one (11).....	S22
2 <i>H</i> -8-Amino-2,3-dihydro-7-methoxynaphtho[<i>b</i>]-1,4-oxazin-3-one (12).....	S22
2,2-Bis-(2 <i>H</i> -benzo[<i>b</i>]-1,4-oxazin-3-one-6-yl)propane (13)	S23
7-Amino-2,2-dimethyl-6-methoxybenzo[<i>b</i>]-1,4-oxazin-3(4 <i>H</i>)-one (14).....	S23
7-Amino-2,3-dihydro-6-methoxy-2-phenylbenzo[<i>b</i>]-1,4-oxazin-3-one (15).....	S23
7-Amino-2,3-dihydro-6-methoxy-2-phenylbenzo[<i>b</i>]-1,4-oxazin-3-one (16).....	S24
2 <i>H</i> -7-Amino-6-methoxy-3-phenylbenzo[<i>b</i>]-1,4-oxazine (17)	S24
5-Fluoro-2-methoxybenzenesulfonyl chloride 21a.....	S25
5-Bromo-2-methoxybenzenesulfonyl chloride 20a	S25
5-Methyl-2-methoxybenzenesulfonyl chloride 22a	S25
5-Fluoro-2-methoxy- <i>N</i> -(6-methoxy-2,2-dimethylbenzo[<i>b</i>]-1,4-oxazin-3(4 <i>H</i>)-one-7-yl)benzenesulfonamide (21)	S25
5-Bromo-2-methoxy- <i>N</i> -(6-methoxy-2,2-dimethylbenzo[<i>b</i>]-1,4-oxazin-3(4 <i>H</i>)-one-7-yl)benzenesulfonamide (20)	S26
5-Methyl-2-methoxy- <i>N</i> -(6-methoxy-2,2-dimethylbenzo[<i>b</i>]-1,4-oxazin-3(4 <i>H</i>)-one-7-yl)benzenesulfonamide (22)	S27
Crystallographic data.....	S28
7-Amino-2,2-dimethyl-6-methoxybenzo[<i>b</i>]-1,4-oxazin-3(4 <i>H</i>)-one (14).....	S28
5-Fluoro-2-methoxy- <i>N</i> -(6-methoxy-2,2-dimethylbenzo[<i>b</i>]-1,4-oxazin-3(4 <i>H</i>)-one-7-yl)benzenesulfonamide (21)	S29
5-Bromo-2-methoxy- <i>N</i> -(6-methoxy-2,2-dimethylbenzo[<i>b</i>]-1,4-oxazin-3(4 <i>H</i>)-one-7-yl)benzenesulfonamide (20)	S30

5-Methyl-2-methoxy- <i>N</i> -(6-methoxy-2,2-dimethylbenzo[<i>b</i>]-1,4-oxazin-3(4 <i>H</i>)-one-7-yl)benzenesulfonamide (22)	S32
NMR spectra	S34
References	S62

Supporting Information

General aspects

All reagents were used in analytical grades, if not indicated differently. Cyclohexane and ethyl acetate were of technical grade and were purified via distillation prior to use. Acetonitrile was of HPLC grade (Thermo Fisher Scientific, Waltham, Massachusetts, USA). Pyridine and tetraethylammonium tetrafluoroborate were purchased from Acros Organics (Thermo Fisher Scientific, Waltham, Massachusetts, USA). BDD electrodes (DIACHEM®, 10 µm boron-doped diamond layer on 3 mm silicon support) were obtained from CONDIAS GmbH (Itzhoë, Germany), isostatic graphite Sigrafine® electrodes were purchased from SGL Carbon (Bonn-Bad Godesberg, Germany).

Column chromatography

Column chromatography was performed on silica gel 60 M (0.040-0.063 mm, Macherey-Nagel GmbH & Co, Düren, Germany) with a maximum pressure of 2.0 bar. A preparative chromatography system (Büchi-Labortechnik GmbH, Essen, Germany) was used with a Büchi Control Unit C-620, an UV detector Büchi UV photometer C-635, Büchi fraction collector C-660 and two Pump Modules C-605 for adjusting the solvent mixtures. Mixtures of cyclohexane and ethyl acetate were used as eluents. Silica gel 60 sheets on aluminium (F254, Merck, Darmstadt, KGaA, Germany) were employed for thin layer chromatography.

Gas chromatography

GC was performed on a Shimadzu GC-2010 (Shimadzu, Kyoto, Japan) using a Zebron ZB-5MSi column (Phenomenex, USA, dim.: 30 m · 0.25 mm · 0.25 µm, carrier gas: hydrogen).

GC-MS measurements were carried out on a Shimadzu GC-2010 (Shimadzu, Kyoto, Japan) using a HP 1 column (Agilent Technologies, USA; length: 30 m, inner diameter: 0.25 mm, film: 0.25 µm, carrier gas: hydrogen). The method was coupled with mass spectrometry on a Shimadzu GCMS-QP2010.

Method "hart": 50 °C starting temperature for 1 min, heating rate 20 °C/min, final temperature: 190 °C for 5 min.

Spectroscopy and spectrometry

^1H NMR, ^{13}C NMR, and ^{19}F spectra were recorded at 25 °C on a Bruker Avance II 400 or Avance III HD 300 instrument (Bruker, Analytische Messtechnik, Karlsruhe, Germany). Chemical shifts (δ) are reported in parts per million (ppm). Traces of non-deuterated solvents were used as internal standard for calibration. For ^{19}F spectra, α -trifluorotoluene served as external standard ($\delta = -63.9$ ppm). Mass spectra and high resolution mass spectra were obtained by using a QToF Ultima 3 (Waters, Milford, Massachusetts, USA) apparatus employing the ESI+ mode.

X-ray analysis

All data were collected on a STOE IPDS2T diffractometer (Oxford Cryostream 700er series, Oxford Cryosystems) using graphite monochromated Mo K_α radiation ($\lambda = 0.71073$ Å). Intensities were measured using fine-slicing ω and ϕ -scans and corrected for background, polarization and Lorentz effects. The structures were solved by direct methods and refined anisotropically by the least-squares procedure implemented in the SHELX program system.^[1]

The supplementary crystallographic data for this paper can be obtained free of charge from The Cambridge Crystallographic Data Center via www.ccdc.cam.ac.uk/data_request/cif. Deposition numbers and further details are given with the individual characterization data.

High Performance Liquid Chromatography (HPLC)

Analytical HPLC were conducted by use of a modular LC-20A Prominence system (Shimadzu, Japan) and a UV detector SPD-20A/AV. For analytical separations a Eurosphere II C18 column (Knauer Wissenschaftliche Geräte, Berlin, Germany) with an inner diameter of 4 mm and a length of 150 mm (pore size: 100 Å; particle size: 5 μm) was employed. Preparative HPLC was performed on a Azura preparative HPLC (KNAUER Wissenschaftliche Geräte GmbH, Berlin, Germany) using an Eurospher II column (pore size: 100 Å, particle size: 5 μm , length: 250 mm, inner diameter: 30 mm), deuterium lamp as a detector and 2.1 L pump.

Cyclic Voltammetry (CV)

CV was performed with a Metrohm 663 VA Stand equipped with a μ -Autolab type III potentiostat (Metrohm AG, Herisau, Switzerland). WE: BDD electrode tip, 2 mm diameter; CE: glassy carbon rod; RE: Ag/AgNO₃ (silver wire in 0.2 M Bu₄NBF₄, 0.01 M AgNO₃, $E_0 = 77$ mV vs. FcH/FcH⁺). Electrolyte: 0.2 M supporting electrolyte/CH₃CN, $c(\text{substrate}) = 2$ mmol.^[2]

A: General protocol for the synthesis of methyl phenoxyacetates

In a round-bottom flask (250 mL), the phenol derivative (18 mmol, 1.0 eq) was dissolved in 120 mL *N,N*-dimethylformamide (DMF) and potassium carbonate (6.21 g, 45 mmol, 2.5 eq) was added. Followed by a slow addition (0.2 mL/min) of 1.9 mL methyl α -bromoacetate (20 mmol, 1.1 eq) to the suspension. The reaction mixture was stirred at room temperature for 18 hours. When thin layer chromatography (TLC) indicated almost disappearance of the phenolic component (ethyl acetate/cyclohexane = 1/1), water (200 mL) was added to the reaction mixture. The mixture was extracted three times with ethyl acetate (200 mL). The combined organic fractions were washed two times with water (50 mL) and two times with saturated sodium chloride solution (50 mL). The organic fraction was dried (MgSO_4) and filtered. Concentration of the solution provided the crude product. Solid products were purified by recrystallization from ethanol/water = 9/1. Liquid products were distilled at reduced pressure. Alternatively, the crude products were purified by column chromatography using ethyl acetate/cyclohexane as eluent mixtures.^[3]

B: General protocol for the synthesis of Weinreb amides

In a round-bottom flask (50 mL), the phenyl acetic acid (0.910 g, 5.0 mmol, 1.0 eq) was dissolved in anhydrous *N,N*-dimethylformamide (10 mL) and cooled to 0 °C. 1,1'-Carbonyl diimidazole (1.054 g, 6.5 mmol, 1.3 eq) was added to the reaction mixture. The solution was stirred at 0-25 °C until carbon dioxide production ceased and imidazole started to precipitate. The suspension was cooled again to 0 °C and trimethylamine (1 mL, 7.0 mmol, 1.5 eq) was added. Subsequently, *N,O*-dimethylhydroxylamine hydrochloride (0.732 g, 7.5 mmol, 1.5 eq) was added in small portions. The reaction temperature was kept at 0 °C. The reaction was stirred overnight at 0-25 °C. The conversion of the reaction was monitored by TLC analysis. Overnight a precipitate formed, which was dissolved by the addition of 15 mL 1 M HCl. The aqueous layer was extracted four times with dichloromethane (15 mL) and washed two times with water and additionally two times with 15% LiCl solution (25 mL) to ensure the removal of all DMF. The combined organic fraction was dried with MgSO_4 and filtered. Concentration of the solution provided crude product. Further purification was done by column chromatography using cyclohexane/ethyl acetate as eluent mixtures.^[4]

C: General protocol for the synthesis of arylketones (Grignard method)

In a round bottom flask (50 mL), the Weinreb amide (5.0. mmol, 1.0 eq) was dissolved in anhydrous THF (20 mL) and cooled to 0 °C. Phenylmagnesium bromide (7.5 mmol, 1.5 eq) was added slowly. The resulting mixture was stirred overnight. The conversion of the reaction was monitored by TLC analysis. The reaction was quenched by a half saturated ammonium chloride solution. The resulting aqueous solution was extracted four times with 20 mL dichloromethane. The combined organic fraction was dried with MgSO₄ and filtered. Concentration of the solution provided the crude product. The crude product was purified by column chromatography using cyclohexane/ethyl acetate as eluent mixtures.

D: General protocol for the synthesis of arylketones (α -halo-acetone)

In a round-bottom flask (100 mL), the phenol derivative (20 mmol, 1.0 eq) was dissolved in 2-butanone (30 mL) and potassium carbonate (5.0 g, 36 mmol, 1.8 eq) as well as potassium iodide (0.2 g, 1.2 mmol, 0.06 eq) were added. To this suspension a solution of bromo acetophenone derivative (4.67 g, 20 mmol, 1.0 eq) in 2-butanone (10 mL) was added dropwise over 15 min. The reaction mixture was stirred under reflux for 3-6 h. The TLC analysis confirmed the almost complete disappearance of the starting material. The solids were filtered off and the solution was concentrated at reduced pressure. The oily residue was extracted into diethylether and washed several times with 1 M NaOH and water. The combined ethereal extract was dried over MgSO₄, filtered, and concentrated to provide the crude product. Further purification was done by column chromatography using cyclohexane/ethyl acetate as eluent mixtures.^[5]

E: General protocol for the synthesis of 1,4-benzoxazin-3-ones

The electrochemical conversion was conducted in divided cells made of Teflon.^[6,7] Thomapor[®] was used as the separator. A platinum plate was employed as the cathode and isostatic graphite was used as anodic material (dimension: 1 cm × 3 cm × 0.3 cm).^[7] The anolyte consisted of 0.5 mmol methyl phenoxyacetate derivative, 1 mL (12 mmol) pyridine and 5 mL 0.2 M Et₄NBF₄ in acetonitrile. To the cathodic compartment 6 mL 0.2 M Et₄NBF₄ in acetonitrile and 0.5 mL trifluoromethane sulfonic acid were added. The first pyridination process was performed with 3.4 F and at 5 mA/cm². The further second pyridination process was conducted at 2.1 F and 10 mA/cm². The electrolysis were conducted at constant current conditions at 20 °C.

Anolyte compartment was transferred into a pressure tube and 1 mL of piperidine was added. This solution was heated to 80 °C for 12-18 hours. The volatiles were removed at reduced pressure and the crude product was purified via column chromatography (ethyl acetate/cyclohexane + 1% triethylamine).^[3]

F: General protocol or the synthesis of benzenesulfonyl chloride

A round bottom flask (100 mL) was charged with chlorosulfonic acid (300 mmol, 20 mL, 7.5 eq) and cooled to 0 °C. The anisole derivative (40 mmol, 1.0 eq) was added slowly. The resulting homogenous mixture was stirred for 30 min at 0-25 °C. After completion (2 h) the reaction mixture was pured slowly into 200 mL crushed ice. A precipitate formed immediately. The crude precipitate was filtered off and washed 5 times with cold water. Where needed, the crude product was purified by recrystallization from cyclohexane/chloroform mixtures.^[8]

G: General protocol for the synthesis of sulfonamides

In a round bottom flask (10 mL) the aniline derivative was dissolved in dichloromethane (2 mL) with pyridine (0.5 mL) and cooled to 0 °C. The benzenesulfonyl chloride derivative was added slowly in portions or dropwise (dissolved in dichlormethane 2 mL). The reaction mixture turned slightly orange. The resulting mixture was stirred for 30 min at 0-25 °C. The conversion of the reaction was monitored by TLC analysis. After completion (1-2 h) 5 mL of 10% HCl solution was added. The aqueous layer was extracted four times with dichloromethane (5 mL) and washed 2 times with water. The combined organic fraction was dried over MgSO₄ and filtered. Concentration of the solution provided the crude product. The crude product was purified by column chromatography (normal phase, C18 reversed phase) using cyclohexane/ethyl acetate and water/acetonitrile as eluent mixtures.^[9]

Cell culture and Cell Viability Assay:

HEK293 cells were cultured in DMEM (Sigma Aldrich, Munic, Germany) supplemented with 10 % FCS (v/v) (Biochrom, Berlin, Germany), 1 % Penicillin/Streptomycin (v/v) (Sigma Aldrich, Munic, Germany) and 1 % L-Glutamine (v/v) (Sigma Aldrich, Munic, Germany). LnCAP cells were cultured in RPMI-1640 (Sigma Aldrich, Munic, Germany) supplemented with 10 % FCS (v/v), 1 % Penicillin/Streptomycin (v/v) and 1 % L-Glutamine (v/v). Cells were grown at 37 °C in 5 % CO₂. For the MTT Cell Viability Assay,^[10] cells were seeded with 25 000 cells/well in 24-well plates. After 24 h and exchange to fresh growth medium without phenol red, cells were treated with a serial dilution of compound 20-22 (1-20 µM, diluted in DMSO of BioScience Grade (Roth, Karlsruhe, Germany)), respectively, with a total volume of 5 µL (0.5 % (v/v) DMSO/well). Every plate also contained control wells where cells were treated with 0.5 % (v/v) DMSO. After an incubation time of 48h, MTT (Sigma Aldrich, Munic, Germany) with an end concentration of 2 mM was added to each well and cells were incubated for 90 minutes at 37 °C and 5 % CO₂. The produced formazan was then solubilized with 10 % (w/v) Triton-X and 0.1 n HCl in 2-propanole. The MTT absorbance was measured at 560 nm and subtracted by cell debris background absorbance at 650 nm. Shown results are normalized on control cells treated with 0.5 % (v/v) DMSO.

Experimental setup

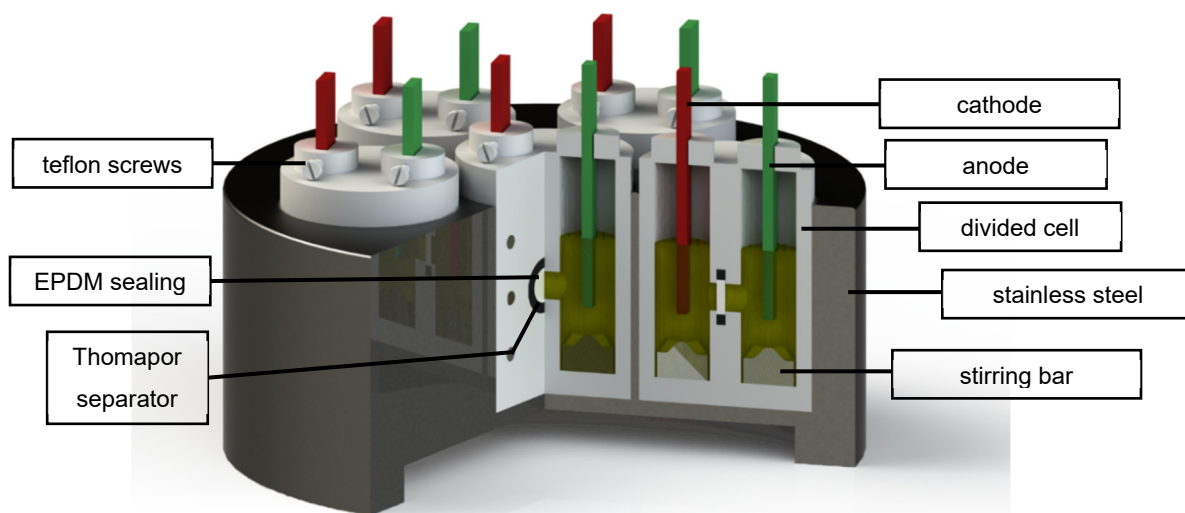


Figure 1: Screening system with 6 divided electrolysis cells fitting on a common magnetic stirrer; electrode gap: 2 cm; active surface of the planar electrode: 3 cm².

Divided screening cells embedded in a stainless steel arranged designed by Waldvogel research group^[6] and were used for the twofold electrochemical C–H amination. The divided cells Divided screening cells embedded in a stainless steel arranged designed by Waldvogel are made of PTFE (polytetrafluoroethylene, Teflon[®]) and were used to conveniently screen several electrolysis parameters in an efficient way and short time.^[6] The volume capacity of electrolyte solution of each chamber is up to 6 mL. Porous glass frits (10-16 μm, ROBU[®] Glasfilter-Geräte GmbH, Hattert, Germany) and Thomapor[®] membranes (Reichelt Chemietechnik GmbH & Co., Heidelberg, Germany) were used as separator materials. An O-ring made of ethylene-propylene-diene-rubber (EPDM) was used to seal the compartments. The electrode gap between cathode and anode was approx. 2 cm in this experimental setup. A multi-channel galvanostate was used as the power source. The screening setup is also commercially available as IKA Screening System (IKA-Werke GmbH & Co. KG, Staufen, Germany).

Thomapor® membrane

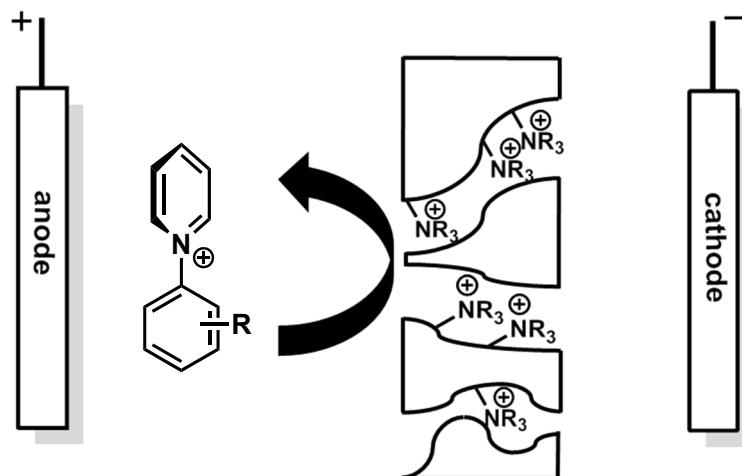


Figure 2: The Thomapor® separator as anion exchange membrane. It is not permeable for positively charged pyridinium intermediates. Functionalization of a polystyrene polymer with quaternary ammonium groups allows this selectivity.^[11]

Thomapor® RCT®-high-mechanical-strength-AMX anion exchange membranes were used as the separator (purchased from Reichelt Chemietechnik GmbH & Co., Heidelberg, Germany).

Cyclic Voltammetry

Analysis of 1,4-dimethoxybenzene (4)

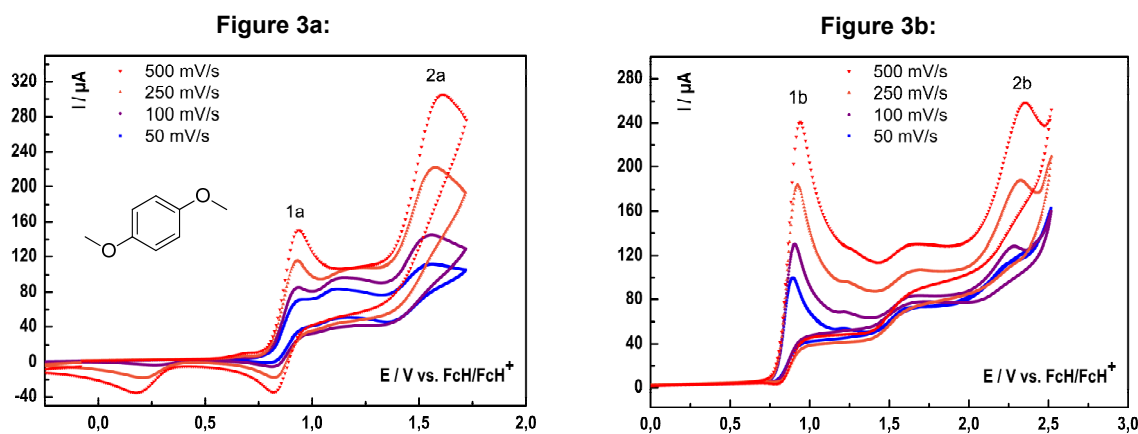
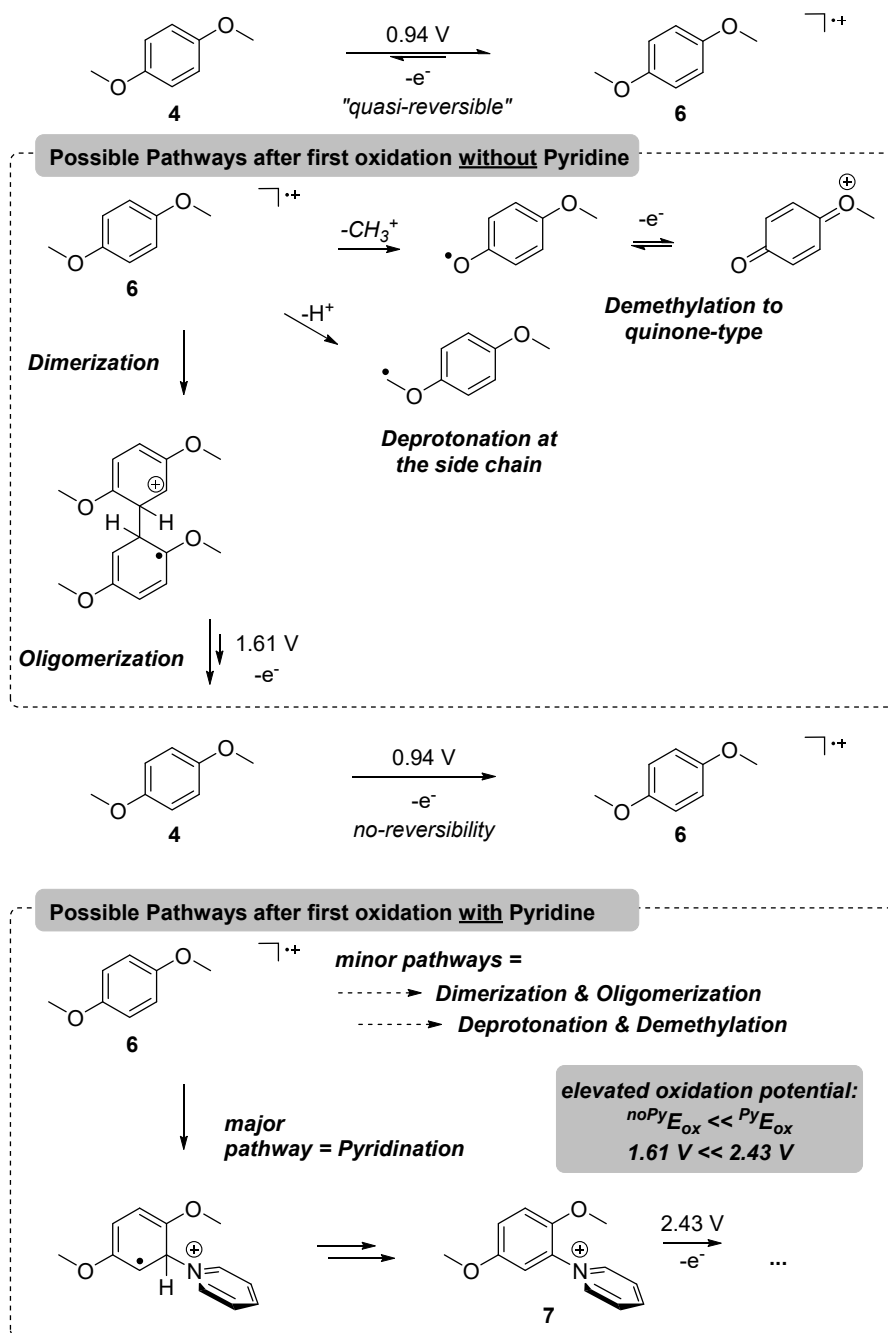


Figure 3: Cyclic voltammograms of 0.1 M Et₄NBF₄/CH₃CN with 1,4-dimethoxybenzene **4** with different scan rates from 50 mV/s to 500 mV/s. (a): without addition of pyridine. (b): With addition of pyridine. Working electrode: BDD; counter electrode: glassy carbon; reference electrode: Ag/AgNO₃.

In the cyclic voltammogram of 1,4-dimethoxybenzene **4** (Figure 3a), one quasi-reversible oxidation step and another oxidation peak were observed ($E_{\text{Ox1a}} = 0.94$ V and $E_{\text{Ox2a}} = 1.61$ V vs. FcH/FcH⁺, respectively). Increasing the scan rate from 50 mV/s to 500 mV/s the first two oxidation peaks unite to one broad oxidation band. This suggests that on a slow time scale the first emerging radical cation **6** has time to be interfered by a chemical reaction, which is also indicated by the absence of a reduction wave at 0.82 V vs. FcH/FcH⁺. Resulting in an intermediate which is oxidized at elevated potential. With the addition of pyridine, the second oxidation peak shifts to higher values ($E_{\text{Ox2b}} = 2.43$ V vs. FcH/FcH⁺, Figure 3b). This indicates that the electron-withdrawing effect of the pyridinium intermediate **7** destabilize the arene system and consequently over-oxidation is suppressed. Thus, the single pyridinium salt **7** accumulates and no further oxidation processes can occur. These data are consistent with the hypothesis postulated by Yoshida and co-workers.^[12]



Scheme 1: Postulated Electrochemical pathways of dimethoxybenzene **4** in a twofold amination reaction according to cyclic voltammetry measurements. To the best of our knowledge the assignment of the oxidation potentials is most likely.^[13]

Analysis of methyl 2-(4-methoxyphenoxy)acetate (**3**)

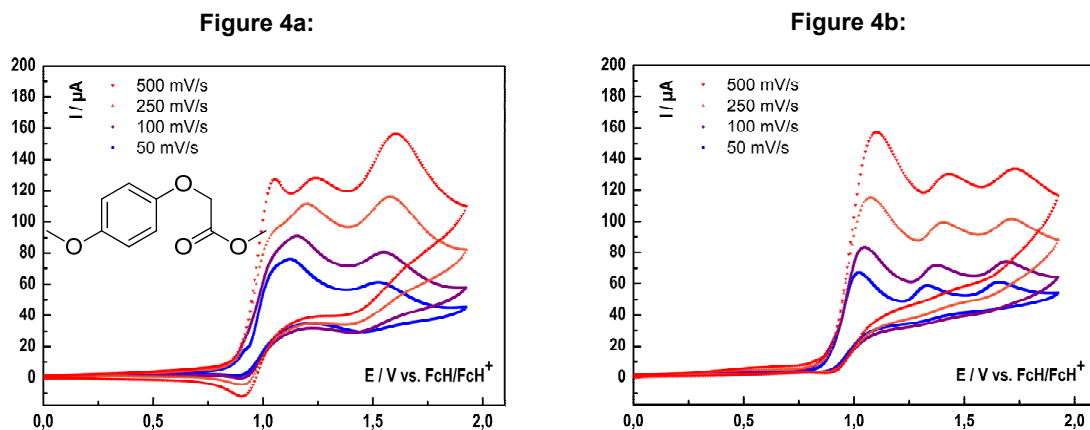
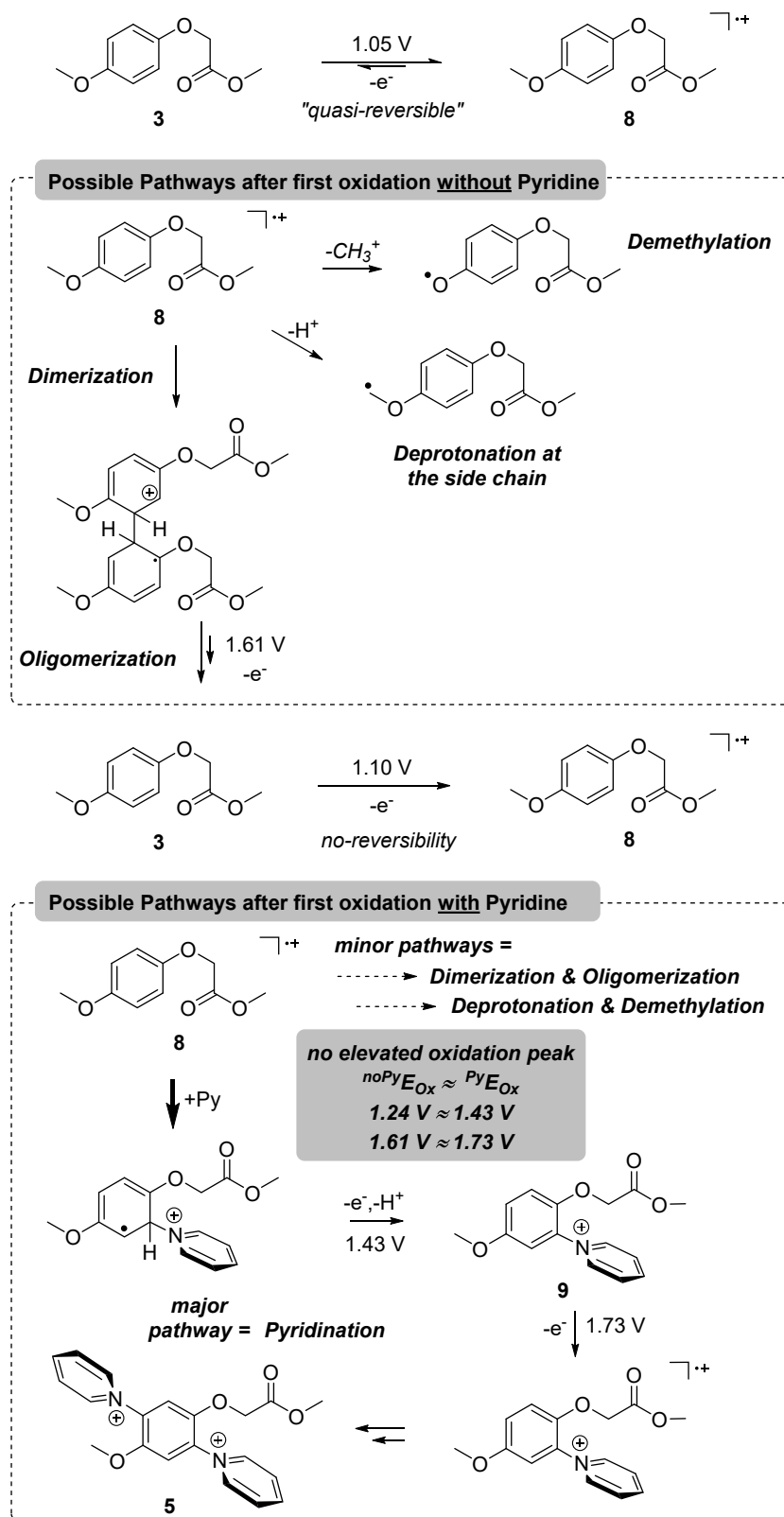


Figure 4: Cyclic voltammograms of 0.1 M Et₄NBF₄/CH₃CN with methyl 2-(4-methoxyphenoxy)acetate **3** with different scan rates from 50 mV/s to 500 mV/s. (a): without addition of pyridine. (b): With addition of pyridine. Working electrode: BDD; counter electrode: glassy carbon; reference electrode: Ag/AgNO₃.

In the cyclic voltammogram of methyl 2-(4-methoxyphenoxy)acetate **3** (Figure 4a), three distinguishable oxidation peaks can be observed ($E_{\text{Ox}1} = 1.05$ V, $E_{\text{Ox}2} = 1.24$ V, and $E_{\text{Ox}3} = 1.61$ V vs. FcH/FcH⁺, respectively). The first oxidation peak seems to be quasi-reversible at high scan rates. Additionally, at 500 mV/s two defined oxidation peaks can be observed, which unite to one broad peak at 50 mV/s. In comparison to the Figure 4b the shape of the cyclic voltammogram seems to be clearly defined by the addition of pyridine and independent to the scan rate. Emerging radical cations **8** will be trapped in-situ by pyridine. This appears to determine the reaction pathway. The trapping mechanism is also monitored by the absence of a reduction wave at 0.9 V vs. FcH/FcH⁺ and consequently no reversibility is observable at any scan rate. Furthermore, no significant shift of the oxidation peaks compared to the elevated oxidation peak with 1,4-dimethoxybenzene as substrate (Figure 3b, $E_{\text{Ox}2a} = 1.61$ V and $E_{\text{Ox}2b} = 2.43$ V vs. FcH/FcH⁺, respectively) could be found. This suggests a shielding and stabilizing effect of the attached ester function.



Scheme 2: Postulated electrochemical pathway of methyl 2-(4-methoxyphenoxy)acetate **3** in a twofold amination reaction according to cyclic voltammetry measurements. To the best of our knowledge the assignment of the oxidation potentials is most likely.^[13]

Screening of Electrolytic Conditions

Porous Glass Frit

Table 1. Screening of electrolysis conditions. 0.5 mmol substrate, 0.2 M supporting electrolyte, 12 mmol pyridine, 5 mmol trifluoromethanesulfonic acid (TfOH), isostatic graphite anode, platinum cathode, divided cell

Entry	Separator	Supporting electrolyte	Current density / mA/cm ⁻²	Applied charge / F/mol	Yield / % ^[a]
1	glass frit	NEt ₄ BF ₄	1	4.2	24
2	glass frit	NEt ₄ BF ₄	3	4.2	32
3	glass frit	NEt ₄ BF ₄	7	4.2	18
4	glass frit	NEt ₄ BF ₄	8	4.2	29
5	glass frit	NEt ₄ BF ₄	9	4.2	25
6	glass frit	NEt ₄ BF ₄	10	4.2	30
7	glass frit	NEt ₄ BF ₄	11	4.2	28
8	glass frit	NEt ₄ BF ₄	12	4.2	30
9	glass frit	NEt ₄ BF ₄	13	4.2	32
10	glass frit	NEt ₄ BF ₄	16	4.2	33

[a] determined via ¹H NMR with 1,1,2,2-tetrachloroethane as ISTD

Supporting Electrolyte Tetraethylammonium Hexafluorophosphate

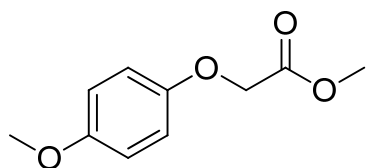
Table 2. Screening of electrolysis conditions. 0.5 mmol substrate, 0.2 M supporting electrolyte, 12 mmol pyridine, 5 mmol trifluoromethanesulfonic acid (TfOH), isostatic graphite anode, platinum cathode, divided cell

Entry	Separator	Supporting electrolyte	Current density / mA/cm ⁻²	Applied charge / F/mol	Yield / % ^[a]
1	Thomapor [®]	NEt ₄ PF ₆	1	5.5	46
2	Thomapor [®]	NEt ₄ PF ₆	3	5.5	42
3	Thomapor [®]	NEt ₄ PF ₆	7	5.5	48
4	Thomapor [®]	NEt ₄ PF ₆	10	5.5	51
5	Thomapor [®]	NEt ₄ PF ₆	13	5.5	47
6	Thomapor [®]	NEt ₄ PF ₆	16	5.5	44

[a] determined via ¹H NMR with 1,1,2,2-tetrachloroethane as ISTD

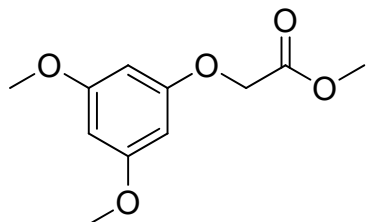
Analytical data

Methyl 2-(4-methoxyphenoxy)acetate (**3**)



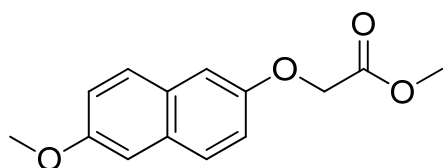
Preparation according to general protocol **A** produced **3** (1.217 g, 6.2 mmol, 34%) as colorless solid. $R_f = 0.30$, (cyclohexane/ethyl acetate = 5/1). $^1\text{H NMR}$ (400 MHz, chloroform-*d*) δ (ppm) = 3.76 (s, 3H), 3.80 (s, 3H), 4.59 (s, 2H), 6.80 – 6.90 (m, 4H). $^{13}\text{C NMR}$ (101 MHz, chloroform-*d*) δ (ppm) = 52.2, 55.7, 66.3, 114.7, 115.9, 152.0, 154.6, 169.7. mp.: 46.4–49.6 °C, crystallized from ethanol. HRMS ESI (m/z) for $[\text{M}+\text{Na}]^+$ $\text{C}_{10}\text{H}_{12}\text{NaO}_4$: calc.: 219.0633, found: 219.0623. The spectroscopic data match those reported in literature.^[14]

Methyl 2-(3,5-dimethoxyphenoxy)acetate (**18**)



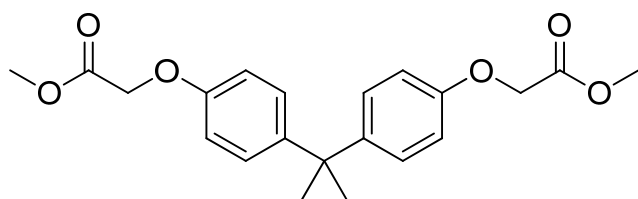
Preparation according to general protocol **A** produced **18** (1.79 g, 7.9 mmol, 79%) as colorless liquid. $R_f = 0.26$ (cyclohexane/ethyl acetate = 5/1). $^1\text{H NMR}$ (400 MHz, chloroform-*d*) δ (ppm) = 3.76 (s, 10H), 3.80 (s, 5H), 4.59 (s, 4H), 6.08 (d, $J=2.1$, 4H), 6.12 (t, $J=2.1$, 2H). $^{13}\text{C NMR}$ (101 MHz, chloroform-*d*) δ (ppm) = 52.4, 55.5, 65.4, 93.6, 94.0, 159.7, 161.7, 169.3. mp.: 56.0–57.9 °C, crystallized from cyclohexane/ethyl acetate. HRMS ESI (m/z) for $[\text{M}+\text{H}]^+$ $\text{C}_{11}\text{H}_{15}\text{O}_5$: calc. 227.0919, found: 227.0910. The spectroscopic data match those reported in literature.^[15]

Methyl 2-(6-methoxynaphthoxy)acetate (**19**)



Preparation according to general protocol **A** produced **19** (1.7 g, 9.4 mmol, 85%) as colorless liquid. $R_f = 0.50$, (cyclohexane/ethyl acetate = 1/2). $^1\text{H NMR}$ (400 MHz, chloroform-*d*) δ (ppm) = 3.83 (s, 3H), 3.90 (s, 3H), 4.73 (s, 2H), 7.05 (d, $J=2.6$, 1H), 7.10 (d, $J=2.6$, 1H), 7.13 (dd, $J=8.9$, 2.6, 1H), 7.21 (dd, $J=8.9$, 2.6, 1H), 7.63 (d, $J=8.9$, 1H), 7.67 (d, $J=8.9$, 1H). $^{13}\text{C NMR}$ (101 MHz, chloroform-*d*) δ (ppm) = 52.4, 55.4, 65.6, 106.1, 107.6, 118.9, 119.3, 128.4, 128.6, 129.5, 130.4, 154.3, 156.6, 169.6. mp.: 123.0–125.4 °C, crystallized from cyclohexane/ethyl acetate. HRMS ESI (m/z) for $[\text{M}+\text{H}]^+$ $\text{C}_{14}\text{H}_{15}\text{O}_4$: calc.: 247.0970, found: 247.0970.

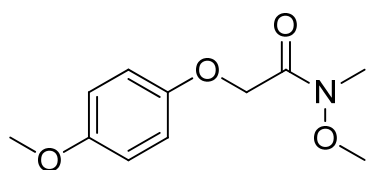
2,2-Bis(4'-methoxycarbonylmethylphenoxy)propane (**23**)



Preparation according to general protocol **A** produced **23** (1.7 g, 9.4 mmol, 85%) as colorless liquid. $R_f = 0.20$, (cyclohexane/ethyl acetate = 5/1). $^1\text{H NMR}$

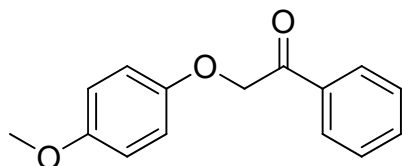
(400 MHz, chloroform- d) δ (ppm) = 1.62 (s, 8H), 3.80 (s, 8H), 4.61 (s, 5H), 6.80 (d, $J=8.9$, 4H), 7.13 (d, $J=8.9$, 4H). $^{13}\text{C NMR}$ (101 MHz, chloroform- d) δ (ppm) = 31.0, 41.8, 52.3, 65.4, 114.0, 127.9, 144.1, 155.6, 169.6. HRMS ESI (m/z) for $[\text{M}+\text{Na}]^+$ $\text{C}_{21}\text{H}_{24}\text{NaO}_6$: calc.: 395.1465, found: 395.1471. The analytical data match those reported in literature.^[16]

N-Methoxy-2-(4-methoxyphenoxy)-N-methylacetamide (24)



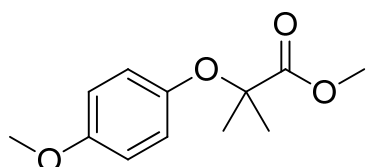
Preparation according to general protocol **B** produced **24** (2.806 g, 12.4 mmol, 87%) as clear oil. $R_f = 0.35$, (cyclohexane/ethyl acetate = 1/1). $^1\text{H NMR}$ (400 MHz, chloroform-*d*) δ (ppm) = 3.23 (s, 2H), 3.74 (s, 1H), 3.76 (s, 1H), 4.76 (s, 1H), 6.80 – 6.86 (m, 1H), 6.88 – 6.93 (m, 1H). $^{13}\text{C NMR}$ (101 MHz, chloroform-*d*) δ (ppm) = 32.5, 55.8, 61.8, 66.7, 77.4, 114.7, 116.2, 152.6, 154.5. HRMS ESI (m/z) for $[\text{M}+\text{H}]^+$ $\text{C}_{11}\text{H}_{16}\text{NO}_4$: calc.: 226.1079, found 226.1079. The spectroscopic data match those reported in literature.^[4]

2-(4-Methoxyphenoxy)acetophenone (25)



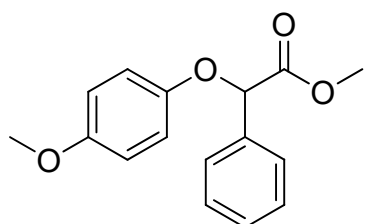
Preparation according to general protocol **C** produced **24** (2.351g, 9.7 mmol, 87%) as colorless solid. $R_f = 0.38$, (cyclohexane/ethyl acetate = 5/1). $^1\text{H NMR}$ (400 MHz, chloroform-*d*) δ (ppm) = 3.76 (s, 2H), 5.23 (s, 1H), 6.80 – 6.86 (m, 1H), 6.87 – 6.93 (m, 1H), 7.44 – 7.54 (m, 1H), 7.57 – 7.66 (m, 1H), 7.93 – 8.09 (m, 1H). $^{13}\text{C NMR}$ (101 MHz, chloroform-*d*) δ (ppm) = 55.8, 71.9, 114.8, 116.1, 128.3, 129.0, 134.0, 134.8, 152.3, 154.6, 195.0. mp.: 64.5–67.5 °C. HRMS ESI (m/z) for $[\text{M}+\text{H}]^+$ $\text{C}_{15}\text{H}_{15}\text{O}_3$: calc.: 243.1021, found: 243.1019. The spectroscopic data match those reported in literature.^[17]

Methyl 2-(4-methoxyphenoxy)-2-methylpropionate (26)



Preparation according to general protocol **A** produced **26** (1.86 g, 8.3 mmol, 83%) as colorless liquid. Reaction temperature was increased to 90 °C. Bromo compound was slowly added over 10 min. $R_f = 0.30$, (cyclohexane/ethyl acetate = 5/1). $^1\text{H NMR}$ (400 MHz, chloroform-*d*) δ (ppm) = 1.53 (s, 3H), 3.76 (s, 2H), 3.78 (s, 2H), 6.75 – 6.80 (m, 1H), 6.80 – 6.87 (m, 1H). $^{13}\text{C NMR}$ (101 MHz, chloroform-*d*) δ (ppm) = 25.4, 52.6, 55.7, 79.9, 114.3, 121.8, 148.9, 155.4, 175.0. HRMS ESI (m/z) for $[\text{M}+\text{H}]^+$ $\text{C}_{12}\text{H}_{17}\text{O}_4$: calc.: 225.1127, found: 225.1127.

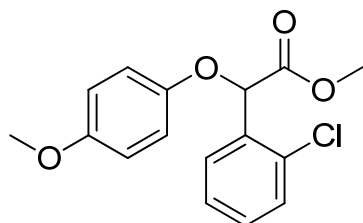
Methyl 2-(4-methoxyphenoxy)-2-phenylacetate (27)



Preparation according to general protocol **D** produced **27** (4.884g, 18.0 mmol, 87%) as colorless solid. $R_f = 0.80$, (cyclohexane/ethyl acetate = 2/1). $^1\text{H NMR}$ (400 MHz, chloroform-*d*) δ (ppm) = 3.74 (s, 1H), 3.75 (s, 2H), 5.56 (s, 0H), 6.75 – 6.85 (m, 1H), 6.86 – 6.94 (m, 1H), 7.33 – 7.45 (m, 2H),

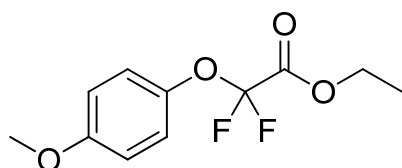
7.53 – 7.61 (m, 1H). ^{13}C NMR (101 MHz, chloroform-*d*) δ (ppm) = 52.7, 55.7, 79.8, 114.8, 117.0, 127.2, 128.9, 129.1, 135.7, 151.5, 154.7, 170.7. mp.: 77.2–80.0 °C. HRMS ESI (*m/z*) for $[\text{M}+\text{Na}]^+$ $\text{C}_{16}\text{H}_{16}\text{NaO}_4$: calc.: 295.0946, found: 295.0943. The spectroscopic data match those reported in literature.^[18]

Methyl 2-(2-chlorophenyl)-2-(4-methoxyphenoxy)acetate (**28**)



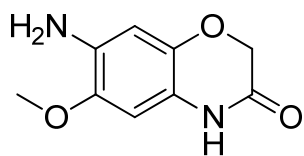
Preparation according to general protocol **D** produced **28** (2.553g, 8.3 mmol, 83 %) as colorless oil. R_f = 0.60, (cyclohexane/ethyl acetate = 5/1). ^1H NMR (400 MHz, chloroform-*d*) δ (ppm) = 3.74 (s, 3H), 3.76 (s, 3H), 6.06 (s, 1H), 6.75 – 6.85 (m, 2H), 6.85 – 6.96 (m, 2H), 7.26 – 7.34 (m, 2H), 7.38 – 7.45 (m, 1H), 7.59 – 7.70 (m, 1H). ^{13}C NMR (101 MHz, chloroform-*d*) δ (ppm) = 52.8, 55.7, 76.1, 114.8, 117.2, 127.5, 128.9, 129.8, 130.3, 133.6, 133.9, 151.3, 154.9, 169.9. HRMS ESI (*m/z*) for $[\text{M}+\text{Na}]^+$ $\text{C}_{16}\text{H}_{15}\text{ClNaO}_4$: calc.: 329.0557 found: 329.0557.

Ethyl 2,2-difluoro-2-(4-methoxyphenoxy)acetate (**29**)



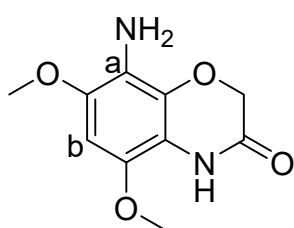
Preparation according to general protocol **A** produced **29** (1.56 g, 634 μmol , 63%) as colorless liquid. Reaction temperature was increased to 70 °C and Diazabicycloundecene (DBU) was used instead of K_2CO_3 . The Bromo derivative was slowly added over 15 min. R_f = 0.45, (cyclohexane/ethyl acetate = 3/1). ^1H NMR (400 MHz, chloroform-*d*) δ (ppm) = 1.37 (t, $J=7.2$, 2H), 3.80 (s, 1H), 4.38 (q, $J=7.1$, 1H), 6.78 – 6.92 (m, 1H), 7.08 – 7.19 (m, 1H). ^{19}F NMR (376 MHz, chloroform-*d*) δ (ppm) = -77.73. ^{13}C NMR (101 MHz, chloroform-*d*) δ (ppm) = 14.0, 55.7, 63.8, 114.1 (t, $J=271.3$), 114.6, 123.2, 142.8, 157.9, 160.1 (t, $J=41.6$). The spectroscopic data match those reported in literature.^[19]

2H-7-Amino-2,3-dihydro-6-methoxybenzo[*b*]-1,4-oxazin-3-one (10)



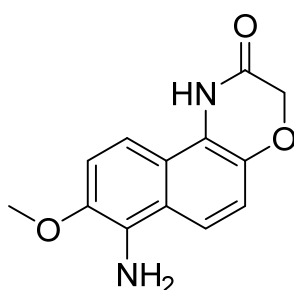
Preparation according to general protocol **E** produced **10** (56 mg, 0.29 mmol, 57%) as slightly yellow solid. $R_f = 0.20$, (cyclohexane/ethyl acetate = 1/2). $^1\text{H NMR}$ (400 MHz, DMSO- d_6) δ (ppm) = 3.67 (s, 3H), 4.37 (s, 2H), 4.54 (s, 2H), 6.29 (s, 1H), 6.38 (s, 1H), 10.21 (s, 1H). $^{13}\text{C NMR}$ (101 MHz, DMSO- d_6) δ (ppm) = 55.9, 67.1, 100.0, 102.4, 116.0, 133.3, 137.4, 141.6, 164.3. mp.: 171.1–173.5 °C, crystallized from cyclohexane/ethyl acetate. HRMS ESI (m/z) for $[\text{M}+\text{H}]^+$ $\text{C}_9\text{H}_{11}\text{N}_2\text{O}_3$: calc.: 195.0770, found: 195.0764.

2H-8-Amino-2,3-dihydro-7-methoxynaphtho[*b*]-1,4-oxazin-3-one (11)



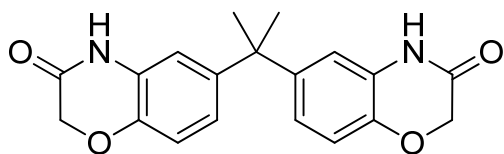
Preparation according to general protocol **E** produced **11a** (23 mg, 0.11 mmol, 21%) and **11b** (39 mg, 0.18 mmol, 35%) as colorless solids. $R_f = 0.28$ (cyclohexane/ethyl acetate = 1/5). Purified by preparative HPLC (eluent mixture of solvent A, solvent B, A: water/acetonitrile/ H_3PO_4 = 950/50/1, B: acetonitrile). $^1\text{H NMR}$ **11a** (400 MHz, DMSO- d_6) δ (ppm) = 3.72 (s, 3H), 3.75 (s, 3H), 3.97 (s, 2H), 4.46 (s, 2H), 6.39 (s, 1H), 9.89 (s, 1H). $^{13}\text{C NMR}$ **11a** (101 MHz, DMSO- d_6) δ (ppm) = 56.2, 57.1, 67.2, 93.0, 111.1, 120.0, 131.9, 137.6, 142.4, 164.1. $^1\text{H NMR}$ **11b** (400 MHz, DMSO- d_6) δ (ppm) = 3.63 (s, 3H), 3.71 (s, 3H), 4.18 (s, 2H), 4.39 (s, 2H), 6.39 (s, 1H), 10.14 (s, 1H). $^{13}\text{C NMR}$ **11b** (101 MHz, DMSO- d_6) δ (ppm) = 55.9, 59.5, 67.3, 96.5, 114.5, 125.6, 134.3, 134.4, 142.3, 164.9. mp. **11a**: 223.0–225.3 °C, mp. **11b**: 222.9–225.3 °C, crystallized from acetonitrile/water. HRMS ESI **11a** (m/z) for $[\text{M}+\text{H}]^+$ $\text{C}_{10}\text{H}_{13}\text{N}_2\text{O}_4$: calc.: 225.0870, found: 225.0869, HRMS ESI **11b** (m/z) for $[\text{M}+\text{H}]^+$ $\text{C}_{10}\text{H}_{13}\text{N}_2\text{O}_4$: calc.: 225.0870, found: 225.0867.

2H-8-Amino-2,3-dihydro-7-methoxynaphtho[*b*]-1,4-oxazin-3-one (12)



Preparation according to general protocol **E** produced **12** (54 mg, 0.24 mmol, 47%) as colorless solid. $R_f = 0.15$ (cyclohexane/ethyl acetate = 1/1). $^1\text{H NMR}$ (400 MHz, DMSO- d_6) δ (ppm) = 3.86 (s, 3H), 4.60 (s, 2H), 5.28 (s, 2H), 7.06 (d, $J=9.1$, 1H), 7.27 (d, $J=9.1$, 1H), 7.46 (d, $J=9.2$, 1H), 7.69 (d, $J=9.2$, 1H), 10.79 (s, 1H). $^{13}\text{C NMR}$ (101 MHz, DMSO- d_6) δ (ppm) = 56.5, 67.1, 107.9, 114.3, 115.3, 117.4, 119.4 (d, $J=1.3$), 120.0, 132.0, 138.5, 140.4, 165.6. mp.: 230.0–232.5 °C, crystallized from cyclohexane/ethyl acetate. HRMS ESI (m/z) for $[\text{M}+\text{H}]^+$ $\text{C}_{13}\text{H}_{13}\text{N}_2\text{O}_3$: calc.: 245.0921, found: 245.0915.

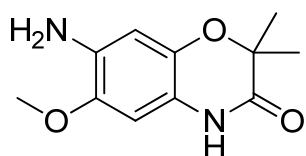
2,2-Bis-(2*H*-benzo[*b*]-1,4-oxazin-3-one-6-yl)propane (**13**)



Preparation according to general protocol **E** produced **13** (159 mg, 0.47 mmol, 94%) as colorless solid. $R_f = 0.24$ (cyclohexane/ethyl acetate = 1/2). ^1H NMR (400 MHz, DMSO- d_6) δ (ppm) = 1.53 (s, 3H),

4.52 (s, 2H), 6.73 (d, $J=2.2$, 1H), 6.77 (dd, $J=8.4, 2.2$, 1H), 6.85 (d, $J=8.4$, 1H), 10.52 (s, 1H). ^{13}C NMR (101 MHz, DMSO- d_6) δ (ppm) = 31.1, 42.0, 67.2, 114.6, 116.0, 121.3, 127.2, 141.6, 145.0, 165.3. mp.: 274.1–275.0 °C, crystallized from cyclohexane/ethyl acetate. HRMS ESI (m/z) for $[\text{M}+\text{H}]^+$ $\text{C}_{19}\text{H}_{19}\text{N}_2\text{O}_4$: calc.: 339.1339, found: 339.1341.

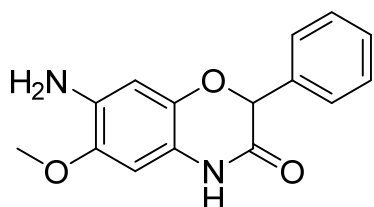
7-Amino-2,2-dimethyl-6-methoxybenzo[*b*]-1,4-oxazin-3(4*H*)-one (**14**)



Preparation according to general protocol **E** produced **14** (76 mg, 0.34 mmol, 68 %) as brown solid. $R_f = 0.5$ (cyclohexane/ethyl acetate = 1/5). ^1H NMR (400 MHz, DMSO- d_6) δ (ppm) = 1.31 (s, 6H), 3.67 (s, 3H), 4.51 (s, 2H), 6.25 (s, 1H), 6.36 (s,

1H), 10.09 (s, 1H). ^{13}C NMR (101 MHz, DMSO- d_6) δ (ppm) = 23.1, 55.8, 76.8, 99.3, 103.2, 116.4, 133.3, 135.7, 141.5, 168.1. mp.: 179–183 °C HRMS ESI (m/z) for $[\text{M}+\text{H}]^+$ $\text{C}_{11}\text{H}_{15}\text{N}_2\text{O}_3$: calc.: 223.1083, found: 223.1079. The spectroscopic data match those reported in literature.^[20]

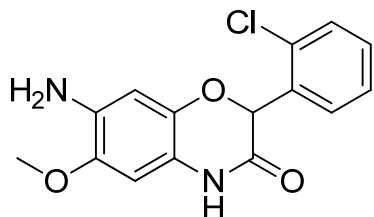
7-Amino-2,3-dihydro-6-methoxy-2-phenylbenzo[*b*]-1,4-oxazin-3-one (**15**)



Preparation according to general protocol **E** produced **15** (46 mg, 0.17 mmol, 33%) as slightly brown solid. $R_f = 0.15$ (cyclohexane/ethyl acetate = 1/1). ^1H NMR (400 MHz, DMSO- d_6) δ (ppm) = 3.67 (s, 3H), 4.57 (s, 2H), 5.56 (s, 1H), 6.32 (s, 1H), 6.37 (s, 1H), 7.25 – 7.42 (m, 5H), 10.46 (s, 1H).

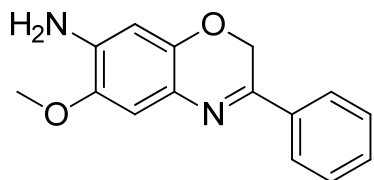
^{13}C NMR (101 MHz, DMSO- d_6) δ (ppm) = 55.7, 77.5, 99.6, 102.9, 115.6, 126.9, 128.4, 128.4, 133.6, 136.1, 136.2, 141.7, 164.2. mp.: 171.4–175.6 °C HRMS ESI (m/z) for $[\text{M}+\text{Na}]^+$ $\text{C}_{15}\text{H}_{14}\text{N}_2\text{NaO}_3$: calc.: 293.0900, found: 293.0892.

7-Amino-2,3-dihydro-6-methoxy-2-phenylbenzo[*b*]-1,4-oxazin-3-one (16)



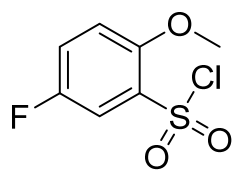
Preparation according to general protocol **E** produced **16** (73 mg, 0.24 mmol, 48%) as slightly brown solid. $R_f = 0.20$ (cyclohexane/ethyl acetate = 1/2). $^1\text{H NMR}$ (400 MHz, DMSO- d_6) δ (ppm) = 3.70 (s, 3H), 4.55 (s, 2H), 5.71 (s, 1H), 6.24 (s, 1H), 6.44 (s, 1H), 7.33 – 7.45 (m, 3H), 7.52 (dd, $J=7.8$, 1.0, 1H), 10.56 (s, 1H). $^{13}\text{C NMR}$ (101 MHz, DMSO- d_6) δ (ppm) = 55.8, 75.9, 99.7, 102.6, 115.8, 127.3, 129.8, 130.0, 130.6, 133.6, 133.7, 133.7, 136.5, 141.8, 163.6. mp.: 192.1–196.3 °C. HRMS ESI (m/z) for $[\text{M}+\text{H}]^+$ calc.: 305.0693, found: 305.0694.

2H-7-Amino-6-methoxy-3-phenylbenzo[*b*]-1,4-oxazine (17)



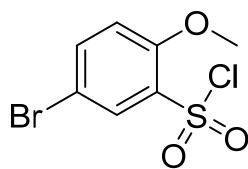
Preparation according to general protocol **A** produced **17** (24 mg, 0.1 mmol, 19%) as yellow oil. $R_f = 0.18$ (cyclohexane/ethyl acetate = 1/2). Purified by preparative HPLC (eluent mixture of solvent A, solvent B, A: water/acetonitrile/ $\text{H}_3\text{PO}_4 = 950/50/1$, B: acetonitrile). $^1\text{H NMR}$ (400 MHz, chloroform- d) δ (ppm) = 3.86 (s, 2H), 4.97 (s, 1H), 6.28 (s, 1H), 6.91 (s, 1H), 7.39 – 7.50 (m, 1H), 7.79 – 7.92 (m, 1H). $^{13}\text{C NMR}$ (101 MHz, chloroform- d) δ (ppm) = 56.2, 63.1, 101.4, 110.1, 125.6, 126.1, 128.8, 130.4, 136.1, 137.1, 141.3, 142.5, 154.2. HRMS ESI (m/z) for $[\text{M}+\text{H}]^+$ $\text{C}_{15}\text{H}_{15}\text{N}_2\text{O}_2$: calc.: 255.1128, found: 225.1128.

5-Fluoro-2-methoxybenzenesulfonyl chloride **21a**



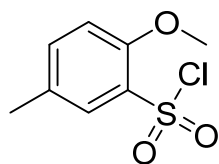
Preparation according to general protocol **F** produced **21a** (8.702 g, 38.7 mmol, 97%) as colorless solid. $R_f = 0.30$ (cyclohexane/ethyl acetate = 3/1). $^1\text{H NMR}$ (400 MHz, Chloroform- d) $\delta = 4.0$ (s, 3H), 7.1 (dd, $J=9.2, 3.8$, 1H), 7.4 – 7.5 (m, 1H), 7.7 (dd, $J=7.4, 3.2$, 1H). $^{19}\text{F NMR}$ (376 MHz, Chloroform- d) $\delta = -121.93$ (td, $J=7.4, 3.9$). $^{13}\text{C NMR}$ (101 MHz, CDCl_3) $\delta = 57.3, 114.7$ (d, $J=7.3$), 116.8 (d, $J=27.2$), 124.1 (d, $J=22.9$), 132.1 (d, $J=7.3$), 153.9 (d, $J=2.3$), 155.2 (d, $J=245.1$). mp.: 75.1–75.9 °C. HRMS ESI (m/z) for $[\text{M}-\text{Cl}+\text{O}]^-$ $\text{C}_7\text{H}_6\text{FO}_4\text{S}$: calc.: 204.9976, found: 204.9973. The spectroscopic data match those reported in literature.^[21]

5-Bromo-2-methoxybenzenesulfonyl chloride **20a**



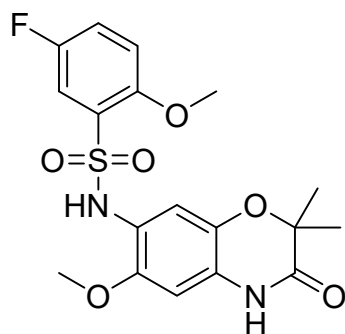
Preparation according to general protocol **F** produced **20a** (8.57 g, 30.0 mmol, 75%) as colorless solid. $R_f = 0.28$ (cyclohexane/ethyl acetate = 3/1). $^1\text{H NMR}$ (400 MHz, $\text{DMSO}-d_6$) $\delta = 3.74$ (s, 3H), 6.94 (d, $J=8.7$, 1H), 7.45 (dd, $J=8.7, 2.7$, 1H), 7.75 (d, $J=2.7$, 1H). $^{13}\text{C NMR}$ (101 MHz, $\text{DMSO}-d_6$) $\delta = 56.2, 110.8, 114.8, 131.2, 133.0, 138.2, 156.1$. mp.: 105.8–107.9 °C. HRMS APCI (m/z) for $[\text{M}-\text{Cl}+\text{O}]^-$ $\text{C}_7\text{H}_6^{79}\text{BrO}_4\text{S}$: calc.: 264.9176, found: 267.9168. The spectroscopic data match those reported in literature.^[8,22]

5-Methyl-2-methoxybenzenesulfonyl chloride **22a**



Preparation according to general protocol **F** produced **22a** (2.693 g, 12.2 mmol, 61%) as colorless crystals. $R_f = 0.45$ (cyclohexane/ethyl acetate = 3/1). The crude product was purified by recrystallization from cyclohexane. $^1\text{H NMR}$ (400 MHz, $\text{DMSO}-d_6$) $\delta = 2.22$ (m, 3H), 3.72 (s, 3H), 6.87 (d, $J=8.3$, 1H), 7.13 (ddd, $J=8.3, 2.4, 0.8$, 1H), 7.50 (dd, $J=2.4, 0.8$, 1H). $^{13}\text{C NMR}$ (101 MHz, $\text{DMSO}-d_6$) $\delta = 20.1, 55.6, 112.1, 127.8, 129.0, 131.0, 134.4, 154.3$. mp.: 78.4–80.1 °C. HRMS ESI (m/z) for $[\text{M}-\text{Cl}+\text{O}]^-$ $\text{C}_8\text{H}_9\text{O}_4\text{S}$: calc.: 201.0227, found: 201.0224. The spectroscopic data match those reported in literature.^[23]

5-Fluoro-2-methoxy-*N*-(6-methoxy-2,2-dimethylbenzo[*b*]-1,4-oxazin-3(4*H*)-one-7-yl)benzenesulfonamide (**21**)

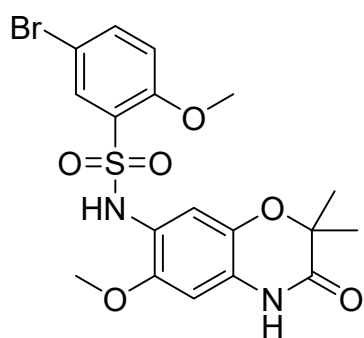


Preparation according to general protocol **G** produced **21** (31 mg, 0.075 mmol, 30%) as colorless crystals. $R_f = 0.10$ (cyclohexane/ethyl acetate = 1/2). The crude product was purified by normal phase column chromatography with eluent mixtures of cyclohexane/ethyl acetate. Further purification was performed by

S25

reversed phase C18 column chromatography (eluent mixtures of solvent A, solvent B, A: water/acetonitrile/formic acid = 950/50/1, B: acetonitrile). ^1H NMR (400 MHz, $\text{DMSO-}d_6$) δ = 1.32 (s, 6H), 3.51 (s, 3H), 3.87 (s, 3H), 6.41 (s, 1H), 6.75 (s, 1H), 7.23 (dd, $J=9.2, 4.0$, 1H), 7.37 (dd, $J=8.1, 3.2$, 1H), 7.46 (ddd, $J=9.2, 8.1, 3.2$, 1H), 8.91 (s, 1H), 10.48 (s, 1H). ^{19}F NMR (376 MHz, $\text{DMSO-}d_6$) δ = -124.46 (td, $J=8.2, 4.1$). ^{13}C NMR (101 MHz, $\text{DMSO-}d_6$) δ = 23.1, 56.0, 56.7, 77.2, 99.1, 114.1, 114.3 (d, $J=7.5$), 116.0 (d, $J=26.1$), 119.5, 121.1 (d, $J=22.7$), 125.7, 128.4 (d, $J=6.5$), 134.5, 147.8, 153.1 (d, $J=2.1$), 154.5 (d, $J=239.6$), 168.6. mp.: 212.3–213.6 °C (under decomposition). HRMS ESI (m/z) for $[\text{M}+\text{K}]$ $\text{C}_{18}\text{H}_{19}\text{FKN}_2\text{O}_6\text{S}$: calc.: 449.0585, found: 449.0579.

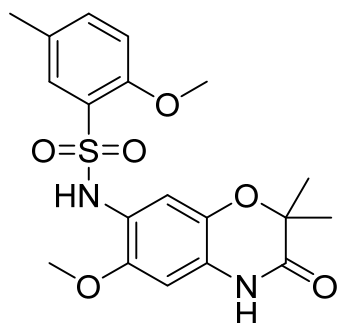
5-Bromo-2-methoxy-*N*-(6-methoxy-2,2-dimethylbenzo[*b*]-1,4-oxazin-3(4H)-one-7-yl)benzenesulfonamide (20)



Preparation according to general protocol **G** produced **20** (98 mg, 0.21 mmol, 83%) as colorless needles. R_f = 0.18 (cyclohexane/ethyl acetate = 1/3). The crude product was purified by normal phase column chromatography with eluent mixtures of cyclohexane/ethyl acetate. Further purification was performed by reversed phase C18 column chromatography (eluent mixtures of solvent A, solvent B, A: water/acetonitrile/formic acid = 950/50/1, B: acetonitrile). ^1H

NMR (400 MHz, $\text{DMSO-}d_6$) δ = 1.33 (s, 6H), 3.52 (s, 3H), 3.89 (s, 3H), 6.43 (s, 1H), 6.76 (s, 1H), 7.20 (d, $J=8.9$, 1H), 7.64 (d, $J=2.5$, 1H), 7.76 (dd, $J=8.9, 2.5$, 1H), 8.32 (s, 1H), 9.00 (s, 1H), 10.50 (s, 1H). ^{13}C NMR (101 MHz, $\text{DMSO-}d_6$) δ = 23.1, 56.0, 56.5, 77.2, 99.0, 110.4, 114.4, 115.2, 119.4, 125.8, 129.4, 131.2, 134.5, 137.1, 147.9, 156.0, 168.6. mp.: 210.0–212.5 °C (under decomposition). HRMS ESI (m/z) for $[\text{M}+\text{Na}]^+$ $\text{C}_{18}\text{H}_{19}^{81}\text{BrN}_2\text{NaO}_6\text{S}$: calc.: 495.0024, found: 495.0021.

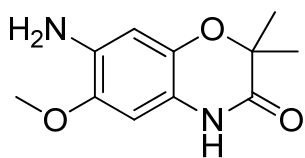
5-Methyl-2-methoxy-N-(6-methoxy-2,2-dimethylbenzo[b]-1,4-oxazin-3(4H)-one-7-yl)benzenesulfonamide (22)



Preparation according to general protocol **G** produced **22** (44 mg, 0.11 mmol, 43%) as colorless solid. $R_f = 0.15$ (cyclohexane/ethyl acetate = 2/3). The crude product was purified by normal phase column chromatography with eluent mixtures of cyclohexane/ethyl acetate. Further purification was performed by reversed phase C18 column chromatography (eluent mixtures of solvent A, solvent B, A: water/acetonitrile/formic acid = 950/50/1, B: acetonitrile). $^1\text{H NMR}$ (400 MHz, DMSO-d_6) $\delta = 1.31$ (s, 6H), 2.21 (s, 3H), 3.57 (s, 3H), 3.85 (s, 3H), 6.41 (s, 1H), 6.80 (s, 1H), 7.08 (d, $J=8.4$, 1H), 7.33 – 7.45 (m, 2H), 8.47 (s, 1H), 10.44 (s, 1H). $^{13}\text{C NMR}$ (101 MHz, DMSO-d_6) $\delta = 19.7$, 23.0, 56.1, 56.1, 77.1, 99.1, 112.5, 112.5, 120.2, 125.0, 126.6, 128.7, 129.5, 134.5, 135.1, 146.8, 154.4, 168.5. mp.: 204.1–205.7°C (under decomposition). HRMS ESI (m/z) for $[\text{M}+\text{Na}]^+$ $\text{C}_{19}\text{H}_{22}\text{N}_2\text{NaO}_6\text{S}$: calc.: 429.1091, found: 429.1092.

Crystallographic data

7-Amino-2,2-dimethyl-6-methoxybenzo[*b*]-1,4-oxazin-3(4*H*)-one (**14**)



Crystallization was carried out by heating the compound in ethyl acetate. Slow cooling and evaporating of the solution resulting in crystal formation. Crystal structure determination of **14**: $C_{11}H_{15}N_2O_3$,

$M_r = 222.24$, colorless block-like crystals ($0.27 \times 0.40 \times 0.49 \text{ mm}^3$), $T = 120 \text{ K}$, MoK_{α} graphite monochromator, monocline space group $P 2_1/c$, $a = 10.2897(9) \text{ \AA}$, $b = 9.9806(9) \text{ \AA}$, $\beta = 106.191(7)^\circ$, $c = 10.6105(9) \text{ \AA}$, $V = 1046.45(16) \text{ \AA}^3$, $z = 4$, $F(000) = 472$, $\rho = 1,411 \text{ g/cm}^3$, $\mu = 0.10 \text{ mm}^{-1}$, 6119 reflexions, 2494 independent reflexions, $wR_2 = 0.1019$ ($R_1 = 0.0362$), 0.45 e/\AA^3 , -0.21 e/\AA^3 , (CCDC 1998475).

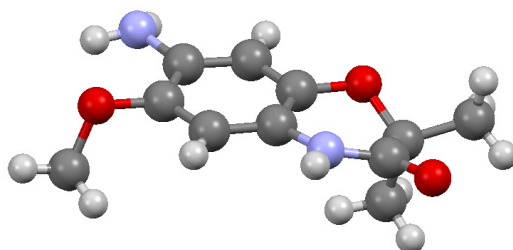


Figure 5: Molecular structure of compound **14**.

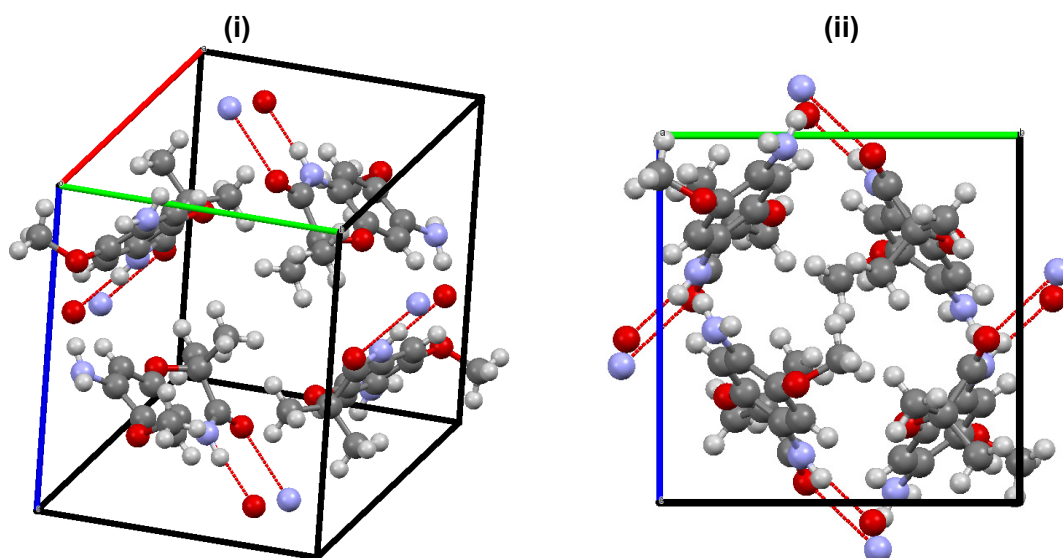
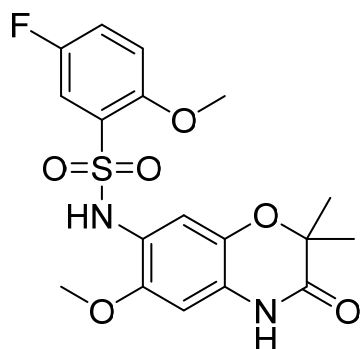


Figure 6: (i) Packing of compound **14** with hydrogen bonding indicated by red dashed lines, (ii) Packing along axis *a*.

5-Fluoro-2-methoxy-N-(6-methoxy-2,2-dimethylbenzo[b]-1,4-oxazin-3(4H)-one-7-yl)benzenesulfonamide (21)



logP = 3.35

-0.40 eÅ³, (CCDC 1998477).

Crystallization was carried out by slow evaporating (over 2 days) of solvent mixture of cyclohexene/ethylacetate = 1/9. Crystal structure determination of **21**: C₁₈H₁₉FN₂O₆S, M_r = 410.42, colorless block-like crystals (0.29 x 0.30 x 0.46 mm³), T = 120 K, MoK_α graphite monochromator, monocline space group P 2₁/n, a = 13.5153(3) Å, b = 9.1007(2) Å, β = 100.977(2)° c = 10.6105(9) Å, V = 1855.54(8) Å³, z = 4, F(000) = 856, ρ = 1.469 g/cm³, μ = 0.223 mm⁻¹, 16916 reflections, 6679 independent reflections, wR₂ = 0.1001 (R1 = 0.0351), 0.55 e/Å³,

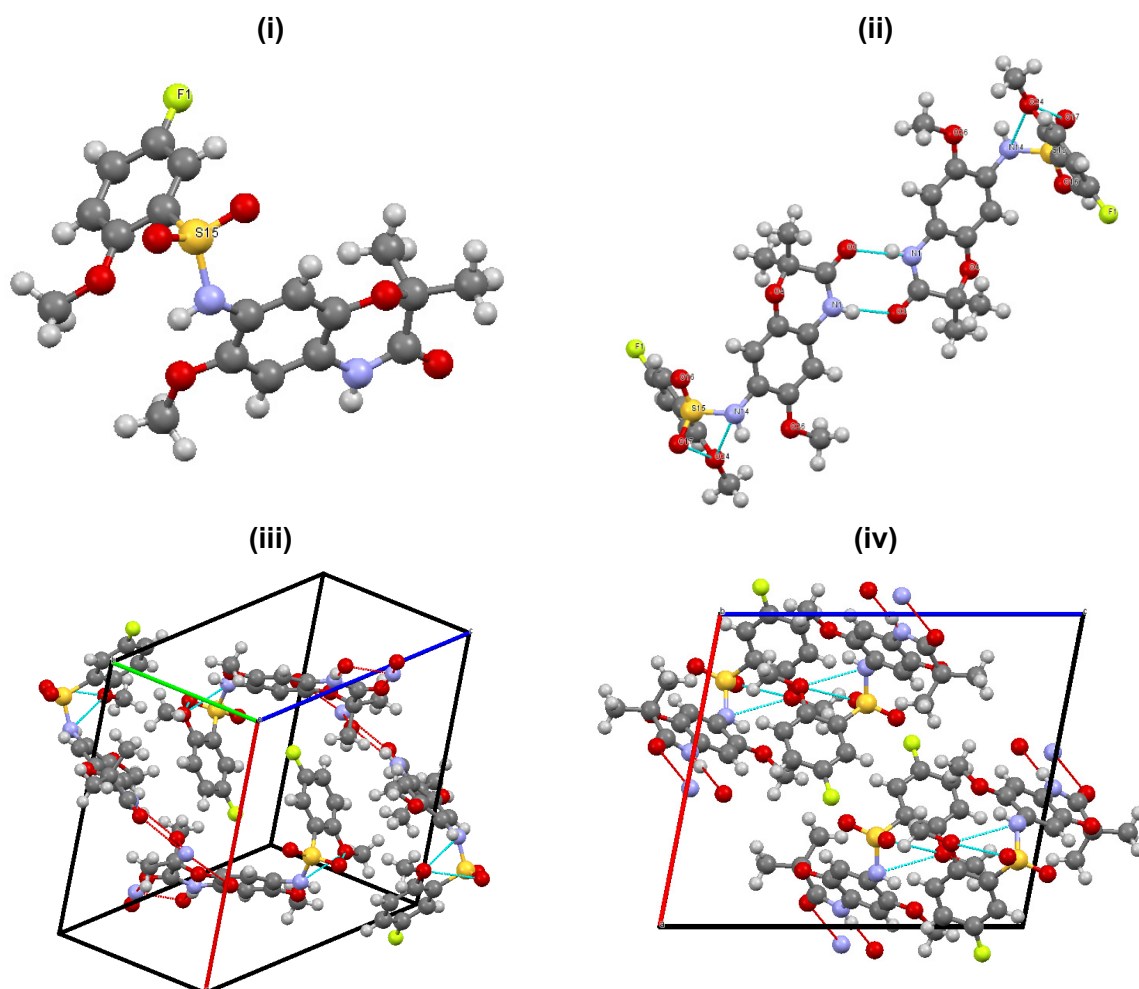
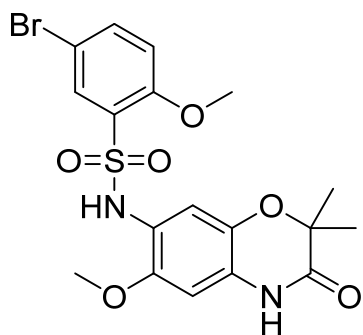


Figure 7: (i) Molecular structure of compound **21** (ii) dimerization of lactame structure with hydrogen bonds indicated by blue dashed lines, (iii) Packing of compound **21** with intermolecular hydrogen bonds indicated by red dashed lines and intramolecular hydrogen bonds indicated by blue dashed lines, (iv) Packing along axis b.

5-Bromo-2-methoxy-*N*-(6-methoxy-2,2-dimethylbenzo[*b*]-1,4-oxazin-3(4*H*)-one-7-yl)benzenesulfonamide (20)



logP = 3.97

Crystallization was carried out by slow evaporating (1 day) of ethylacetate, prior heated solvent. Crystal structure determination of **20**. C₁₈H₁₉BrN₂O₆S, M_r = 471.32, colorless needles (0.09 x 0.13 x 0.67 mm³), T = 120 K, MoK_α graphite monochromator, orthorhombic P bca, a = 8.1077(3) Å, b = 16.3138(5) Å, β = 100.977(2)° c = 29.4116(10) Å, V = 3890.2(2) Å³, z = 8, F(000) = 1920, ρ = 1.609 g/cm³, μ = 2.27 mm⁻¹, 12307 reflections, 4628 independent reflections, wR₂ = 0.0884 (R1 = 0.0347), 0.44 e/Å³, -0.60 e/Å³, (CCDC

1998476).

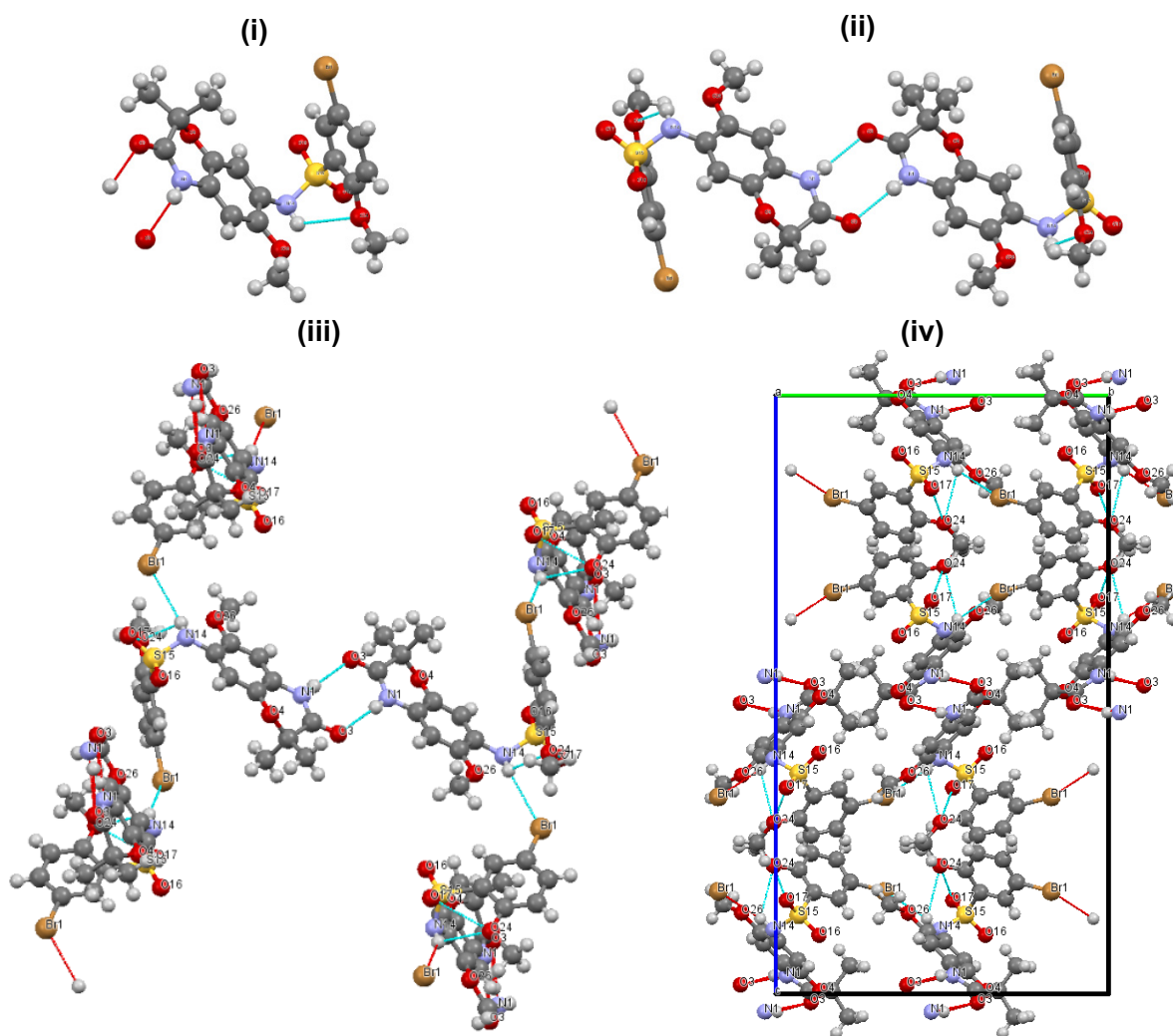


Figure 8: (i) Molecular structure of **20**, (ii) dimerization of lactame structure with hydrogen bonds indicated by blue dashed lines, (iii) dimerization of lactame structure in the middle with chain substructure via hydrogen bonds with bromine as donor atom, (iv) packing along a axis

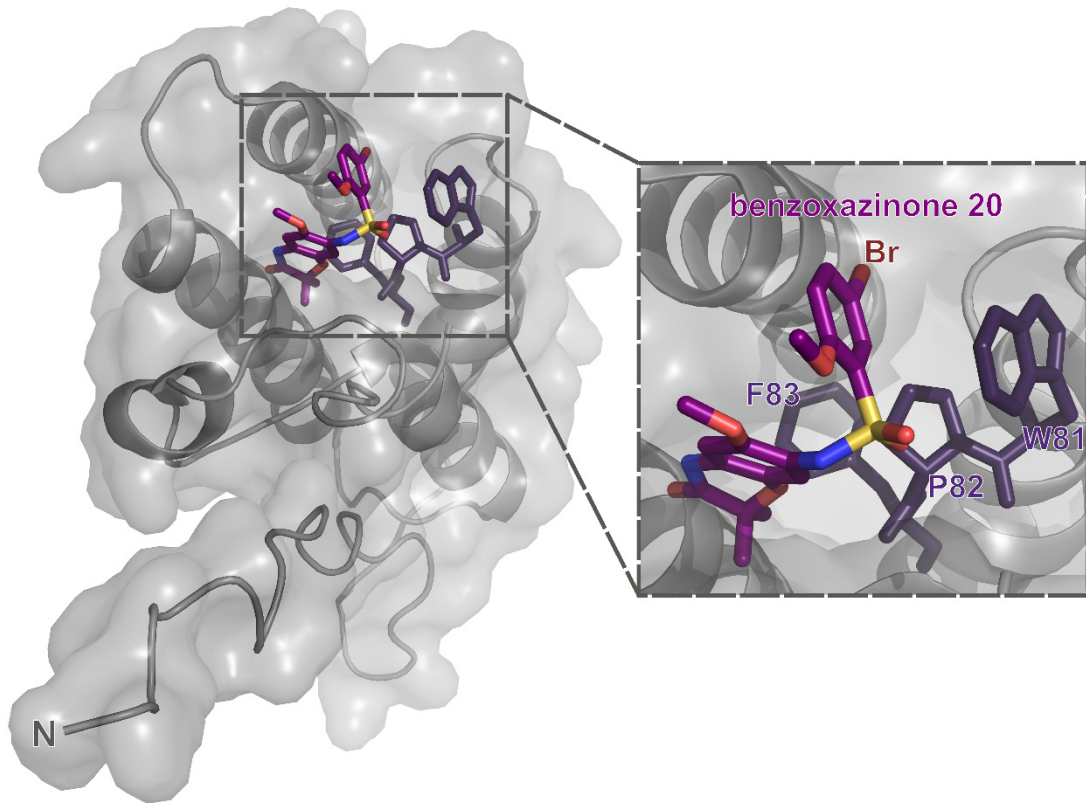
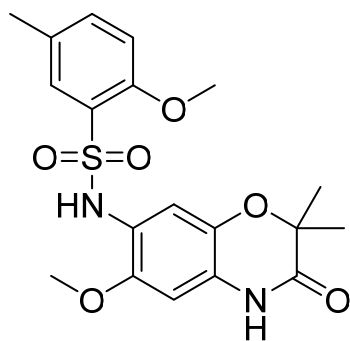


Figure 9: Crystal structure of BRD4 bound to benzoxazinone 20 (PDB: 5Z1R) with the BRD4 WPF shelf (W81, P82, F83) indicated as sticks.^[20]

5-Methyl-2-methoxy-N-(6-methoxy-2,2-dimethylbenzo[b]-1,4-oxazin-3(4H)-one-7-yl)benzenesulfonamide (22)



logP = 3.52

(CCDC 1998478).

Crystallization was carried out by slow evaporating (over 1 day) of ethylacetate, prior heated solvent. Crystal structure determination of **22**. C₁₉H₂₂N₂O₆S, M_r = 406.45, colorless crystals (0.42 x 0.56 x 0.80 mm³), T = 120 K, MoK_α graphite monochromator, triclin P -1, a = 7.6744(4) Å, α = 87.544(5)°, b = 8.8073(6) Å, β = 100.977(2)° c = 29.4116(10) Å, γ = 70.785(5)° V = 922.76(10) Å³, z = 2, F(000) = 428, ρ = 1.463 g/cm³, μ = 0.216 mm⁻¹, 8142 reflexions, 4372 independent reflexions, wR₂ = 0.0952 (R1 = 0.0351), 0.44 e/Å³, -0.44 e/Å³,

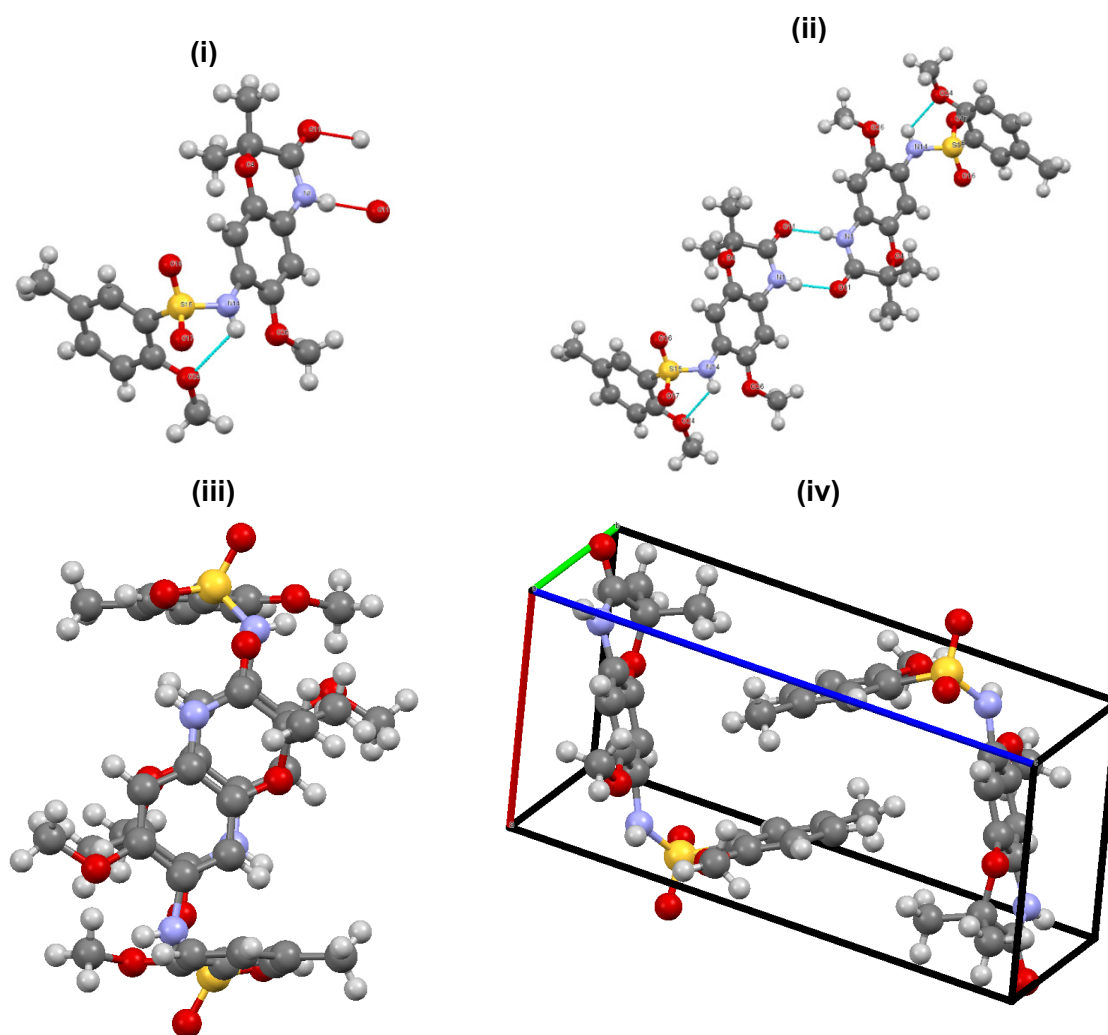
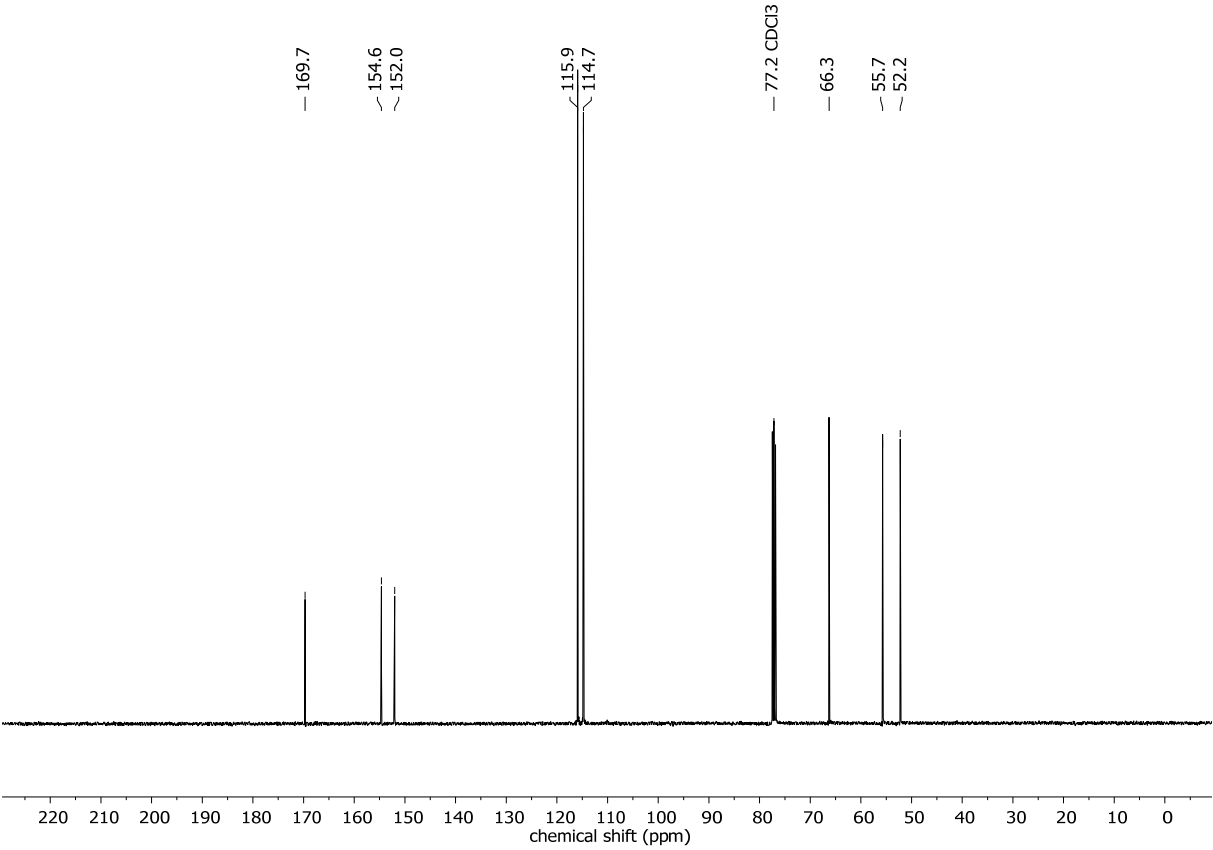
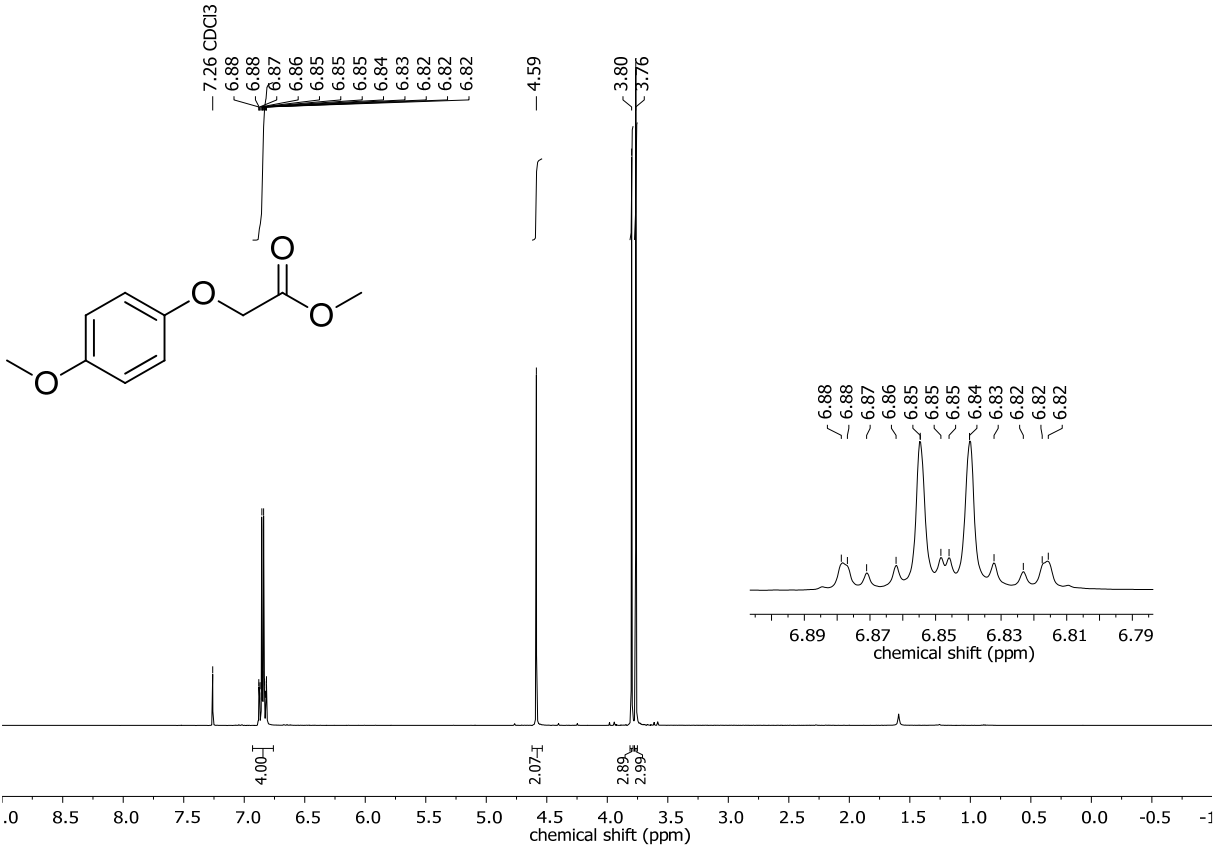


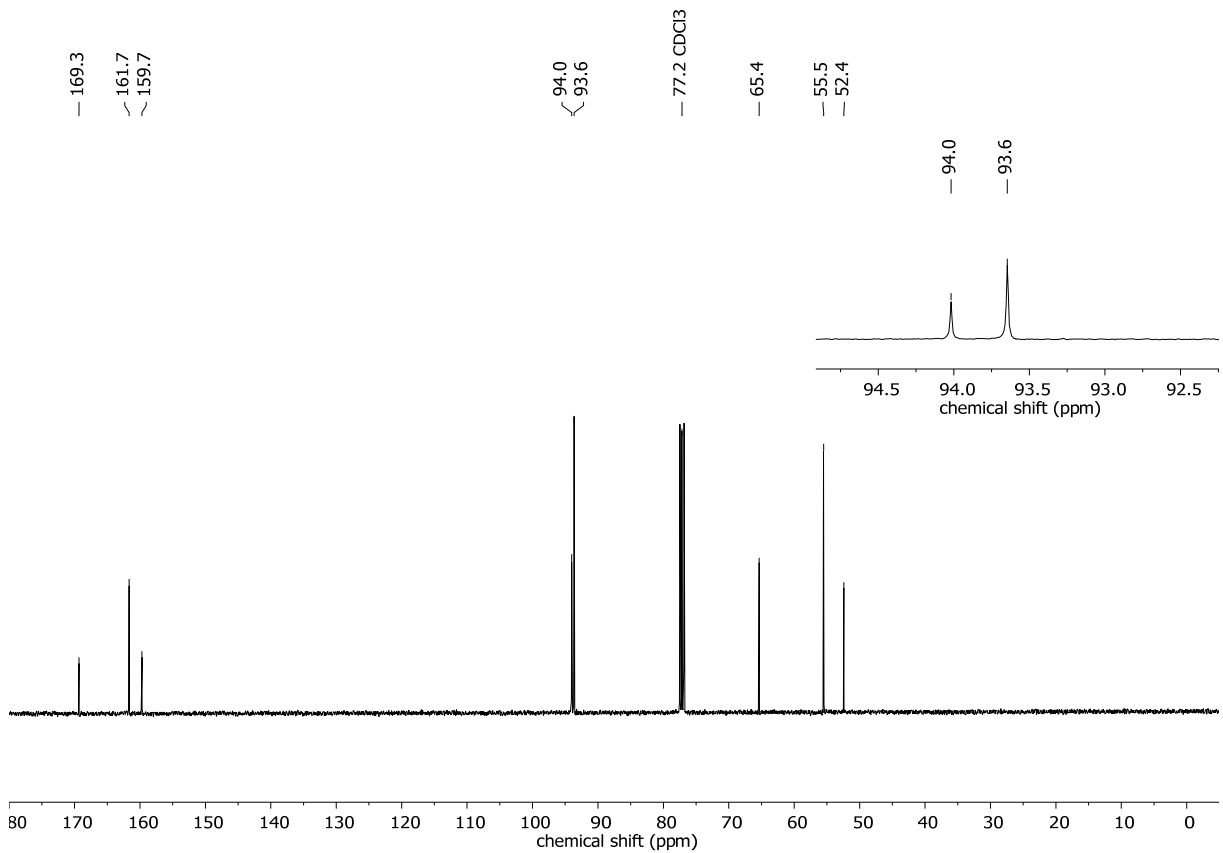
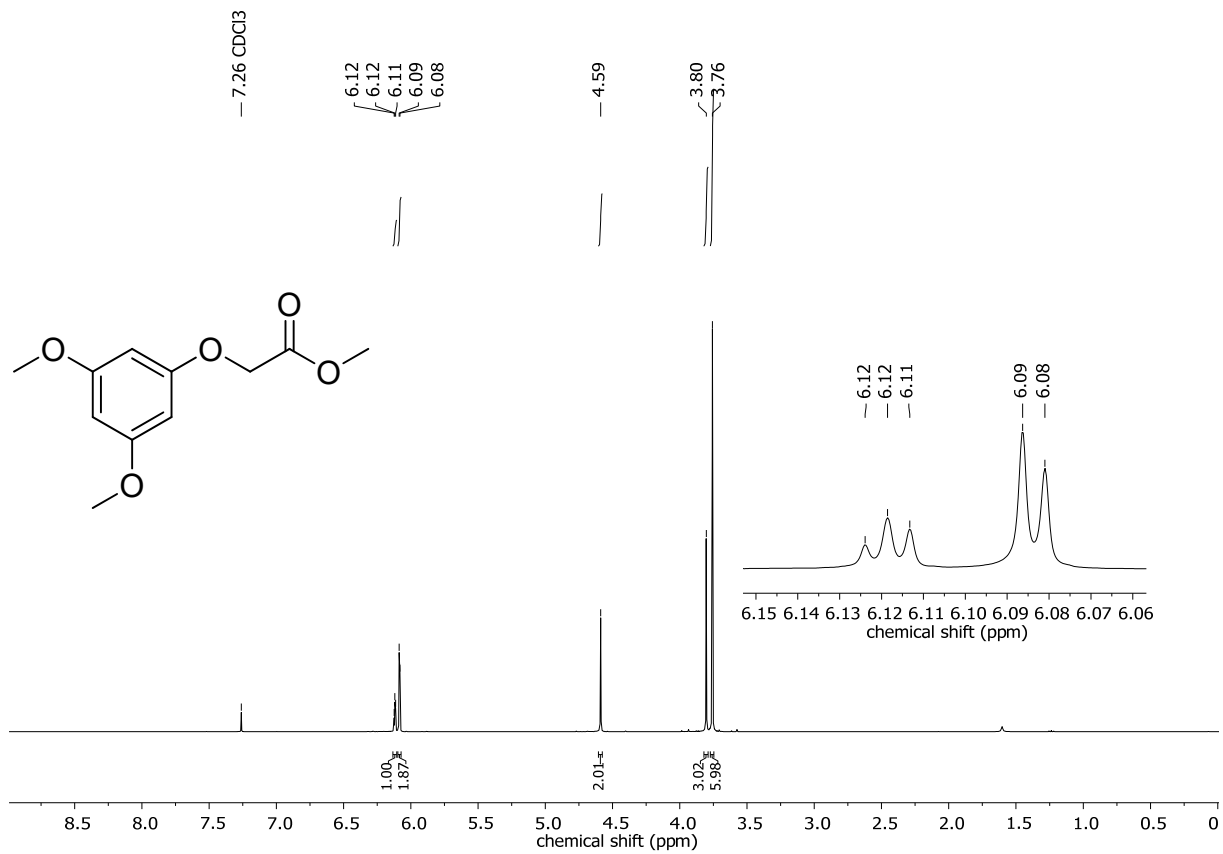
Figure 10: (i) Molecular structure of **22**, (ii) dimerization of lactame structure with hydrogen bonds indicated by blue dashed lines, (iii) pi-pi-stacking of benzoxazinone substructure, (iv) Packing of compound **22**.

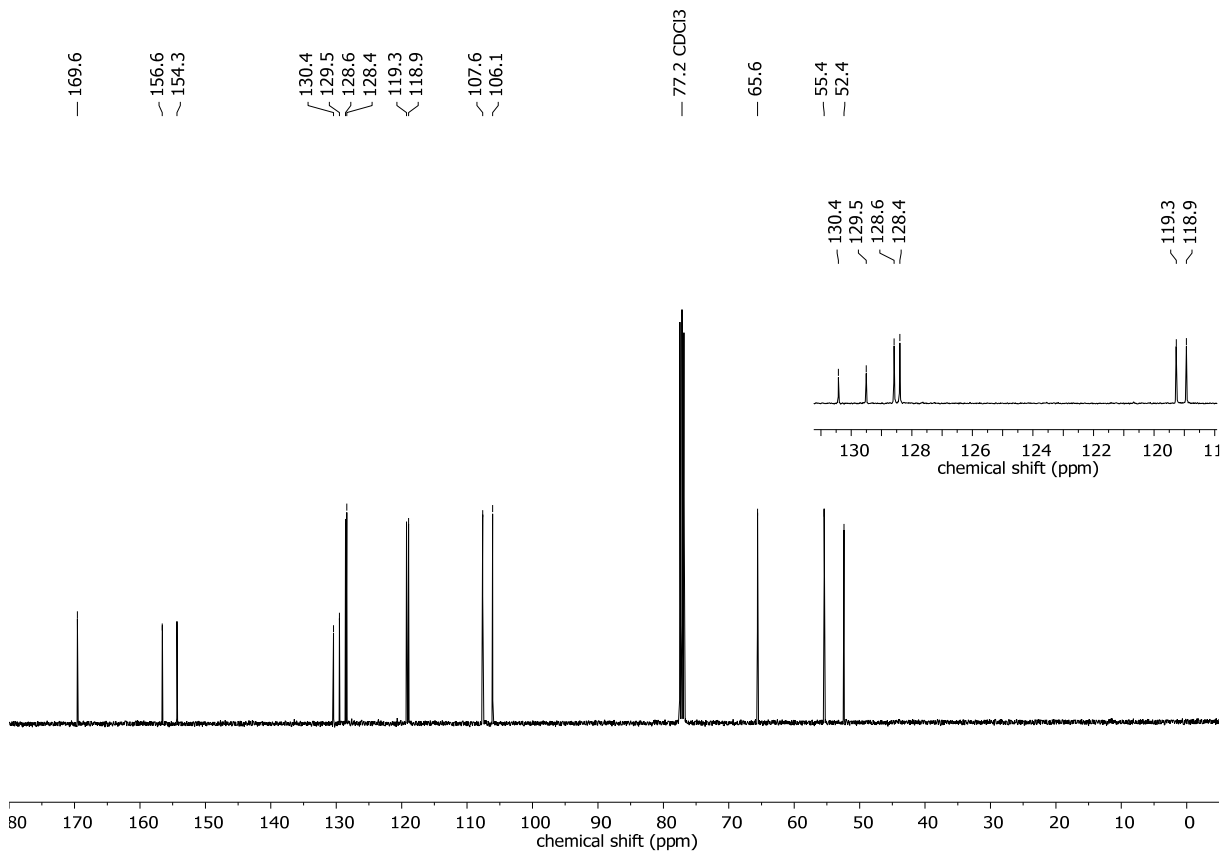
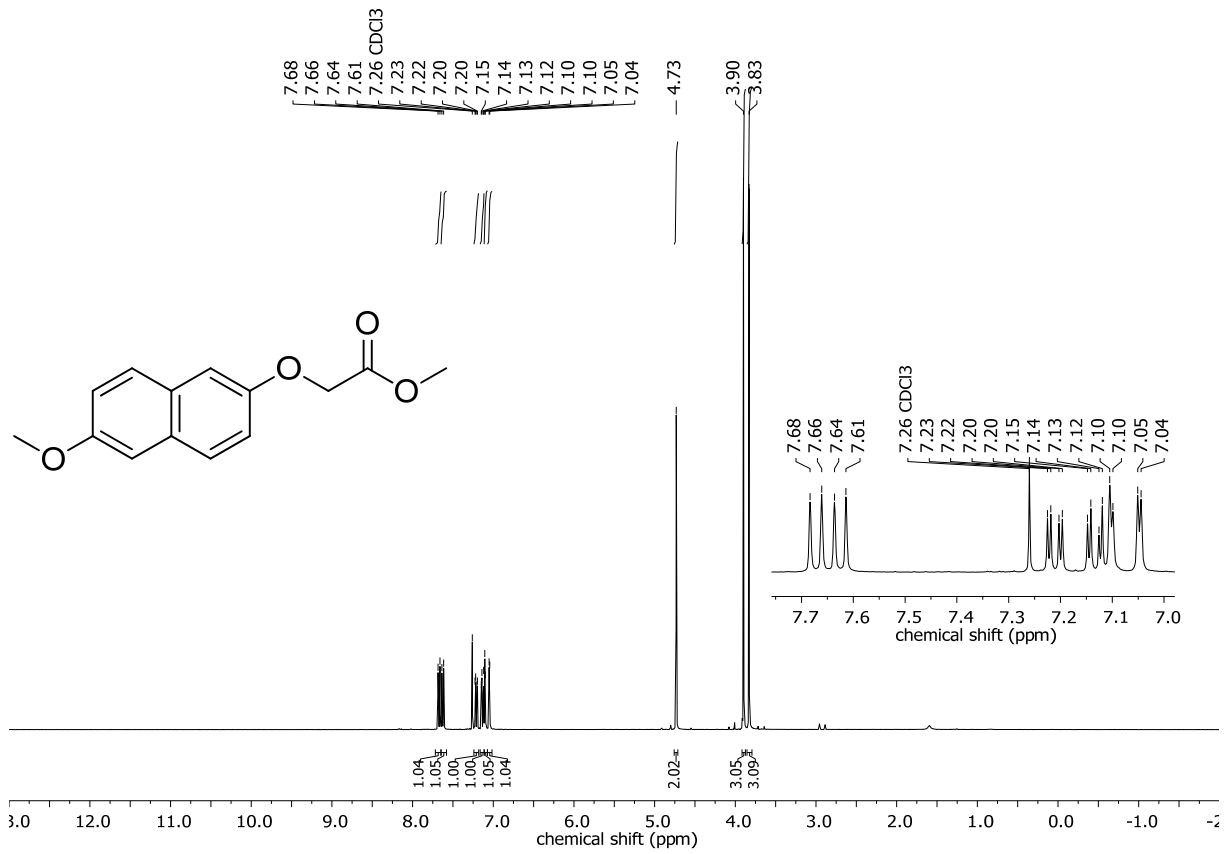
LogP - Values:

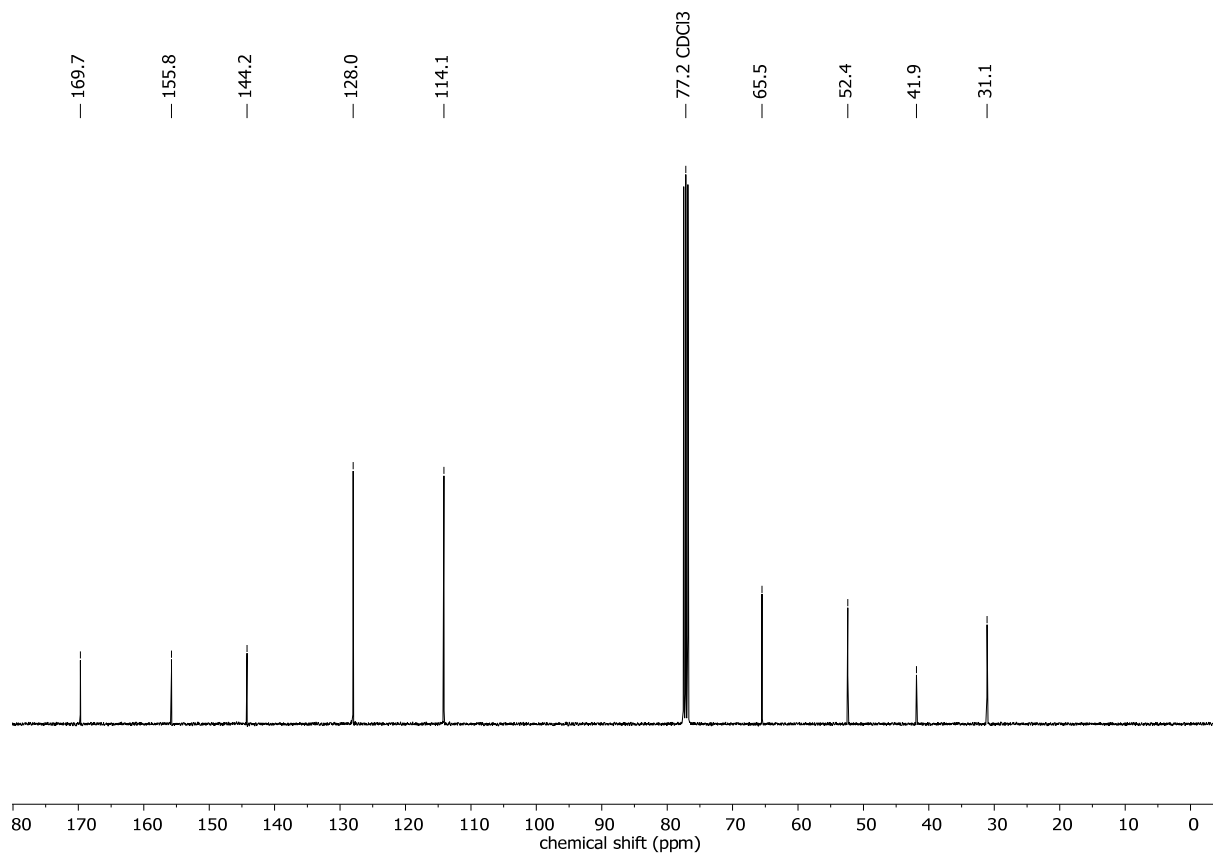
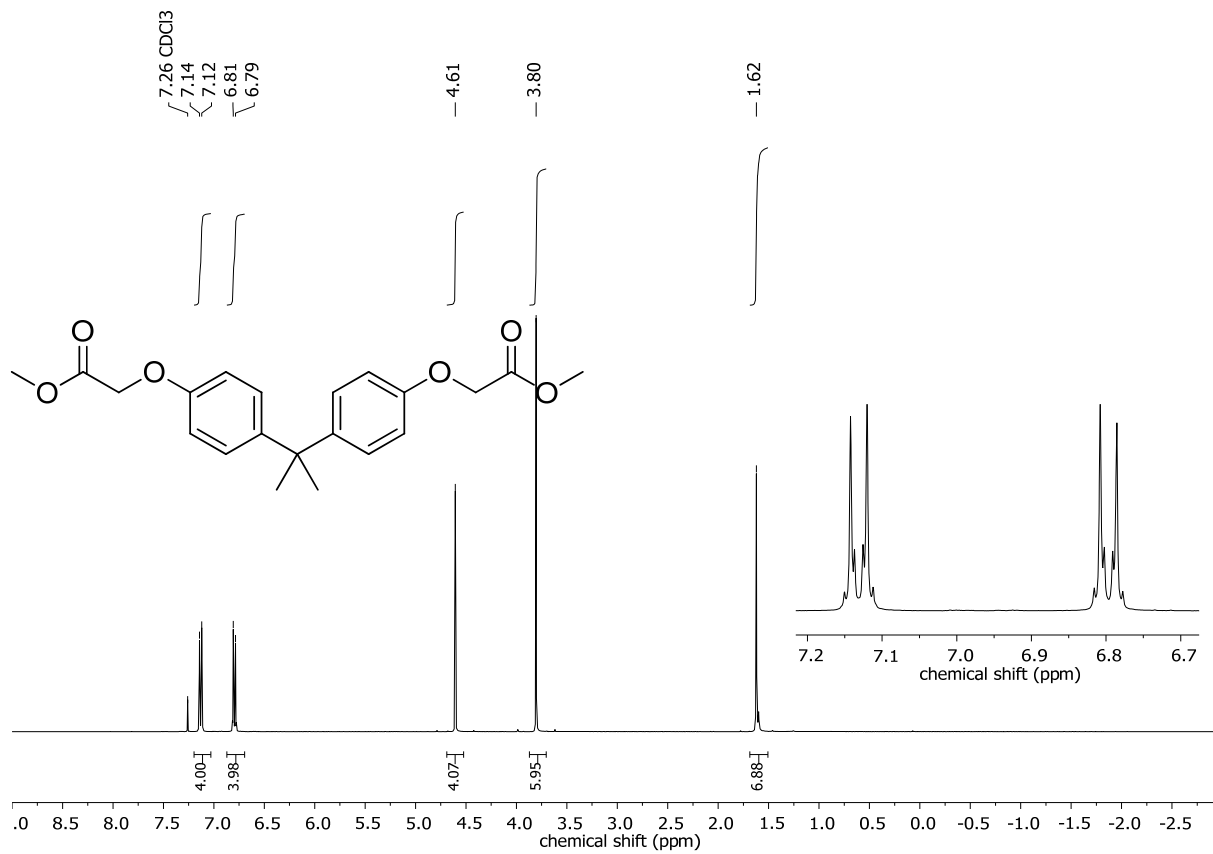
Calculated MOE2015 (*Molecular Operating Environment (MOE), 2019.01; Chemical Computing Group ULC: Montreal, QC, Canada, 2019.*) nach Wildman, S.A., Crippen, G.M.; *Prediction of Physicochemical Parameters by Atomic Contributions; J. Chem. Inf. Comput. Sci.* 39 No. 5 (1999) 868–873.

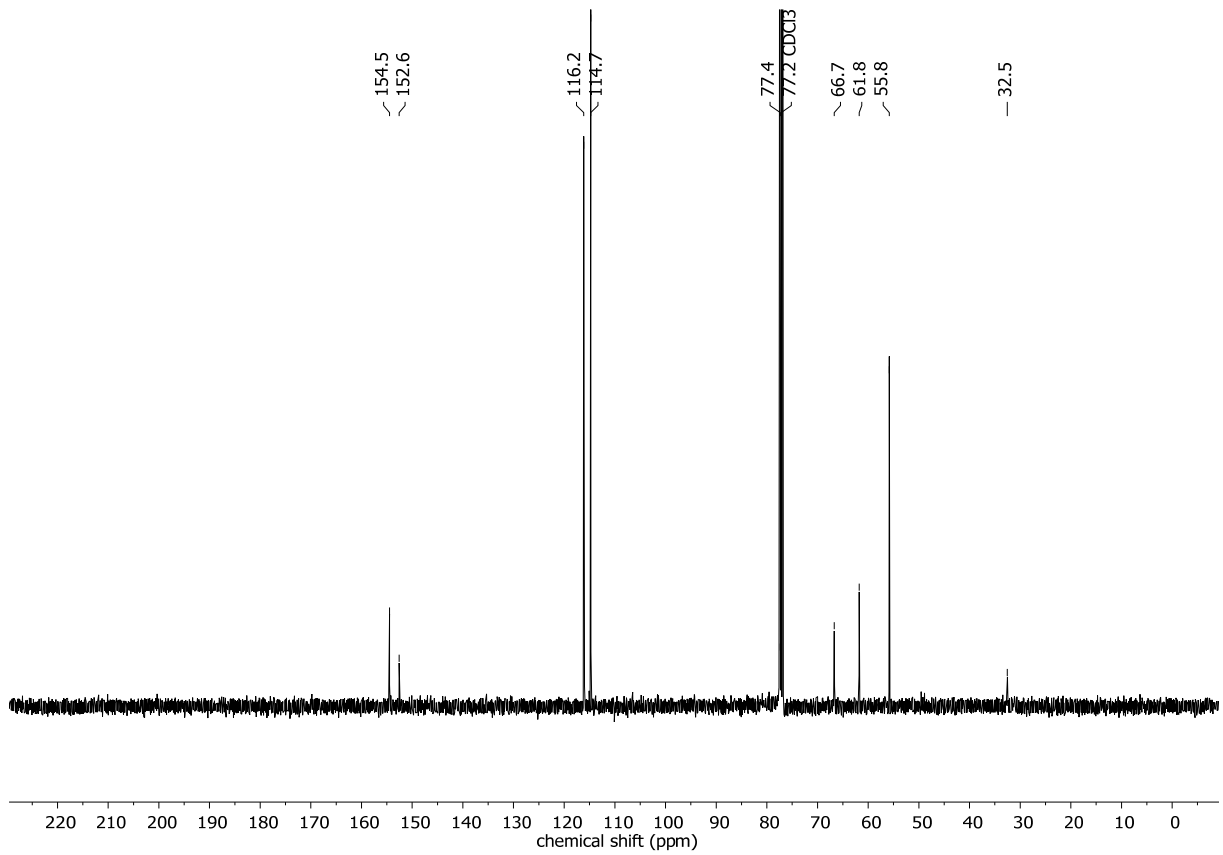
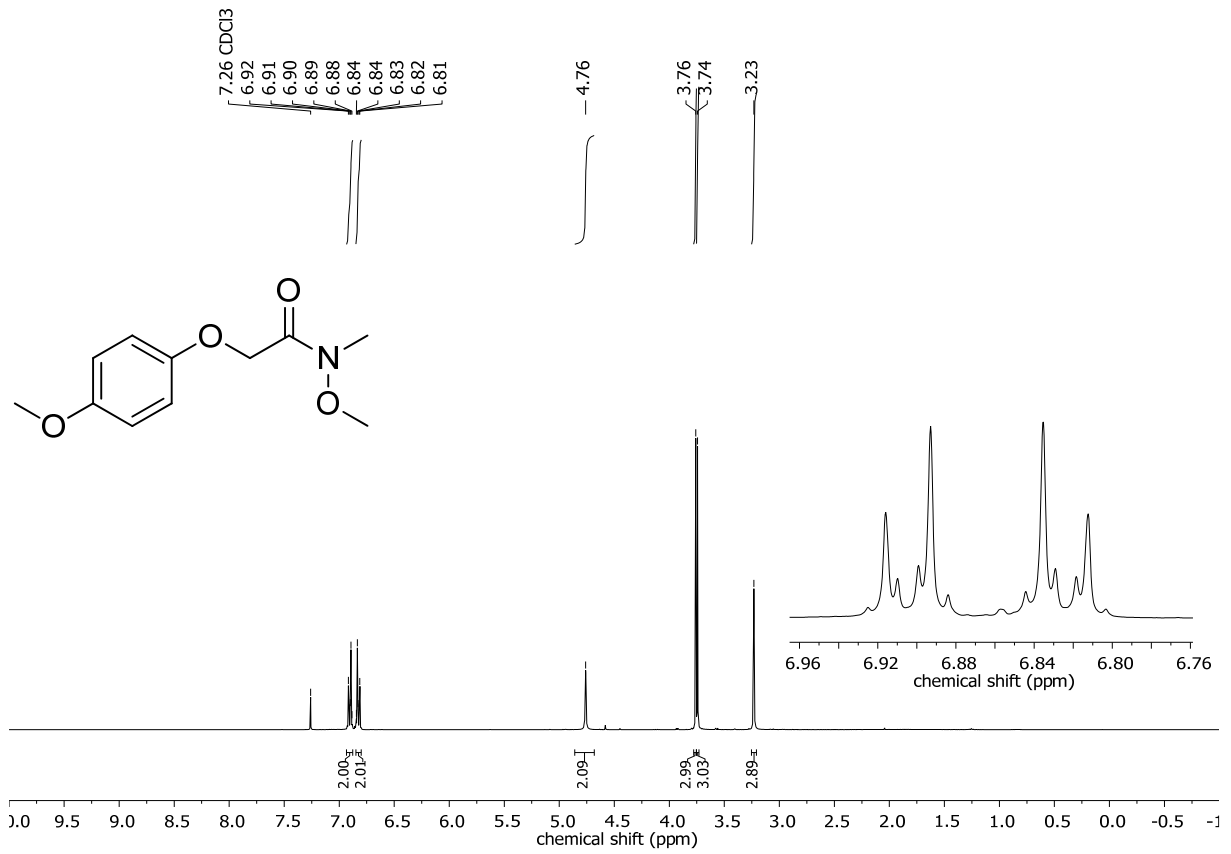
NMR spectra

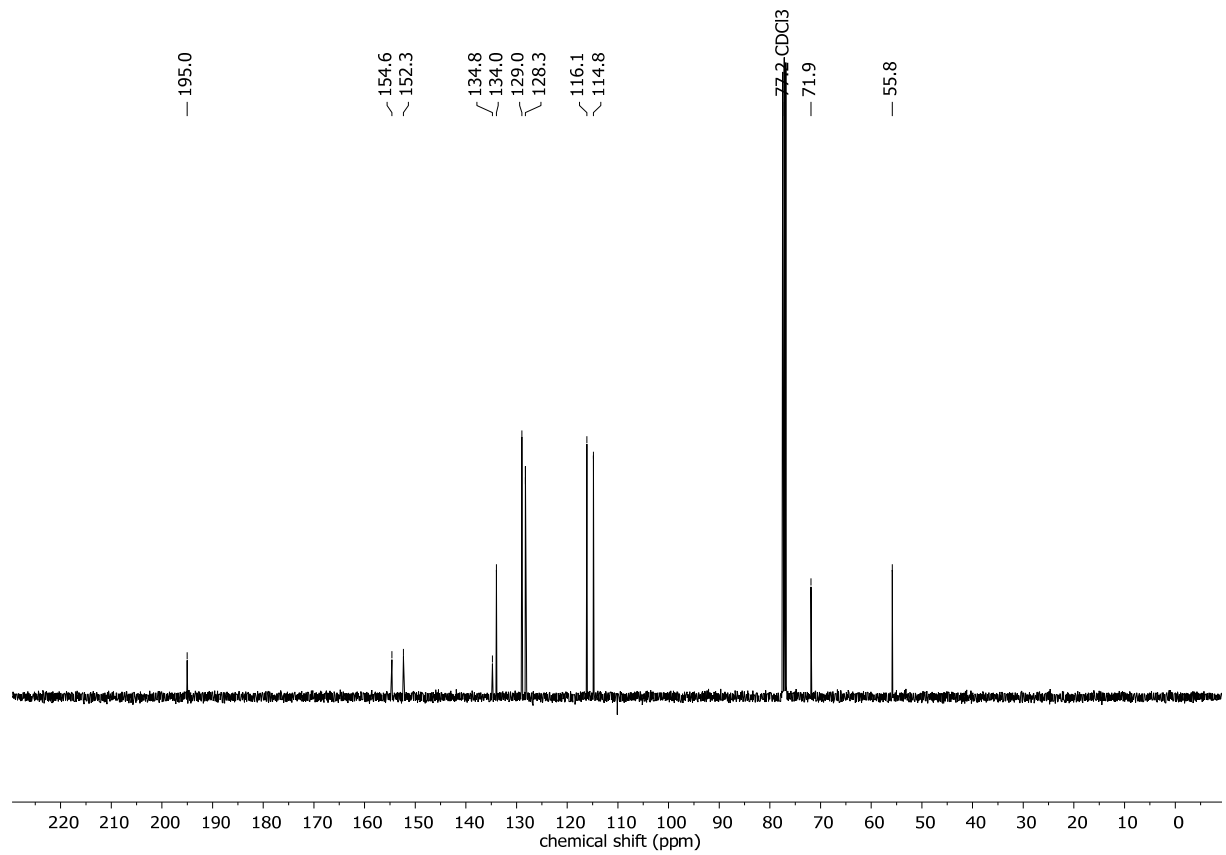
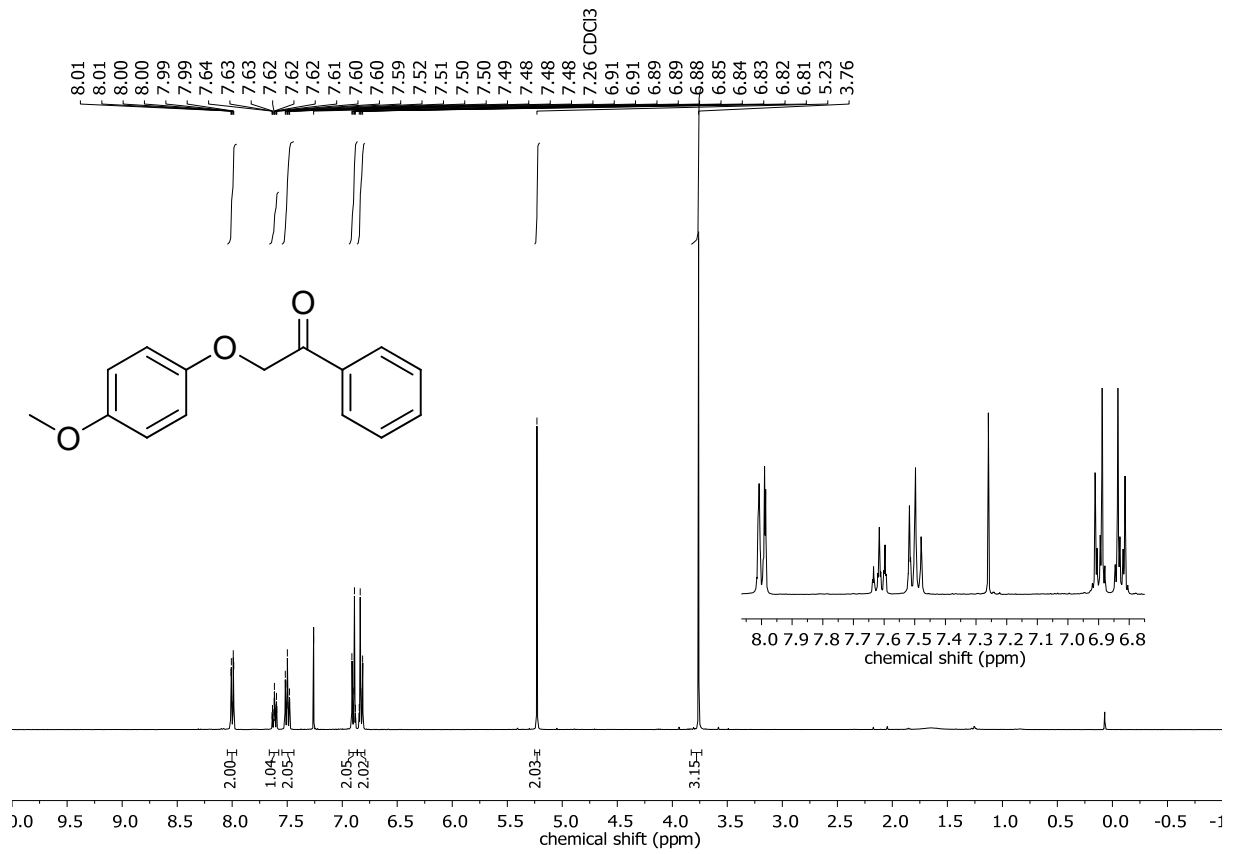


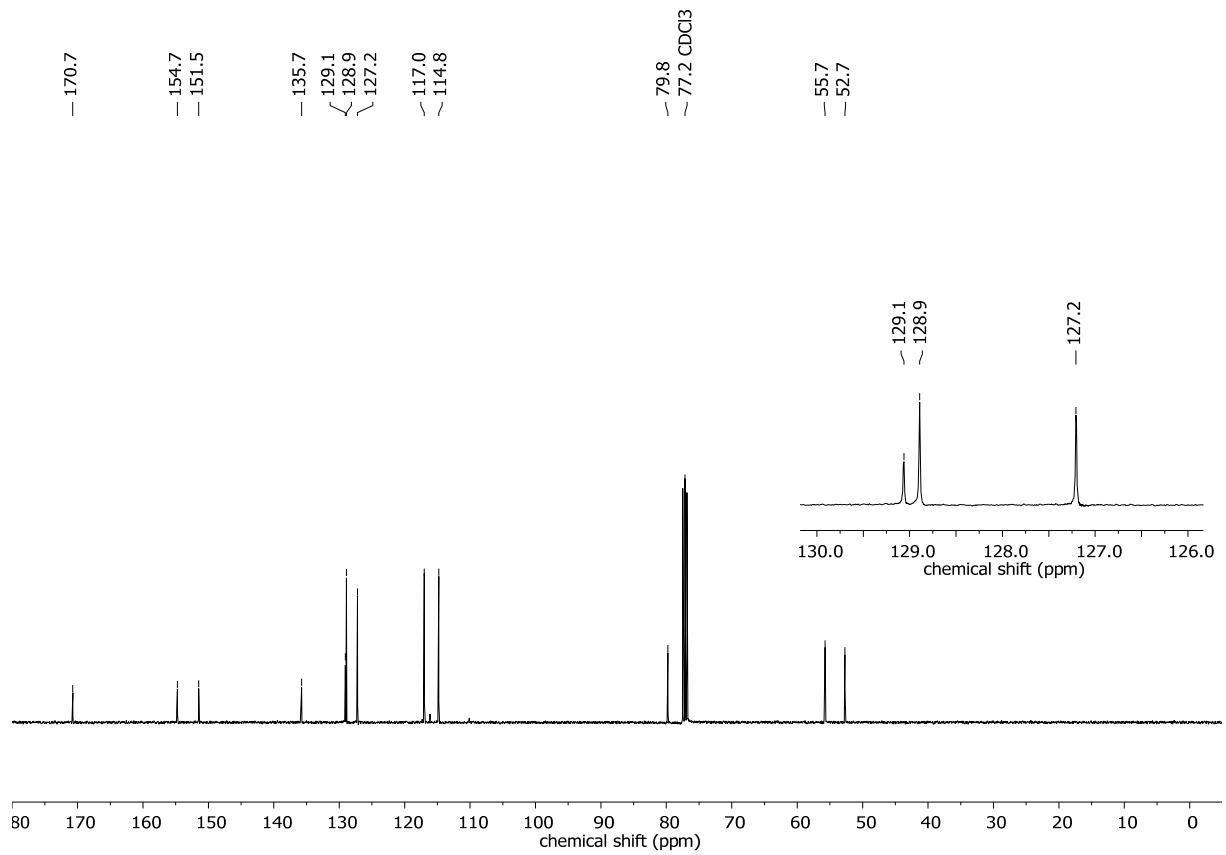
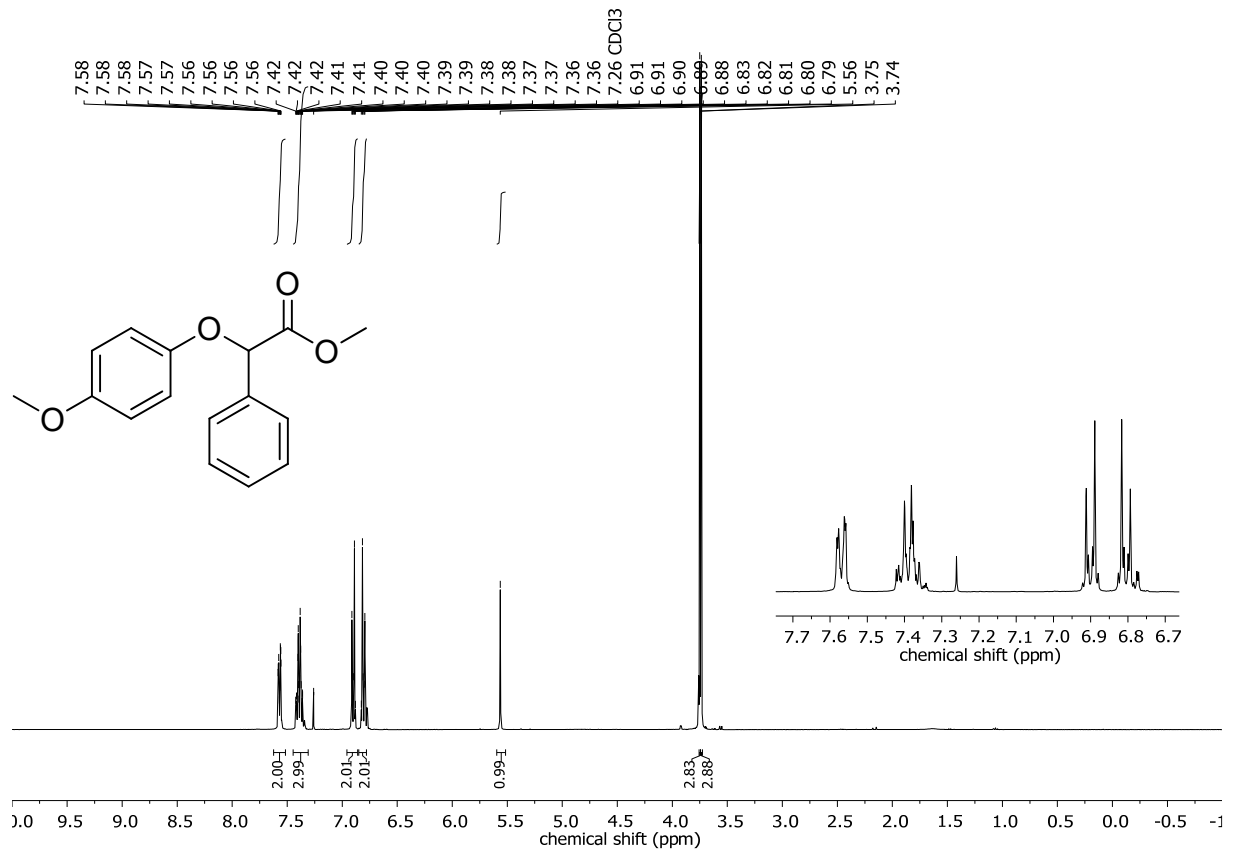


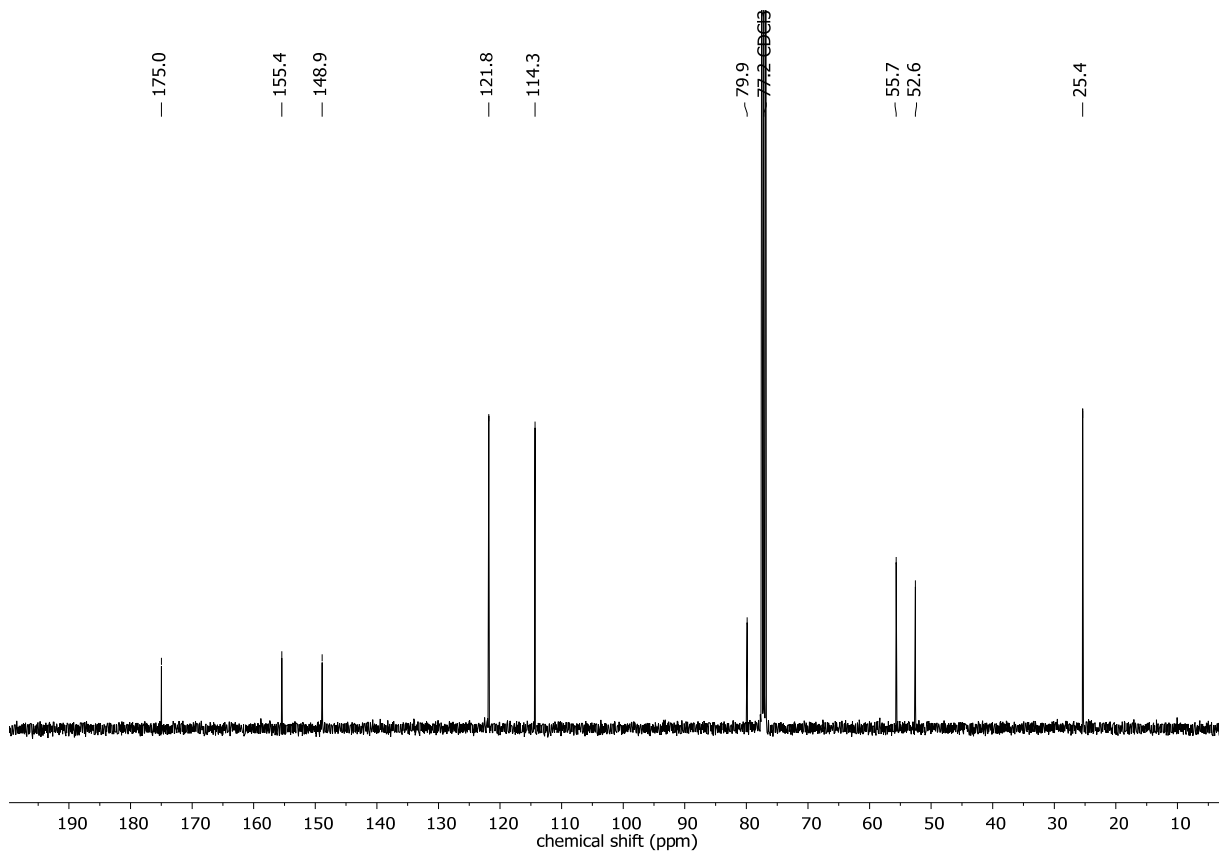
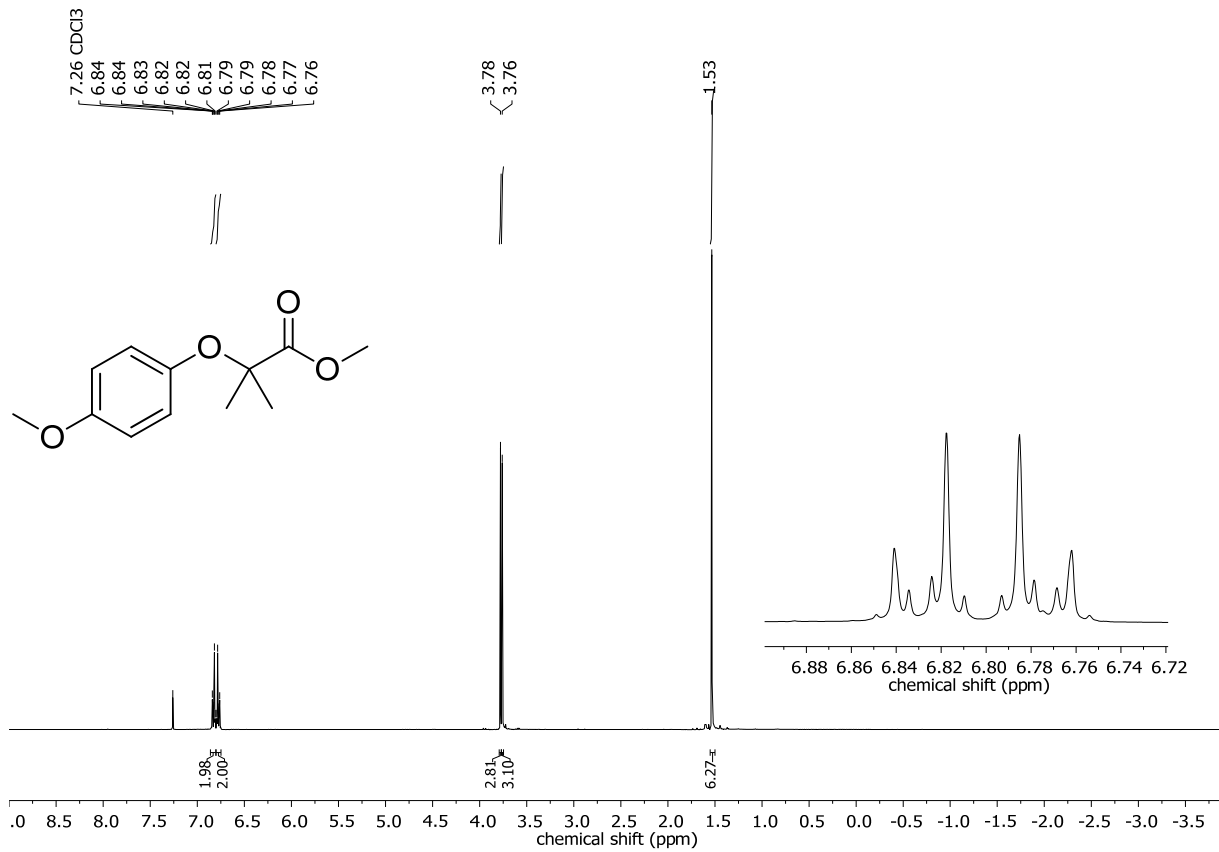


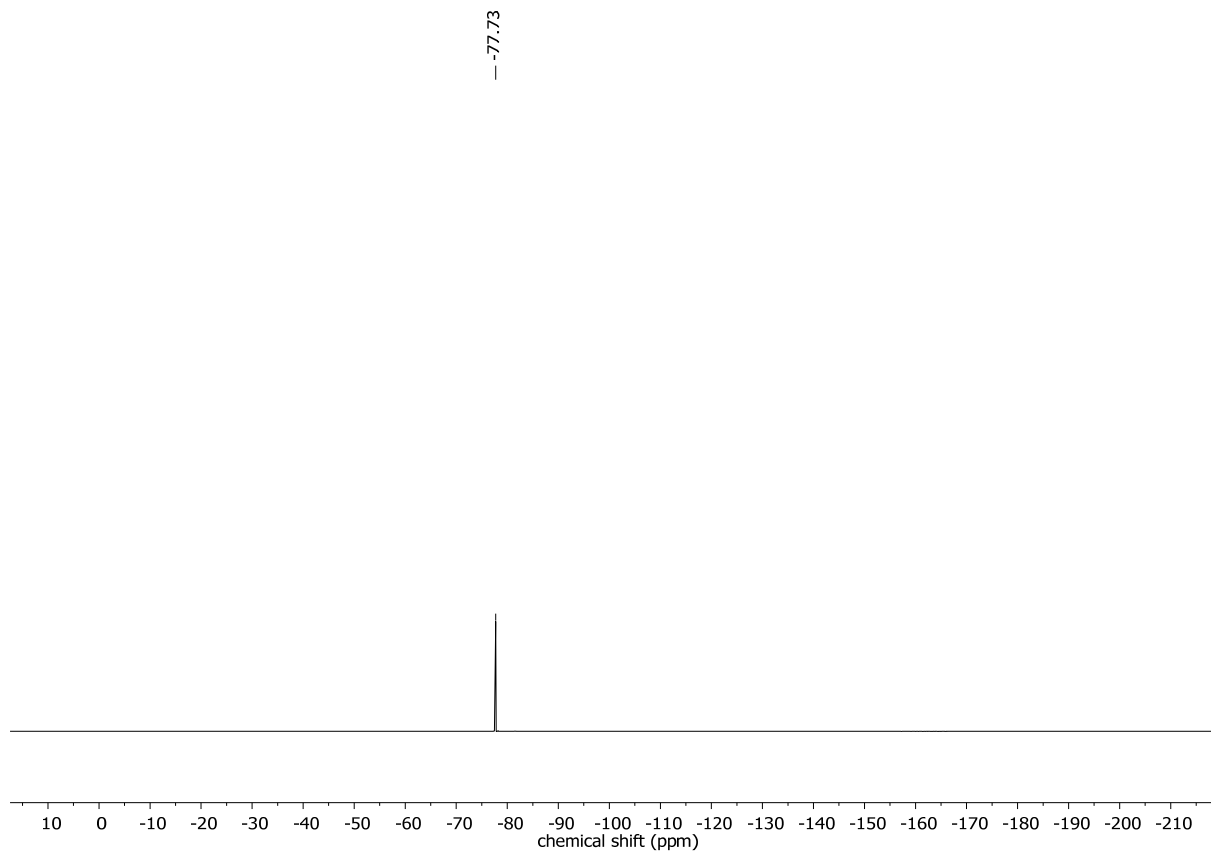
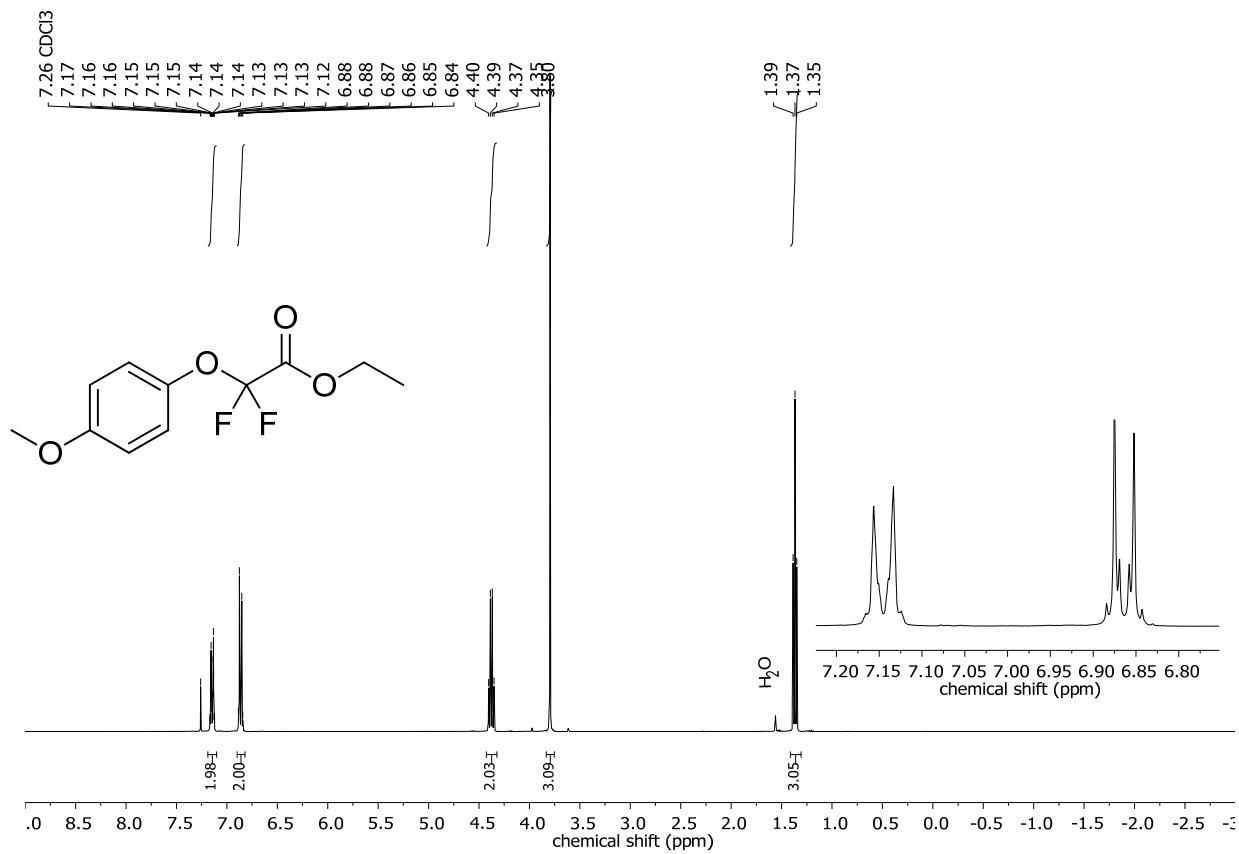


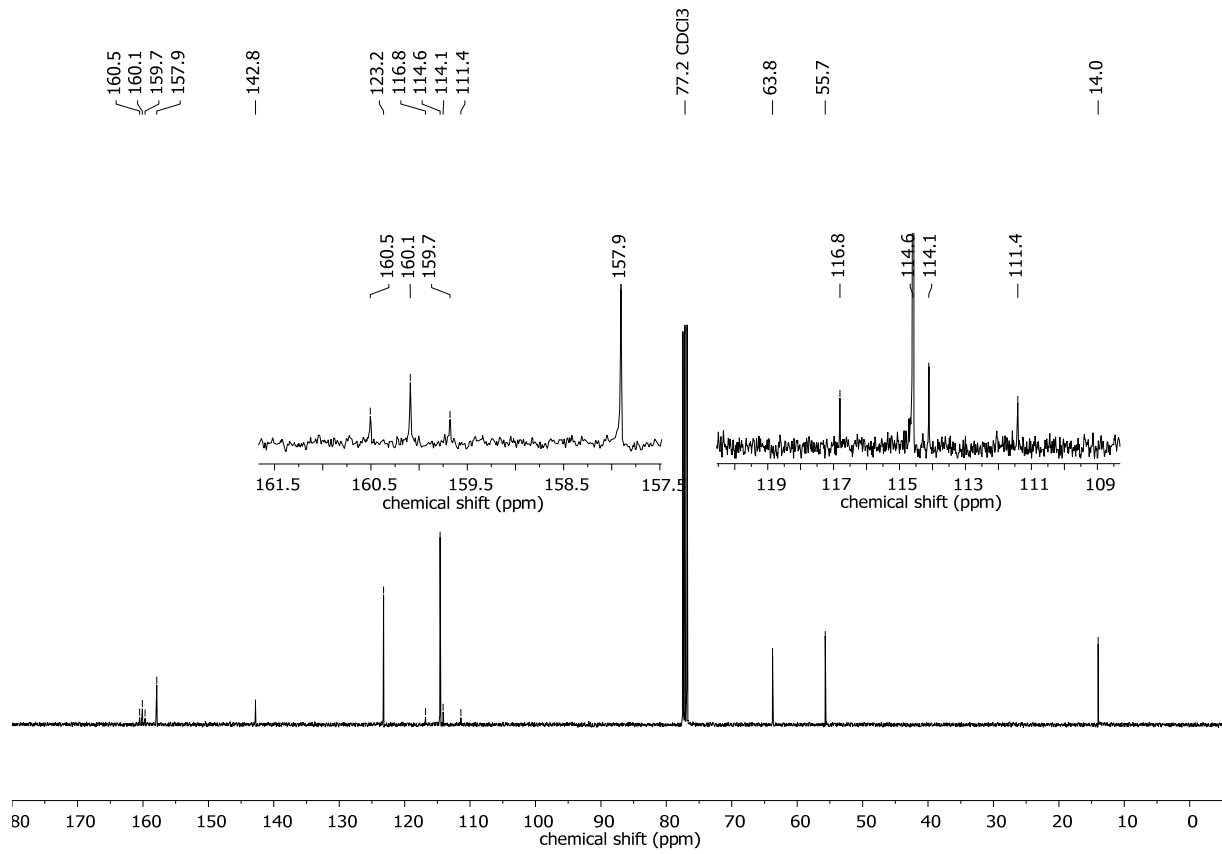


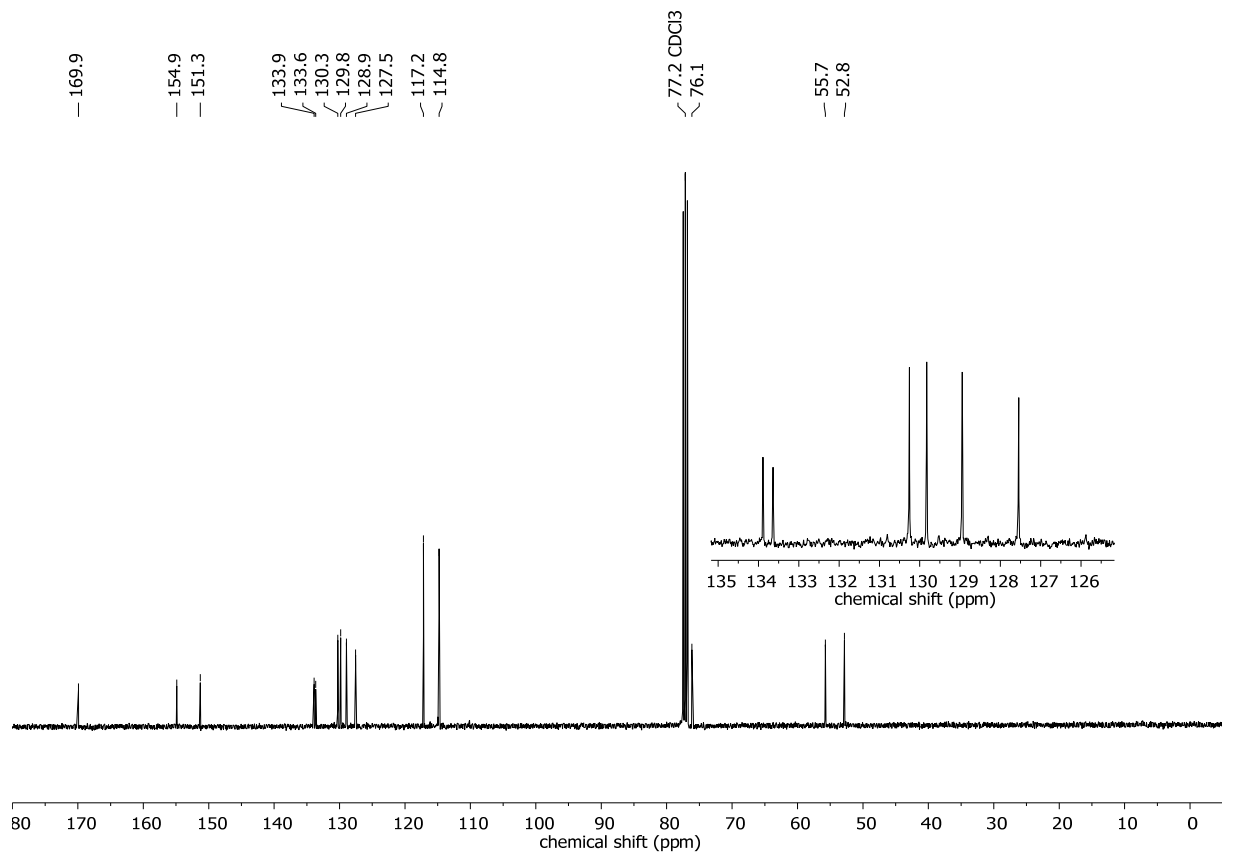
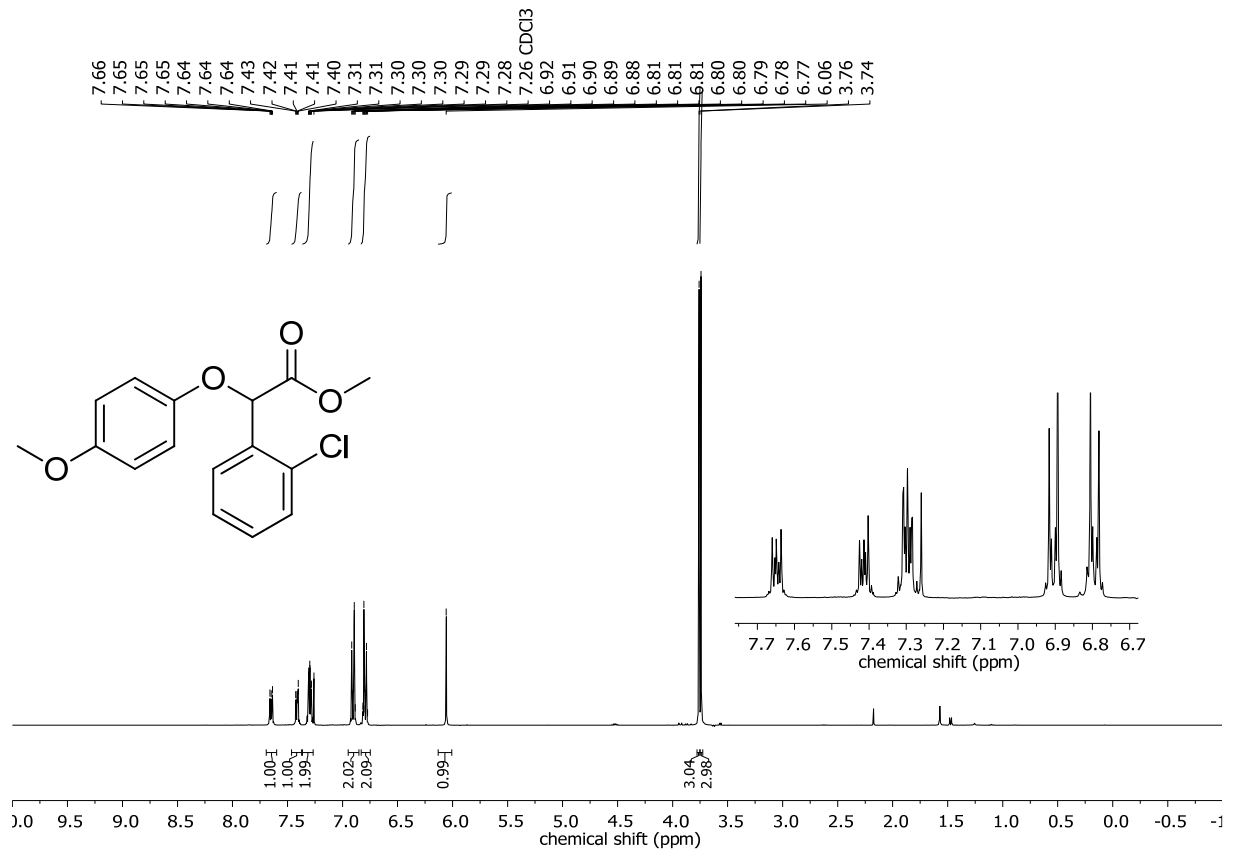


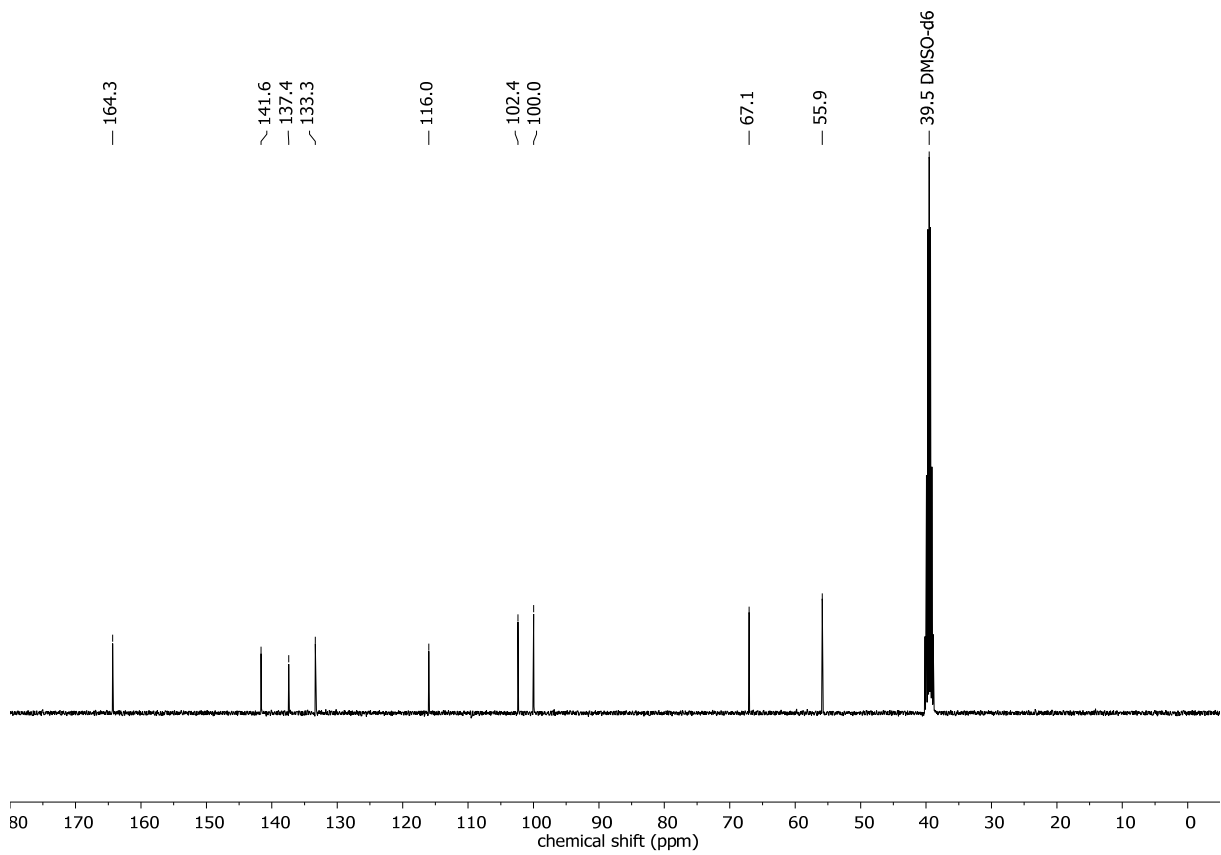
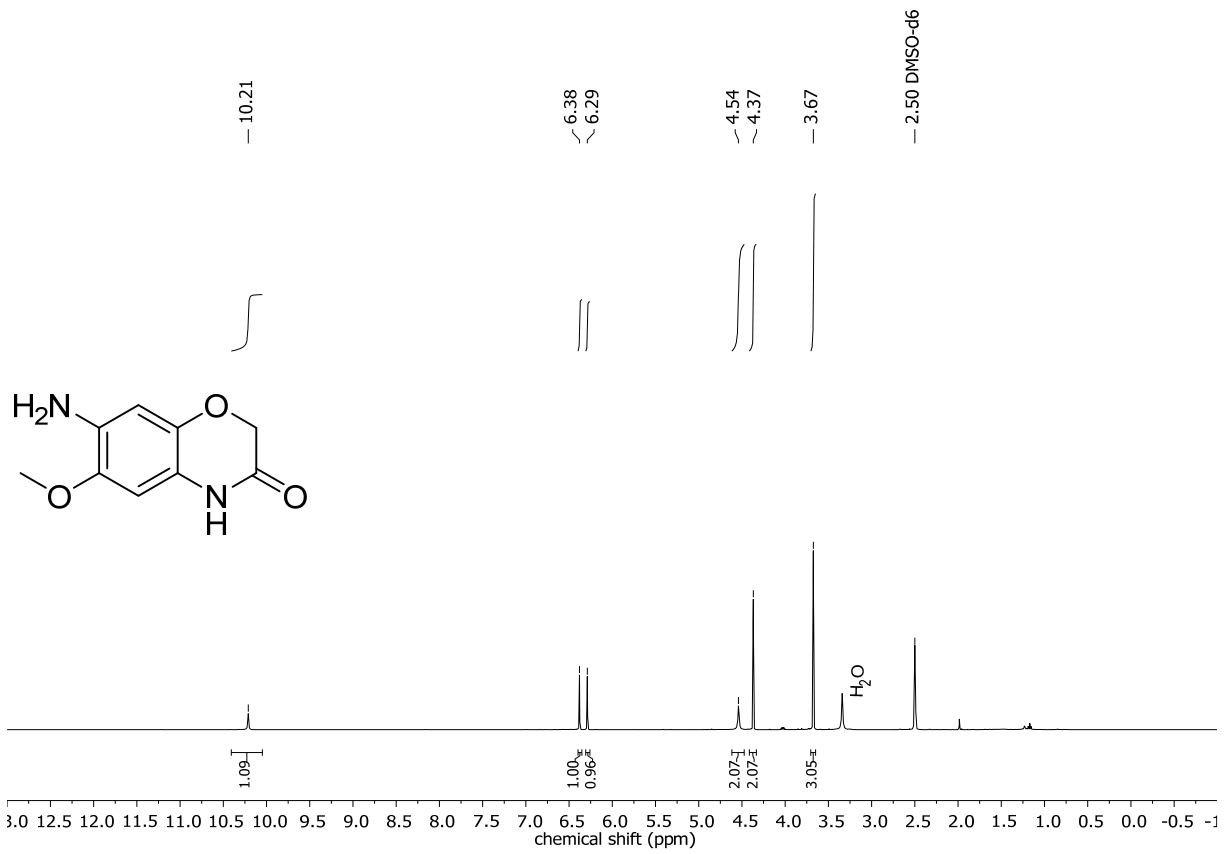


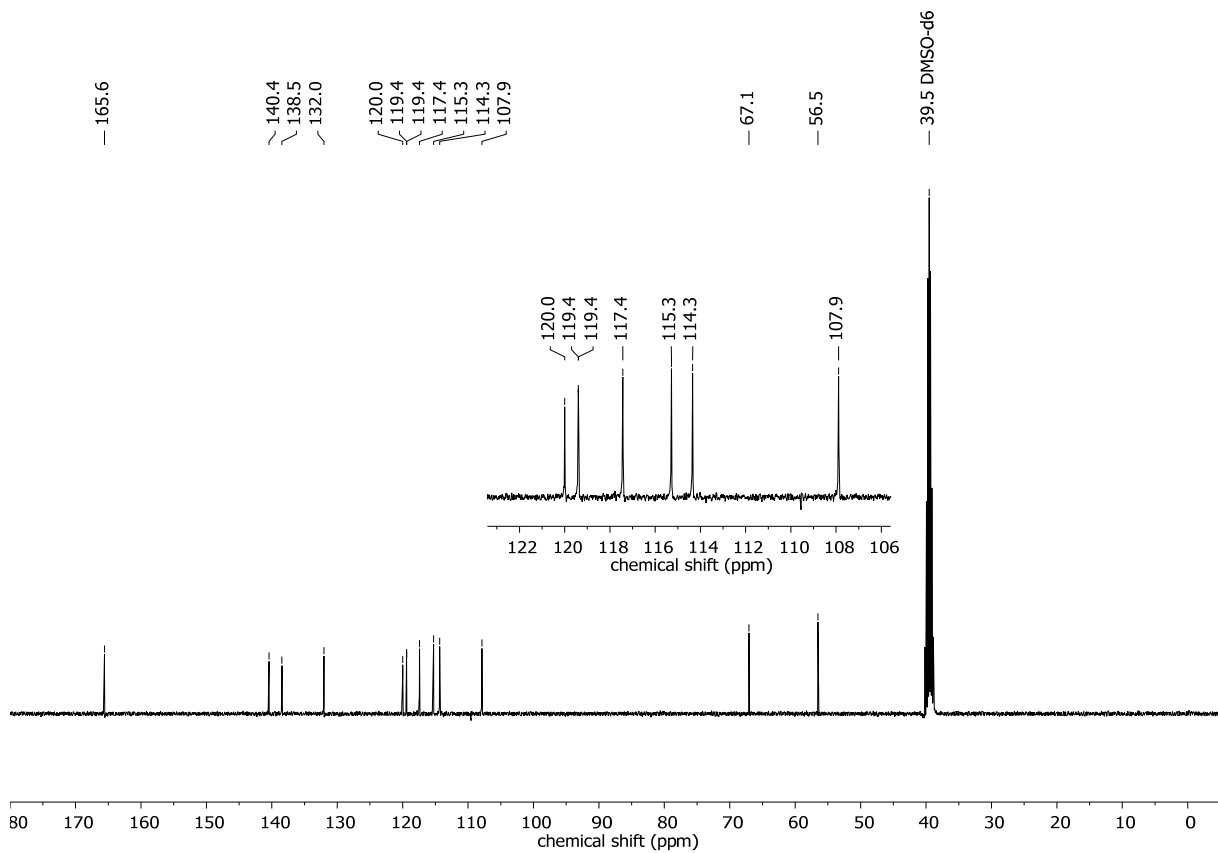
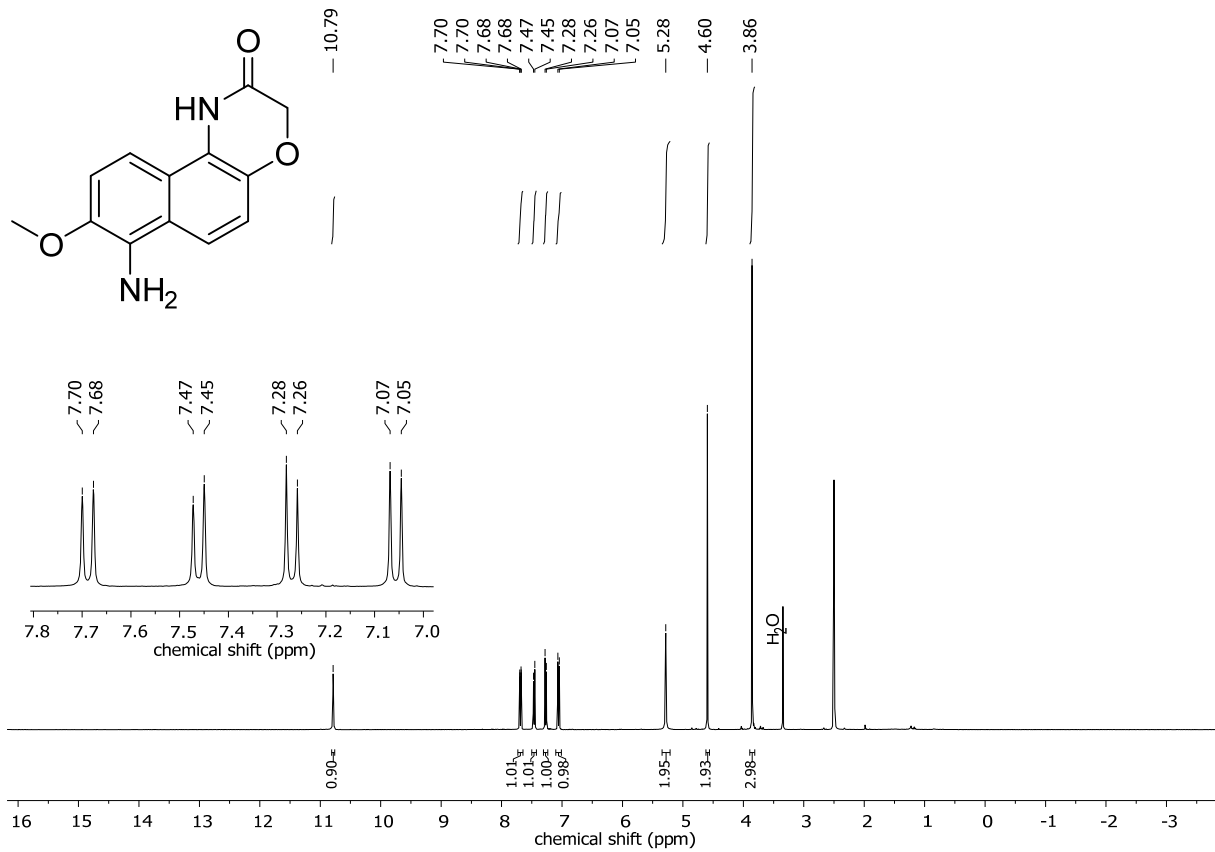


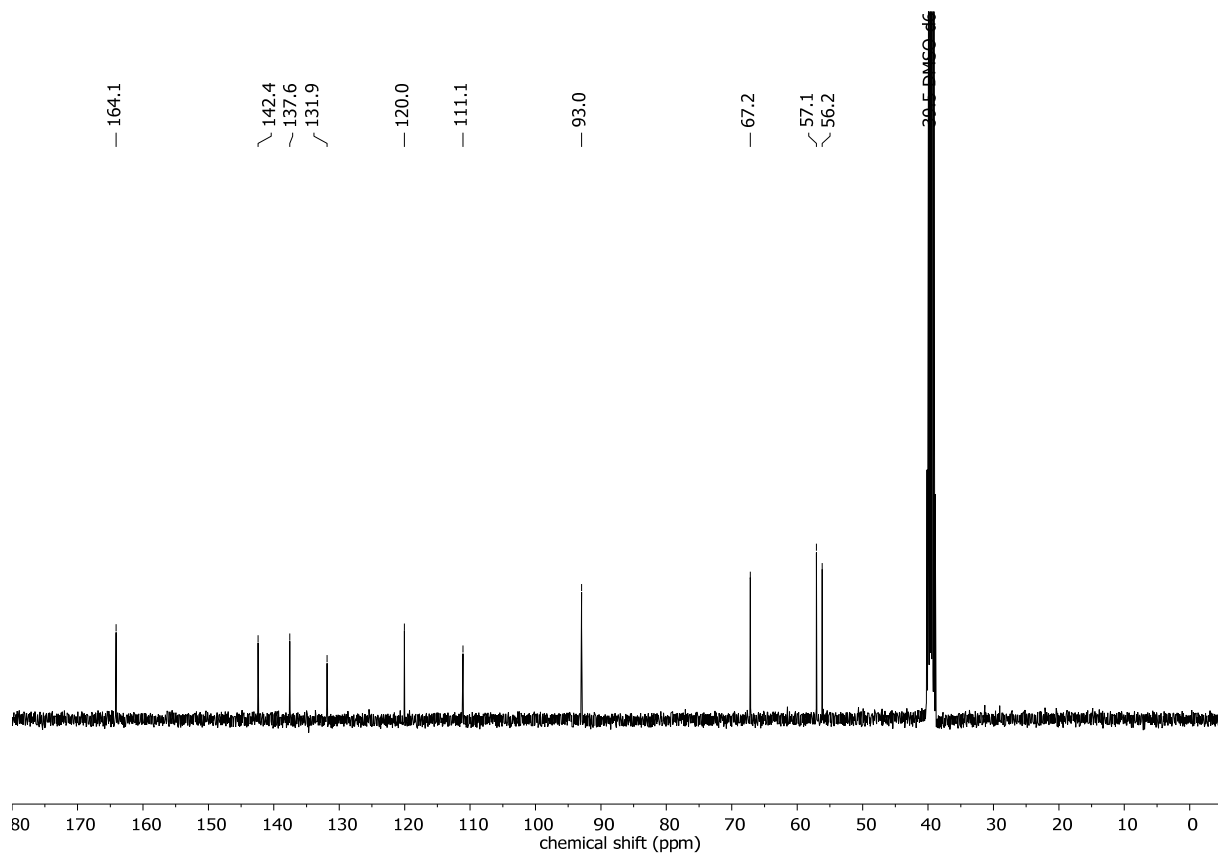
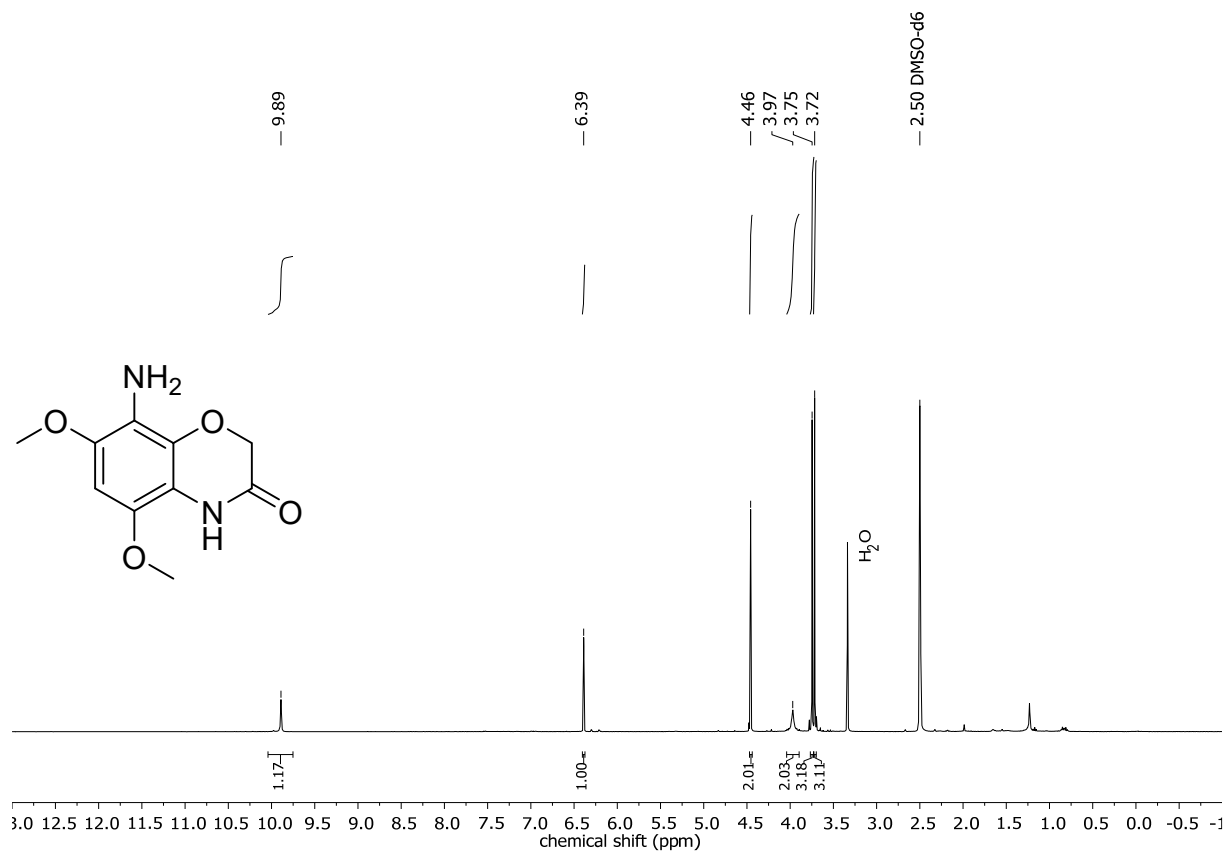


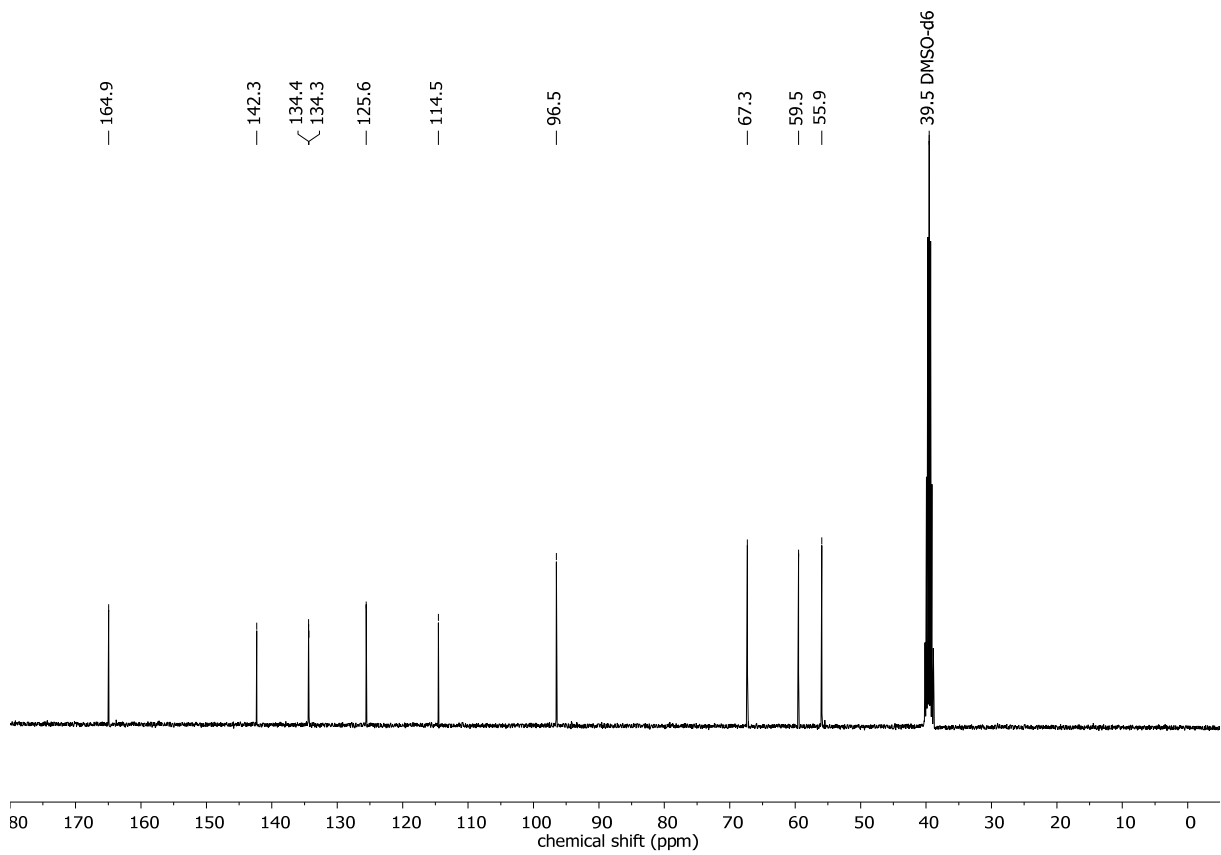
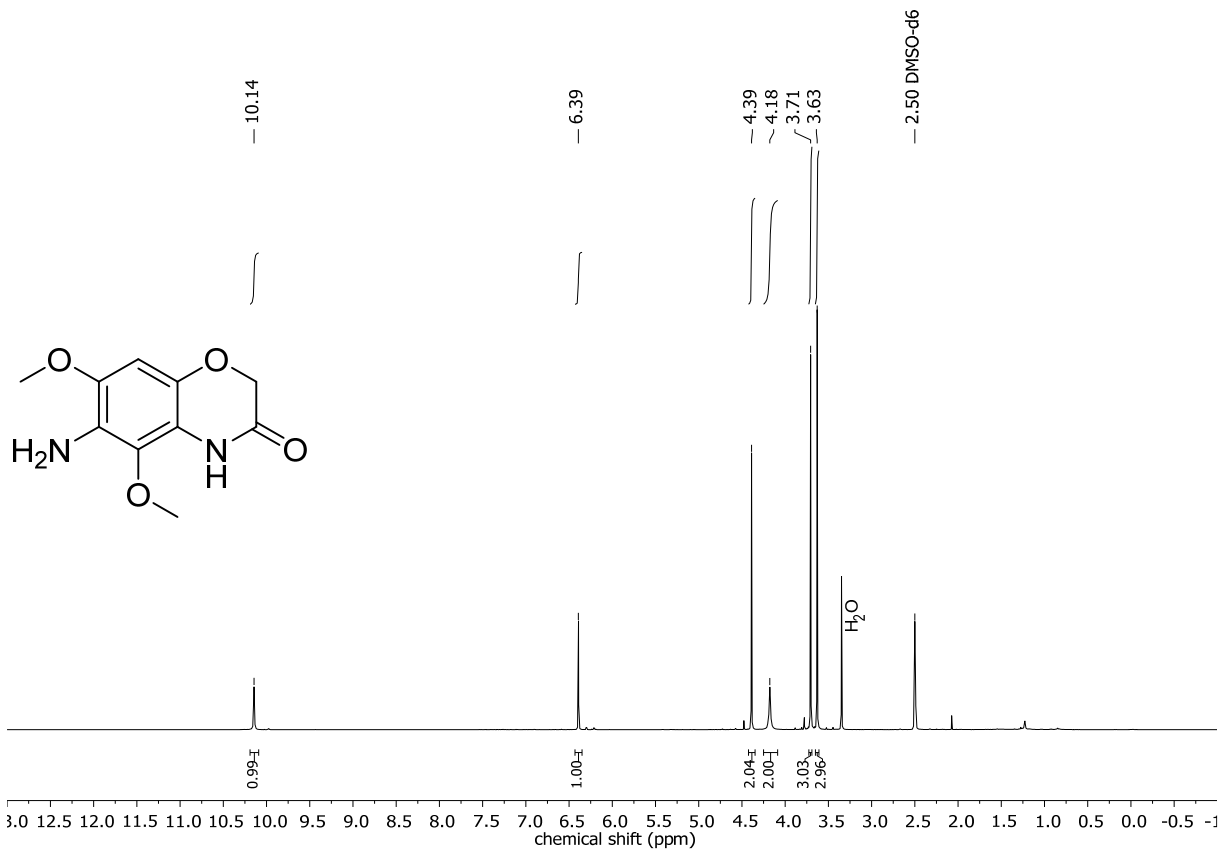


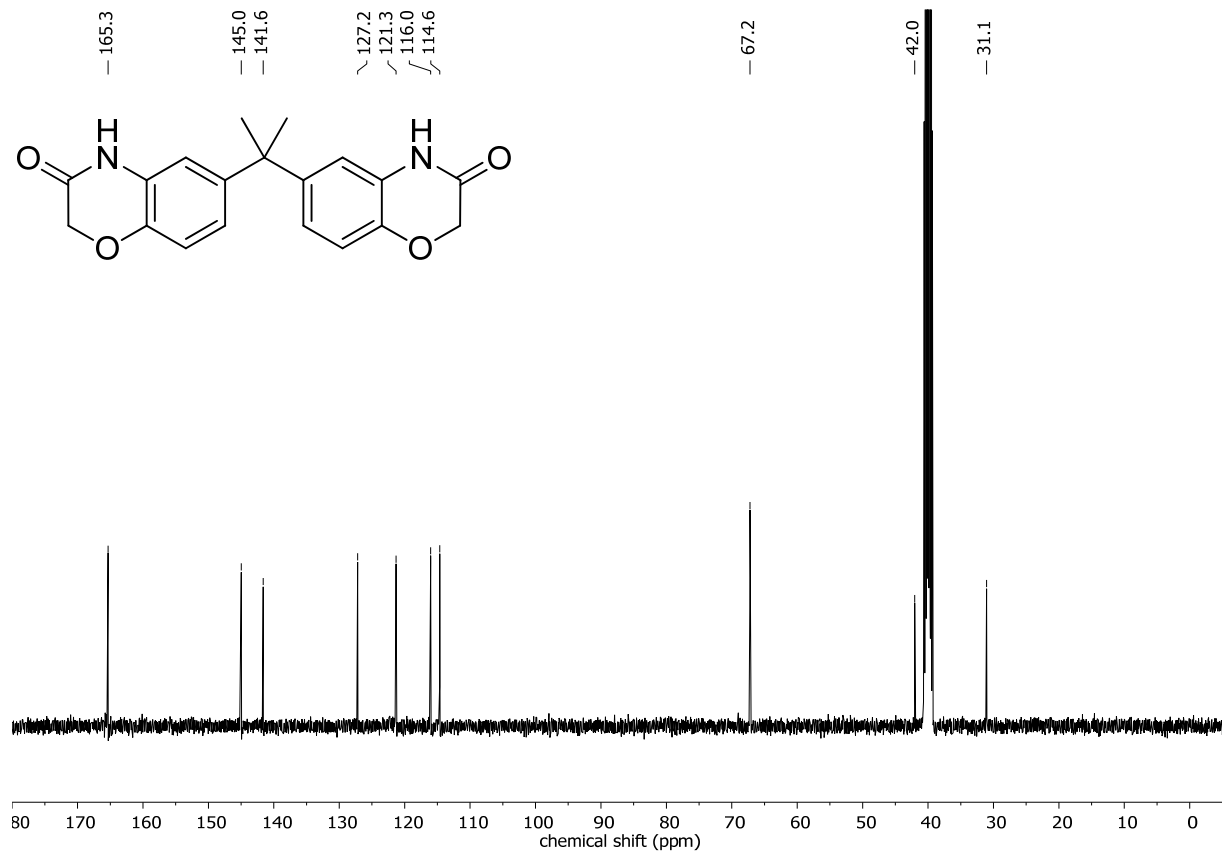
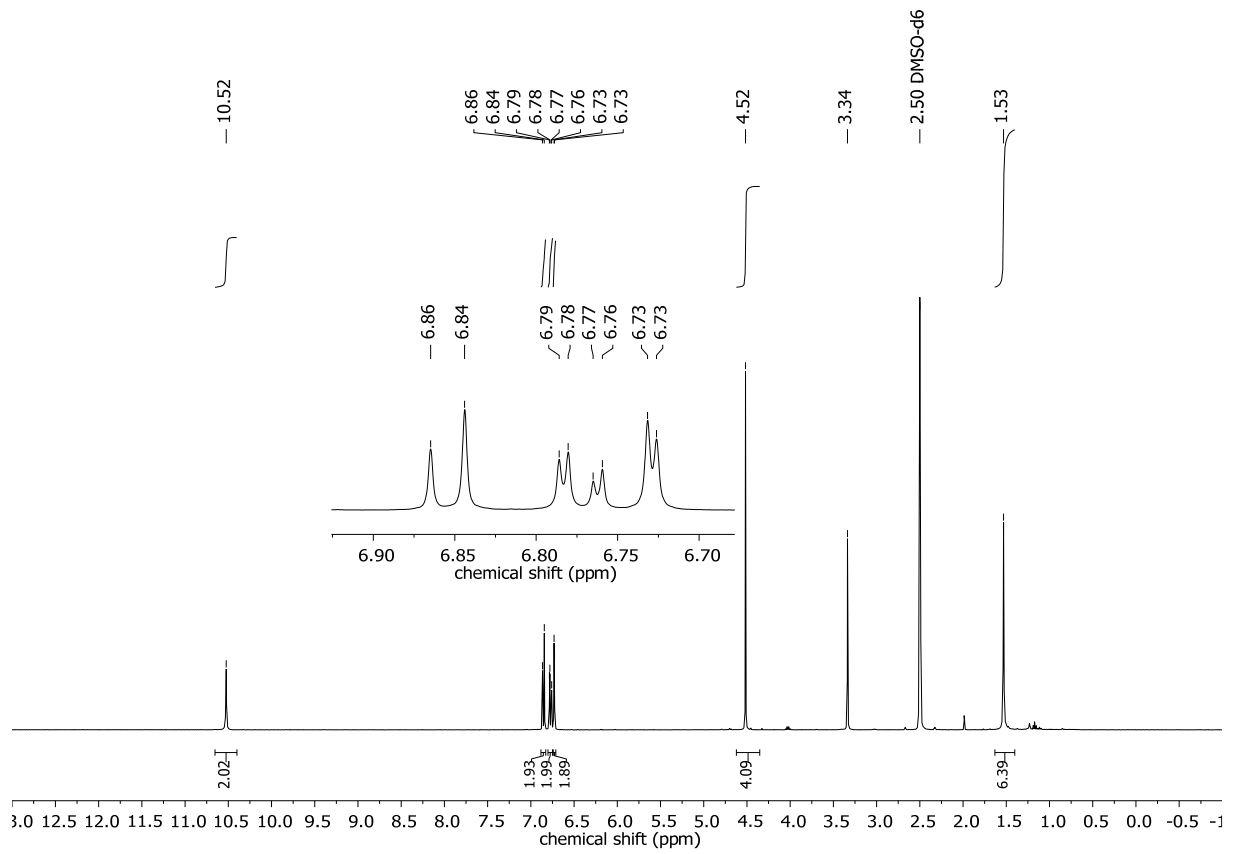


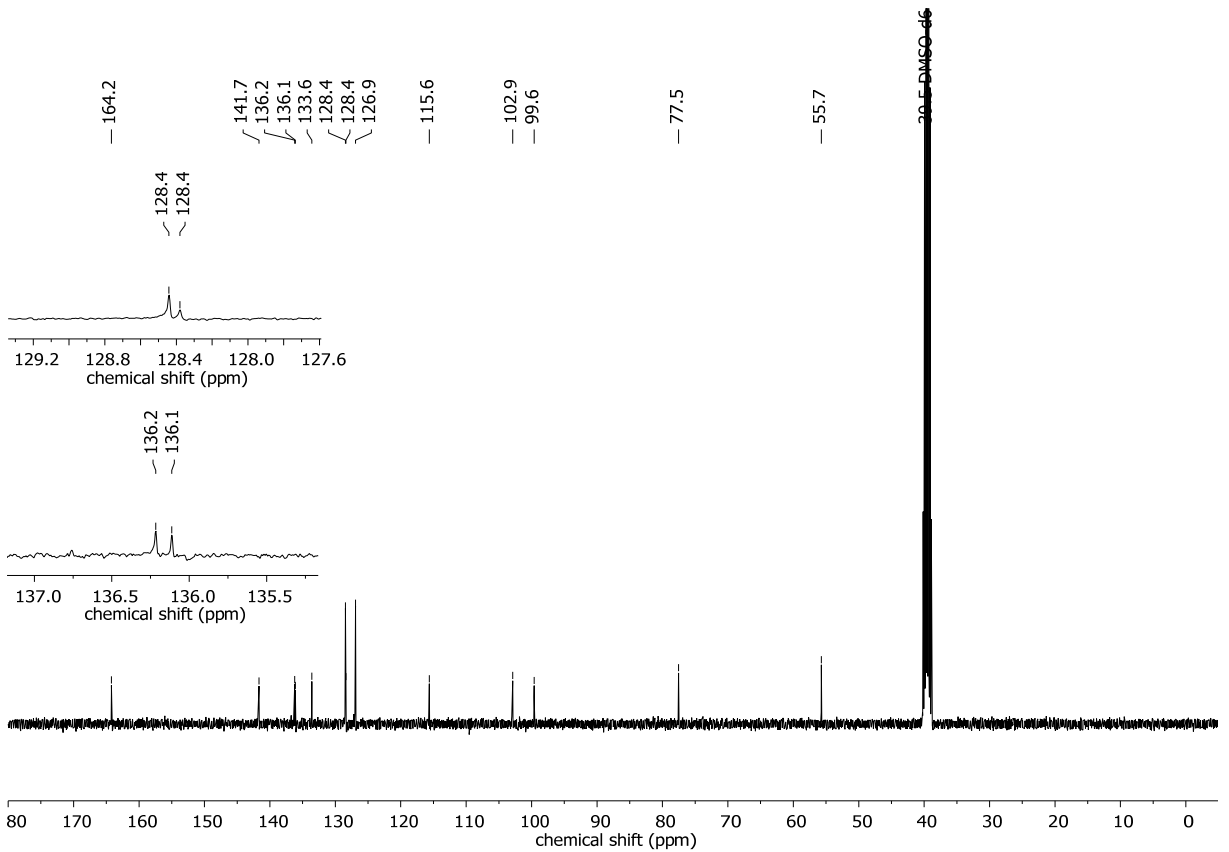
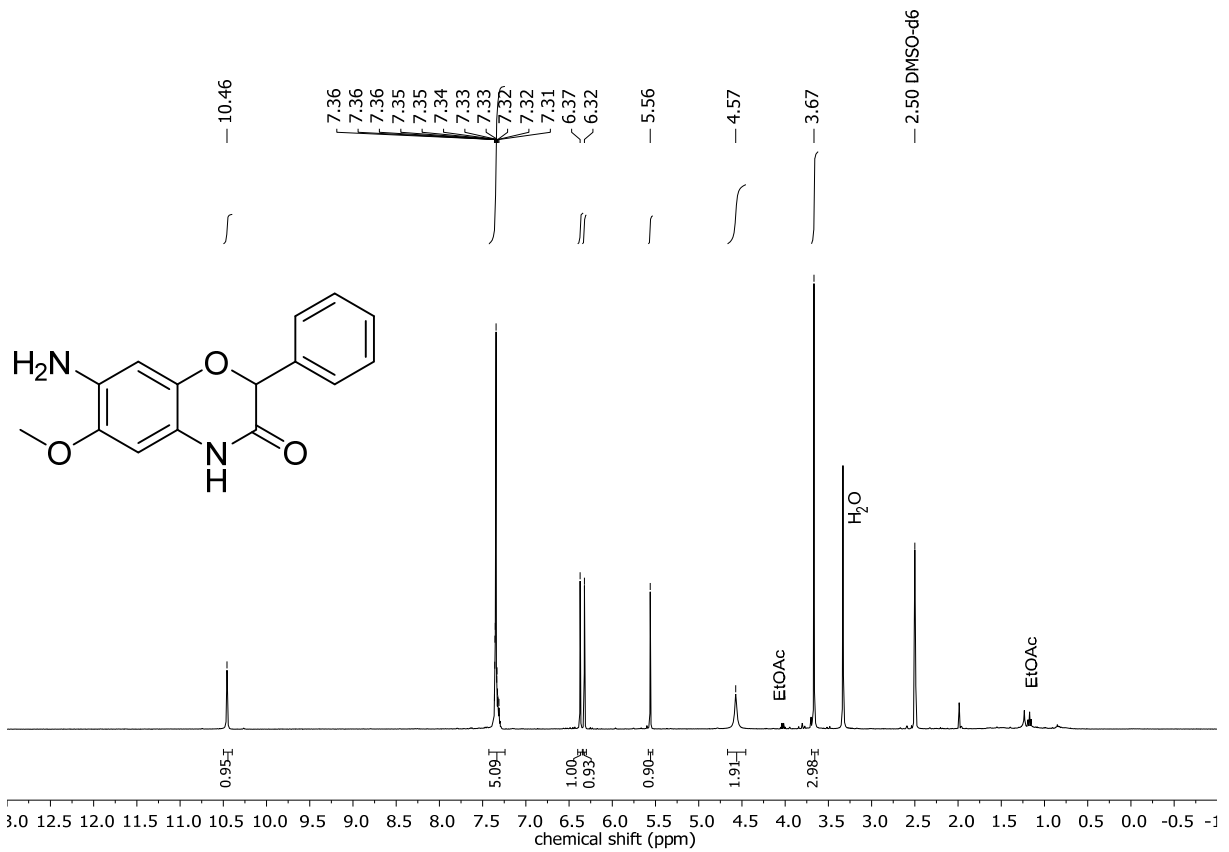


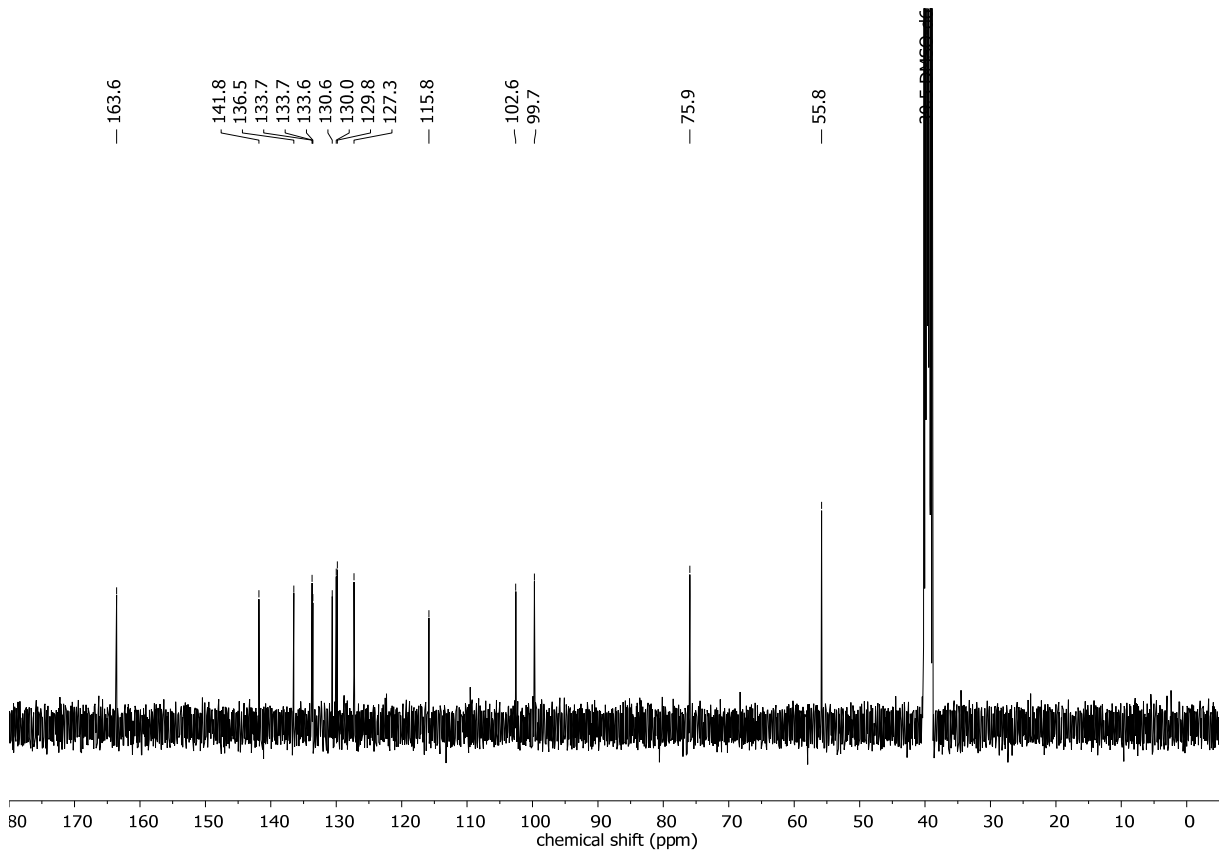
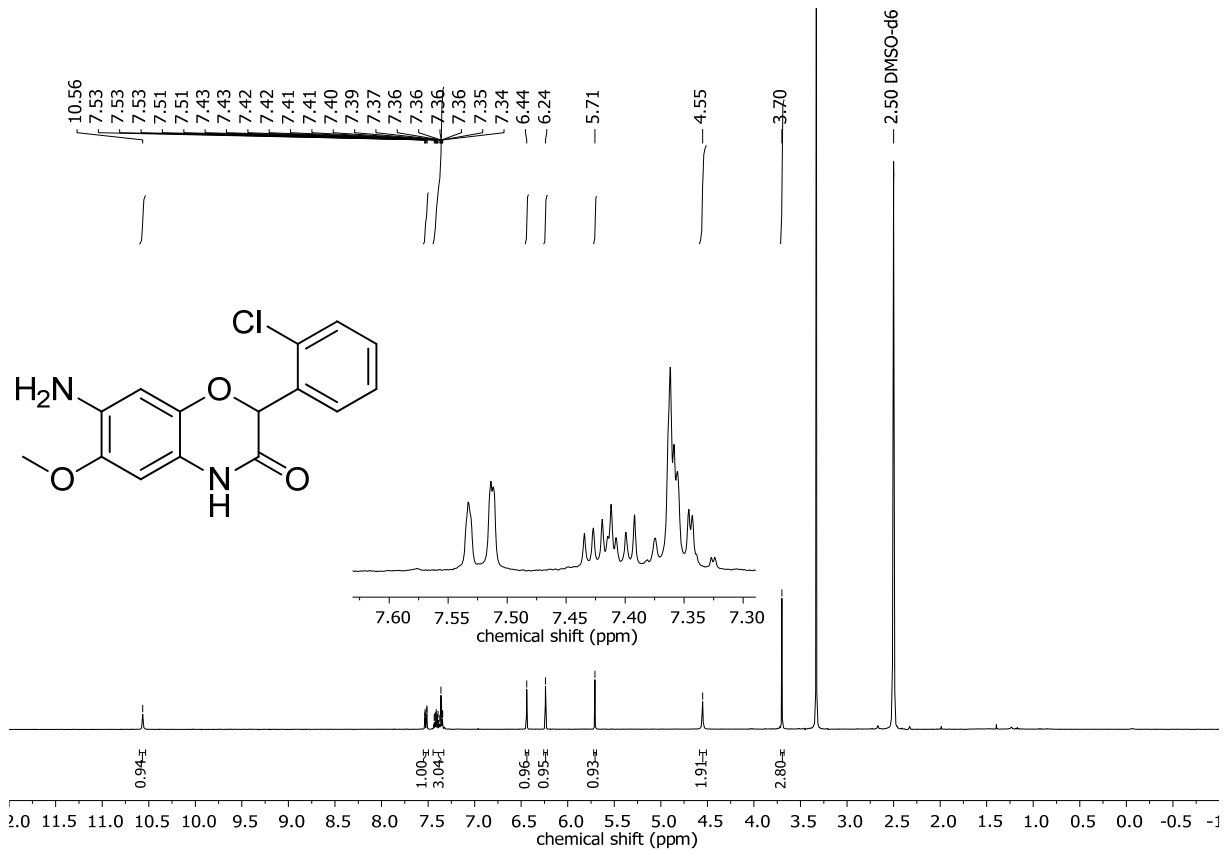


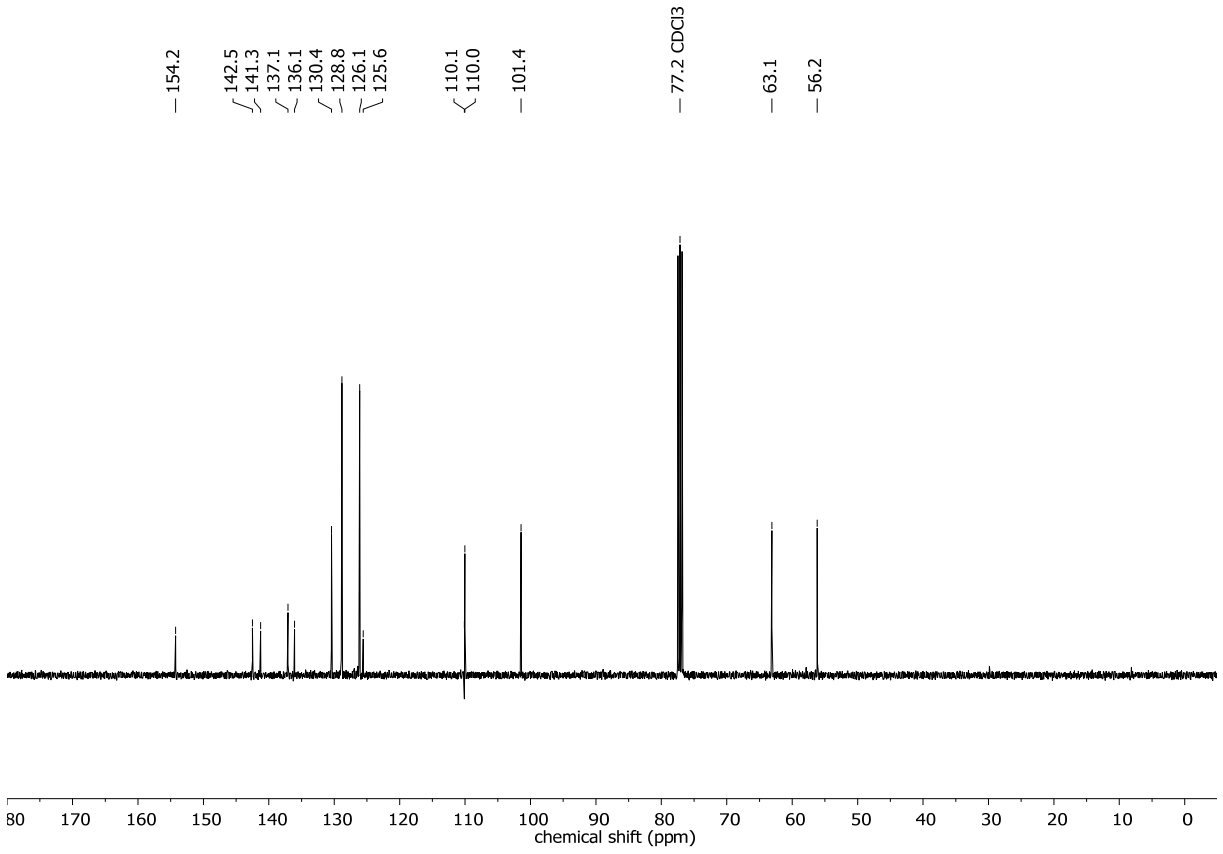
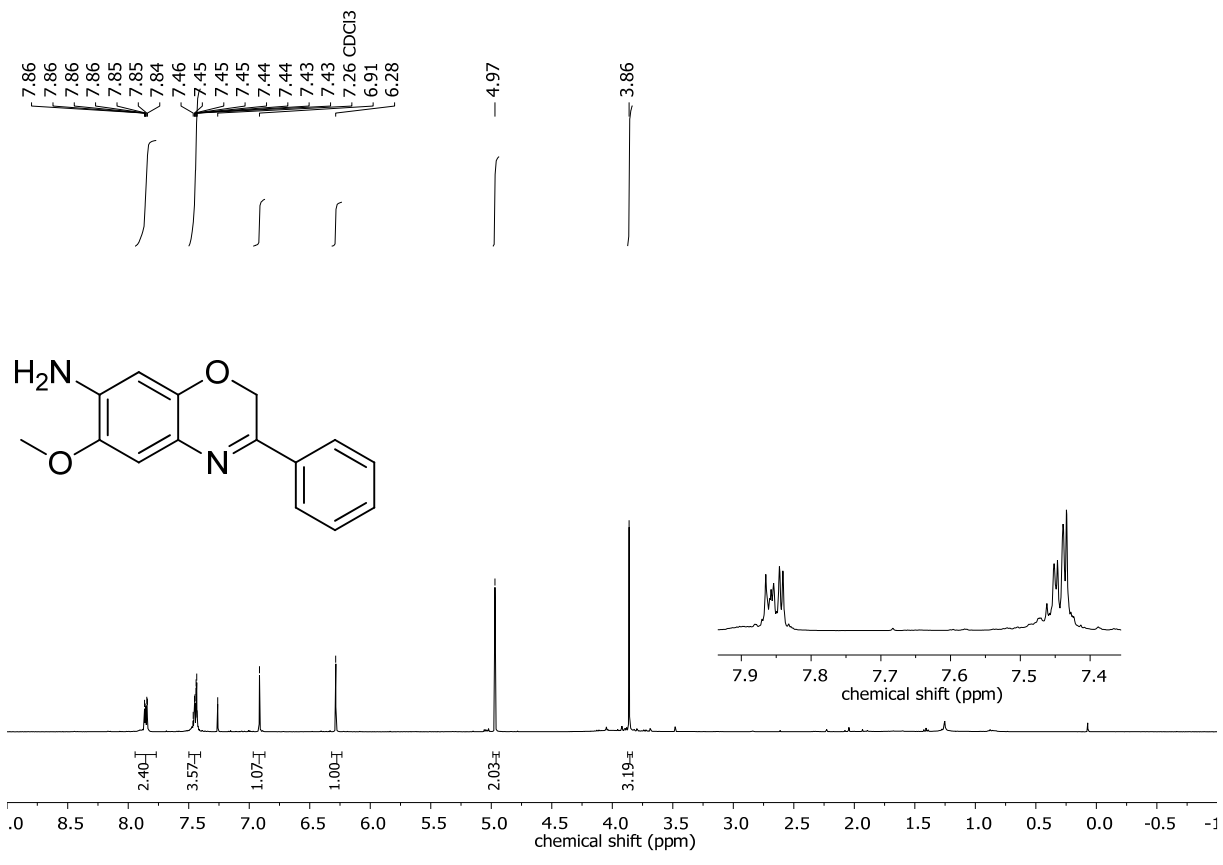


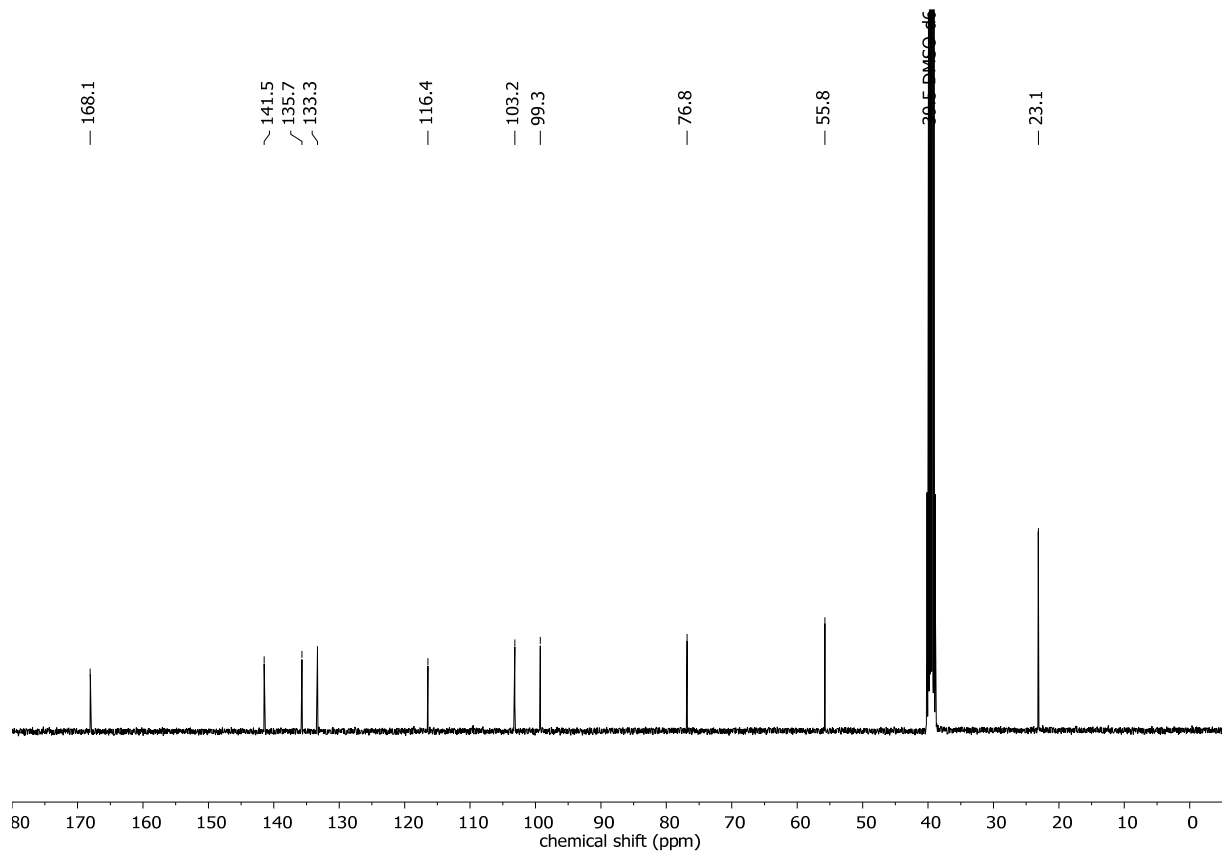
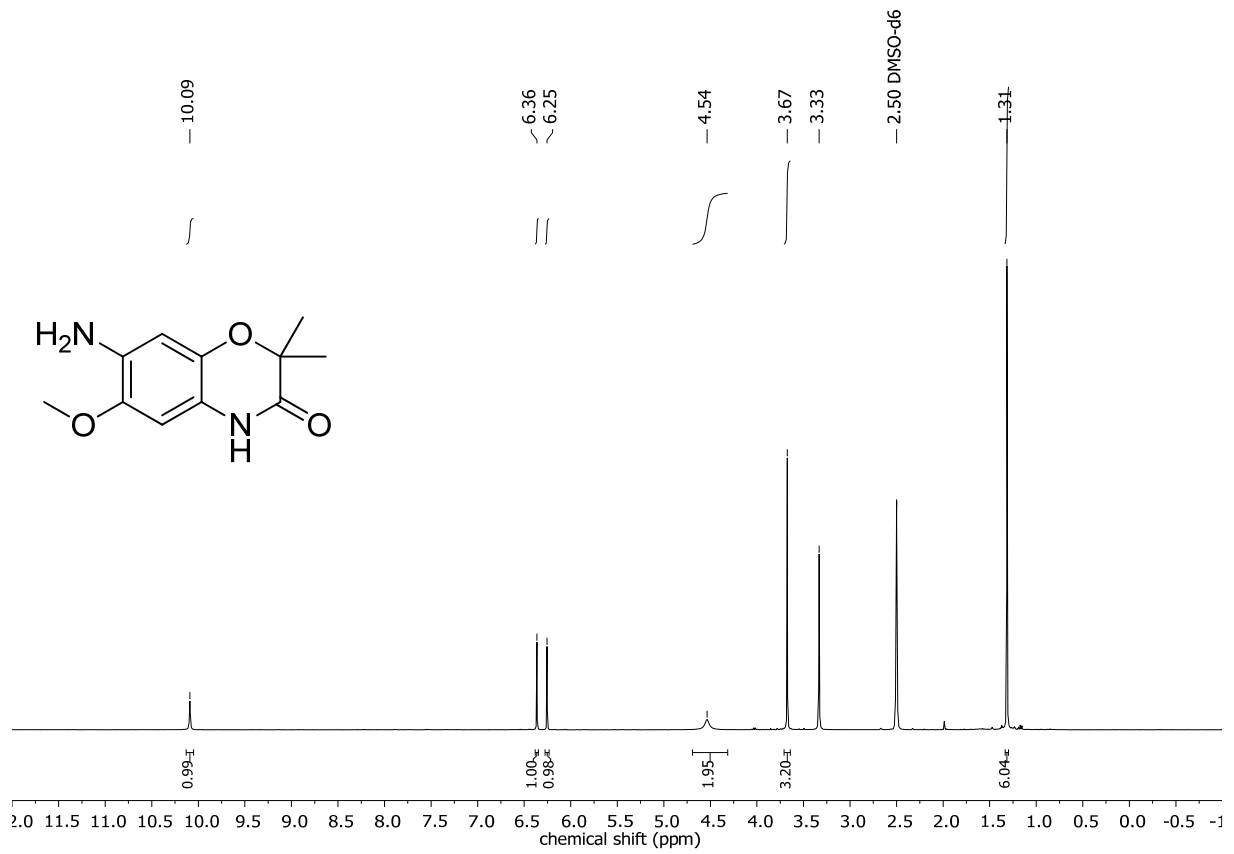


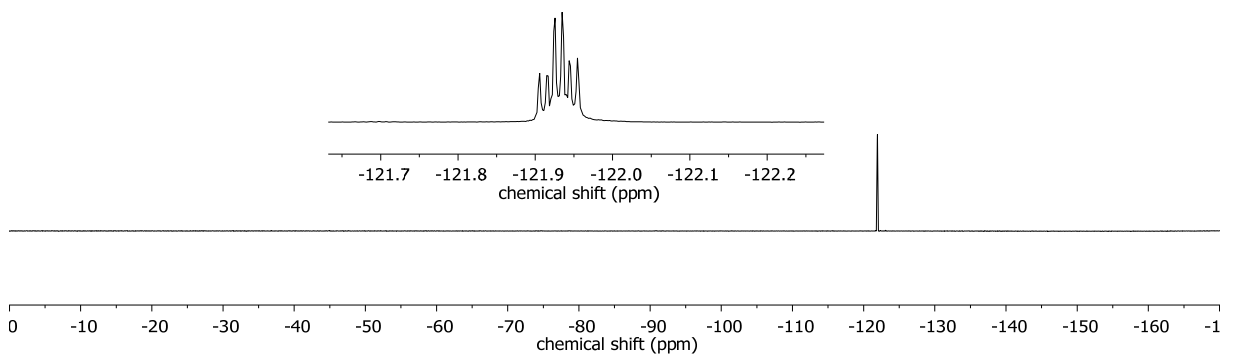
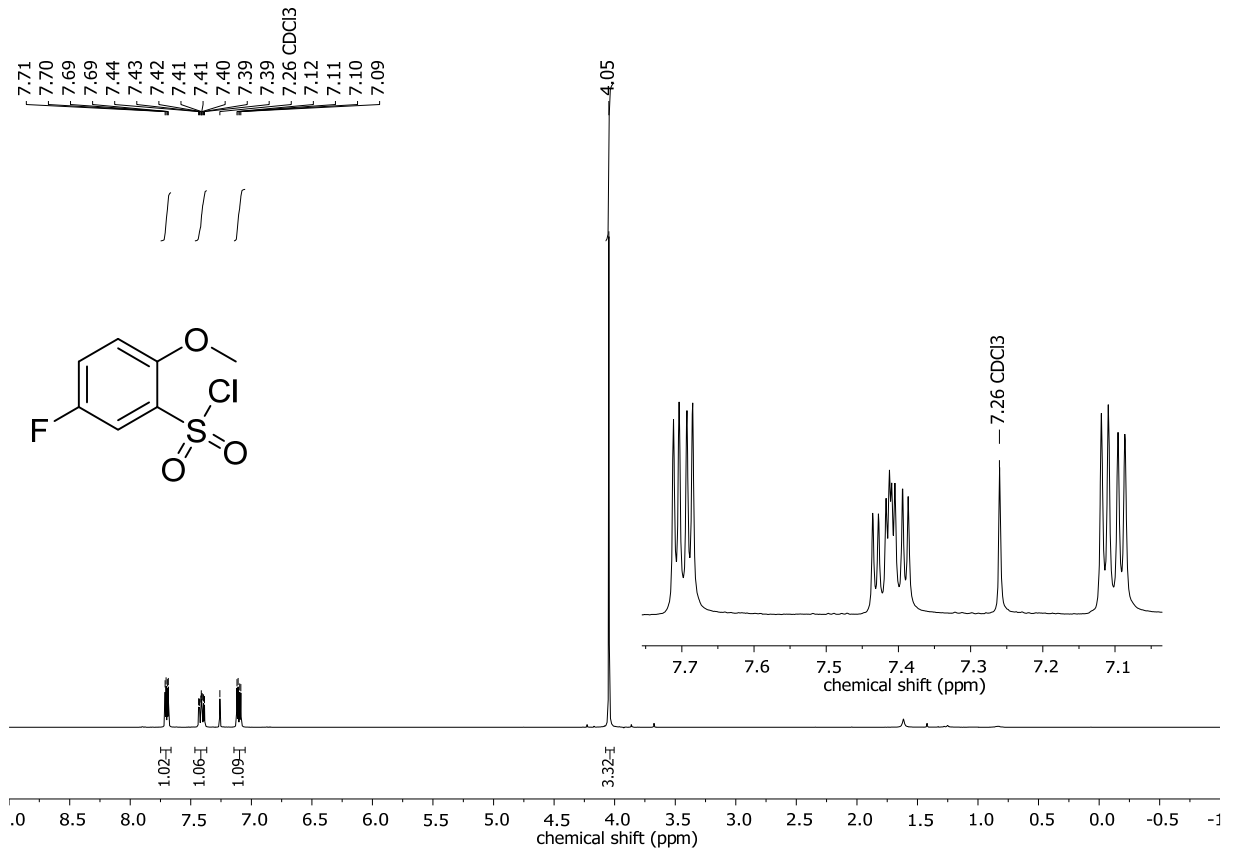


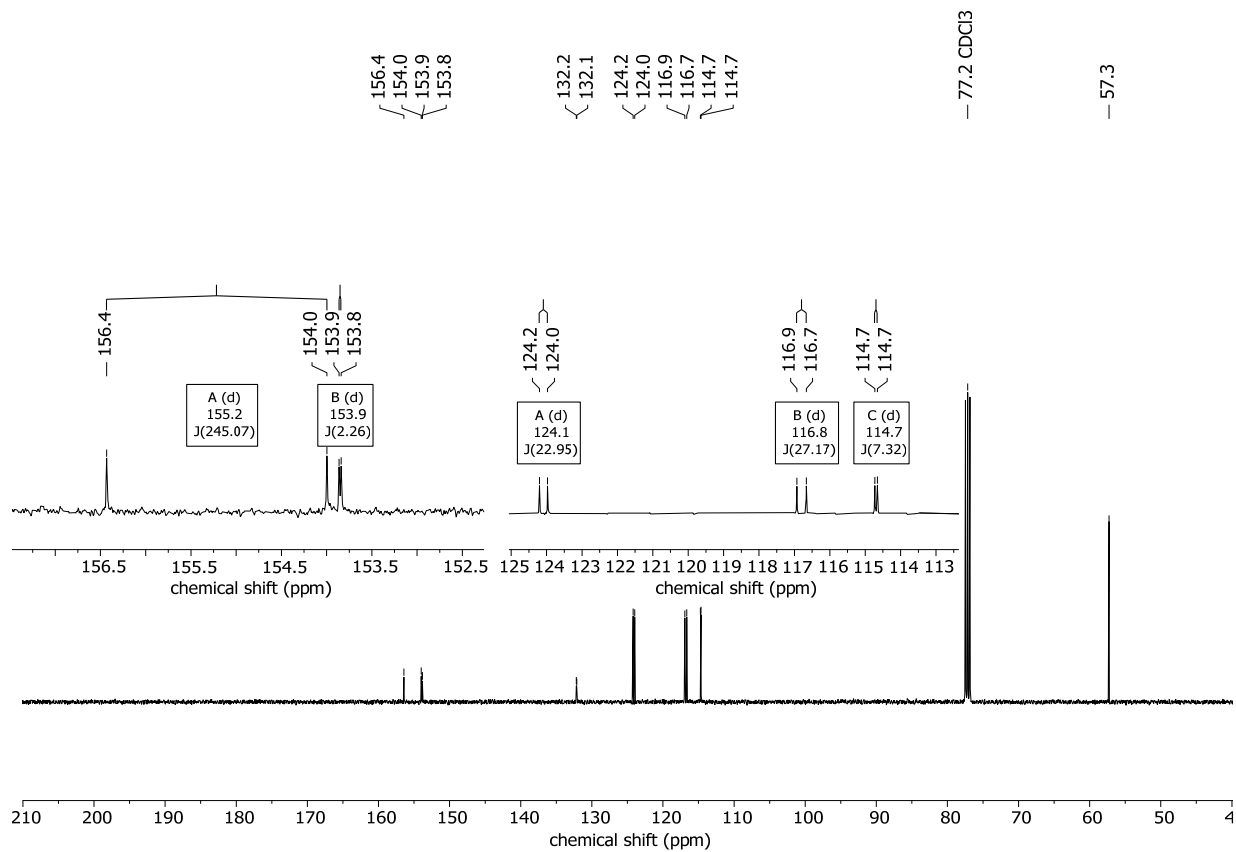


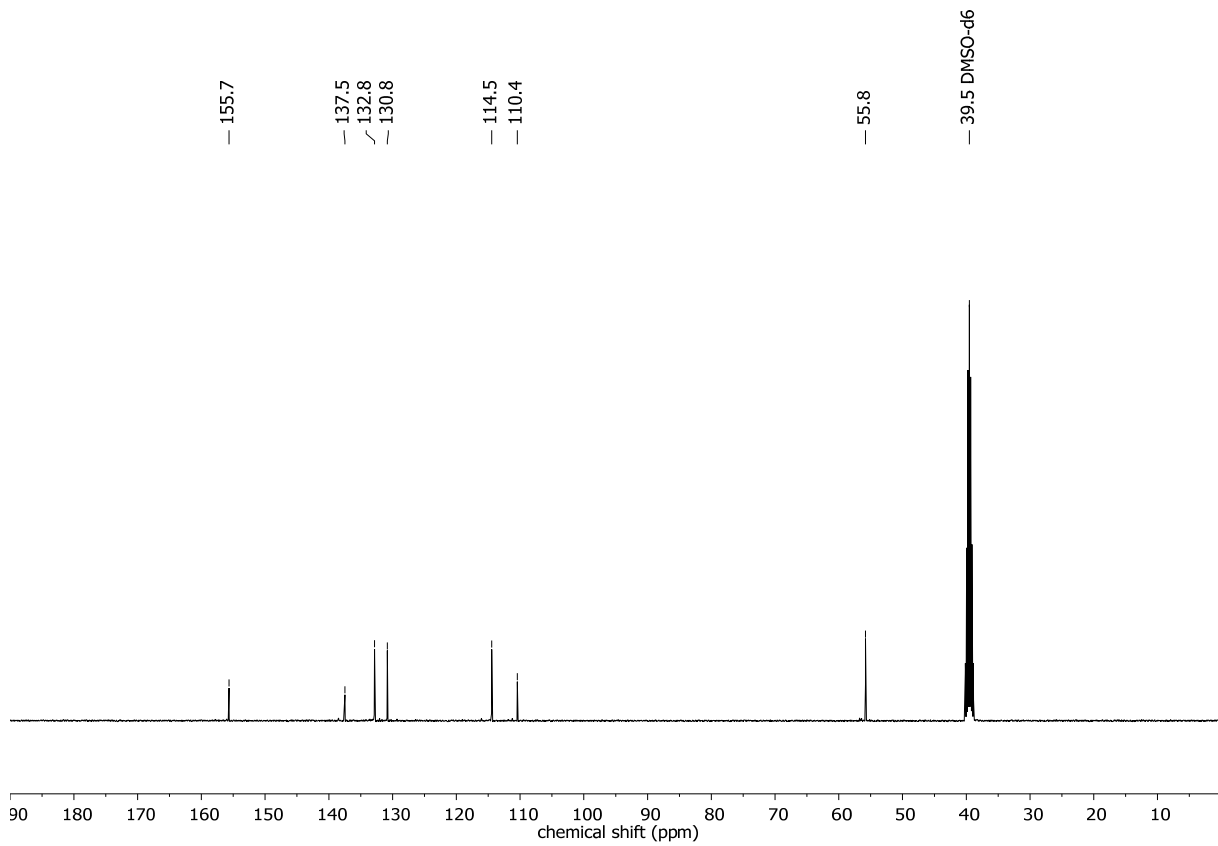
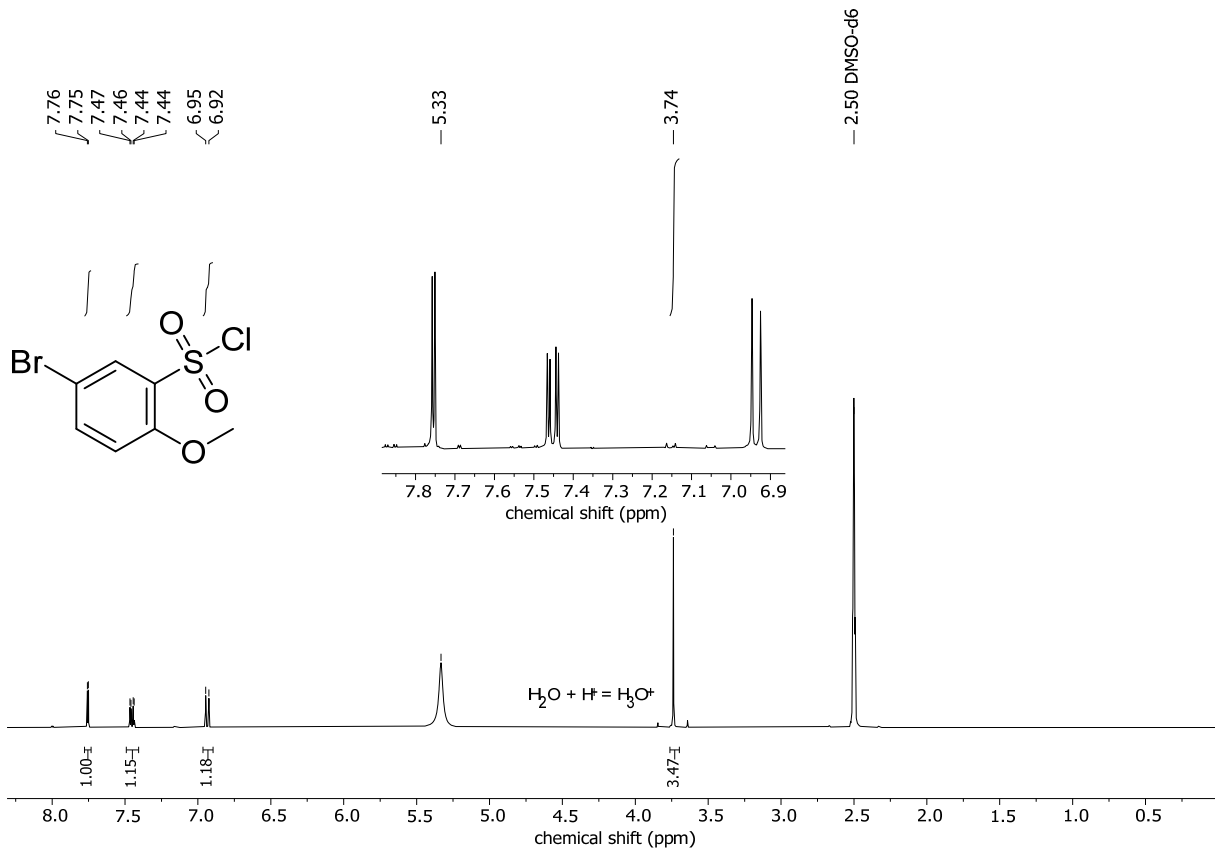


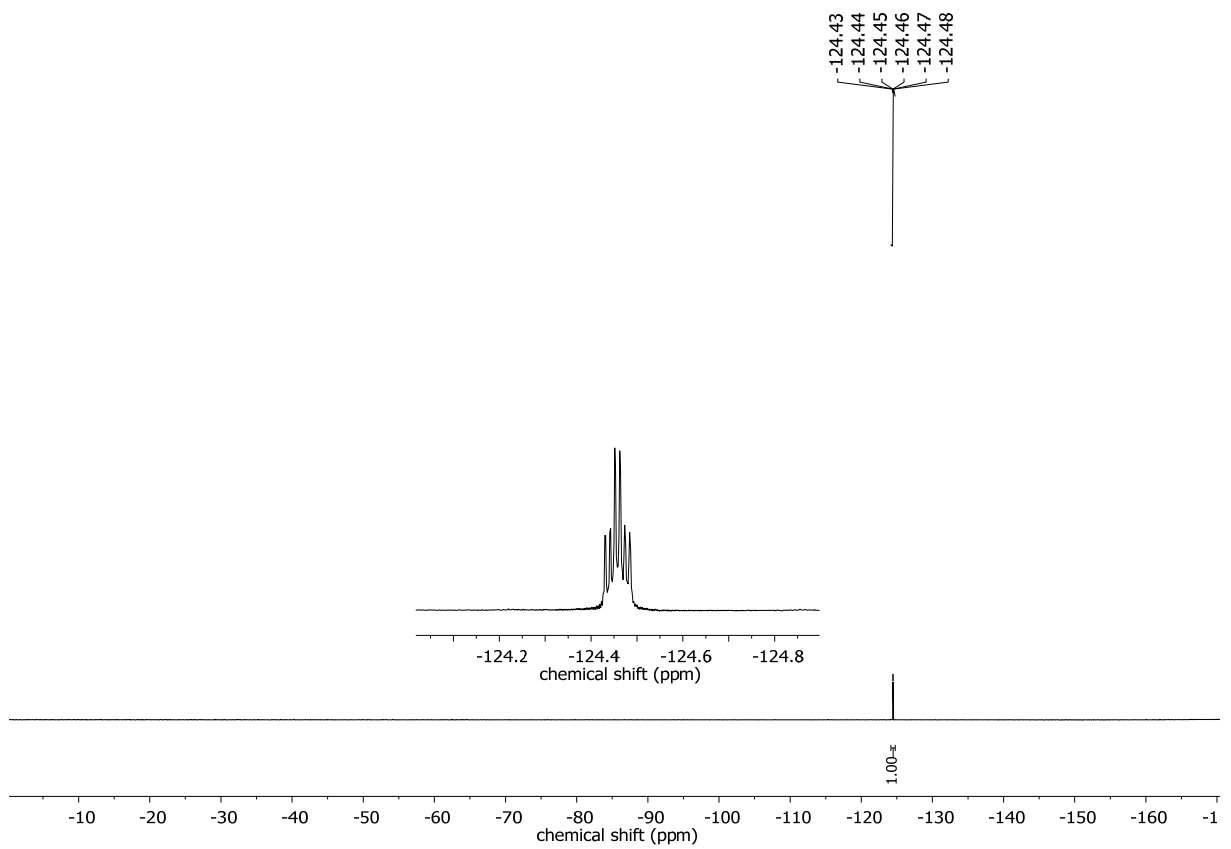
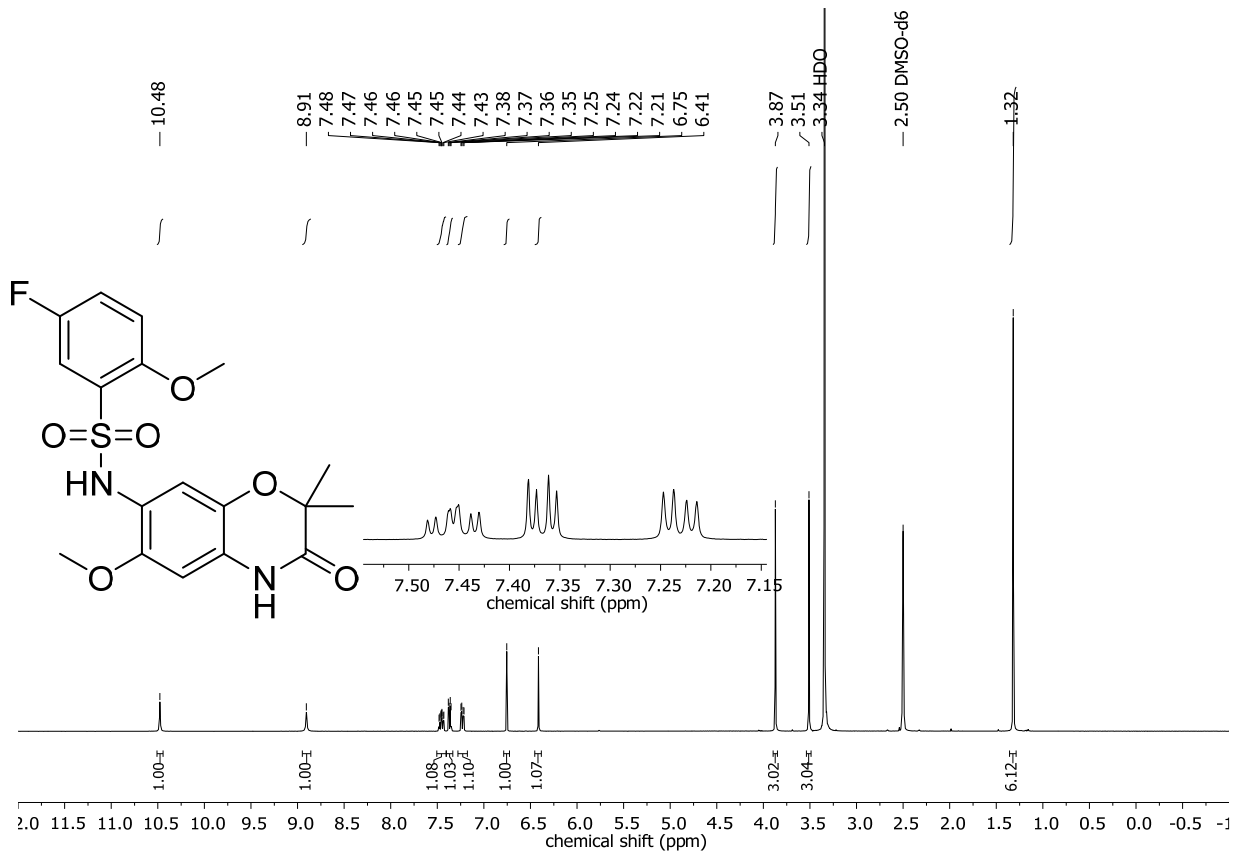


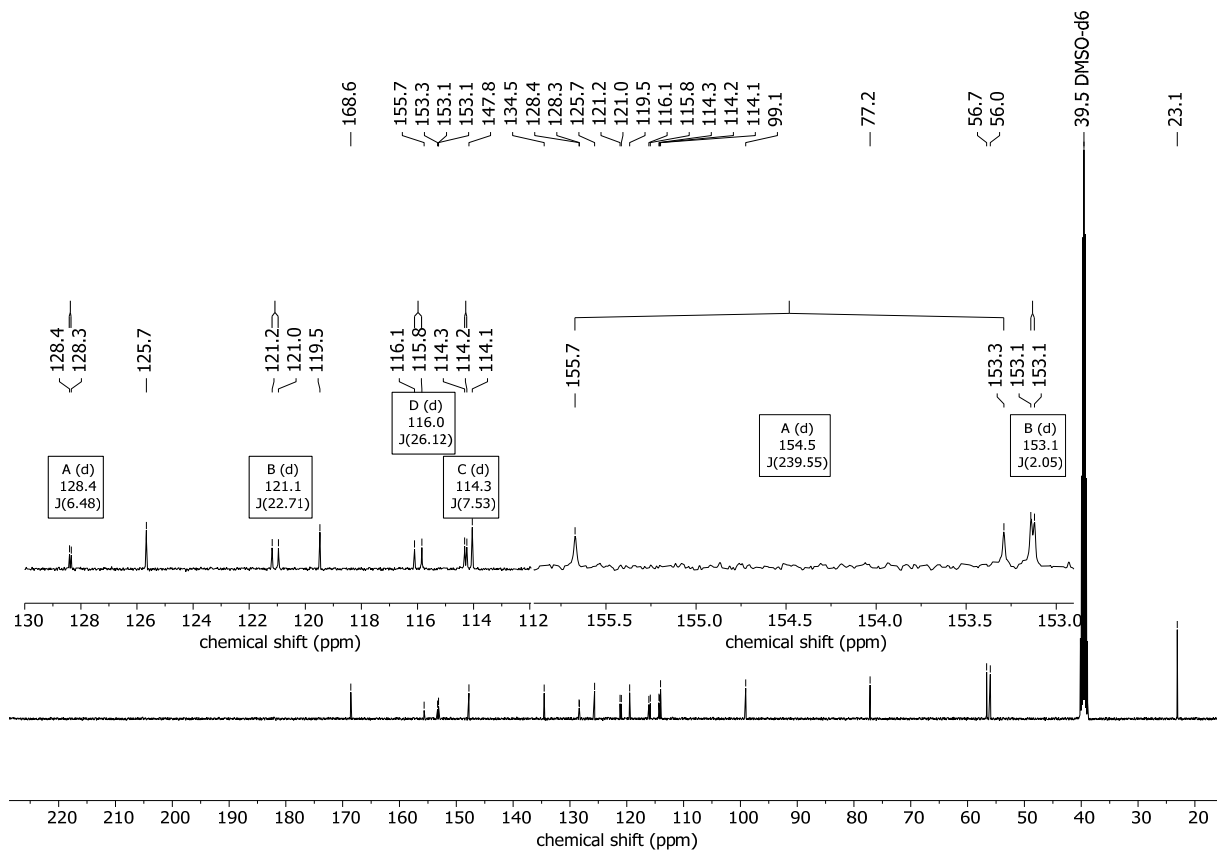


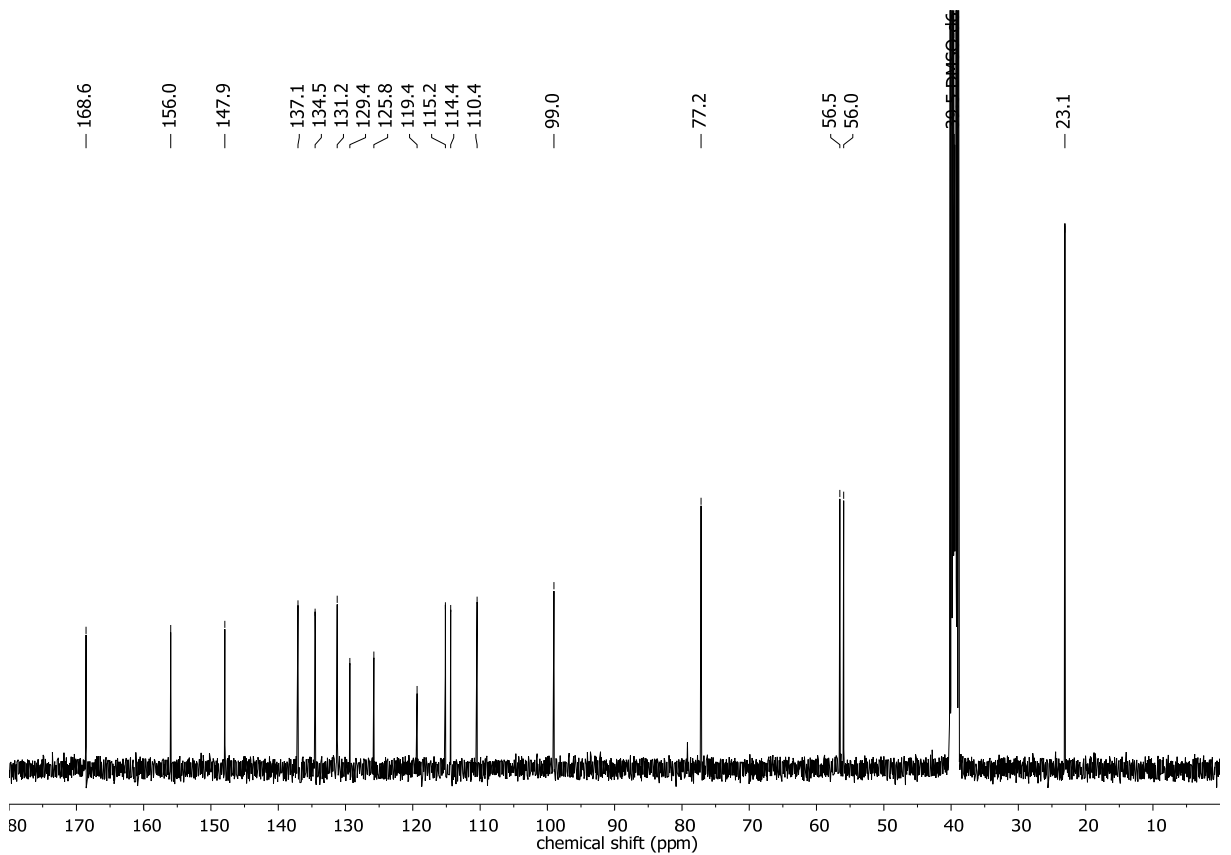
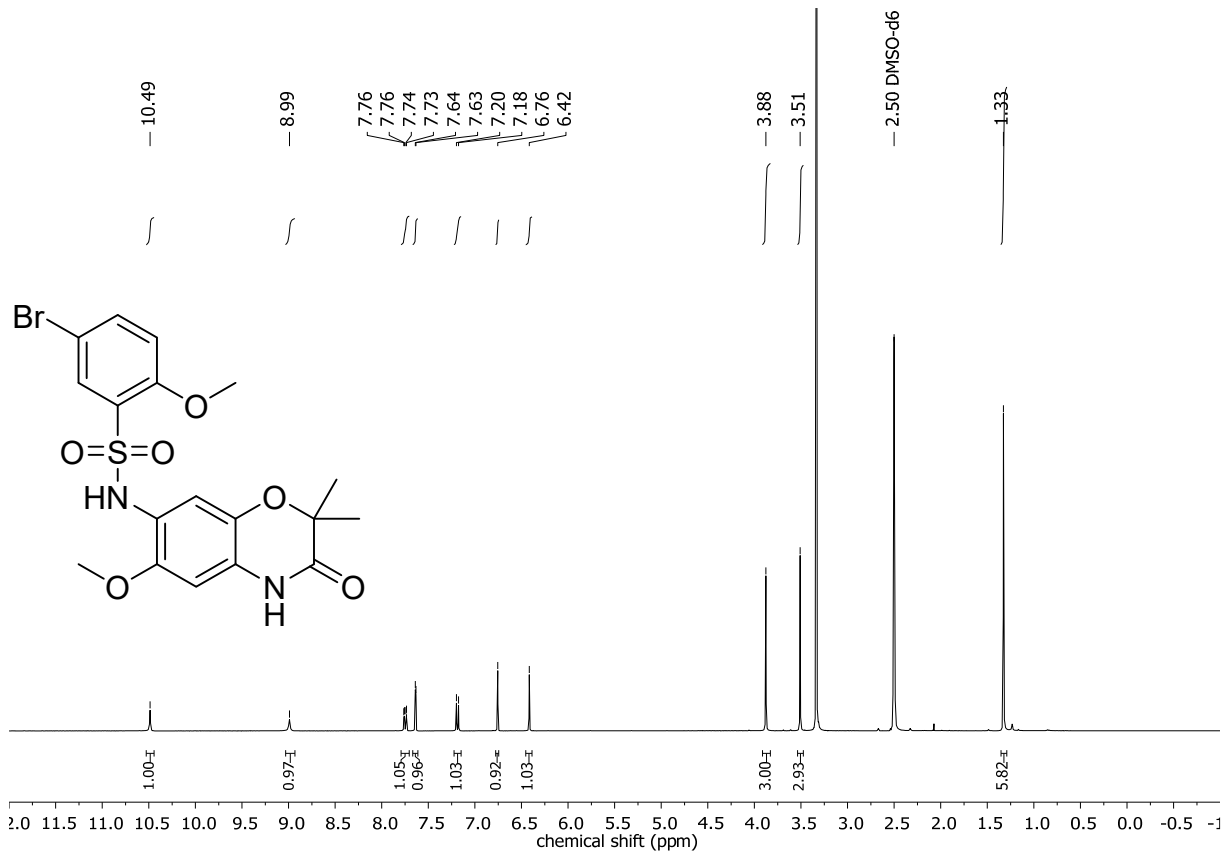


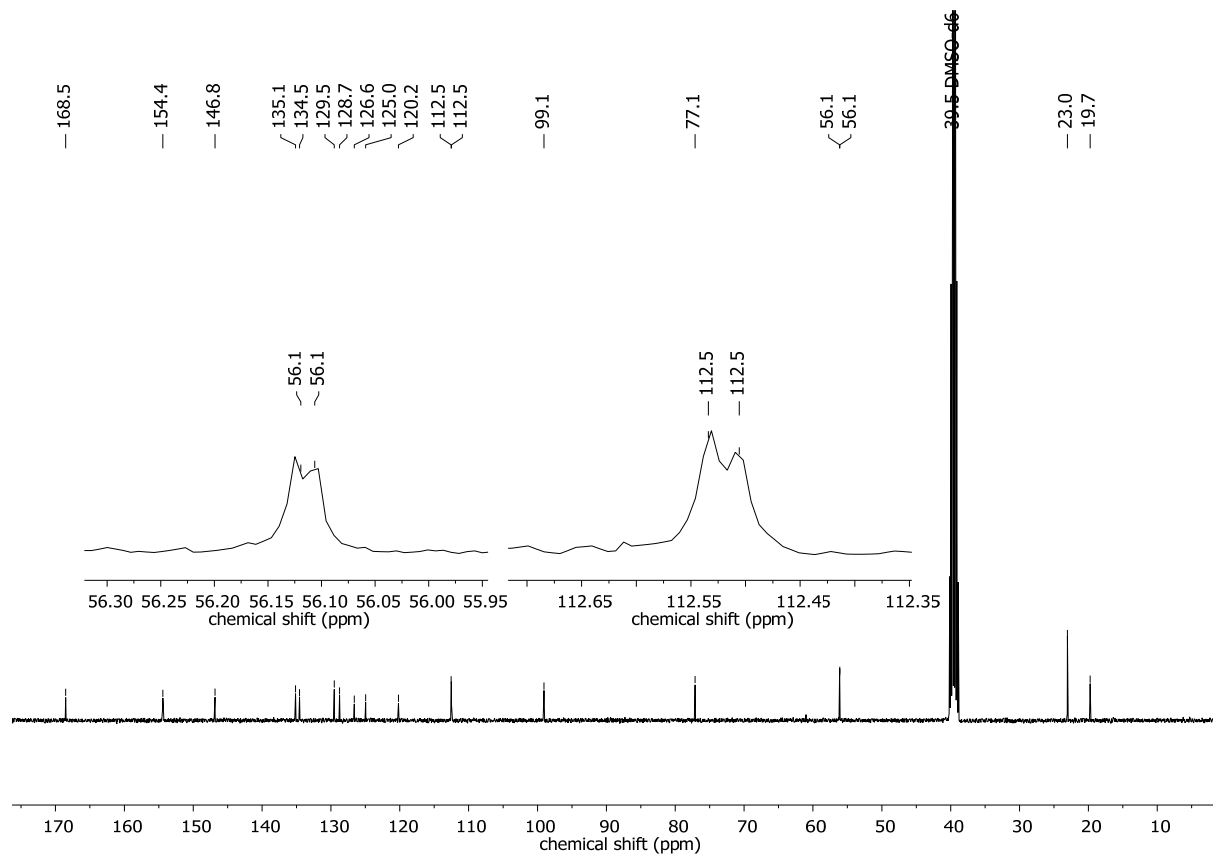
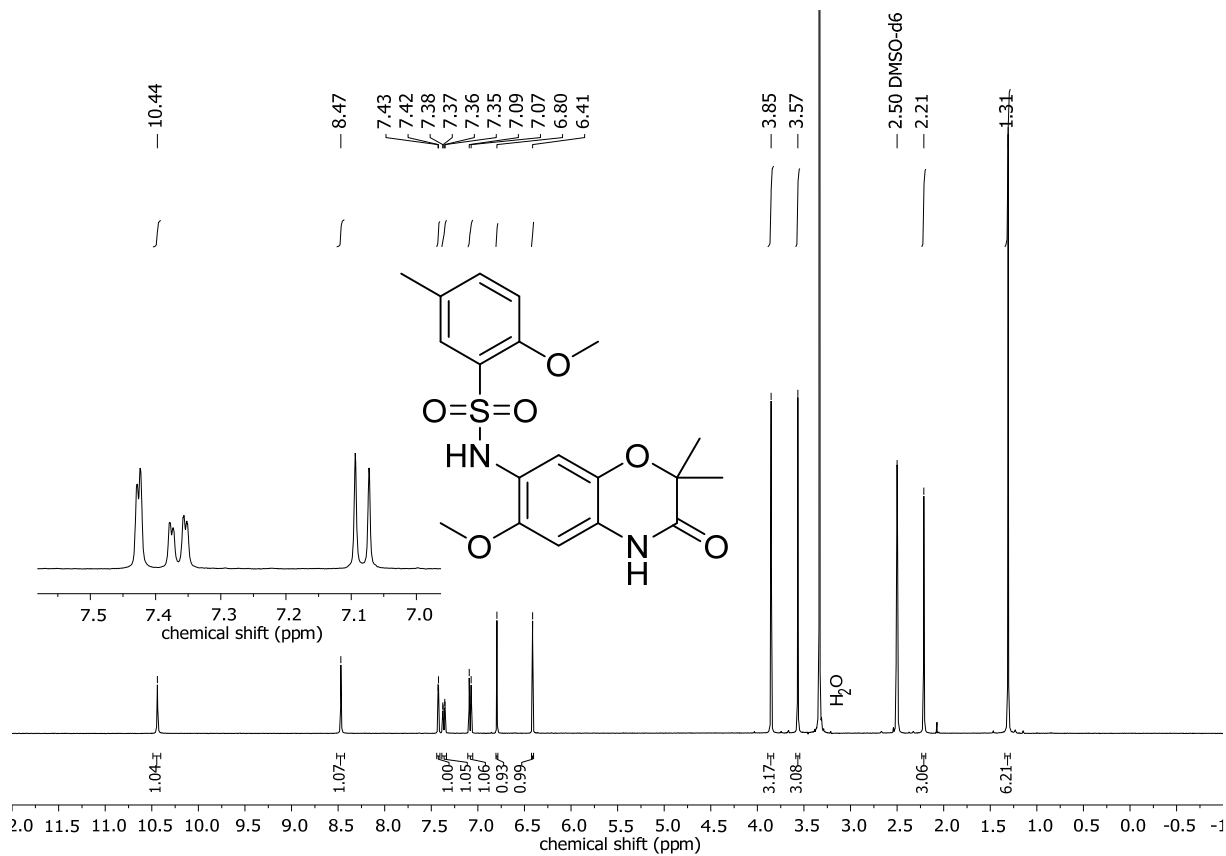












References

- [1] Sheldrick, G. M., SHELXS97 and SHELXL97: program of X-ray crystal structure refinement: Dept. of Structural Chemistry, University Göttingen, Germany, 1997.
- [2] N. Elgrishi, K. J. Rountree, B. D. McCarthy, E. S. Rountree, T. T. Eisenhart, J. L. Dempsey, *J. Chem. Educ.* **2017**, *95*, 197–206.
- [3] L. J. Wesenberg, S. Herold, A. Shimizu, J.-i. Yoshida, S. R. Waldvogel, *Chem. - Eur. J.* **2017**, *23*, 12096–12099.
- [4] G. L. Beutner, J. T. Kuethe, M. M. Kim, N. Yasuda, *Am. J. Org. Chem.* **2009**, *74*, 789–794.
- [5] a) M. K. M. Dirania, J. Hill, *J. Chem. Soc. C* **1969**, *0*, 2144–2147; b) C. D. Hurd, P. Perletz, *J. Am. Chem. Soc.* **1946**, *68*, 38–40.
- [6] C. Gütz, M. Bänziger, C. Bucher, T. R. Galvão, S. R. Waldvogel, *Org. Process Res. Dev.* **2015**, *19*, 1428–1433.
- [7] C. Gütz, B. Klöckner, S. R. Waldvogel, *Org. Process Res. Dev.* **2016**, *20*, 26–32.
- [8] R. J. W. Cremllyn, R. Hornby, *J. Chem. Soc. C* **1969**, 1341.
- [9] J. K. Laha, K. P. Jethava, N. Dayal, *Am. J. Org. Chem.* **2014**, *79*, 8010–8019.
- [10] P. Kumar, A. Nagarajan, P. D. Uchil, *Cold Spring Harbor protocols* **2018**, 2018.
- [11] S. Möhle, S. Herold, F. Richter, H. Nefzger, S. R. Waldvogel, *ChemElectroChem.* **2017**, *4*, 2196–2210.
- [12] T. Morofuji, A. Shimizu, J.-i. Yoshida, *J. Am. Chem. Soc.* **2013**, *135*, 5000–5003.
- [13] R. S. Assary, L. Zhang, J. Huang, L. A. Curtiss, *J. Phys. Chem. C* **2016**, *120*, 14531–14538.
- [14] S. T. Heller, R. Sarpong, *Org. Lett.* **2010**, *12*, 4572–4575.
- [15] D. W. Manley, A. Mills, C. O'Rourke, A. M. Z. Slawin, J. C. Walton, *Chem. - Eur. J.* **2014**, *20*, 5492–5500.
- [16] S. A. Lyakhov, E. A. Lyakhova, N. N. Panchenko, L. A. Litvinova, S. A. Andronati, *Pharm. Chem. J.* **2001**, *35*, 653–656.
- [17] J. C. Netto-Ferreira, I. G. J. Avellar, J. C. Scaiano, *Am. J. Org. Chem.* **1990**, *55*, 89–92.
- [18] K. J. Park, Y. Kim, M.-s. Lee, Y. S. Park, *Eur. J. Org. Chem.* **2014**, *2014*, 1645–1652.
- [19] C. Chatalova-Sazepin, M. Binayeva, M. Epifanov, W. Zhang, P. Foth, C. Amador, M. Jagdeo, B. R. Boswell, G. M. Sammis, *Org. Lett.* **2016**, *18*, 4570–4573.
- [20] Q. Xiang, Y. Zhang, J. Li, X. Xue, C. Wang, M. Song, C. Zhang, R. Wang, C. Li, C. Wu et al., *ACS Med. Chem. Lett.* **2018**, *9*, 262–267.
- [21] A. Sapegin, V. Panova, E. Reutskaya, A. V. Smirnov, M. Krasavin, *Tetrahedron* **2016**, *72*, 7570–7578.

- [22] A. B. Pinkerton, R. Dahl, N. D. P. Cosford, J. L. Millan, WO2013/126608 A1.
- [23] C. Guo, J. Qiu, X. Zhang, D. Verdugo, M. L. Larter, R. Christie, P. Kenney, P. J. Walsh, *Tetrahedron* **1997**, 53, 4145–4158.

Charged Tags for the Identification of Oxidative Drug Metabolites Based on Electrochemistry and Mass Spectrometry

Alexandra Gutmann,^[a] Lars Julian Wesenberg,^[a] Nadine Peez,^[a, b] Siegfried R. Waldvogel,^{*,[a]} and Thorsten Hoffmann^[a]

In memory of Prof. Dr. Jun-ichi Yoshida


Most of the active pharmaceutical ingredients like Metoprolol are oxidatively metabolized by liver enzymes, such as Cytochrome P450 monooxygenases into oxygenates and therefore hydrophilic products. It is of utmost importance to identify the metabolites and to gain knowledge on their toxic impacts. By using electrochemistry, it is possible to mimic enzymatic transformations and to identify metabolic hot spots. By introducing charged-tags into the intermediate, it is possible to detect and isolate metabolic products. The identification and synthesis of initially oxidized metabolites are important to understand possible toxic activities. The gained knowledge about the metabolism will simplify interpretation and predictions of metabolic pathways. The oxidized products were analyzed with high performance liquid chromatography-mass spectrometry using electrospray ionization (HPLC-ESI-MS) and nuclear magnetic resonance (NMR) spectroscopy. For proof-of-principle, we present a synthesis of one pyridinated main oxidation product of Metoprolol.


Most of the active pharmaceutical ingredients are oxidatively transformed by the liver into metabolites. In order to evaluate pharmacologic or even toxic effects, it is of high importance to know the metabolic products and to gain knowledge about their potential health impacts.^[1,2,3] Biotransformation reactions in the liver mainly lead to hydrolysis or oxidation (phase-1 drug metabolism) and biosynthetic reactions conjugating metabo-

lites with glutathione, sulfates, amino acids or acetates (phase-2 drug metabolism, leads to deactivated metabolites).^[3-5] Phase-1 metabolism is mainly performed (75%) by Cytochrom P450 monooxygenases.^[5,6] It is assumed that Cytochrom P450 monooxygenases use electrophilic oxoferryl-porphyrin-cation radicals to catalyze *N*-dealkylation, *O*-dealkylation, aromatic hydroxylation, oxidation of alcohols and aldehydes and Baeyer-Villiger oxidations.^[2,6-9] Application of electrochemistry in this field is intended to partly simulate the enzymatic oxidation of Cytochrome P450 to form metabolic products of the phase-1 metabolism.^[3,8] Besides the cost-benefit assessment, it is also of great interest for ethical reasons to find alternatives to in vivo experiments.^[5,10] Furthermore, electrochemical synthesis might enable quantitative synthesis of metabolites and reduction of critical waste due to the absence of any reducing and/or oxidizing reagents. Consequently, electrochemistry has already been employed in drug metabolism research.^[7,11] Direct hydroxylation of aromatic compounds leads to labile intermediates that are significantly more prone to further oxidation. Therefore, usually over-oxidized reaction products are formed. Using an electrochemical oxidation system with addition of nucleophilic compounds, which can trap the radical-cationic intermediates, it is possible to detect and isolate these metabolic products. The electrochemical C–H amination of aromatic compounds in the presence of pyridine has already been reported.^[12,13] Pyridine as tag molecule is suitable for the following reasons: the high oxidation potential of pyridine enables selective oxidation of aromatic compounds in the presence of pyridine, furthermore the nucleophilic nature and the excessive use of pyridine lead to a trapping mechanism of occurring radical cation being electrochemically generated. After a second oxidation step the *N*-arylpyridinium cation will be formed. Yoshida and co-workers postulated that any over-oxidation is suppressed because of strong electron-withdrawing effect of a positive charge on the pyridinium nitrogen and the electrostatic repulsion towards the positively polarized anode, avoiding introduction of multiple groups and subsequent degradation.^[12] Therefore, accumulation of the main oxidation product takes place and the most reactive positions in a molecule might reveal metabolic hot spots of a drug entity. When charged tags are incorporated into the target molecules not only the reactive sites of initial oxidation are marked, also the metabolite detection with mass spectrometry is facilitated. Subsequent

[a] A. Gutmann, L. J. Wesenberg, N. Peez, Prof. Dr. S. R. Waldvogel, Prof. Dr. T. Hoffmann
Department of Chemistry
Johannes Gutenberg University Mainz
Duesbergweg 10–14
55128 Mainz (Germany)
E-mail: waldvogel@uni-mainz.de

[b] N. Peez
Institute for Integrated Natural Sciences
University of Koblenz
Universitätsstraße 1
56072 Koblenz (Germany)

 Supporting information for this article is available on the WWW under <https://doi.org/10.1002/open.202000084>

 © 2020 The Authors. Published by Wiley-VCH Verlag GmbH & Co. KGaA. This is an open access article under the terms of the Creative Commons Attribution Non-Commercial License, which permits use, distribution and reproduction in any medium, provided the original work is properly cited and is not used for commercial purposes.

introduction of OH-groups enables synthesis of real drug metabolites.^[14,15]

Metoprolol was chosen as a test molecule for proof-of-principle. Metoprolol is a selective β_1 -receptor blocker and it is mainly used to treat high blood pressure and to prevent further heart problems after myocardial infarction. It is also used when conditions with chest pain occur due to poor blood supply to the heart and abnormally fast heart rate. Metoprolol metabolism has been investigated in many studies over decades.^[16] The electrochemical adaption seems to proceed by the initial one-electron oxidation of an aromatic compound **1** to produce the radical cation. Pyridine is present in abundantly amounts and leads to a subsequent nucleophilic attack on the radical cation species followed by one electron oxidation and elimination of a proton gives the arylpyridinium ion **2** (Scheme 1)

This work presents a reliable and cost-efficient method for synthesizing tagged and oxidized Metoprolol derivatives via electrochemistry and identification with high performance liquid chromatography-mass spectrometry using electrospray ionization (HPLC-ESI-MS) and nuclear magnetic resonance (NMR) spectroscopy. The work is focused on the identification of the main oxidation product and the optimization of the method with respect to yield the major product from oxidation.

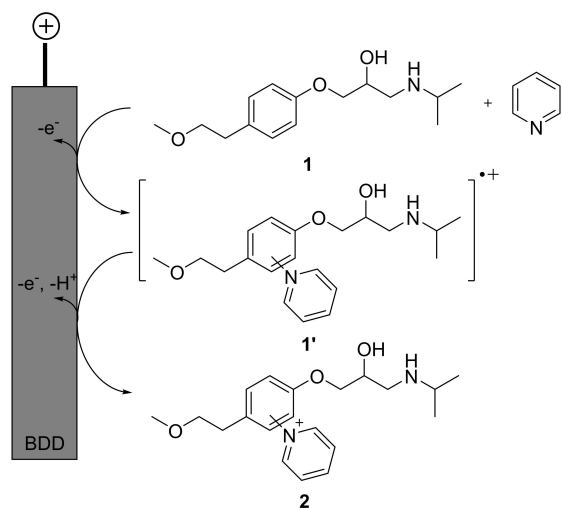
The galvanostatic electrolysis of Metoprolol was carried out in divided cells. Electrosynthesis in presence of pyridine favoured one main oxidation product **2** with a m/z ratio of 345 (positive mode). Structural clarification based on interpretation of MS^2 -, MS^3 - and 2-dimensional nuclear magnetic resonance

(NMR) data revealed following pyridinated charge tag **2** (Figure 1).

Structural isomers containing *N*-pyridinium tags at side chains are suppressed due to inaccessibility of $C(sp^3)$ -H moieties for anodic oxidation.^[17] However, especially at higher applied charge (5 F) beside the main oxidation products other pyridinated side oxidation products (**3**) were detected. Apart from single aromatic pyridination, aliphatic positions were oxidized and transformed into advanced degraded products. Especially, amine and alcohol functionalities are facilitated for these over-oxidation processes (for detailed structure analysis see Supporting Information, chapter 1.4). Beside pyridinium-tagged products, traces of non-pyridinated side oxidation products (**4**) were observed. MS^2 -experiments of these products show similarity with Metoprolol spectra.^[18] Oxidation products of this group contain a modified *O*-containing functional group instead of a pyridinium tag. This suggests that a competitive reaction mechanism occurs during electrolysis. The used boron-doped diamond (BDD)-electrode is thought to enable an 'indirect' electron transfer via OH radicals if water content is significant.^[19] Spectra and postulated structures are provided in the supplementary material (see Supporting Information, chapter 1.4).

Screening of electrochemical reaction conditions were carried out in divided Teflon cells with different separator materials e.g. glass frit or a proton exchange membrane like FAPQ® (for more details see Supporting Information, chapter 1.1). This screening technique is very time efficient and allows the variation of several parameters simultaneously, e.g. current density and applied charge (for more details see Supporting Information chapter 1.1).^[20] Platinum was used as the cathode material due to its low over-potential for the required hydrogen evolution ($\eta^{H_2} = -0.40$ V vs. Ag/AgCl).^[21-23] The BDD electrode was chosen due to the extraordinary properties of BDD as electrode material for electro-organic synthesis.^[24] BDD is well known for its high robustness in electrochemical reactions and large chemical window, caused by high over-potential for the evolution of molecular hydrogen and oxygen ($\eta^{H_2} = -1.10$ V vs. Ag/AgCl; $\eta^{O_2} = 2.30$ V vs. Ag/AgCl).^[21-23] Besides these beneficial electro-organic properties, BDD was already used to mimic enzymatic oxidation reactions.^[25]

The influence of supporting electrolytes such as lithium perchlorate ($LiClO_4$), ammonium acetate (NH_4OAc), and the absence of any supporting electrolyte has been investigated (applied charge 2.5 F, current density: 1 mA/cm², Metoprolol: 0.25 mmol, separation: glass frit). Results were normalized within this test sequence. An insufficient reproducibility was observed, when $LiClO_4$ was used as supporting electrolyte. This could be related to precipitation of the supporting electrolyte. Another disadvantage was the tedious workup procedure, regarding the removal of $LiClO_4$. Ammonium acetate (NH_4OAc) is vaporizable (decomposition at 90 °C). No workup procedure for the crude product after electrolysis is needed for measurements with ESI-MS-systems. Even though 4% water needed to be added to enhance solubility of ammonium acetate and increase conductivity. Applying $LiClO_4$ and NH_4OAc a similar relative conversion to main oxidation products **2** of $71 \pm 3\%$ and $71 \pm 5\%$ could be obtained, respectively. However, without



Scheme 1. Proposed mechanism of anodic oxidation of Metoprolol **1**.

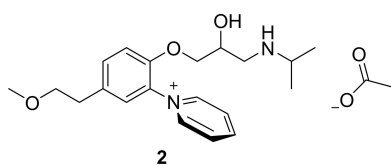


Figure 1. Main oxidation product of Metoprolol in presence of pyridine. For more information on the analytical data see Supporting Information.

supporting electrolytes the relative result of 65 ± 2 % main oxidation product is decreased. To ensure conductivity a water content of 4.5 % was applied in the anodic half-cell. Increased water contents in anodic half-cells led to an enhanced formation of OH radicals and therefore increased formation of non-pyridinated side oxidation products (4) (see table 1)

Subsequently, we investigated the efficiency of Metoprolol electrooxidation. Experimental data indicates that the conversion depends on the Metoprolol concentration containing 20.8 mmol/L (0.125 mmol Metoprolol), 41.7 mmol/L (0.250 mmol Metoprolol) and 62.5 mmol/L (0.375 mmol Metoprolol) (supporting electrolyte: NH_4OAc , current density: 1 mA/cm² with 2.5 F applied charge, separation: glass frit). Results were normalized within this test sequence. With decreased Metoprolol concentration (0.125 mmol) lowest Metoprolol conversion has been observed (see table 2). Best results of the formation of compound 2 were obtained with 0.250 mmol Metoprolol, while increased Metoprolol concentration (0.375 mmol Metoprolol) decreased relative yields of 2 from 87 % to 67 % respectively. Further increased formation of non-pyridinium-tagged oxidation products (4) was obtained. A Metoprolol concentration of 41.67 mmol/L (0.250 mmol) seems to be optimal for the formation of 2.

Next, the influence of the separator material was investigated. Due to their positive charge, pyridinium-tagged derivatives are prevented from further oxidation from the anode. However, oxidized positive charged intermediates or products are attracted by the cathode. Furthermore, the concentration gradient between anodic and cathodic compartments increases during electrolysis. Both effects lead to an

increasing trend of oxidation products diffusing towards the cathode. For preventing migration of oxidation products and starting material towards the cathodic compartment a divided cell set-up was used with separator membranes. Applied separation membranes require permeaselectivity towards exclusively protons while maintaining low electrical resistivity and prevent diffusion of analytes in the cathodic compartment. Here, porous glass frits and FAPQ® membranes have been compared for their permeaselectivity. Therefore, the analyte concentrations were determined in both half-cells after electrolysis. The values shown in figure 2 were calculated as fraction in the cathodic half-cell to the total sum found in both compartments. Experiments with glass frits as separator membrane have shown that (independently from supporting electrolytes used) 71.2 % of Metoprolol in particular was found in the cathodic compartment (impedes a full conversion, see figure 2A). The backwards diffusion of Metoprolol from the cathodic half-cell to the anodic half-cell seems to be too slow to equilibrate Metoprolol conversion by oxidation. Separation with glass frit also resulted in 20 % of main oxidation product 2 in the cathodic half cell (decreasing obtained yields). An applied FAPQ®-membrane was able to prevent diffusion in the cathodic compartment almost quantitatively for compound 2 and decreased the diffusion of Metoprolol to 4.5 %.

FAPQ® is a proton permeable exchange membrane, (for further details see chapter 1.1). The current density is related to the radical spin density close to the electrode surface. Controlled radical formation is desired, hence lower current densities might be beneficial. Higher current densities tend to lead to uncontrolled reaction pathways, which is certainly undesired with fragile substrates. The influence of the current density on oxidation products formation was investigated for 1 and 10 mA/cm² (supporting electrolyte: NH_4OAc or none, amount of charge: 2.5 F, Metoprolol: 0.25 mmol, separator: glass frit). Increased current density caused a decreased conversion of Metoprolol and the formation

Table 1. Relative conversion dependent on supporting electrolyte and water content (note: Relative yields are based on the highest result in the experiment series (in this case the sum of compounds (3) with LiClO_4 as supporting electrolyte)).

Supporting electrolyte	Water content	[U _{iv}]=V	2 ^[a]	3 ^[b]	4 ^[c]
LiClO_4 *	0.0 %	2.5	77 ± 3%	100 ± 2%	1 ± 0%
NH_4OAc	4.0 %	2.9	76 ± 5%	99 ± 1%	4 ± 1%
None	4.5 %	3.6	70 ± 2%	93 ± 2%	6 ± 1%

*not further pursued, due to lack of reproducibility, [a] 2 = main oxidation product, [b] 3 = pyridinated side oxidation products, [c] 4 = non-pyridinated side oxidation products; U_{iv} = terminal voltage; for electrolysis conditions see text.

Table 2. Influence of provided Metoprolol on product formation (note: Relative yields are based on the highest result in the experiment series (in this case the sum of compounds (3) with 0.250 mmol as supporting electrolyte)).

Metoprolol molarity	Metoprolol recovery	[U _{iv}]=V	2 ^[a]	3 ^[b]	4 ^[c]
0.125 mmol	53 %	2.4	45 %	56 %	2 %
0.250 mmol	6 %	2.4	87 %	100 %	5 %
0.375 mmol	8 %	2.5	67 %	80 %	10 %

[a] 2 = main oxidation product, [b] 3 = pyridinated side oxidation products, [c] 4 = non-pyridinated side oxidation products; U_{iv} = terminal voltage; for electrolysis conditions see text.

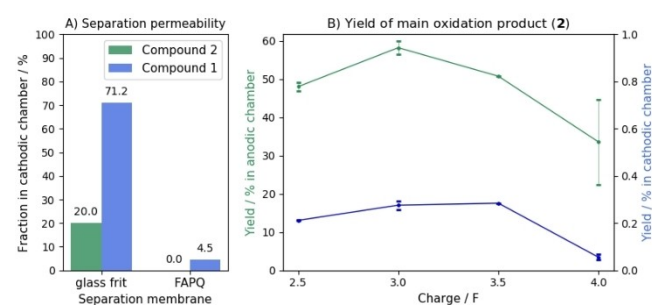


Figure 2. (A): Efficiency of half-cell separation using different membranes. Values were calculated as fraction in cathodic compartment to the total sum found in both half-cells. Separation with glass frit resulted in 20 % of 2 (green) or even above 70 % for Metoprolol (blue). An applied FAPQ membrane was able to prevent diffusion in cathodic compartment almost quantitatively for main oxidation product 2 and decreased diffusion to 4.5 % for Metoprolol. (B): Obtained yield of 2 dependent on applied charge. A maximal formation of compound 2 of 58 ± 2 % was obtained at 3.0 F. The observation of cathodic half-cell concentrations for main oxidation product 2 confirmed that diffusion into the cathodic compartment does not increase with increased applied charge (also resulting in increased reaction time). For error calculation every charge has been applied twice.

of the main oxidation product decreased by 20% (with NH_4OAc as supporting electrolyte) or even 50% (without any supporting electrolyte) respectively. The theoretical amount of charge of Metoprolol is 2 F. The increase of applied charge from 2.5 F stepwise to 5.0 F resulted in depletion of Metoprolol with 3.5 F (see Figure 3, red values). However, increased Metoprolol conversion does not lead to increased formation of the main oxidation product (2, green values). Increased applied charges form pyridinated side oxidation products (3, dark blue) might result from further oxidation of 2. Non-pyridinated side oxidation products (4, light blue) seem not to be heavily affected by increased applied charges (Electrolysis conditions: Charge: 2.5–5 F, stepwise, supporting electrolyte: NH_4OAc , current density: 1 mA/cm^2 , 0.25 mmol Metoprolol, membrane: FAPQ®).

This study enabled synthesis of pyridinium-tagged Metoprolol derivatives and revealed an active side at the *ortho*-position of the phenoxy ether of Metoprolol, while avoiding multi oxidation reactions (one main oxidation product). A maximal formation of main oxidation product 2 via electrolysis of $58 \pm 2\%$ was obtained with supporting electrolyte NH_4OAc , 0.25 mmol Metoprolol content, half-cell separation with FAPQ®-membrane, applied current density of 1 mA/cm^2 and applied charge of 3.0 F. Traces of pyridinium tagged (3) and non-

pyridinium tagged side oxidation products (4) have been minimized. Therefore, oxidized products bearing a pyridinium moiety can be enriched during electrolysis and isolated for metabolite synthesis. Transition metal catalysis of pyridinium substituted groups on specifically selected oxygen nucleophiles might lead to an effective synthesis of metabolic products (Scheme 2). Recently, studies on this field are emerging, focusing on pyridinium salts as redox-active functional group transfer reagents.^[14] Hence, this method might be able to provide a new reliable pathway for the synthesis of metabolites and supports further research into drug metabolism since direct hydroxylation reactions would lead to an over-oxidation caused by lower oxidation potential of the new electron-rich aromatic system. Consequently, further reactions occur, and the original metabolites would be only found in low yields.

Acknowledgements

Support of the Advanced Lab of Electrochemistry and Electrosynthesis – ELYSION (Carl Zeiss Stiftung) is gratefully acknowledged.

Conflict of Interest

The authors declare no conflict of interest.

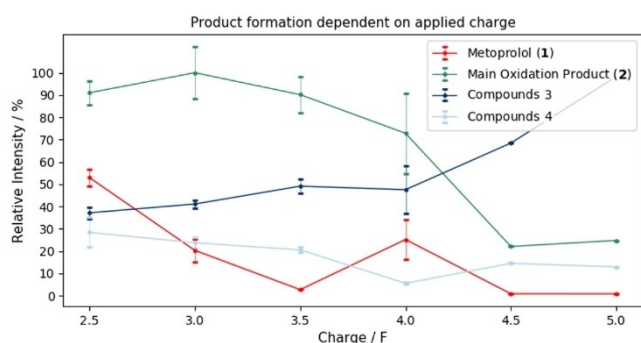
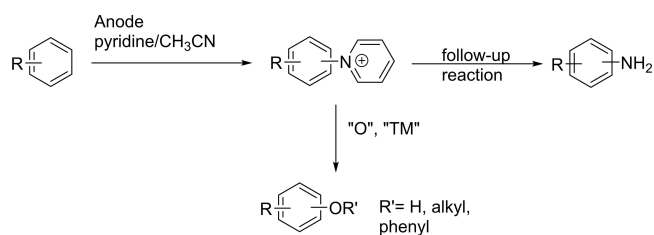


Figure 3. Metoprolol conversion and formation of side products dependent on applied charge. Red data reveal increased conversion of Metoprolol with elevated amount of charge. Increased Metoprolol conversion does not lead to increased formation of the main oxidation product (2, green values). Non-pyridinated side oxidation products (4, light blue) seem to decrease slightly by elevated amount of charges. Increased applied charges form pyridine tagged side oxidation products (3, dark blue) which might result from further oxidation of 2 or derivatization of (4) with pyridine. For error calculation every charge has been applied three times, except 4.5 and 5.0 F, which have been tested only once. For further experimental descriptions see text.



Scheme 2. Anodic oxidation of arenes in presence of pyridine and conversion to metabolites; TM = transition metal

Keywords: anodic oxidation · charged tags · drug metabolites · electrochemistry · mass spectrometry

- [1] a) J. Genovino, D. Sames, L. G. Hamann, B. B. Touré, *Angew. Chem. Int. Ed.* **2016**, *55*, 14218–14238; *Angew. Chem.* **2016**, *128*, 14430–1445; b) S. D. Krämer, B. Testa, *Chem. Biodiversity* **2009**, *6*, 1477–660; c) A. F. Stepan, D. P. Walker, J. Bauman, D. A. Price, T. A. Baillie, A. S. Kalgutkar, M. D. Aleo, *Chem. Res. Toxicol.* **2011**, *24*, 1345–1410; d) B. Testa, S. D. Krämer, *Chem. Biodiversity* **2006**, *3*, 1053–1101.
- [2] T. Johansson, L. Weidolf, U. Jurva, *Rapid Commun. Mass Spectrom.* **2007**, *21*, 2323–2331.
- [3] K. G. Madsen, J. Olsen, C. Skonberg, S. H. Hansen, U. Jurva, *Chem. Res. Toxicol.* **2007**, *20*, 821–831.
- [4] S. Sozzani, D. Bosisio, A. Mantovani, P. Ghezzi, *Eur. J. Immunol.* **2005**, *35*, 3095–3098.
- [5] K. Schroer, M. Kittelmann, S. Lütz, *Biotechnol. Bioeng.* **2010**, *106*, 699–706.
- [6] R. Bernhardt, *J. Biotechnol.* **2006**, *124*, 128–145.
- [7] U. Jurva, H. V. Wikstrom, L. Weidolf, A. P. Bruins, *Rapid Commun. Mass Spectrom.* **2003**, *17*, 800–810.
- [8] F. P. Guengerich, *AAPS J.* **2006**, *8*, E101–11.
- [9] A. Chefson, K. Auclair, *Mol. Biosyst.* **2006**, *2*, 462–469.
- [10] a) H. U. Schulze, H. Staudinger, *Die Naturwissenschaften* **1975**, *62*, 331–340; b) H. Zhang, D. Zhang, W. Li, M. Yao, C. D'Arienzo, Y.-X. Li, W. R. Ewing, Z. Gu, Y. Zhu, N. Murugesan, W.-C. Shyu, W. G. Humphreys, *Drug Metab. Dispos.* **2007**, *35*, 795–805; c) J. Kiebish, W. Holla, J. Heidrich, M. Poraj-Kobielska, M. Sandvoss, R. Simonis, G. Gröbe, J. Atzrodt, M. Hofrichter, K. Scheibner, *Bioorg. Med. Chem.* **2015**, *23*, 4324–4332.
- [11] a) M. K. Eberle, A.-M. Jutzi-Eme, F. Nüniger, *Bioorg. Med. Chem. Lett.* **1995**, *5*, 1725–1728; b) L. R. Hall, R. T. Iwamoto, R. P. Hanzlik, *Am. J. Org. Chem.* **1989**, *54*, 2446–2451; c) S. Khera, N. Hu, *Anal. Bioanal. Chem.* **2013**, *405*, 6009–6018; d) W. Lohmann, R. Dötzer, G. Gütter, S. M. van Leeuwen, U. Karst, *J. Am. Soc. Mass Spectrom.* **2009**, *20*, 138–145; e) R. Stalder, G. P. Roth, *ACS Med. Chem. Lett.* **2013**, *4*, 1119–1123; f) K. Pelivan, L. Frensemeier, U. Karst, G. Koellensperger, B. Bielec, S. Hager, P. Heffeter, B. K. Keppler, C. R. Kowol, *Analyst* **2017**, *142*, 3165–3176; g) T. Wigger, A. Seidel, U. Karst, *Chemosphere* **2017**, *176*, 202–211; h) A. Paci,

- T. Martens, J. Royer, *Bioorg. Med. Chem. Lett.* **2001**, *11*, 1347–1349; i) K. G. Madsen, G. Grönberg, C. Skonberg, U. Jurva, S. H. Hansen, J. Olsen, *Chem. Res. Toxicol.* **2008**, *21*, 2035–2041; j) M. K. Bal, C. E. Banks, A. M. Jones, *ChemElectroChem*. **2019**, *6*, 4284–4291; k) M. H. Rahman, M. K. Bal, A. M. Jones, *ChemElectroChem*. **2019**, *6*, 4093–4104.
- [12] T. Morofuji, A. Shimizu, J.-i. Yoshida, *J. Am. Chem. Soc.* **2013**, *135*, 5000–5003.
- [13] a) S. R. Waldvogel, S. Möhle, *Angew. Chem. Int. Ed.* **2015**, *54*, 6398–6399; *Angew. Chem.* **2015**, *127*, 6496–6497; b) L. J. Wesenberg, S. Herold, A. Shimizu, J. -i Yoshida, S. R. Waldvogel, *Chem. Eur. J.* **2017**, *23*, 12096–12099.
- [14] A. Togni, S. L. Rössler, B. J. Jelier, E. Magnier, G. Dagousset, E. M. Carreira, *Angew. Chem. Int. Ed.* **2019**; *Angew. Chem.* **2019**; in press. [Doi.org/10.1002/anie.201911660].
- [15] D. Moser, Y. Duan, F. Wang, Y. Ma, M. J. O'Neill, J. Cornella, *Angew. Chem. Int. Ed.* **2018**, *57*, 11035–11039; *Angew. Chem.* **2018**, *130*, 11201–11205.
- [16] a) J. C. McGourty, J. H. Silas, M. S. Lennard, G. T. Tucker, H. F. Woods, *Br. J. Clin. Pharmacol.* **1985**, *20*, 555–566; b) S. S. Murthy, H. U. Shetty, W. L. Nelson, P. R. Jackson, M. S. Lennard, *Biochem. Pharmacol.* **1990**, *40*, 1637–1644; c) N. Bodor, P. Buchwald, *AAPS J.* **2005**, *7*, E820–33; d) V. K. H. Barclay, N. L. Tyrefors, I. M. Johansson, C. E. Pettersson, *J. Chromatogr. A* **2012**, *1269*, 208–217; e) T. Xu, S. Bao, P. Geng, J. Luo, L. Yu, P. Pan, Y. Chen, G. Hu, *J. Chromatogr. B* **2013**, *937*, 60–66.
- [17] Q.-L. Yang, Y.-Q. Li, C. Ma, P. Fang, X.-J. Zhang, T.-S. Mei, *J. Am. Chem. Soc.* **2017**, *139*, 3293–3298.
- [18] M. D. Hernando, M. J. Gómez, A. Agüera, A. R. Fernández-Alba, *TrAC Trends Anal. Chem.* **2007**, *26*, 581–594.
- [19] a) M. Panizza, P. A. Michaud, G. Cerisola, C. Comninellis, *J. Electroanal. Chem.* **2001**, *507*, 206–214; b) A. Kirste, G. Schnakenburg, F. Stecker, A. Fischer, S. R. Waldvogel, *Angew. Chem. Int. Ed.* **2010**, *49*, 971–975; *Angew. Chem.* **2010**, *122*, 983–987; c) B. Marselli, J. Garcia-Gomez, P.-A. Michaud, M. A. Rodrigo, C. Comninellis, *J. Electroanal. Chem. Interfacial Electrochem.* **2003**, *150*, D79; d) A. Stefanova, S. Ayata, A. Erem, S. Ernst, H. Baltruschat, *Electrochim. Acta* **2013**, *110*, 560–569.
- [20] C. Gütz, B. Klöckner, S. R. Waldvogel, *Org. Process Res. Dev.* **2016**, *20*, 26–32.
- [21] S. R. Waldvogel, S. Mentizi, A. Kirste, *Top. Curr. Chem.* **2012**, *320*, 1–31.
- [22] S. R. Waldvogel, B. Elsler, *Electrochim. Acta* **2012**, *82*, 434–443.
- [23] S. Lips, S. R. Waldvogel, *ChemElectroChem*. **2019**, *6*, 1649–1660.
- [24] a) J. L. Röckl, D. Pollok, R. Franke, S. R. Waldvogel, *Acc. Chem. Res.* **2020**, *53*, 45–61; b) S. Möhle, M. Zirbes, E. Rodrigo, T. Gieshoff, A. Wiebe, S. R. Waldvogel, *Angew. Chem. Int. Ed.* **2018**, *57*, 6018–6041; *Angew. Chem.* **2018**, *130*, 6124–6149; c) B. Gleede, T. Yamamoto, K. Nakahara, A. Botz, T. Graßl, R. Neuber, T. Matthée, Y. Einaga, W. Schuhmann, S. R. Waldvogel, *ChemElectroChem*. **2019**, *6*, 2771–2776; d) A. Wiebe, T. Gieshoff, S. Möhle, E. Rodrigo, M. Zirbes, S. R. Waldvogel, *Angew. Chem. Int. Ed.* **2018**, *57*, 5594–5619; *Angew. Chem.* **2018**, *130*, 5694–5721.
- [25] a) H. Faber, D. Melles, C. Brauckmann, C. A. Wehe, K. Wentker, U. Karst, *Anal. Bioanal. Chem.* **2012**, *403*, 345–354; b) P. Mielczarek, M. Smoluch, J. H. Kotlinska, K. Labuz, T. Gotszalk, M. Babij, P. Suder, J. Silberring, *J. Chromatogr. A* **2015**, *1389*, 96–103.

Manuscript received: March 27, 2020

ChemistryOpen

Supporting Information

Charged Tags for the Identification of Oxidative Drug Metabolites Based on Electrochemistry and Mass Spectrometry

Alexandra Gutmann, Lars Julian Wesenberg, Nadine Peez, Siegfried R. Waldvogel,* and Thorsten Hoffmann © 2020 The Authors. Published by Wiley-VCH Verlag GmbH & Co. KGaA. This is an open access article under the terms of the Creative Commons Attribution Non-Commercial License, which permits use, distribution and reproduction in any medium, provided the original work is properly cited and is not used for commercial purposes.

Table of Content

1. Supporting Information	2
1.1. Electrolysis setup	2
1.2. Preparative purification chromatography	2
1.3. Analytics	2
1.3.1 Solid phase extraction	2
1.3.2 Liquid Chromatography-mass spectrometry.....	3
1.3.3 Nuclear magnetic resonance	4
1.4. Chromatograms and MS-Spectra	5
1.4.1 Metoprolol	6
1.4.2 Main oxidation product 2	7
1.4.3 Pyridinium tagged side oxidation products 3	8
1.4.4 Non-pyridinated side oxidation products 4	12
1.5. NMR Spectra.....	14
2. References	16

1. Supporting Information

1.1. Electrolysis setup

In this study, applications of screening-electrolysis half cells of PTFE (Polytetrafluorethylen, Teflon) were used for the oxidation of Metoprolol.^[1] Electrolysis half cells were separated with a porous glass frit (10–16 µm, ROBU® Glasfilter-Geräte GmbH, Hattert, Deutschland) or FAPQ®-membrane (75 µm, FUMATECH BWT GmbH, Bietigheim-Bissingen, Deutschland). The membrane diameter was 14 mm. The anode was a boron-doped diamond electrode BDD (70x10x3 mm) while the cathode was made of platinum sheet (70x10 mm). Each half cell was filled with 6 mL solvent. The electrochemical oxidation of Metoprolol was carried out in a solution of two different supporting electrolytes (lithium perchlorate and ammonium acetate) and experiments without supporting electrolytes. Therefore, the anodic compartment was filled with 5 mL acetonitrile (water content 0% (LiClO₄), 4% (NH₄OAc) or 4.55% (using no supporting electrolyte)), 1 mL pyridine, 0.25 mmol supporting electrolyte (if used), and 0.25 mmol Metoprolol. The cathodic compartment was filled with 6 mL acetonitrile (water content 0% (LiClO₄), 4% (NH₄OAc) or 4.55% using no supporting electrolyte), 0.3 mmol supporting electrolyte, and 0.4 mL trifluoromethanesulfonic acid. The electrolysis was performed under constant current conditions with current densities of 1 or 10 mA/cm² with an amount of charge of 2.5-5.0 F (0.5 steps).

1.2. Preparative purification chromatography

Pre-cleaning of electrolysis products has been carried out at a preparative chromatography system (Büchi-Labortechnik GmbH, Essen, Germany) with puriFlash® C18AQ columns (pore size: 200 Å, particle size: 15 µm, length 78 mm /inner diameter: 21 mm) or length 193 mm (inner diameter: 31 mm). Mixtures of water with 0.1% formic acid (solvent A) and acetonitrile (solvent B) were used as eluents (flow rate: 20 mL/min, detection at λ = 254 nm). Method: 0-15 min (holding isocratic A:B = 95:5), 15-25 min (gradient up to A:B = 90:10), 25-55 min (gradient up to A:B = 70:30), 55-70 min (holding isocratic A:B = 0:100).

Purification occurred on an Azura preparative HPLC (KNAUER Wissenschaftliche Geräte GmbH, Berlin, Germany) using an eurospher II column (pore size: 100 Å, particle size: 5 µm, length: 250 mm, inner diameter: 30 mm, flow rate: 10 mL/min, detection at λ = 254 nm). Mixtures of water with 0.1% formic acid (solvent A) and acetonitrile (solvent B) were used as eluents. Method: 0-30 min (holding isocratic A:B = 97:3), 30-60 min (gradient up to A:B = 92:8), 60-80 min (gradient up to A:B = 80:20), 80-110 min (holding isocratic A:B = 80:20).

1.3. Analytics

Derivatized analytes were analyzed with high-pressure liquid chromatography-mass spectrometry using an electrospray ionization. If necessary, samples have been preconcentrated via solid phase extraction (SPE). External calibration was used for quantification.

1.3.1 Solid phase extraction

The supporting electrolyte lithium perchlorate (LiClO₄) is a non-volatile salt. Since we used an ESI-MS system for analysis removal of the supporting electrolyte in samples became mandatory. Nevertheless,

since LiClO_4 is a widely used supporting electrolyte its influence has been proven in the current experiments as well. Therefore, a work up procedure based on solid phase extraction to remove supporting electrolytes and for pre-concentration has been developed.

Applied pre-concentration procedures of Vieno et al.^[2] has been optimized as follows: Oasis HLB SPE cartridges (3cc, 60 mg, Waters) were conditioned with 1 mL Methanol and 1 mL ultrapure water (pH 10, adjusted with NaOH). The dried sample was solved in 1 mL ultrapure water (pH 10, adjusted with NaOH) and loaded onto the cartridges. The cartridges were washed once with 1 mL of a 5 % methanol solution generated from a 2 % aqueous NH_4OH solution and dried for 15 min by using a vacuum manifold. Analytes were eluted with four portions of 0.5 mL methanol. The solvent was evaporated to dryness under a gentle nitrogen stream at 35 °C.

Recovery and reproducibility of the solid phase extraction have been analyzed by using ammonium acetate (NH_4OAc , volatile with ESI conditions) as supporting electrolyte (1 mA/cm², 2.5 F, glass frit). Divided electrolysis samples enabled comparison of pretreated and non-treated samples. A recovery of $106 \pm 4 \%$ for the main oxidation product and $93 \pm 3 \%$ for Metoprolol have been observed.

1.3.2 Liquid Chromatography-mass spectrometry

High-pressure liquid chromatography coupled to electrospray ionization tandem mass spectrometry (HPLC-ESI-MS/MS) was performed on an Agilent 1100 series (Agilent Technologies, Germany) coupled to a HCT-Plus ion trap mass spectrometer (Bruker-Daltonics, Germany).

The HPLC parameters were optimized for baseline separation in extracted ion chromatograms and short retention times of oxidation products. Separation was tested using C18, C8, and phenylhexyl columns and solvent gradients of acetonitrile/water and methanol/water mixtures respectively. The best results based on peak shape and retention time were observed using an Atlantis T3 C18 2.1x150 mm, 3 μm particle size (Waters, Germany) heated to 35 °C during analysis. A gradient of eluent A (ultrapure water including 400 μL formic acid) to eluent B (methanol) was used, starting with 5 % eluent B that was held for 3 min. Then eluent B was raised up to 41 % within 3 min, raised further to 90 % within 2 min and up to 99 % eluent B within the next 5 min. 99 % eluent B was held for 7 min before decreasing back to 5 % eluent B and equilibration for 30 min. The flow rate was constant at 200 $\mu\text{L}/\text{min}$ and an autosampler performed 2 μL injection volume.

The use of electrospray ionization (ESI) to create ions from analytes with distinct ionization potentials may lead to decreased ionization of analytes with low potentials and therefore decreased signal intensities (so called ion suppression).^[3] The positive charge of the pyridinium-tag prevents this effect since analytes are already ionized. Therefore, the ionization efficiency of analytes during electrospray-ionization for pyridinium-tagged analytes is assumed to be equal. Because of the positive charged pyridinium tag the electrospray ionization source was used in the positive mode. The capillary voltage was +3.5 kV, 300 °C dry gas temperature, 10 L/min dry gas flow (N_2), and 35 psi nebulizer pressure. The mass spectrometer was operated in ultra-scan mode. MS^n -experiments were performed using the multi reaction monitoring (MRM) mode. Given molecules were isolated and fragmented in the ion trap using collisional induced dissociation (CID). Helium was used as collision gas.

1.3.3 Nuclear magnetic resonance

^1H NMR, ^{13}C NMR, 2D-NMR spectra were recorded at 25 °C on a Bruker Avance II 400 or Avance III HD 300 instrument (*Bruker*, Analytische Messtechnik, Karlsruhe, Germany). Chemical shifts (δ) are reported in parts per million (ppm). Traces of non-deuterated solvents were used as internal standard for calibration. Identification of substitution pattern of charged tagged metoprolol **2** were realized by 2D-NOESY NMR experiment. With this technique dipole-dipole coupling processes of protons can be observed (for more details see chapter 1.5).

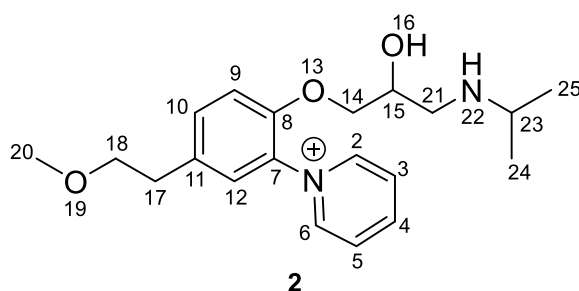


Figure S1: NMR-analytic of the main oxidation product in ortho position to the phenoxy ether

^1H NMR (400 MHz, acetonitrile- d_3) δ = 1.23 (t, J = 6.4, 6H, H-25, H-24), 2.75 – 2.82 (m, 1H, H-21''), 2.89 (t, J = 6.4, 3H, H-17), 2.94 – 3.02 (m, 1H, H-21'), 3.28 (s, 3H, H-20), 3.32 (hept, J = 6.5, 1H, H-23), 3.61 (t, J = 6.4, 3H, H-18), 4.10 (m, 3H, H-14, H-15), 7.25 (d, J = 8.6, 1H, H-9), 7.46 (d, J = 2.1, 1H, H-12), 7.54 (dd, J = 8.6, 2.2, 1H, H-10), 8.15 – 8.23 (m, 2H, H-3), 8.64 – 8.73 (m, 1H, H-4), 8.76 – 8.86 (m, 2H, H-2).

^{13}C NMR (101 MHz, acetonitrile- d_3) δ = 17.2 (s, C-25), 17.5 (s, C-24), 33.5 (s, C-17), 46.3 (s, C-21), 50.6 (s, C-23), 56.8 (s, C-20), 64.2 (s, C-15), 69.8 (s, C-14), 71.5 (s, C-18), 113.3 (s, C-9), 125.9 (s, C-12), 127.2 (s, C-3, C-5), 130.2 (s, C-7), 132.6 (s, C-10), 133.2 (s, C-11), 145.4 (s, C-2, C-6), 146.2 (s, C-4), 148.3 (s, C-8).

1.4. Chromatograms and MS-Spectra

For reaction monitoring and structure analysis an HPLC-ESI-MS system was used (for further description and applied chromatography method see main article). Figure S1 shows chromatogram (total ion current) of optimized electrolysis. MS²- and MS³-experiments revealed substructures that support prediction of suggested structures. Table S1 gives an overview on all found products and Figure S2 shows details on formation of tracked side oxidation products.

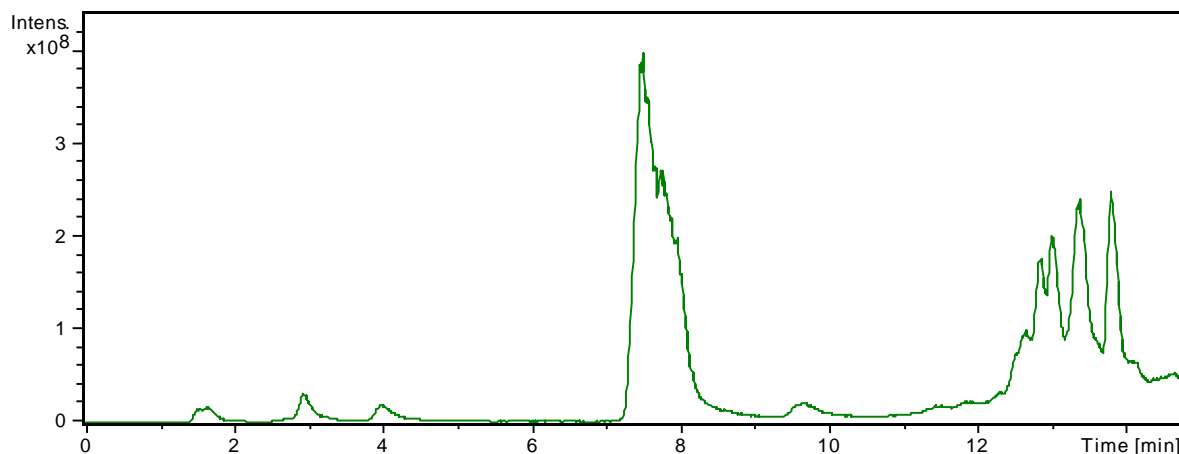
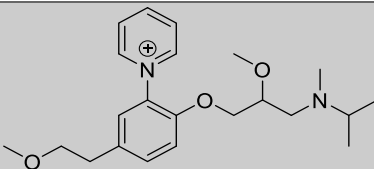
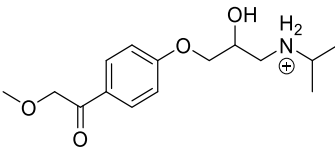
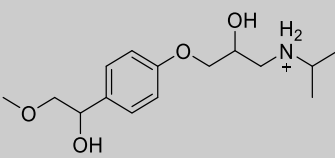


Figure S2: Chromatogram (total ion current) of electrolysis (supporting electrolyte: NH_4OAc , current density: 1 mA/cm^2 , 0.25 mmol Metoprolol, Charge: 3 F , membrane: FAPQ®)

Table S1: overview of tracked compounds

Compound	Suggested structure	Retention time [min]	Considered m/z ratios
Metoprolol		13.8	268
Main oxidation product (MOP, 2)		7.6	345, 303, 230
Pyridinium tagged side oxidation products (PSOP, 3)		1.6	422, 343, 307, 228
		2.9	361, 319, 246

	Isomer of 2	4.0	345, 303, 230
	Isomer of 2	9.6	345, 303, 230
	Isomer of 2	11.4	345, 303, 230
	Isomer of 2	12.6	345, 303, 230
		13.2	373
Non-pyridinated side oxidation products (NSOP, 4)		13.0	282
	Isomer of α -hydroxy-metoprolol	12.8	284
		13.5	284

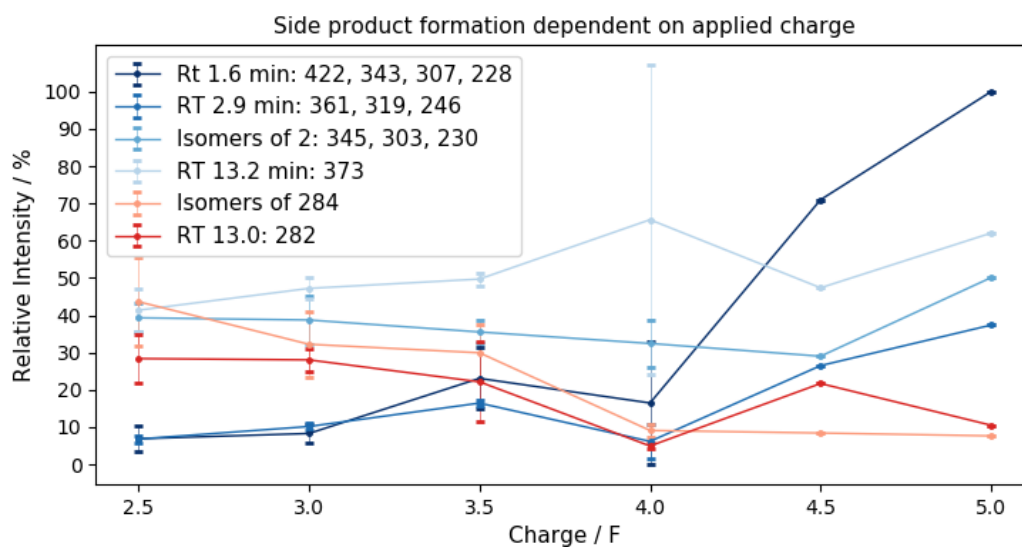


Figure S3: formation of side oxidation product dependent on applied charge. Pyridinated side oxidation products (3) in blue show a general increase with increased charge while non pyridinated side oxidation products (4) in red show a slight decrease. For compound details compare Table S1.

1.4.1 Metoprolol

Observed MS spectra and suggested structures have been compared and are consistent with former structure analysis.)^[4]

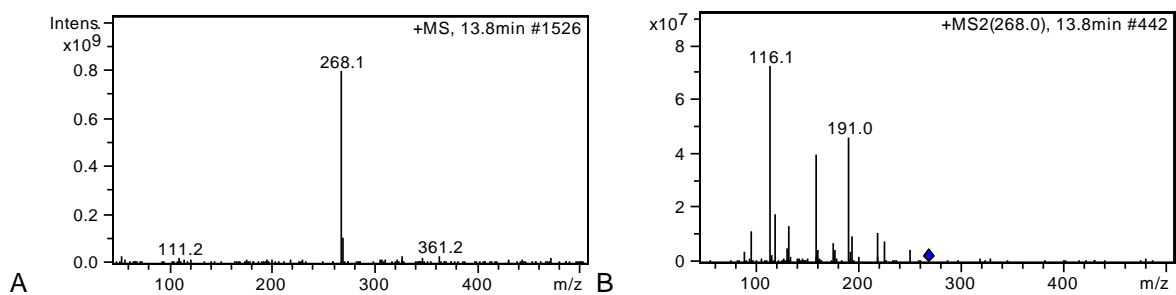
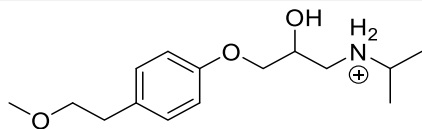


Figure S4: MS spectra of Metoprolol at retention time 13.8 min. A: Spectrum of the total ion current at retention time 13.8 min shows m/z of 268 for Metoprolol. B: MS^2 -spectrum of isolated m/z 268 at retention time 13.8 min results in main peaks of m/z 191 (65%), 159 (53%) and 116 (100%).

Table S2: Suggested MS^2 -fractions for Metoprolol at retention time 13.8 min.

ESI-MS $[M+H]^+$	MS^2 -fragments $[m/z]$ of 268
268	191: $C_{12}H_{15}O_2^+$
	159: $C_{11}H_{11}O^+$
	116: $C_6H_{14}NO^+$



1.4.2 Main oxidation product 2

The main oxidation product was found with a m/z ratio of 345 and its fractions 303 and 230 at 7.6 min retention time. MS^n -experiments supported the assumption that the pyridinium tag is located at the aromatic ring system of Metoprolol. The exact assignment of the pyridinium-tag's position in the ring was revealed by 2-dimensional-NMR-spectroscopy.

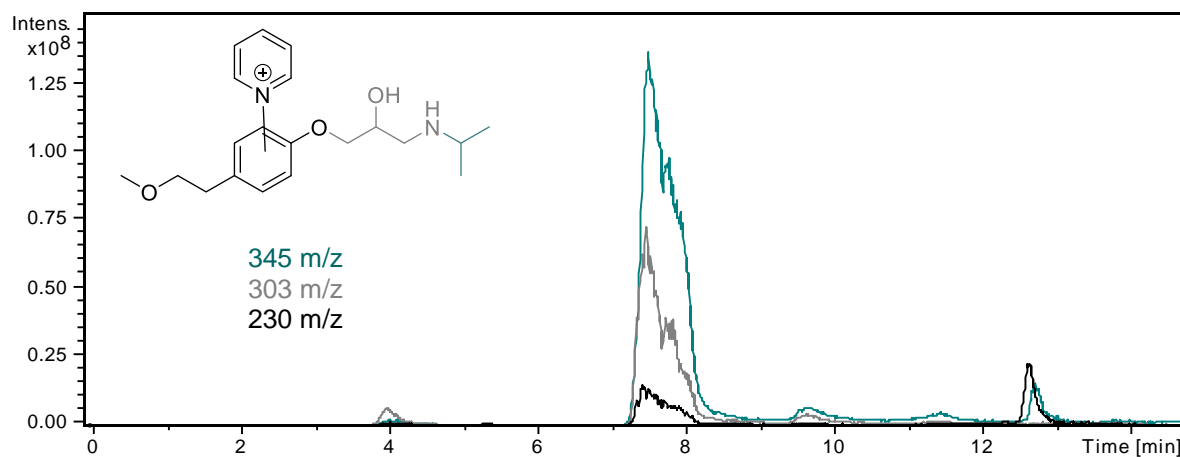


Figure S5: Extracted chromatogram of m/z ratios 345 (green), 303 (grey) and 230 (black). Main oxidation product 2 at retention time 7.6 min. Oxidation side products with same m/z ratios at 4.0, 9.6, 11.4 and 12.6 min.

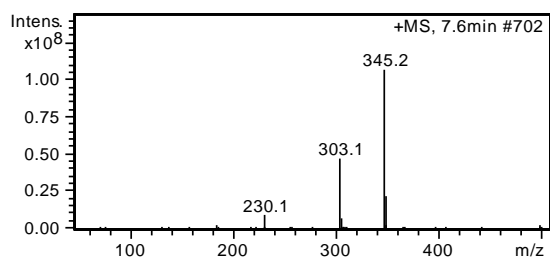
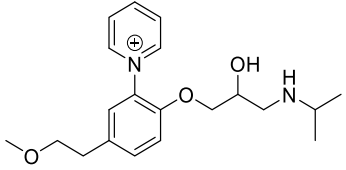
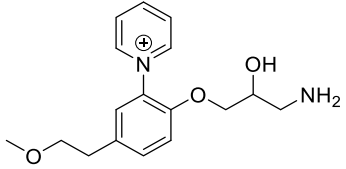
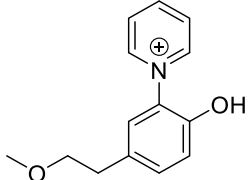


Figure S6: MS spectrum of the total ion current at retention time 7.6 min shows compounds with main m/z of 345 (100%) and fragments 303 (44%) and 230 (9%)

Table S3: Suggested structures of main oxidation product **2** m/z 345 and its MS^2 - and MS^3 -fragments with relative intensities at retention time 7.6 min

ESI-MS	MS^2 -fragments [m/z] of 345	MS^3 -fragments [m/z] of 345→230
345 (100%) 	230 (100%): $C_{14}H_{16}NO_2^+$	198 (49%): $C_{13}H_{12}NO^+$ 185 (100%): $C_{12}H_{11}NO^{++}$
303 (44%) 	230 (100%): $C_{14}H_{16}NO_2^+$	198 (69%): $C_{13}H_{12}NO^+$ 185 (100%): $C_{12}H_{11}NO^{++}$
230 (9%) 	198 (56%): $C_{13}H_{12}NO^+$ 185 (100%): $C_{12}H_{11}NO^{++}$	

1.4.3 Pyridinium tagged side oxidation products 3

1.4.3.1 m/z 345, 303, 230 – Isomers of main oxidation product **2**

Beside the main oxidation product **2** traces of four further oxidation products with m/z 345 (and fragments 303 and 230) were observed at retention times 4.0 min, 9.6 min, 11.4 min and 12.6 min (see Chromatogram Figure S3). Structures are suggested to be isomers of main oxidation product (**2**, see Table S3).

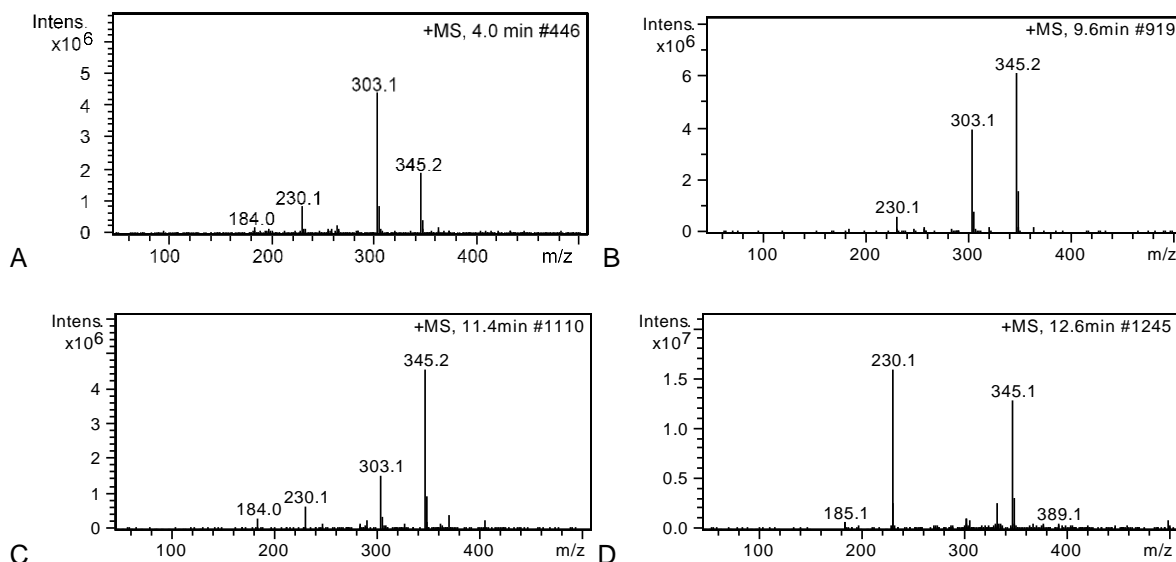


Figure S7: MS spectra of main oxidation products isomers

A: Spectrum of the total ion current at retention time 4.0 min shows main compounds with m/z of 345 (42%) and fragments 303 (100%) and 230 (19%).

B: Spectrum of the total ion current at retention time 9.6 min shows compounds with main m/z of 345 (100%) and fragments 303 (63%) and 230 (10%)

C: Spectrum of the total ion current at retention time 11.4 min shows compounds with main m/z of 345 (100%) and fragments 303 (35%) and 230 (100%).

D: Spectrum of the total ion current at retention time 12.6 min shows compounds with main m/z of 345 (81%) and fragments 303 (2%) and 230 (100%).

1.4.3.2 m/z 422, 343, 307, 228

At 1.6 min a compound were observed that resulted in m/z ratios of 422, 343, 307 and 228. Structure analysis assumes a compound of m/z 343 that is associated to pyridine (m/z 79). Although, it is unlikely that a clustered compound withstands MS^n -experiments. To reveal if pyridine is associated as a cluster or covalent bonded is beyond the scope of this work. However, structure analysis assumes a pyridinium tag in the aromatic system and therefore classifies this compound as a pyridinated side oxidation product (3).

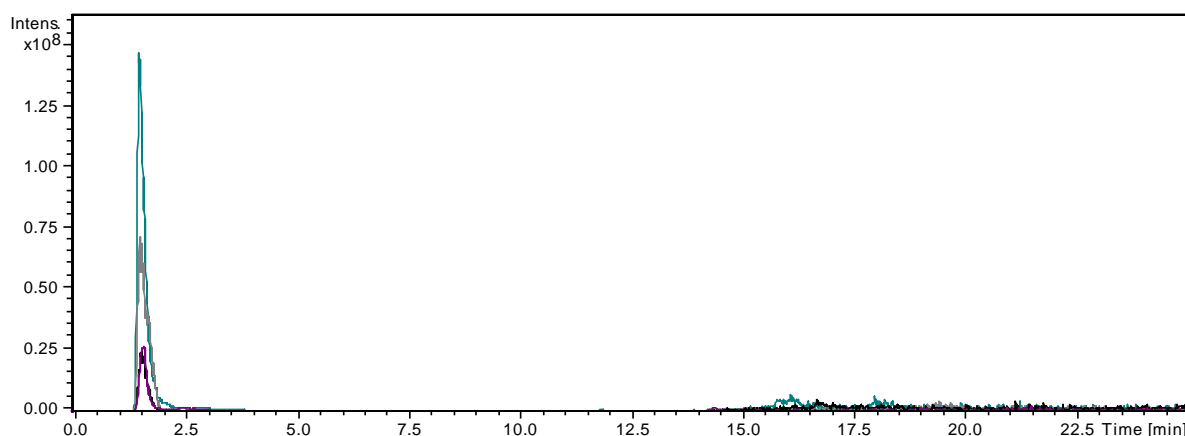


Figure S8: Extracted chromatogram of m/z ratios 422, 343, 307 and 228 at retention time 1.6 min.

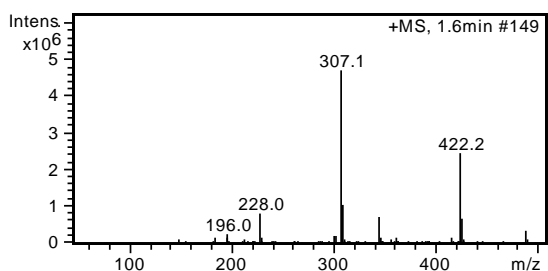
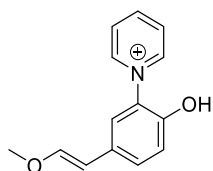


Figure S9: MS spectrum of the total ion current at retention time 1.6 min shows compounds with main m/z of 422 (52%) and fragments 343 (15%), 307 (100%) and 228 (17%).

Table S4: Suggested structures of m/z 422, 343, 307 and 228 and its MS^2 - and MS^3 -fragments with relative intensities at retention time 1.6 min

ESI-MS	MS^2 -fragments [m/z] of 422	
422 (52%)	343 (68%): $C_{20}H_{27}N_2O_3^+$	
343 + 79		MS^3 -fragments [m/z] 422 \rightarrow 307
	307 (100%): $C_{19}H_{19}N_2O_2^+$	275 (45%): $C_{18}H_{15}N_2O^+$
		262 (100%): $C_{17}H_{14}N_2O^{++}$
		228 (24%): $C_{14}H_{14}NO_2^+$
		183 (19%): $C_{12}H_9NO^+$
	MS^2 -fragment [m/z] of 343	MS^3 -fragments [m/z] 343 \rightarrow 240
343 (15%)	240 (25%): $C_{15}H_{14}NO_2^+$	197 (100%): $C_{13}H_{11}NO^+$
		MS^3 -fragments [m/z] 343 \rightarrow 228
	228 (100%): $C_{14}H_{14}NO_2^+$	213 (100%): $C_{13}H_{11}NO_2^{++}$
		197 (33%): $C_{13}H_{11}NO^+$
		149 (82%): $C_9H_9O_2^+$
	MS^2 -fragments [m/z] of 307	MS^3 -fragments [m/z] 307 \rightarrow 262
307 (100%)	275 (41%): $C_{18}H_{15}N_2O^+$	260: $C_{17}H_{12}N_2O^{++}$
228 + 79		196: $C_{13}H_{10}NO^+$
		MS^3 -fragments [m/z] 307 \rightarrow 262
	262 (100%): $C_{17}H_{14}N_2O^{++}$	183 (100%): $C_{12}H_9NO^+$
		155 (61%): $C_{11}H_9N^+$
		MS^3 -fragments [m/z] 307 \rightarrow 228
	228 (84%): $C_{14}H_{14}NO_2^+$	213: $C_{13}H_{11}NO_2^{++}$
		197: $C_{13}H_{11}NO^+$
		149: $C_9H_9O_2^+$
		MS^3 -fragments [m/z] 307 \rightarrow 183
	183 (20%): $C_{12}H_9NO^+$	155 (100%): $C_{11}H_9N^+$
	MS^2 -fragments [m/z] 228	MS^3 -fragments [m/z] 228 \rightarrow 213
228 (17%)	213 (14%): $C_{13}H_{11}NO_2^{++}$	185: $C_{12}H_{11}NO^+$
		133: $C_9H_9O^+$
	197 (26%): $C_{13}H_{11}NO^{++}$	



149 (100%): C₉H₉O₂⁺

1.4.3.3 *m/z* 361, 319, 246: Pyridinium tagged α -Hydroxy-metoprolol

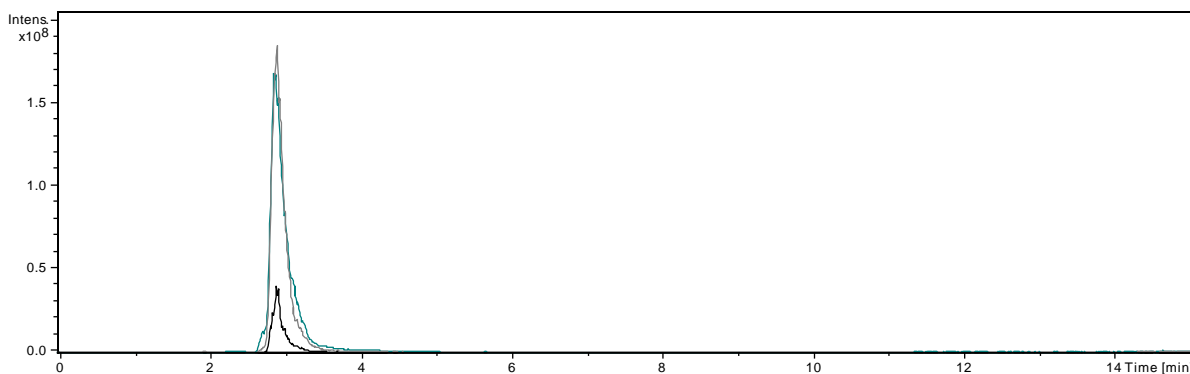


Figure S10: Extracted chromatogram of *m/z* ratios 361 (grey), 319 (green) and 246 (black) at retention time 2.9 min.

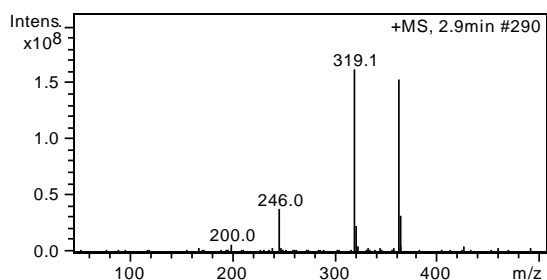
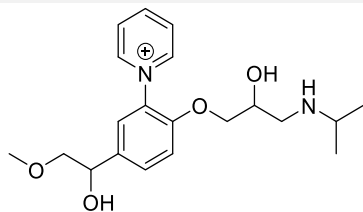


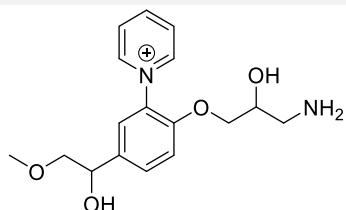
Figure S11: MS spectrum of the total ion current at retention time 2.9 min shows compounds with main *m/z* of 361 (94%) and fragments 319 (100%) and 246 (24%).

Table S5: Suggested structures of *m/z* 361, 319 and 246 and its MS²- and MS³-fragments with relative intensities at retention time 2.9 min

ESI-MS	MS ² -fragments [m/z] of 361	MS ³ -fragments [m/z] 361→246
361 (94%)	246 (100%): C ₁₄ H ₁₆ NO ₃ ⁺	201 (100%): C ₁₂ H ₁₁ NO ₂ ^{•+}

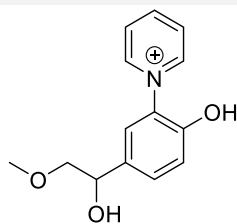


MS ² -fragments [m/z] of 319	MS ³ -fragments [m/z] 319→246
246 (100%): C ₁₄ H ₁₆ NO ₃ ⁺	201 (100%): C ₁₂ H ₁₁ NO ₂ ^{•+}



MS²-fragments [m/z] of 246

246 (24%)

201 (100%): C₁₂H₁₁NO₂^{•+}1.4.3.4 *m/z* 373

Possibly formed methyl radicals during electrolysis derivatize main oxidation product **2**.

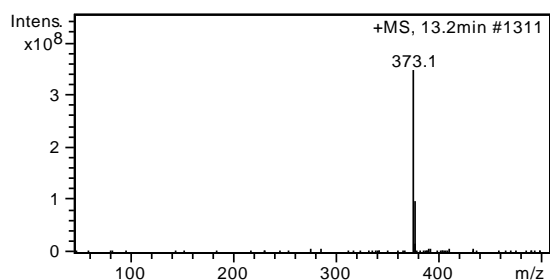
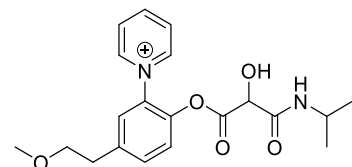


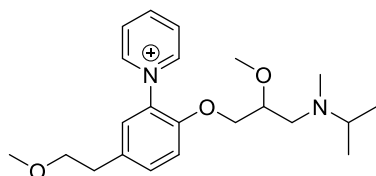
Figure S12: MS spectrum of the total ion current at retention time 13.2 min shows compounds with *m/z* of 373 (100%).

Table S6: Suggested structures of *m/z* 373 and its MS²- and MS³-fragments at retention time 13.2 min

ESI-MS	MS ² -fragments [m/z] of 373	MS ³ -fragments [m/z] 373->230
373 (100%)	230 (100%): C ₁₄ H ₁₆ NO ₂ ⁺	198 (72%): C ₁₃ H ₁₂ NO ⁺
Isomer of		185 (100%): C ₁₂ H ₁₁ NO ⁺
		MS ³ -fragments [m/z] 373->144
	144 (38%): C ₈ H ₁₈ NO ⁺	102 (100%): C ₅ H ₁₂ NO ⁺
		100 (100%): C ₆ H ₁₄ N ⁺



or also possible



1.4.4 Non-pyridinated side oxidation products (4)

1.4.4.1 *m/z* 282

An α -ketone derivatizes Metoprolol was already suggested as Metoprolol metabolite. [5] Alternatively, derivatization due to possible formation of methyl radicals during electrolysis might have occurred.

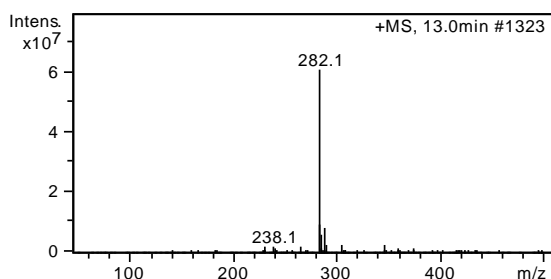


Figure S13: MS spectrum of the total ion current at retention time 13.0 min shows compound with m/z of 282 (100%).

Table S14: Suggested structures of m/z 282 and its MS^2 - and MS^3 -fragments with relative intensities at retention time 13.0 min

ESI-MS	MS^2 -fragments [m/z] of 282	MS^3 -fragments [m/z]
282 (100%)	264 (18%): $C_{15}H_{22}NO_3^+$	
 or less plausible	240 (40%): $C_{12}H_{18}NO_4^+$	MS^3-fragments [m/z] 282→240 167: $C_9H_{13}NO_2^{*+}$ 135: $C_8H_7O_2^+$
	205 (99%): $C_{12}H_{13}O_3^+$	MS^3-fragments [m/z] 282→205 145 unknown molecular formula due to lack of data
	167 (76%): $C_9H_{13}NO_2^+$	MS^3-fragments [m/z] 282→167 135 (100%): $C_8H_7O_2^+$ 107 (23%): $C_7H_7O^+$
	135 (56%): $C_8H_7O_2^+$	
	133 (40%): $C_9H_9O^+$	
	116 (100%): $C_6H_{14}NO^+$	

1.4.4.2 m/z 284: α -Hydroxy-metoprolol

α -Hydroxy-metoprolol has been already analyzed and described as Metoprolol metabolite. [5,6] We observed two isomers at retention times 12.8 min and 13.5 min.

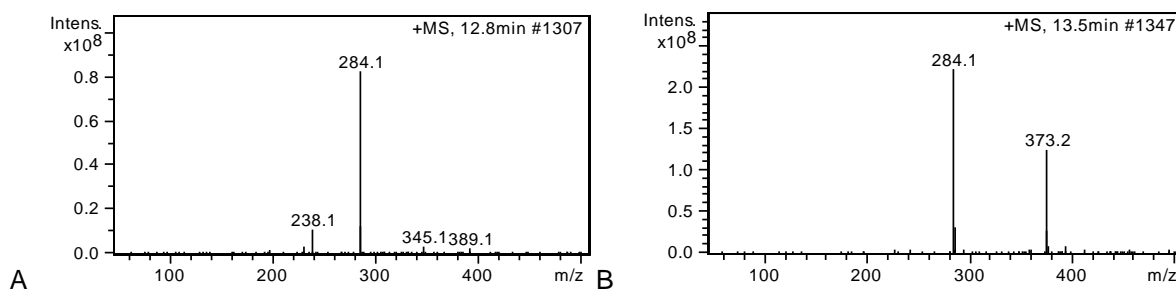


Figure S14: MS spectra of m/z 284 at 12.8 and 13.5 min

A: Spectrum of the total ion current at retention time 12.8 min shows compounds with m/z of 284 (100%) and 238 (13%).

B: Spectrum of the total ion current at retention time 13.5 min shows compounds with m/z of 284 (100%) and tailing from 373 (56%, maximum at 13.2 min).

Table S7: Suggested structure of m/z 284 and its MS^2 - and MS^3 -fragments with relative intensities at retention time 12.8 min

ESI-MS	MS^2 -fragments [m/z] of 284	MS^3 -fragments [m/z]
--------	------------------------------------	-----------------------------

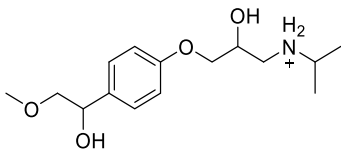
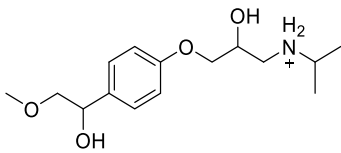
284 (100%)	266 (9%): C ₁₅ H ₂₄ NO ₃ ⁺	MS ³ -fragments [m/z] of 284 -> 207	
Isomer of	248 (7%): C ₁₅ H ₂₂ NO ₂ ⁺		
	224 (15%): C ₁₂ H ₁₈ NO ₃ ⁺		
	207 (22%): C ₁₂ H ₁₅ O ₃ ⁺		198 (41%): C ₁₂ H ₁₃ O ₂ ⁺
	175 (19%): C ₁₁ H ₁₁ O ₂ ⁺		175 (100%):
	116 (100%): C ₆ H ₁₄ NO ⁺		

Table S8: Suggested structure of m/z 284 and its MS²- and MS³-fragments with relative intensities at retention time 13.5 min.

ESI-MS	MS ² -fragments [m/z]
284 (100%)	266 (15%): C ₁₅ H ₂₄ NO ₃ ⁺
Isomer of	234 (18%): C ₁₄ H ₂₀ NO ₂ ⁺
	175 (34%): C ₁₁ H ₁₁ O ₂ ⁺
	116 (100%): C ₆ H ₁₄ NO ⁺

1.5. NMR Spectra

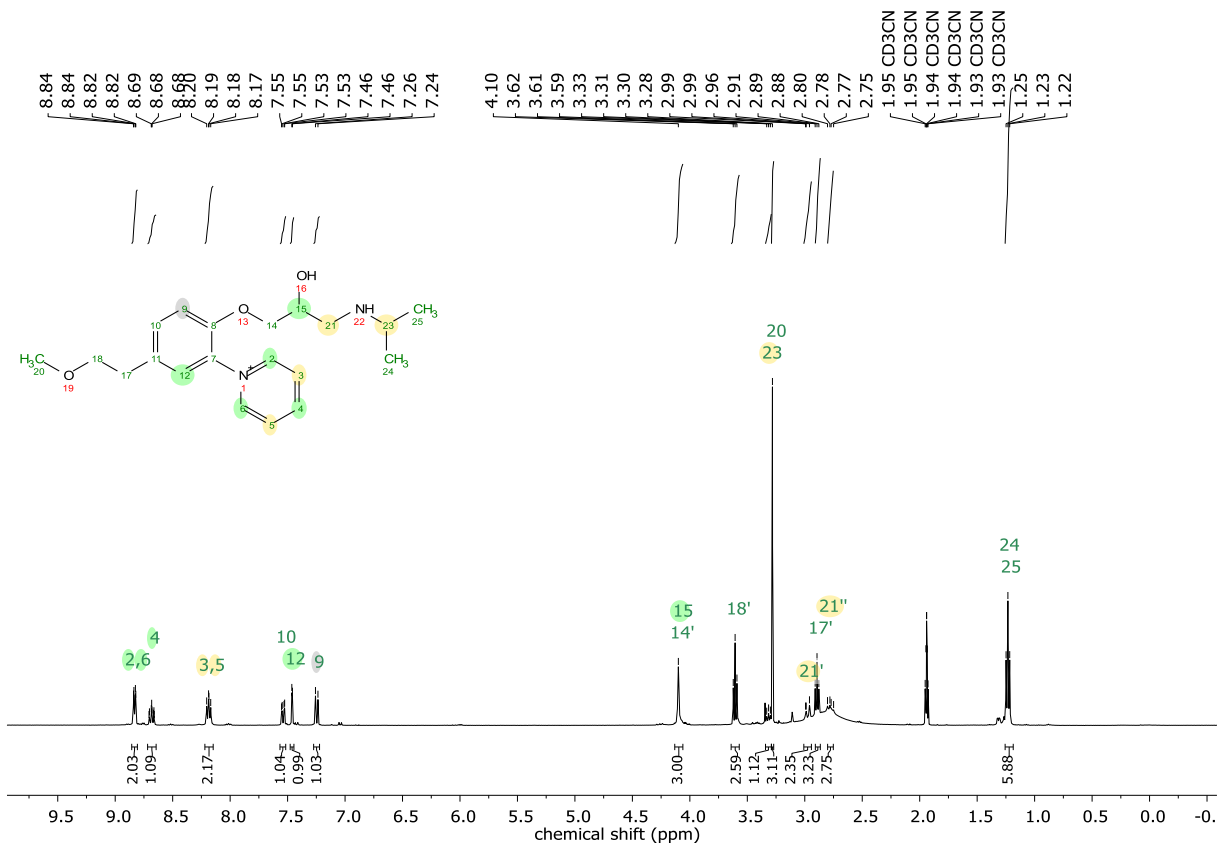


Figure S15: ¹H NMR of charge-tagged Metoprolol 2. 400 MHz NMR

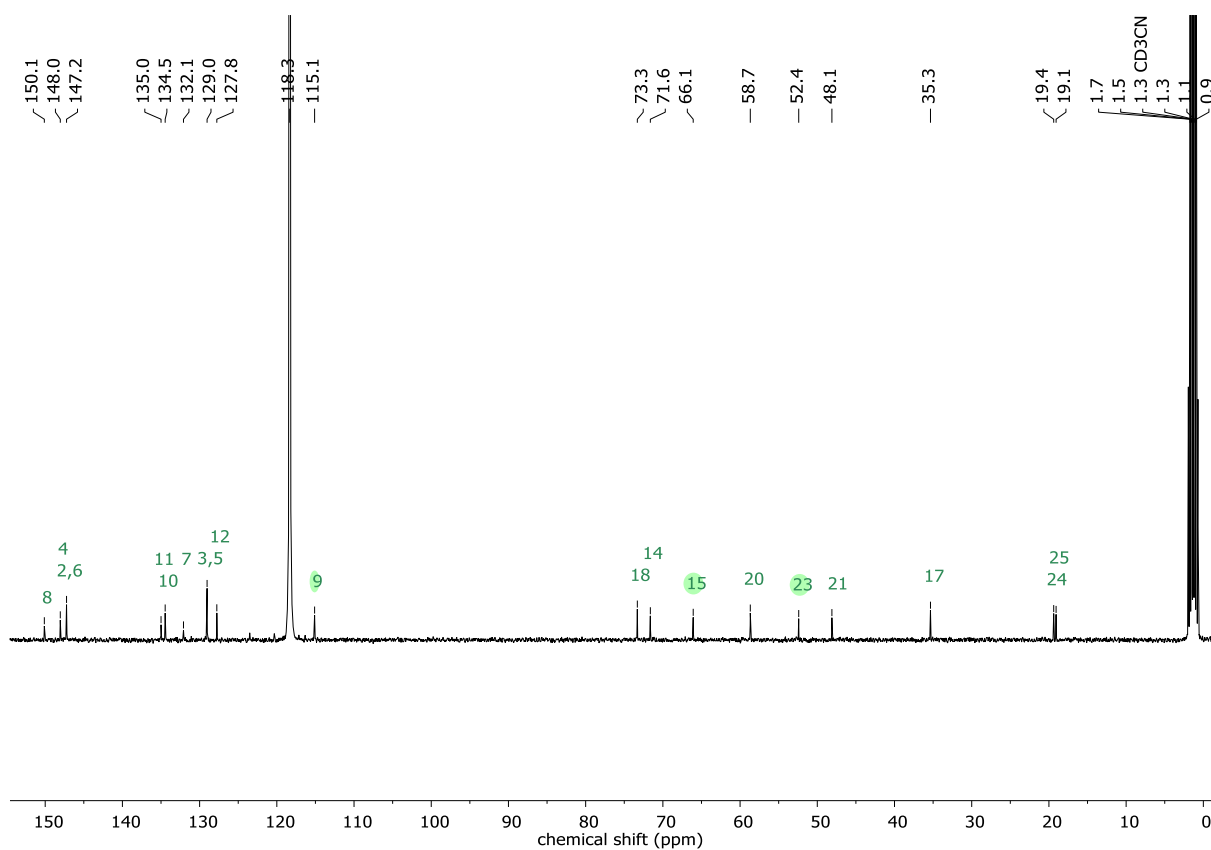


Figure S16: ^{13}C NMR of charged tag metoprolol **2**. 101 MHz NMR

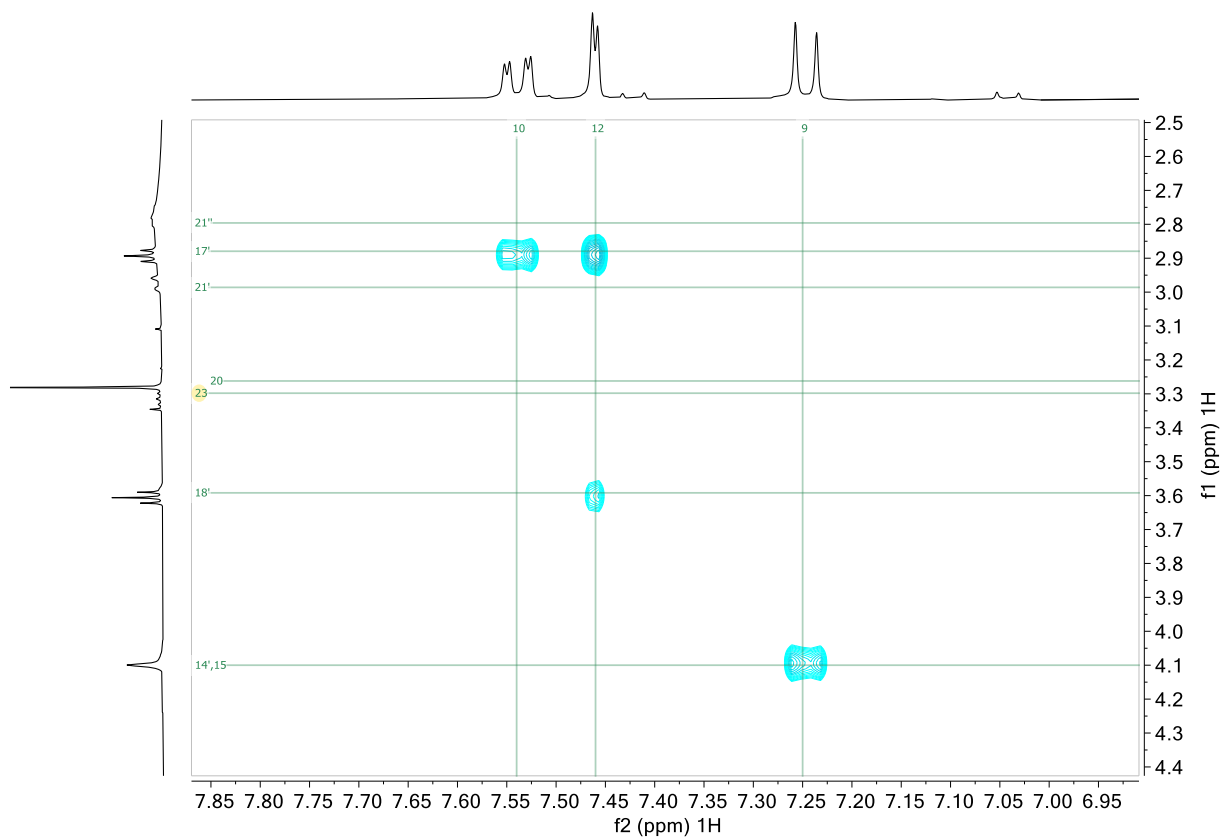


Figure S17: NOESY-NMR of charged tag metoprolol **2**. 400 MHz NMR.

2. References

- [1] a) C. Gütz, B. Klöckner, S. R. Waldvogel, *Org. Process Res. Dev.* **2016**, *20*, 26–32; b) C. Gütz, M. Bänziger, C. Bucher, T. R. Galvão, S. R. Waldvogel, *Org. Process Res. Dev.* **2015**, *19*, 1428–1433.
- [2] N. M. Vieno, T. Tuhkanen, L. Kronberg, *JOURNAL OF CHROMATOGRAPHY* **2006**, *1134*, 101–111.
- [3] B. K. Matuszewski, M. L. Constanzer, C. M. Chavez-Eng, *Anal. Chem.* **2003**, *75*, 3019–3030.
- [4] T. Schulze, "MassBank Record: UF407204", can be found:
<https://massbank.eu/MassBank/RecordDisplay.jsp?id=UF407204&dsn=UFZ>.
- [5] M. Poraj-Kobielska, M. Kinne, R. Ullrich, K. Scheibner, G. Kayser, K. E. Hammel, M. Hofrichter, *Biochemical Pharmacology* **2011**, *82*, 789–796.
- [6] N. D. J. Antunes, R. C. Cavalli, M. P. Marques, V. L. Lanchote, *Chirality* **2013**, *25*, 1–7.